Untersuchungen zur hypothalamischen Kontrolle thermoregulatorischer Effektororgane der Ratte

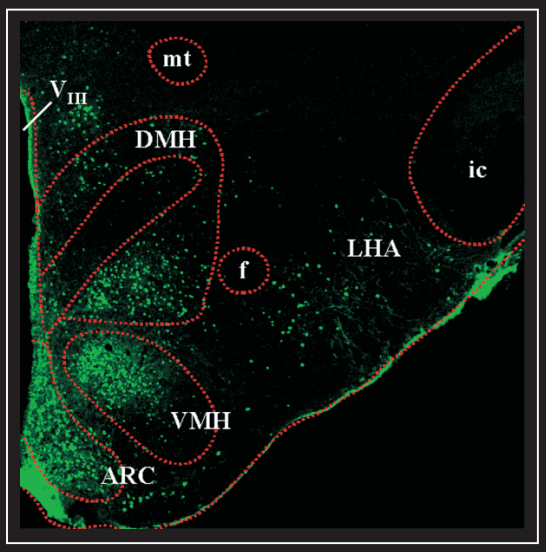

Habilitationsschrift
vorgelegt dem Fachbereich Veterinärmedizin
der Justus-Liebig-Universität Gießen

Dr. rer. nat. Thomas Hübschle

ISBN 3-89687-681-3

VVB LAUFERSWEILER VERLAG
édition scientifique

1. Auflage 2004

1st Edition 2004

VVB LAUFERSWEILER VERLAG
édition scientifique

GLEIBERGER WEG 4, D-35435 WETTENBERG
Tel: 06406-4413 Fax: 06406-72757
Email: VVB-IPS@T-ONLINE.DE

www.doktorverlag.de

Aus dem Institut für Veterinär-Physiologie
der Justus-Liebig-Universität Gießen

Untersuchungen zur hypothalamischen Kontrolle thermoregulatorischer Effektororgane der Ratte

Habilitationsschrift
vorgelegt dem Fachbereich Veterinärmedizin
der Justus-Liebig-Universität Gießen

von
Dr. rer. nat. Thomas Hübschle
aus Fürstenfeldbruck

Gießen 2004

INHALTSVERZEICHNIS **Seite**

Seite

Sabine und Benedikt

LEONARDO DA VINCI (1452-1519)

„All unser Wissen gründet sich auf Wahrnehmung“

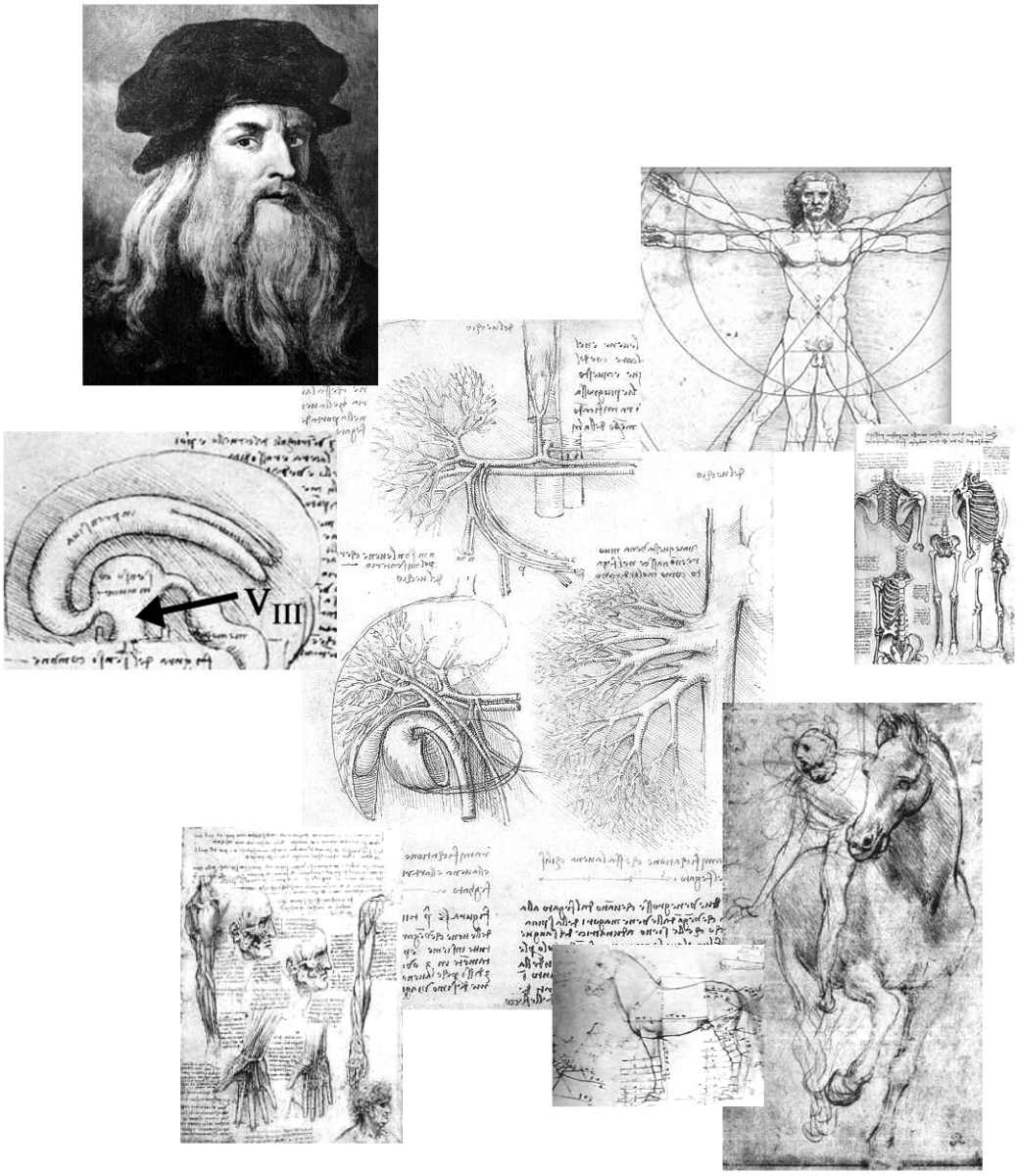

Diverse anatomische Zeichnungen und Skizzen von Leonardo da Vinci. Zu sehen sind unter anderem Studien zu den menschlichen Proportionen (Federzeichnung mit leichter Aquarellierung, 1509, heute in der Galleria dell Accademia, Venedig, Italien), zur Gefäßanatomie der menschlichen Leber (Federzeichnung del vechio, ca. 1508, heute im Besitz der englischen Königin, Windsor, England) und zum Ventrikelsystem des menschlichen Gehirns (Rötelzeichnung, 1508-1509, heute im Besitz der englischen Königin, Windsor, England). Der dritte Hirnventrikel (V_{III}) ist mit Pfeil hervorgehoben. Die Erkenntnis zur Anatomie des Ventrikelsystems verdankte Leonardo da Vinci seinen Wachs-ausgusspräparaten. **Der Hypothalamus liegt seitlich des dritten Hirnventrikels.**

1. Abkürzungen

AG	Arbeitsgruppe
AgRP	Agouti-verwandtes Peptid
AH	anteriorer Hypothalamus
AT1	Angiotensin II Rezeptor vom AT1-Subtyp
CART	Cocain-Amphetamin-verwandtes Transkript
COX2	Cyclooxygenase-2
CVOs	cirkumventrikulären Organe
DAPI	4',6-Diamidino-2-Phenylindol-Dilacetat, Kernfärbung
DMH	dorsomedialer Hypothalamus
DNA	Desoxyribonukleinsäure
EP3R	Prostaglandin E-Rezeptorsubtyp 3
EP4R	Prostaglandin E-Rezeptorsubtyp 4
Fos	Fos-Protein, Transkriptionsfaktor, Onkogen
icv	intracerebroventrikulär
IL-1	Interleukin-1
IL-1ß	Interleukin-1 beta
IL-6	Interleukin-6
IML	intermediolaterale Zellkolumne
JAKs	Janus-Kinasen
JAK2	Janus-Kinase 2
LH	lateraler Hypothalamus
LPS	Lipopolysaccharid
MFB	mediales Vorderhirnbündel
MnPO	*Nucleus praeopticus medianus*
MPO	mediale präoptische Region
NADPH	Nicotinamid-Adenin-Dinukleotid-Phosphat
NeuN	neuronspezifischer nukleärer Faktor
NO	Stickstoffmonoxid
nNOS	neuronale NO-Synthase
Ob-Rb	funktionelle, lange Form des Leptinrezeptors
OVLT	*Organum vasculosum laminae terminalis*
PAG	zentrales Höhlengrau, graue Substanz um den *Aquaeductus mesencephali*
cPAG	caudales PAG
PGE2	Prostaglandin-E2
PH	posteriorer Hypothalamus

POMC	Pro-Opiomelanocortin
PRV	Pseudorabiesviren
PRV-Bartha	attenuierter Pseudorabiesviren-Impfstamm Bartha
PVN	*Nucleus paraventricularis hypothalami*
Raphé	medulläre Kerngebiete an der Mittelnaht
RF	*Formatio reticularis*
RRF	Mittelhirngebiet hinter dem Nucleus ruber (engl: retrorubal field)
SFO	Subfornikalorgan (*Organum subfornicale*)
SON	*Nucleus supraopticus*
SSN	*Nucleus salivatorius superior*
sst1 - sst5	Somatostatin-Rezeptorsubtypen
STAT	STAT-Transkriptionsfaktorfamilie
	(engl: **s**ignal **t**ransducers and **a**ctivators of **t**ranscription)
STAT3	STAT-Transkriptionsfaktor 3
VMH	ventromedialer Hypothalamus
VMPO	ventromediale präoptische Region
VTA	ventrales *Tegmentum mesencephali*
V_{III}	dritter Hirnventrikel
ZNS	zentrales Nervensystem
[Imp/s]	neuronale Entladungsrate
[T_B]	Körperkerntemperatur

2. Einleitung

2.1. Der Hypothalamus

2.1.1. Hypothalamische Kontrolle homöostatischer Systeme

Parameter des „milieu intérieur“ eines tierischen Organismus werden in einem Zustand des Fließgleichgewichts gehalten [Bernard 1878-1879, Cannon 1932]. Diesen Zustand nennt man Homöostase. Die der Homöostase zu Grunde liegenden Mechanismen stellen eine unabdingbare Voraussetzung für die Funktionalität lebenswichtiger Vorgänge aller höheren Vertebraten dar. Homöostase wird durch ein komplexes Aufeinanderabstimmen afferenter und efferenter Kontrollmechanismen im Rahmen autonomer Regelkreise ermöglicht. Der Hypothalamus, die basale Komponente des Zwischenhirns, gilt als übergeordnetes Kontrollzentrum solcher Regelkreise und ist damit Schlüsselstruktur des Zentralen Nervensystems (ZNS) für die Regulation homöostatischer Systeme. Vereinfacht dargestellt vergleicht der Hypothalamus (patho-)physiologische Abweichungen der zu regelnden, physiologischen Größe (Istwerte) mit vorgegebenen Sollwerten. Nach neuronaler Integration zahlreicher afferenter Signale moduliert er die Aktivität bestimmter peripherer Effektororgane, die durch Anpassung an den geforderten Sollwert einen neuen Istwert einstellen: Entspricht der Istwert dem geforderten Sollwert, so ist das innere Fließgleichgewicht hergestellt.

Die Komplexität und Diversität des Hypothalamus zeigt sich in seiner Zytoarchitektur, Transmitter- und Rezeptorausstattung sowie seiner multiplen neuronalen Verbindungen zu anderen Anteilen des Gehirns. Ausgeprägte, teils reziproke Verbindungen sind beispielsweise zu Strukturen des sogenannten limbischen Systems, wie z.B. Cortex, Amygdala und Hippocampus vorhanden. Diese neuronalen Verbindungen bilden die neuroanatomische Grundlage für eine Gewährleistung lebenswichtiger Körperfunktionen auch beim Auftreten starker emotionaler Belastungen des Organismus. Generell funktionieren hypothalamisch kontrollierte Regelsysteme nicht nur unter Ruhebedingungen, sondern auch bei größter körperlicher Aktivität oder Krankheit oft fehlerfrei.

Neben den vitalen Körperfunktionen wird vom Hypothalamus auch das hierfür adäquate Verhalten gesteuert. Dies verdeutlicht, dass nicht nur interne Kontrollmechanismen des Individuums für die Aufrechterhaltung der Homöostase entscheidend sind. Umweltfaktoren sind ebenso wichtig, und zumeist ist es noch wichtiger, wie die Umwelt in die Regulation

vitaler Körperfunktionen mit einbezogen wird. Als Beispiel kann man die Regulation der Körperkerntemperatur (Thermoregulation) anführen, die nicht nur auf internen, unbewusst ablaufenden Kontrollmechanismen (autonome Thermoregulation, siehe 2.1.2), sondern auch auf dem Verhalten des einzelnen Individuums beruht (Verhaltensthermoregulation). So werden an einem heißen Sommertag Tiere auf einer Weide bei Bedarf und Möglichkeit den Schatten eines Baumes aufsuchen, um der Hitze besser entgehen zu können. Dieses Beispiel soll verdeutlichen, dass die bedarfsgerechte Regulation lebenswichtiger Funktionen sowohl intern durch körpereigene Systeme erfolgt als auch durch den Zwang, sich entsprechend der Bedürfnisse des Organismus zu verhalten.

Im Blickpunkt dieser Habilitationsschrift stehen hypothalamische Kontrollmechanismen, die an der Interaktion der autonomen Thermoregulation mit anderen homöostatischen Regelsystemen beteiligt sind (Abb. 1).

Interaktion der Thermoregulation mit anderen homöostatischen Systemen

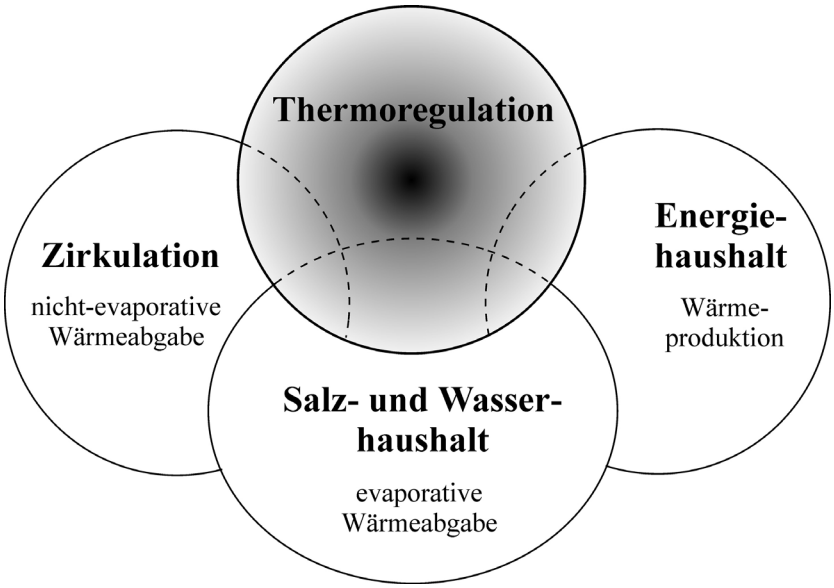

Abbildung 1
Die Regulation der Körperkerntemperatur (Thermoregulation) sollte nur bei vereinfachter Darstellung und zum besseren Verständnis als isolierter Regelkreis betrachtet werden. Die Kontrolle der Körperkerntemperatur ist ansonsten nur im integralen Verbund mit der Regulation anderer lebenswichtiger Funktionen zu verstehen. Diese Habilitationsschrift befasst sich überwiegend mit hypothalamisch kontrollierten Regelleistungen der Schnittmenge der Thermoregulation mit zwei anderen homöostatischen Systemen, dem Salz- und Wasserhaushalt sowie dem Energiehaushalt.

Unter extremer Hitze werden Wärmeabgabemechanismen aktiviert. Diese unterteilt man in evaporative und nicht-evaporative Wärmeabgabemechanismen. Bei der evaporativen Wärme-

abgabe ist der entscheidende Faktor die Verdunstung von Wasser, z.B. von Schweißdrüsensekret an der Körperoberfläche (Verdunstungskälte). Dieser Verlust von Körperwasser hat somit auch Auswirkungen auf die Regulation des Salz- und Wasserhaushaltes. Die evaporative Wärmeabgabe kann daher als integrative Regelleistung von einerseits thermoregulatorischen Belangen und andererseits Anforderungen zur Regulation des Salz- und Wasserhaushaltes angesehen werden. **Hypothalamische Kontrollmechanismen der evaporativen Wärmeabgabe werden unter 4.1ff in vier von zehn für diese Habilitationsschrift relevanten Publikationen näher untersucht.** Die nicht-evaporative Wärmeabgabe des sogenannten inneren Wärmestroms kann dagegen als integrative Regelleistung von einerseits thermoregulatorischen Belangen und andererseits Anforderungen zur Regulation des Herz-Kreislaufssystems (Zirkulation) aufgefasst werden.
Alle vitalen Körperfunktionen und Stoffwechselprozesse homöothermer Tiere werden in ihrer Geschwindigkeit und ihrer Ausrichtung von der Körpertemperatur beeinflusst. Wärmebildung ist ein Resultat des Energieumsatzes aus Nährstoffen. Die Wärmebildung kann daher als integrative Regelleistung von einerseits thermoregulatorischen Belangen und andererseits Anforderungen zur Regulation des Energiehaushaltes angesehen werden. **Hypothalamische Kontrollmechanismen der Wärmebildung werden in 4.2ff in sechs von zehn für diese Habilitationsschrift relevanten Publikationen näher untersucht.**

2.1.2. Hypothalamische Kontrolle der Körperkerntemperatur

Wie bereits erwähnt, ist der übergeordnete Regler der Körperkerntemperatur, der auch als Thermostat bezeichnet werden kann, im Hypothalamus installiert. Nach heutigem Lehrbuchwissen scheinen insbesondere zwei hypothalamische Regionen für die Temperaturregulation von wichtiger Bedeutung zu sein (Abb. 2):

(1) Die präoptische Region als anteriore Komponente des Hypothalamus steuert Mechanismen der Wärmeabwehr. Wird diese hypothalamische Region in tierexperimentellen Läsionsstudien zerstört, so können Wärmeabgabemechanismen nicht mehr oder nur noch ungenügend aktiviert werden.
(2) Eine caudale Komponente des Hypothalamus steuert die Wärmebildung. Zerstört man diese Hirnregion in tierexperimentellen Läsionsstudien, so können Wärmebildungsmechanismen nicht mehr oder nur noch ungenügend aktiviert werden.

Der Hypothalamus – ein neurobiologischer Thermostat

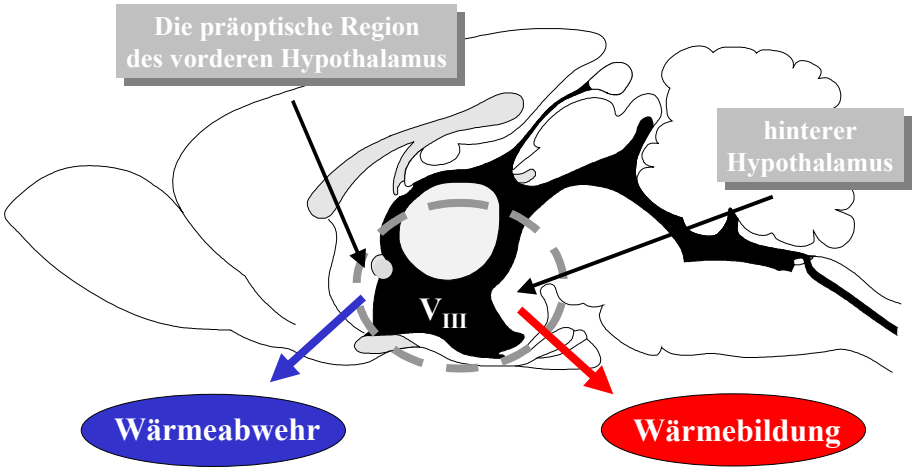

Abbildung 2
Der Sagitalschnitt durch das Gehirn einer Ratte verdeutlicht die Lage des Hypothalamus. Der Hypothalamus bildet die basale Komponente des Zwischenhirns und liegt seitlich des dritten Hirnventrikels (V_{III}). Zwei hypothalamische Regionen sind nach heutigem Lehrbuchwissen wichtig für die Regulation der Körpertemperatur. Die präoptische Region ist essentiell für die Wärmeabwehr, der hintere Hypothalamus für die Wärmebildung.

Diese vereinfachte Sichtweise der hypothalamischen „Zentrums-Theorie“, welche einzelne Regionen bzw. Komponenten als verantwortlich für die Regulation lebenswichtiger Körperfunktionen beschreibt, kann die Komplexität hypothalamischer Regelkreise nur unzureichend beschreiben. Nach aktuellem Stand der Forschung lässt sich zumindest für die differenzielle efferente Aktivierung von Stellgliedern der autonomen Thermoregulation ein weit detaillierteres Modell wiedergeben [Nagashima et al. 2000]. Dies ist in Abbildung 3 für die Ratte gezeigt.

Unter Bedingungen erhöhter externer und interner Wärmebelastung aktivieren Ratten zur regulatorischen Senkung der Körperkerntemperatur zwei Wärmeabgabemechanismen: (1) Vasodilatation von Blutgefäßen der Haut und (2) Speichelsekretion aus der Submandibular- bzw. Sublingualdrüse. Zur Bildung von Körperwärme, z.B. bei Kälteexposition, werden andererseits die beiden Effektororgane Skelettmuskulatur und braunes Fettgewebe genutzt. Dabei werden die unterschiedlichen thermoregulatorischen Effektororgane in kompliziert verschalteten Neuronenketten ausgehend von hypothalamischen Kerngebieten über Zentren des Mittelhirns, der *Medulla oblongata* sowie des Rückenmarks efferent innerviert. Ausgangspunkt dieser multisynaptischen Nervenbahnen vom Gehirn zur Körperperipherie stellen hypothalamische Neurone der präoptischen Region dar. Dabei zeigen die präoptischen

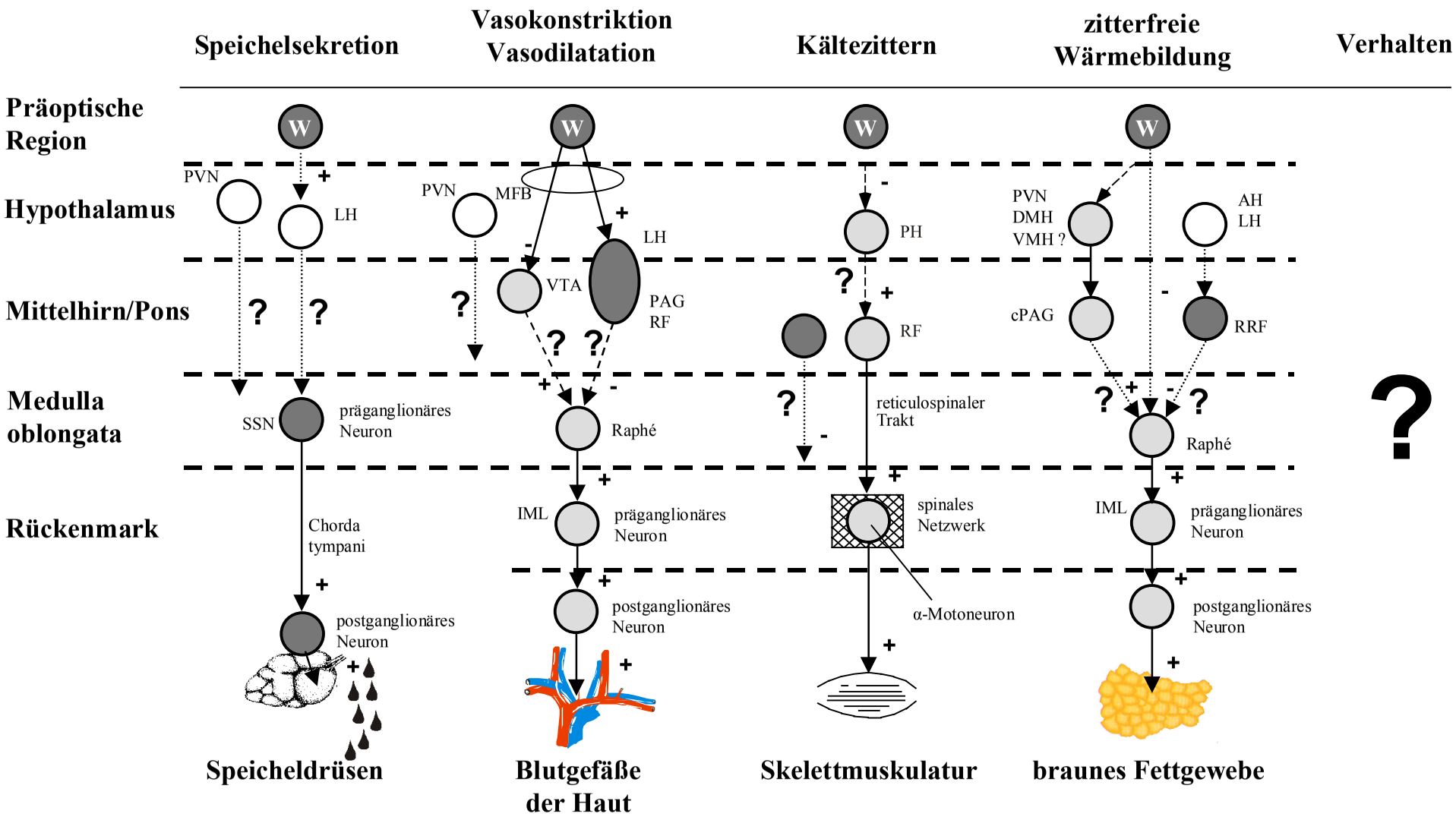

Abbildung 3
Schematische Darstellung der Efferenzen zu thermoregulatorischen Effektororganen der Ratte (modifiziert nach Nagashima et al. 2000). Gemeinsamer Ausgangspunkt der in die Körperperipherie ziehenden efferenten Neuronenketten ist die präoptische Region. Diese Mechanismen der autonomen Thermoregulation sind deutlich besser untersucht als die der Verhaltensthermoregulation, deren neuroanatomisches Korrelat noch völlig unklar ist. W = warmsensitives Neuron, + = Aktivierung, - = Hemmung. Dunkelgrau bzw. hellgrau eingefärbte Projektionen entsprechen Körpertemperatur senkenden bzw. steigernden Projektionen. (Abkürzungen siehe gesonderte Liste, weitere Erläuterungen siehe Text).

Neurone nach diesem Modell eine intrinsische Warmsensitivität [Hammel 1965, 1968, Boulant 2000], d.h. sie selbst fungieren als Thermosensoren des Körperinneren und messen die Istwerte der Körperkerntemperatur. Sie senden exzitatorische Signale zu efferenten Nervenbahnen der Wärmeabgabe und inhibitorische Signale zu Efferenzen der Wärmebildung.

Die alleinige Einbeziehung warmsensitiver präoptischer Neurone in dieses Modell beruht auf Befunden, dass die Messfühler der Körpertemperatur des Körperinneren bzw. des ZNS überwiegend warmsensitive Neurone sind [Hammel 1965, 1968, Boulant 2000]. Nur wenige Thermosensoren des ZNS haben sich *in vivo* und *in vitro* (Gehirnschnittpräparationen) als kaltsensitiv erwiesen. Interessanterweise besitzt gerade die präoptische Region der Säugetiere einen ausgeprägt hohen Prozentsatz warmsensitiver Neurone. Jedoch findet man eine generalisierte Thermoresponsivität neuronaler Zellen in zahlreichen anderen hypothalamischen und extrahypothalamischen Gehirnregionen. Warum ist nach diesem Modell nun gerade die präoptische Region von so großer Bedeutung für die Regulation der Körperkerntemperatur? Die Entscheidungskriterien zur Einordnung von Thermosensitivität bzw. –responsivität von Nervenzellen des ZNS wurden willkürlich festgelegt und das dadurch ermittelte Verteilungsmuster thermosensitiver bzw. thermorezeptiver ZNS-Strukturen ist diffus und wenig aussagekräftig. Das viel entscheidendere Kriterium nach heutiger Sicht ist die Signalverarbeitung solch hypothalamischer bzw. extrahypothalamischer Neurone mittels ihrer afferenten und efferenten neuronalen Verbindungen. Für warmsensitive Neurone der präoptischen Region ist eine ausgeprägte, nachgeschaltete Verarbeitung thermoregulatorischer Signale beschrieben [Nagashima et al. 2000]. Dies trifft für viele andere thermosensitive bzw. thermorezeptive ZNS-Strukturen jedoch nicht zu.

Thermorezeptoren spielen als Bestandteil des afferenten Astes des Regelkreises zur Regulation der Körpertemperatur eine wichtige Rolle. Neben den für die präoptische Region beschriebenen sind solche Temperaturmessfühler sowohl im Körperkern als auch in der Körperperipherie (Haut) zu finden. Die Thermorezeptoren des Körperkerns sind überwiegend warmsensitiv, die der Peripherie vornehmlich kaltsensitiv. Diese Messfühler senden Informationen über die Istwerte der Temperaturen aus dem Körperkern sowie der Peripherie zum Hypothalamus. Bei den thermoafferenten Nervenbahnen der Peripherie handelt es sich um myelinisierte Typ-III und -IV-Fasern, die wahrscheinlich multisynaptische Abzweigungen des spinothalamischen Traktes repräsentieren. Die thermoafferente Information aus dem Hypothalamus selbst wird intrinsisch unter Einbeziehung präoptischer Konnektivitäten vermittelt. Im Hypothalamus wird dann der Sollwert mit den gemessenen Istwerten

verglichen (Abb. 4). Warmrezeptoren zeigen bei steigender Körpertemperatur eine Zunahme, Kaltrezeptoren dagegen eine Abnahme der neuronalen Entladungsrate. Im Bereich des Schnittpunktes beider Kurvenverläufe lässt sich die Temperaturzone des Sollwertes ablesen. Wie wir im nächsten Kapitel sehen werden, wird diese Sollwertzone mittels efferenter Regelleistungen aktiv verteidigt. Liegen jedoch die Istwerte innerhalb dieser Sollwertzone und halten sich die efferenten Regelleistungen die Waage, so stellt sich die geregelte Körpertemperatur dem Sollwert entsprechend ein.

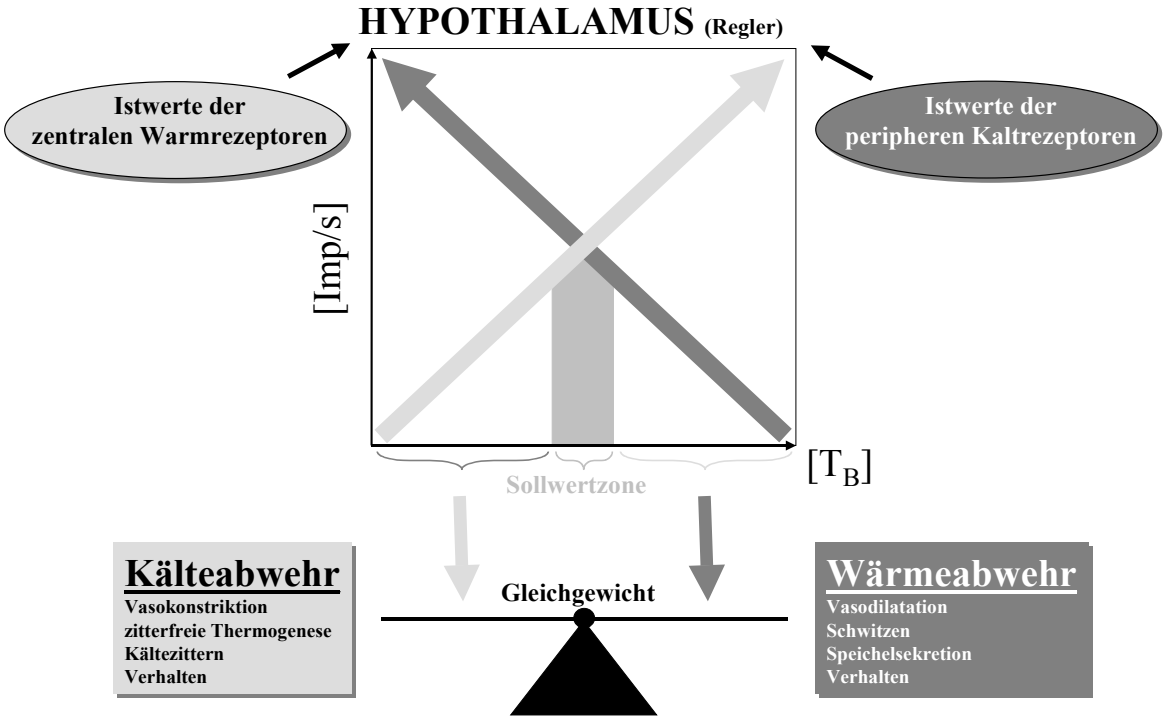

Abbildung 4
Der Hypothalamus als Regler der Körpertemperatur. Eine stabile Körperkerntemperatur stellt sich dann ein, wenn die Wärmebildung der Wärmeabgabe entspricht. Dazu werden die Istwerte der Warm- bzw. Kaltrezeptoren im Hypothalamus verrechnet und durch differentielle Modulation spezifischer thermoregulatorischer Effektororgane efferent beantwortet. [T_B] = Körperkerntemperatur, [Imp/s] = Entladungsrate der Warm- bzw. Kaltrezeptoren (weitere Erläuterungen siehe Text).

Die exakte Verschaltung der thermoregulatorischen Signale aus der präoptischen Region zum entsprechenden Effektororgan kann nach momentanem Wissensstand nur lückenhaft wiedergegeben werden (Abb. 3). Am Ende der Neuronenketten stehen entweder Neurone des autonomen Nervensystems wie z.B. für die Innervation der Speicheldrüsen, des braunen Fettgewebes und der kutanen Zirkulation oder aber α-Motoneurone für die Innervation der Skelettmuskulatur. Prinzipiell können die Regelleistungen der thermoregulatorischen

Effektororgane in zwei Kategorien eingeteilt werden, die Mechanismen der Kälteabwehr bzw. die Mechanismen der Wärmeabwehr (Abb. 4). Im Rahmen der autonomen Thermoregulation werden zur Kälteabwehr Vasokonstriktion der Blutgefäße in der Körperschale, Kältezittern der Skelettmuskulatur und zitterfreie Thermogenese des braunen Fettgewebes als adäquate Antwort, z.B. auf kalte Umgebungstemperaturen aktiviert. Demgegenüber steht die Wärmeabwehr, die z.B. bei heißen Umgebungstemperaturen, durch Aktivierung der Vasodilatation der Blutgefäße in der Körperschale, Schwitzen und bei einigen Tierarten durch verstärkte Speichelsekretion charakterisiert ist. Welche Wärmeabwehrmechanismen Ratten bei extrem hohen Umgebungstemperaturen aktivieren und welche hypothalamischen Kontrollmechanismen dabei wichtig sind, soll im nächsten Kapitel erläutert werden.

2.1.3. Hypothalamische Kontrolle der Körperkerntemperatur bei Hitzestress: Interaktion der Thermoregulation mit der Regulation des Salz- und Wasserhaushaltes

Ratten, die einem extremen Hitzestress bzw. einer Hitzebelastung ausgesetzt werden, aktivieren zunächst nicht-evaporative Wärmeabgabemechanismen und erst bei unzureichender Kühlungsleistung anschließend evaporative Wärmeabgabemechanismen. Der Einsatz evaporativer Kühlung bei dieser Tierart muss als ausgesprochener Notmechanismus angesehen werden. Da Ratten nicht schwitzen können, sind die thermoregulatorischen Effektororgane hierbei nicht die Schweiß-, sondern die Speicheldrüsen [Hainsworth and Stricker 1971]. Der Temperaturschwellenwert, bei dem die evaporative Kühlung aktiviert wird, liegt etwa bei 39,4-40,4°C [Horowitz et al. 1983, 1999, Kanosue et al. 1986]. Der bei Überschreitung des Schwellenwertes aus den Submandibular- und Sublingualdrüsen freigesetzte Speichel wird dann vom Tier auf dem Fell verteilt („grooming“-Verhalten) und die bei der Verdunstung des Speichels entstehende Kälte wird zum Kühlen des Organismus eingesetzt. Es handelt sich somit um eine komplexe Interaktion efferent autonomer und verhaltensrelevanter Regulationsmechanismen. Wie in Abbildung 3 gezeigt, scheinen warmsensitive Neurone der präoptischen Region bei der Initiierung dieser thermoregulatorischen Regelleistung eine wichtige Rolle zu spielen. Die Warmrezeptoren melden einen erhöhten Istwert der lokal gemessenen Temperatur und konsequenterweise werden unter diesen hyperthermen Bedingungen vermehrt Wärmeabwehrmechanismen aktiviert (Abb. 5). Ein weiteres Kennzeichen der Hyperthermie, in Abgrenzung etwa zur Pathophysiologie des Fiebers, stellt der unveränderte Sollwert der Temperaturregulation dar.

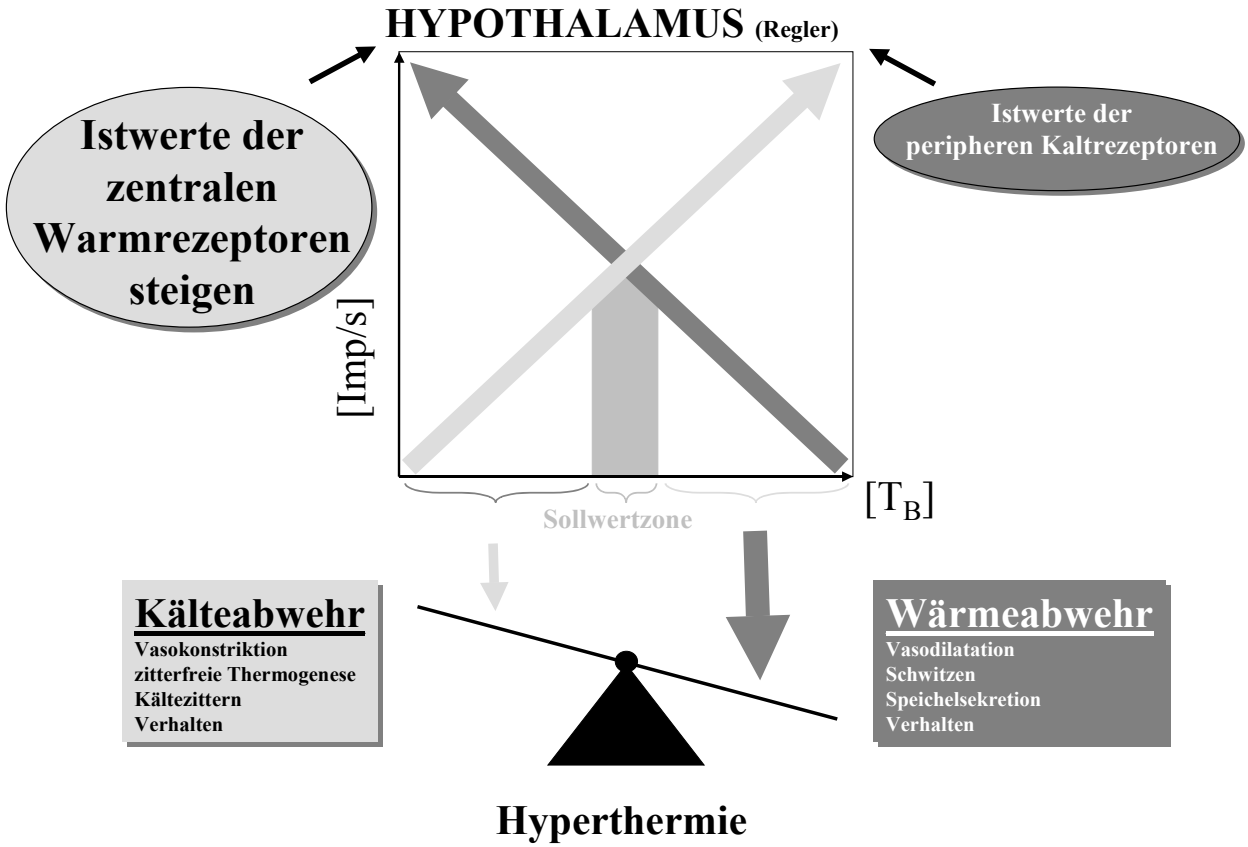

Abbildung 5
Bei Hyperthermie steigen die Istwerte der Körpertemperatur an. Um den geforderten Sollwert einzustellen, werden vermehrt Wärmeabwehrmechanismen aktiviert. [T_B] = Körperkerntemperatur, [Imp/s] = Entladungsrate der Warm- bzw. Kaltrezeptoren (weitere Erläuterungen siehe Text).

Bei länger anhaltendem Hitzestress trägt die vermehrte Abgabe hypotonen Speichels schnell zur thermischen Dehydrierung des tierischen Organismus bei [Hainsworth et al. 1968, Ritter und Epstein 1974, Barney et al. 1991]. Steht in solch einer Situation nicht ausreichend Trink- oder metabolisches Oxidationswasser zur Verfügung, so tritt schnell eine Situation ein, in der Belange des Salz- und Wasserhaushaltes mit thermoregulatorischen Anforderungen abgeglichen werden müssen. Diese integrative Leistung wird im vorderen Hypothalamus koordiniert. Die hypothalamische Kontrolle des Salz- und Wasserhaushaltes ist neuroanatomisch wie auch funktionell physiologisch gut untersucht. Osmoregulatorisch wichtige hypothalamische Strukturen finden sich entlang der Wand, die den dritten Hirnventrikel (V_{III}) nach rostral begrenzt [McKinley et al. 1992, 1996]. Diese als *Lamina terminalis* bezeichnete Hirnstruktur besteht aus 3 Teilkomponenten, dem *Organum vasculosum laminae terminalis* (OVLT), dem Subfornikalorgan (SFO), sowie dem *Nucleus praeopticus medianus* (MnPO). Aufgrund ihrer topographischen Lage werden zwei dieser

Strukturen zu den sogenannten circumventrikulären Organen (CVOs) gezählt, neuroglialen Kerngebieten mit offener bzw. teilweise offener Blut-Hirn-Schranke entlang des Ventrikelsystems des Gehirns (siehe Abb. 7, 13). Bedingt durch das Vorkommen vorwiegend fenestrierter und nicht für das ZNS üblicher dichter Kapillarendothelien können dort im Blut zirkulierende Ionen und Botenstoffe direkt in Wechselwirkung mit Nerven- oder Gliazellen des Gehirns treten. So führt Dehydrierung des Körpers u.a. zum Anstieg des Hormons Angiotensin II (AII) in der Blutbahn, und AII induziert über Wechselwirkung mit dem SFO und OVLT die Wasseraufnahme. Werden Teilkomponenten oder auch die gesamte *Lamina terminalis* in tierexperimentellen Läsionsstudien zerstört, so ist das Trinkverhalten der Tiere entscheidend gestört.

Interessanterweise liegt die *Lamina terminalis* in unmittelbarer Nähe zur präoptischen Region, die für die Thermoregulation von herausragender Bedeutung ist [Nakayama 1985, Boulant 2000, Nagashima et al. 2000]. Wird der ventrale Anteil der *Lamina terminalis* elektrolytisch zerstört, können Ratten ihre Wärmeabgabemechanismen nur noch unzureichend aktivieren. Dies wurde, zumindest teilweise, mit einer verringerten hitzeinduzierten Speichelsekretion erklärt [Whyte and Johnson 2002].

Es könnte daher spekuliert werden, dass sich das neuroanatomische Korrelat der Interaktion von Thermo- und Osmoregulation bei hitzeinduzierter Hyperthermie in diesem Anteil des vorderen Hypothalamus befindet, und dass die hitzeinduzierte Speichelsekretion von dort efferent gesteuert wird (siehe Abb. 3, links). Diese Hypothese sollte mittels funktionell neuroanatomischen Methoden überprüft werden. Neuronale Verbindungen dieser Hirnregionen zur autonomen Innervation der thermoregulatorisch relevanten Speicheldrüsen der Ratte waren in der Literatur nicht beschrieben. Zusammengefasst sollten folgende Fragestellungen untersucht werden:

- Sind neuronale Konnektivitäten der *Lamina terminalis* und der umgebenden präoptischen Region zu den thermoregulatorischen Effektororganen Submandibular- und Sublingualdrüse vorhanden? Wenn ja, welche efferenten, multisynaptischen Nervenbahnen werden zur Kontrolle hitzeinduzierter Speichelsekretion benutzt?
- Welche Rezeptor- bzw. Transmittersysteme sind bei der zentralen Kontrolle hitzeinduzierter Speichelsekretion beteiligt?

2.1.4. Hypothalamische Kontrolle der Thermogenese: Interaktion der Thermoregulation mit der Regulation des Energiehaushaltes

Die Wärmeproduktion des Organismus ändert sich mit dem Energieumsatz. Dieses Prinzip wird bei der Messung des letzteren über die direkte Bestimmung der Wärmeabgabe genutzt (= direkte Kalorimetrie). Eine langfristig ausgeglichene Bilanz von Energiezufuhr und Energieverbrauch ist damit genauso eine Grundvoraussetzung für die Homöostase des Körpers wie die Gleichheit Wärme bildender und Wärme abgebender thermoregulatorischer Mechanismen. Erneut sind es hypothalamische Kontrollmechanismen, welche zur Bildung von Wärme die Anforderungen des Energiehaushaltes mit Belangen der Thermoregulation koordinieren.

Im Rahmen der Homöostase des Energiehaushaltes kommen den Triglyceriden des weißen Speicherfetts – neben der Glukose bzw. dem Speicherglykogen von Leber und Muskel – eine besondere Bedeutung zu. Lipolyse mit nachfolgender mitochondrialer ß-Oxidation der Fettsäuren und Lipogenese unterliegen einer komplexen multihormonalen Kontrolle. Die Menge an langfristig eingelagertem Speicherfett wird so u.a. von einem im Blut zirkulierenden Zytokin reguliert, das nach seiner Entdeckung Anfang der 90er-Jahre die Bezeichnung Leptin erhalten hat. Leptin wird von Adipozyten des weißen Fettgewebes gebildet und in die Blutbahn sezerniert. Dabei spiegelt die Menge an im Blut zirkulierendem Leptin die Menge der im Organismus vorhandenen Fettmasse wieder, d.h. je mehr Körperfett vorhanden ist, umso höher ist der Leptinspiegel. Im Sinne eines „feedback“ Kontrollmechanismus wirkt zirkulierendes Leptin auf Zielstrukturen im Hypothalamus, die den funktionellen Leptinrezeptor exprimieren. Der Hypothalamus wiederum beantwortet das afferente Leptinsignal über adäquate efferente Mechanismen. Klassische Leptin-induzierte Effekte, die zentralnervös vermittelt sind, sind z.B. die Hemmung der Nahrungsaufnahme und die Steigerung des Energieverbrauchs [Friedman 1998, Elmquist et al. 1999, Simon 1999, Meister 2000].

In manchen Deletionsmutanten oder „knock out“ Tieren kann entweder Leptin nicht hergestellt werden ((ob/ob)-Maus), oder aber der Leptinrezeptor weist Defekte auf ((db/db)-Maus, (fa/fa)-Zucker-Ratte). In solchen Tieren ist die Balance der langfristigen Körperfettregulation gestört und sie werden auf Dauer fettleibig. Interessanterweise ändert sich in solchen Tieren auch die Thermogenese. So zeigen homozygot fette Zucker-Ratten (fa/fa) im Vergleich zu ihren homo- bzw. heterozygot schlanken Geschwistern ((Fa/Fa) bzw. (Fa/fa)) einen niedrigeren Energieumsatz, was sich auch in einer niedrigeren

Körpertemperatur unter Normalbedingungen ausdrückt [Armitage et al. 1984, Maskrey et al. 2001, Ivanov und Romanovsky 2002]. Auch wenn der exakte Mechanismus dafür noch unklar ist [Maskrey et al. 2001], könnte im (fa/fa)-Tier der defekte Leptinrezeptor für das Ausbleiben eines gesteigerten Energieverbrauchs mitverantwortlich sein.

Dieses Beispiel aus der Physiologie soll verdeutlichen, warum die Aufklärung einer potenziellen Wechselwirkung der Regulation von Energiehaushalt und Körpertemperatur auf neuroanatomischer Ebene sinnvoll und notwendig ist. Wie bereits in klassischen Studien unter 2.1.2 gezeigt, kontrolliert der caudale Hypothalamus die Wärmebildung. Exakt dieselbe hypothalamische Region zeigt eine hohe Dichte an funktionell exprimierten Leptinrezeptoren [Mercer et al. 1996, Guan et al. 1997]. Diese Rezeptoren sind dadurch gekennzeichnet, dass sie in der Lage sind, einen Zytokin-spezifischen Signalweg, die sogenannte Jak-STAT-Signalkaskade, zu aktivieren (siehe 4.2.1). Leptin könnte somit Wärmebildungsmechanismen über Kerngebiete des hinteren Hypothalamus steuern.

Zur Untersuchung dieser Hypothese muss zunächst eine Kartierungsmethode etabliert werden, die Leptineffekte funktionell neuroanatomisch aufzeigen kann. In einem zweiten Schritt ist es dann von besonderem Interesse zu ermitteln, ob es sich bei Kerngebieten mit hoher Leptin-Sensitivität tatsächlich um diejenigen Hirnstrukturen handelt, die Wärmebildung induzieren können. Zudem ist interessant, welche anderen Regelleistungen von diesen Leptin-sensitiven Kerngebieten gesteuert werden. Vielfältige hypothalamische Kofaktoren (z.B. Neuropeptid Y, Orexin) samt ihrer Rezeptorsysteme komplementieren das Leptin-System in der Regulation des Energiehaushaltes. Weitgehend unbekannt sind die hypothalamischen Wechselwirkungen zwischen dem Leptin-System und dem Neuropeptid Somatostatin. Diese sollen ebenso neuroanatomisch dargestellt werden. Zusammengefasst sollen folgende Fragestellungen untersucht werden:

- Lässt sich eine funktionell neuroanatomische Kartierungsmethode etablieren, welche in der Lage ist, hypothalamische Zielstrukturen des Zytokins Leptin aufzuzeigen?
- Inwieweit sind Leptin-sensitive Kerngebiete des caudalen Hypothalamus von Bedeutung für die hypothalamische Kontrolle der Wärmebildung?
- Handelt es sich bei Kerngebieten mit hoher Leptin-Sensitivität tatsächlich um diejenigen Kerngebiete, welche die efferente Kontrolle der zitterfreien Thermogenese regulieren?
- Welche Rezeptor- bzw. Transmittersysteme könnten mit dem hypothalamischen Leptin-System interagieren?

2.1.5. Hypothalamische Kontrolle der Körperkerntemperatur bei Fieber

Das aus aktivierten Monozyten und Makrophagen freigesetzte, proinflammatorische Zytokin Interleukin-6 (IL-6) spielt eine zentrale Rolle bei der Kommunikation des aktivierten Immunsystems mit dem Gehirn. IL-6 induziert eine Vielzahl von unspezifischen Krankheitsbegleiterscheinungen, von denen die meisten durch pathophysiologisch modulierte hypothalamische Kontrollmechanismen gesteuert werden [Le May et al. 1990, Chai et al. 1996, Plata-Salaman 1996, Lenczowski et al. 1999, Roth et al. 2004]. Dazu zählen z.B. Appetitlosigkeit, Aktivierung der hypothalamo-hypophysär-adrenalen Achse und besonders eine fieberhaft erhöhte Körperkerntemperatur. Die hypothalamische Regulation der Körpertemperatur wird durch erhöhte IL-6 Konzentrationen im Blut im Sinne einer Pyreseentwicklung beeinflusst. Dabei ist humoral wirkendes IL-6 *per se* eher ein schwaches, endogenes Pyrogen, trägt aber zur Bildung weiterer Fiebermediatoren bei, die teilweise erst IL-6-induziert im Gehirn gebildet werden. Aus einer ganzen Gruppe von Stoffen, die Fieber auslösen, sind nach heutigem Wissensstand Prostaglandine die finalen Fiebermediatoren [Roth et al. 2002, Ross et al. 2003].

Der vordere Hypothalamus zeigt eine ausgeprägte Sensitivität gegenüber Prostaglandinen. So kann bei lokaler Mikroapplikation von Prostaglandin in die präoptische Region, welche über einen hohen Anteil warmsensitiver Neurone verfügt [Ranels und Griffin 2003], Fieber ausgelöst werden [Feldberg und Saxena 1971, Stitt 1973, Williams et al. 1977]. Bei der zentralnervös vermittelten Initiierung von Fieber ist die Prostaglandin-E2 (PGE2)-vermittelte Hemmung warmsensitiver Neurone in der präoptischen Region als einer der entscheidenden Mechanismen anzusehen [Matsuda et al. 1992]. Als Konsequenz der geringeren Entladungsrate hypothalamischer Warmrezeptoren verstärkt sich der Einfluss zentraler und vor allem peripherer Kaltrezeptoren. Die Sollwertzone verschiebt sich folgerichtig in einen Bereich höherer Körperkerntemperatur. Fieber ist also durch das Auftreten einer Sollwertverstellung charakterisiert (Abb. 6). Die thermoregulatorischen Regelleistungen, die daraufhin efferent aktiviert werden, entsprechen den klassischen Kälteabwehrmechanismen periphere Vasokonstriktion und Thermogenese, wodurch ein Anstieg der Körperkern-temperatur bewirkt wird.

Wie beschrieben, trägt IL-6 als humoraler Faktor zur Initiierung und Etablierung von Fieber bei. Bei der dabei erforderlichen Aktivierung von Hirnstrukturen ist die Molekülgröße dieses Zytokins ein Hindernis. Zytokine sind große Proteine mit einem Molekulargewicht von ca. 15-30 kDa, die ausgeprägte hydrophile Eigenschaften zeigen. Im Blut zirkulierende Zytokine

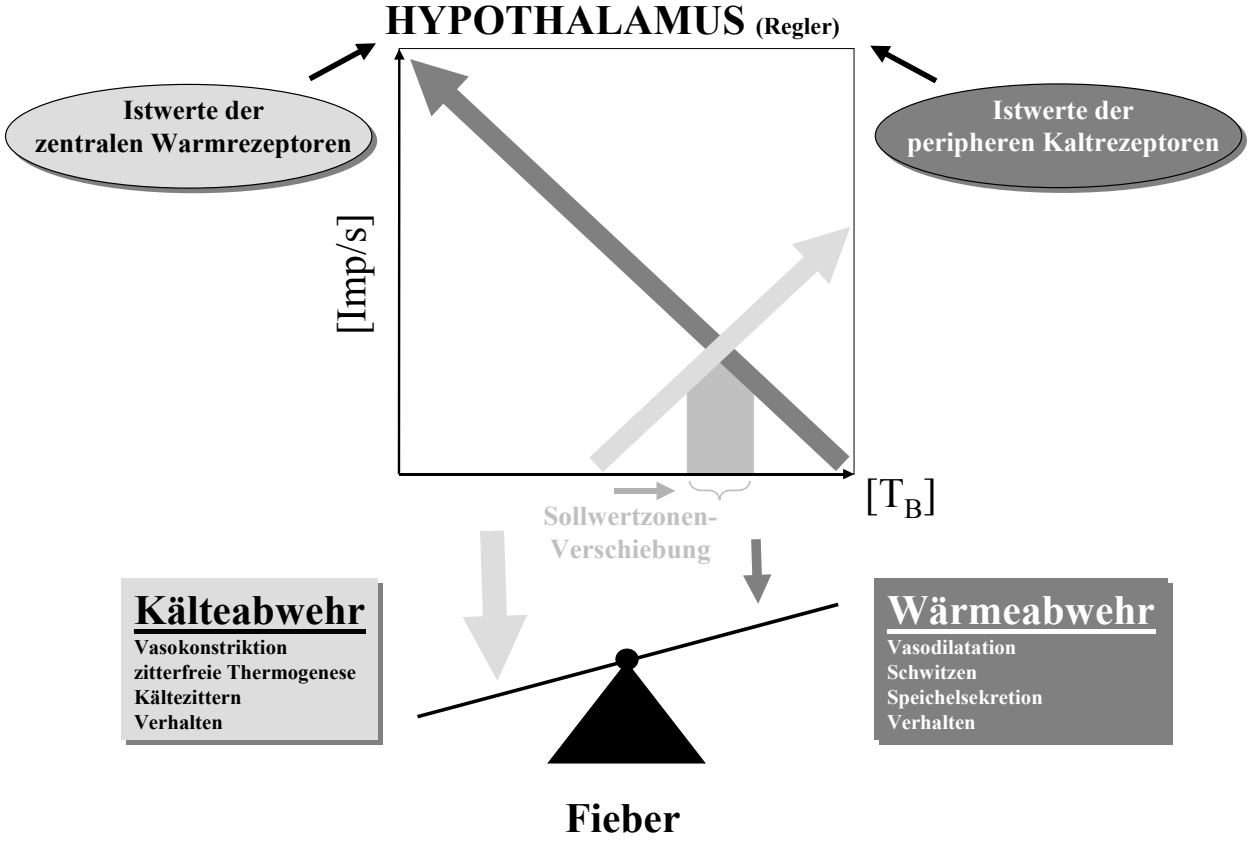

Abbildung 6
Bei Fieber kommt es zu einer Prostaglandin-vermittelten Hemmung der zentralen Warmrezeptoren. Dadurch verstärkt sich der Einfluss der Kaltrezeptoren und es kommt zu einer Verschiebung der Sollwertzone zu höheren Körpertemperaturen. Um den neuen Sollwert einzustellen, werden vermehrt Kälteabwehrmechanismen aktiviert. [T_B] = Körpertemperatur, [Imp/s] = Entladungsrate der Warm- bzw. Kaltrezeptoren.

können folglich die Blut-Hirn-Schranke nicht passieren. Daher braucht IL-6 spezifische Mechanismen, um die Blut-Hirn-Schranke zu umgehen. Hierzu werden mehrere Möglichkeiten diskutiert. Zum einen könnten aktive Transportmechanismen involviert sein. IL-6 könnte über die Adergeflechte der Hirnventrikel (*Plexus choroidei*) aktiv in die Cerebrospinalflüssigkeit transportiert werden. Es könnte auch ein aktiver Transport an Blutgefäßen des Gehirns stattfinden (Kapillartranszytose). Eine weitere Alternative ist die direkte Diffusion aus dem Blut ins Gehirn. Dies geschieht nur an einigen wenigen Hirnstrukturen, die eine offene bzw. teilweise offene Blut-Hirn-Schranke besitzen (Abb. 7).
Den beiden CVOs der *Lamina terminalis* (siehe 2.1.3., Abb. 7, 13), OVLT und SFO, könnte dabei eine wichtige Bedeutung zukommen. Sie liegen in unmittelbarer Nähe der präoptischen Region, sind mit dieser reziprok neuronal verbunden und könnten aufgrund ihrer fehlenden Blut-Hirn-Schranke für im Blut zirkulierendes IL-6 als Eintrittspforte zur wichtigsten pyrogenen Zone des Gehirns fungieren. Zentralnervöse Zielstrukturen für das proinflammato-

Hirngebiete mit offener bzw. teilweise offener Blut-Hirn-Schranke
- Circumventrikuläre Organe (CVOs)

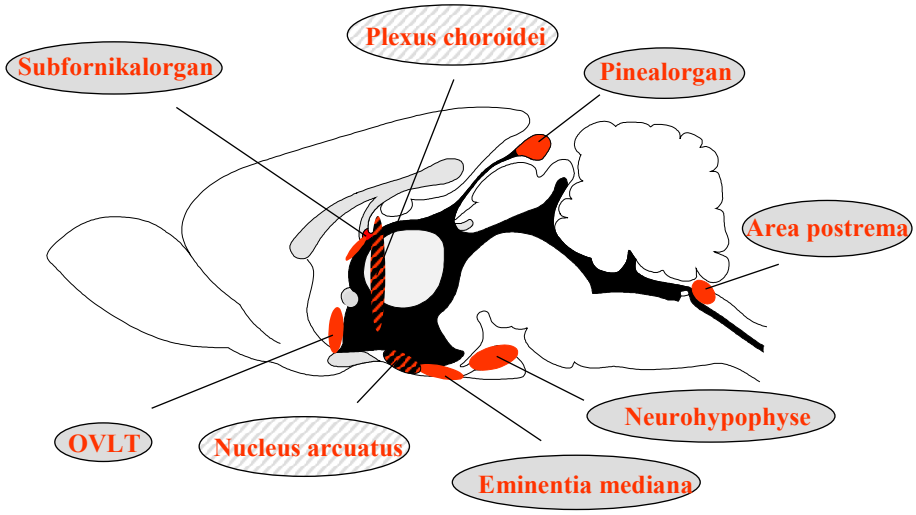

Abbildung 7
Der Sagitalschnitt durch das Gehirn einer Ratte verdeutlicht die Lage der Hirngebiete mit offener bzw. teilweise offener Blut-Hirn-Schranke. Zu diesen Hirnstrukturen zählen die sogenannten circumventrikulären Organe (CVOs), die dunkelgrau eingezeichnet sind. Die CVOs sind entlang des Ventrikelsystems des Gehirns (schwarz hervorgehoben) angeordnet. Die beiden im vorderen Hypothalamus gelegenen CVOs, das *Organum vasculosum laminae terminalis* (OVLT) und das Subfornikalorgan gehören zur *Lamina terminalis*, die den dritten Hirnventrikel nach rostral begrenzt.

rische Zytokin IL-6 sollen daher während des Fieberverlaufes funktionell neuroanatomisch dargestellt werden. Wie bereits für Leptin in 2.1.2. und 4.2.1. beschrieben, soll diese Untersuchung methodisch anhand des Zytokin-spezifischen Signalwegs, der sogenannten Jak-STAT-Signalkaskade erfolgen. Dabei sollen Zielzellen des Gehirns, die möglicherweise durch IL-6 direkt aktiviert werden, mittels der nukleären Translokation des für die IL-6-Signalkaskade spezifischen Transkriptionsfaktors STAT3 nachgewiesen werden.

Wie oben beschrieben, wird die während des Fiebers auftretende Sollwertverstellung durch PGE2-Wirkung auf warmsensitive Neurone der präoptischen Region vermittelt. Mehrere Subtypen der PGE2-spezifischen Rezeptoren könnten dafür verantwortlich zeichnen, wobei insbesondere der Rezeptorsubtyp 3 (EP3R) von Bedeutung zu sein scheint. Dies lassen Studien an transgenen Mäusen vermuten, in denen das Gen für den EP3R künstlich entfernt wurde. In diesen Tieren konnte nach Pyrogenstimulation mit Zytokinen oder bakteriellen Lipopolysaccharid (LPS) experimentell kein Fieber erzeugt werden [Ushikubi et al. 1998]. In der Tat wurde später ein efferenter Signalweg postuliert, der ausgehend von EP3R-

exprimierenden Neuronen der präoptischen Region pyrogene Signale zur Aktivierung der Thermogenese in die Körperperipherie sendet [Nakamura et al. 2002]. In dieser Studie ließen physiologische Messungen der Wärmebildung direkt am brauen Fettgewebe der Ratte auf die Beteiligung der zitterfreien Thermogenese schließen. Es soll nun der neuroanatomische Nachweis erbracht werden, dass neuronale Verbindungen von EP3R-exprimierenden, präoptischen Neuronen zur autonomen Innervation des braunen Fettes wirklich bestehen.

Zusammengefasst sollten folgende Fragestellungen untersucht werden:

- Tragen erhöhte Werte des zirkulierenden, proinflammatorischen Zytokins IL-6, wie sie z.B. nach peripherer Stimulation des Immunsystems mit LPS entstehen, zur Aktivierung fieberrelevanter Strukturen im Hypothalamus bei?
- Kann dies funktionell neuroanatomisch mittels immunhistochemischem Nachweis der nukleären Translokation des IL-6-spezifischen Transkriptionsfaktors STAT3 in Zellen fieberrelevanter Strukturen des Hypothalamus gezeigt werden?
- Welche Zelltypen fieberrelevanter Strukturen des Hypothalamus werden durch IL-6 genomisch aktiviert?
- Welche Bedeutung hat zirkulierendes IL-6 im Vergleich zu Hirn-intrinsisch gebildetem IL-6 bei der Fieberentstehung und der genomischen Aktivierung fieberrelevanter ZNS-Strukturen?
- Welche pyrogenen Signalwege ziehen vom Hypothalamus zur Körperperipherie und wie wird durch sie die zitterfreie Thermogenese des braunen Fettgewebes kontrolliert?

3. Methoden

Der Methodenteil soll einen kurzen Einblick in die wichtigsten Techniken geben, die in den der vorliegenden Arbeit zugrunde liegenden Versuchsansätzen angewandt wurden. Eine detaillierte methodische Beschreibung der physiologischen und neuroanatomischen Studien ist den jeweiligen relevanten Originalpublikationen zu entnehmen (siehe 5. Anlagen). Alle Tierversuche waren von den örtlichen Ethikkomitees und den zuständigen Behörden genehmigt.

3.1. Physiologie

3.1.1. Messung der Körperkerntemperatur

Die Körperkerntemperatur ist für die meisten Untersuchungen mittels Radiotelemetrie (Übermittlung von Funksignalen eines Miniatursenders aus dem Körperinneren) bestimmt worden. In Abbildung 8 ist der Versuchsaufbau gezeigt.

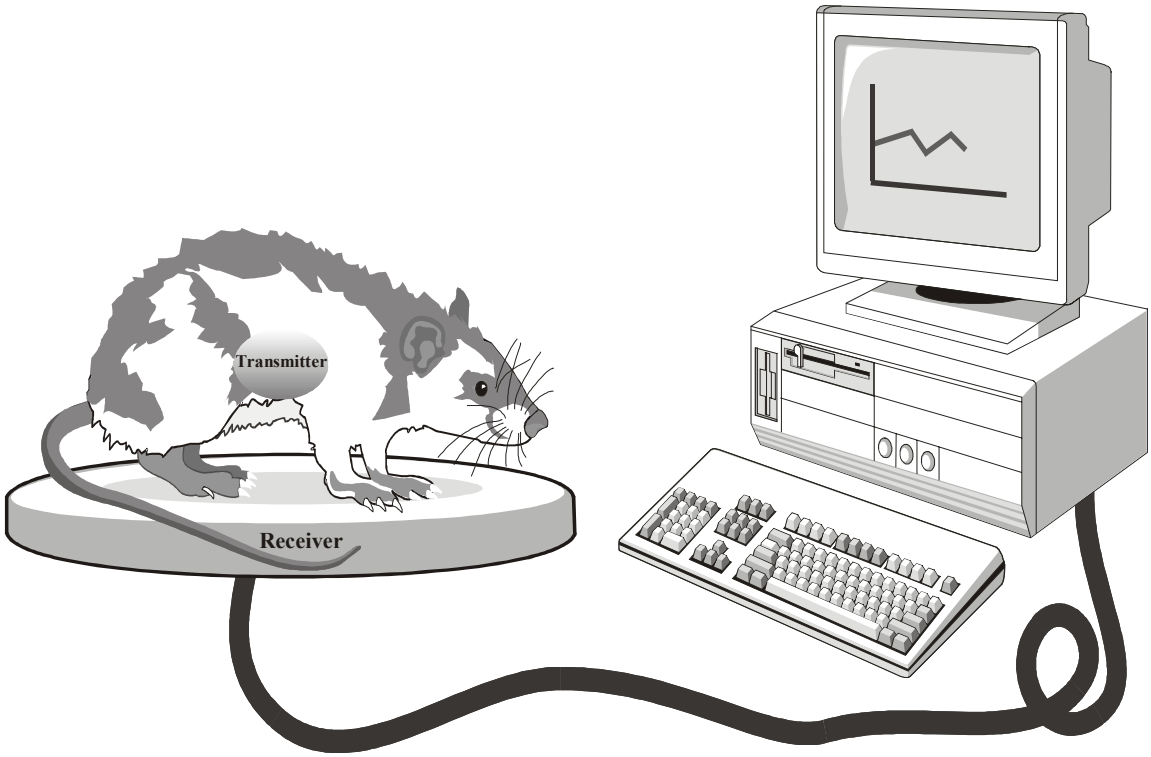

Abbildung 8
Schematische Übersicht der einzelnen Komponenten des telemetrischen Systems. Es ist zu beachten, dass sich das Tier in einem Standard-Typ-III-Käfig zu jeder Zeit frei bewegen kann und sich somit in seiner gewohnten Umgebung unter stressfreien Bedingungen aufhält.

Die notwendigen Einzelkomponenten bestehen aus einem wärmeempfindlichen, batteriebetriebenen Transistor/Thermistor (Transmitter), einem Radioempfänger (Receiver-Platte) und geeigneter Hard- bzw. Software zur kontinuierlichen Datenerfassung. Die Temperaturmessungen erfolgen mit einer Sensitivität von ±0,1°C. Proportional zur Temperaturänderung ändern sich die Radiofrequenzen der vom Transmitter abgegebenen Signale. Der Transmitter wird im Versuchstier intraperitoneal platziert.

3.1.2. Zytokin-Analytik

Zur Quantifizierung von Zytokinen im Blutplasma IL-6- und LPS-behandelter bzw. unbehandelter Tiere werden zwei Bioassays benutzt, die durch Herrn PD Dr. Roth am Institut für Veterinär-Physiologie etabliert sind. Besonderes Augenmerk ist auf die beiden proinflammatorischen Zytokine IL-6 und TNFα gerichtet. Biologisch aktives IL-6 wird in Plasmaproben mittels seiner hochspezifischen, wachstumsfördernden Eigenschaften auf Zellen der Hybridoma Zelllinie B 9 quantitativ bestimmt. Das IL-6-induzierte Wachstum wird durch Zugabe des Farbstoffes MTT (3-4,5-dimethylthiazol-2-yl-2-5-diphenyl-tetrazolium-bromid) bestimmt. Bei Inkubation lebender B9-Zellen mit MTT kommt es zur Bildung dunkelblauer MTT-Formazan-Kristalle, die anschließend mit einem ELISA-Reader bei einer Wellenlänge von 550 nm ausgewertet werden.
Biologisch aktives TNFα wurde mit Hilfe der zytotoxischen Effekte bestimmt, die TNFα in Zellen der Maus Fibrosarkoma Zelllinie WEHI Subklon 13 induziert. Zellen dieser Zelllinie zeichnen sich durch eine hohe Sensitivität gegenüber TNFα aus und sterben schon bei geringsten Mengen (pg/ml) des Zytokins im Zellmedium ab. Die quantitative Auswertung erfolgt wie bei IL-6 mit Hilfe der MTT-Reaktion und eines ELISA-Readers.

3.2. Funktionelle Neuroanatomie

3.2.1. Virales transneuronales Tracing mit Pseudorabiesviren

Eine neuroanatomische Darstellung von funktionell hintereinander geschalteten Nervenzellen als Projektionsbahnen zu thermo- bzw. osmoregulatorischen Effektororganen in der Körperperipherie wurde erst in jüngster Zeit durch die Entwicklung des viralen transneuronalen Tracings möglich. Diese Methode wurde von mir zunächst in Melbourne, Australien angewandt [Hübschle et al. 1998, 2001a] und später in Zusammenarbeit mit dem

Institut für Virologie (Prof. Thiel) an der Justus-Liebig-Universität Giessen etabliert [Yoshida et al. 2003]. Die Anwendung des transneuronalen Tracings erlaubt es, Nervenzellen im ZNS zu identifizieren, die spezifisch mit der vegetativen Innervation der thermo- bzw. osmoregulatorischen Effektororgane verknüpft sind.

Pseudorabiesviren (Familie der Herpesviren) sind tier-, aber nicht humanpathogen. Primaten und der Mensch weisen eine hohe natürliche Resistenz selbst gegen hoch virulente Wildstämme der Pseudorabiesviren auf. Der natürliche Wirt ist das Schwein, und Pseudorabies-Wildstämme verursachen in dieser Spezies die Aujeszky`sche Krankheit. PRV-Bartha zeigt eine zu den Wildstämmen vergleichsweise deutlich abgeschwächte Virulenz und wird daher als attenuierte Lebendvakzine zur Bekämpfung der Aujeszky-Krankheit eingesetzt [Lomniczi 1988, Mettenleiter 1994].

Das Prinzip des viralen transneuronalen Tracings als *in vivo* Markierungsmethode multisynaptischer, efferenter Nervenbahnen soll nachfolgend kurz erläutert werden [Aston-Jones und Card 2000, Card et al. 1990]. Nach Injektion neurotroper Pseudorabiesviren des attenuierten Impfstammes Bartha (PRV-Bartha) in ein peripheres Körperorgan werden die Viren spezifisch von Nervenfaserendigungen aufgenommen, die das entsprechende Organ efferent innervieren. Nach zellulär retrogradem Transport zum Zellkörper der zugehörigen Nervenzelle wird das Virus-Genom vervielfältigt (Abb. 9).

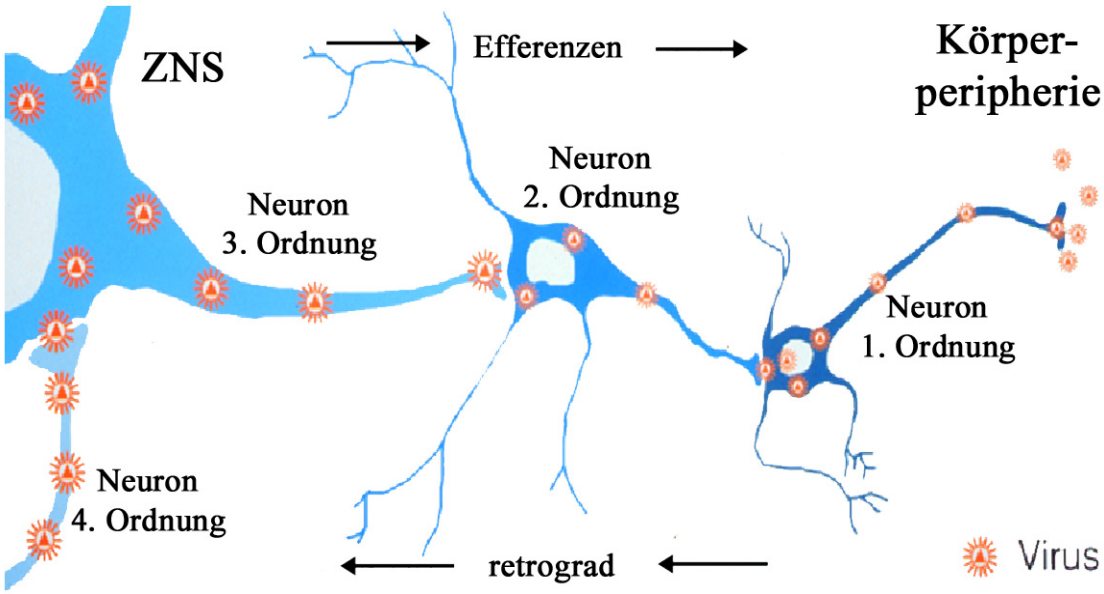

Abbildung 9
Prinzip der viralen transneuronalen Tracing-Methode (Erläuterungen siehe Text).

Die DNA bzw. mRNA spezifischer Virusproteine werden abgelesen und neue, infektiöse Viruspartikel, sogenannte Virione, werden in der infizierten Nervenzelle erster Ordnung gebildet. Es folgt die exozytotische Freisetzung von Viruspartikeln in den synaptischen Spalt.

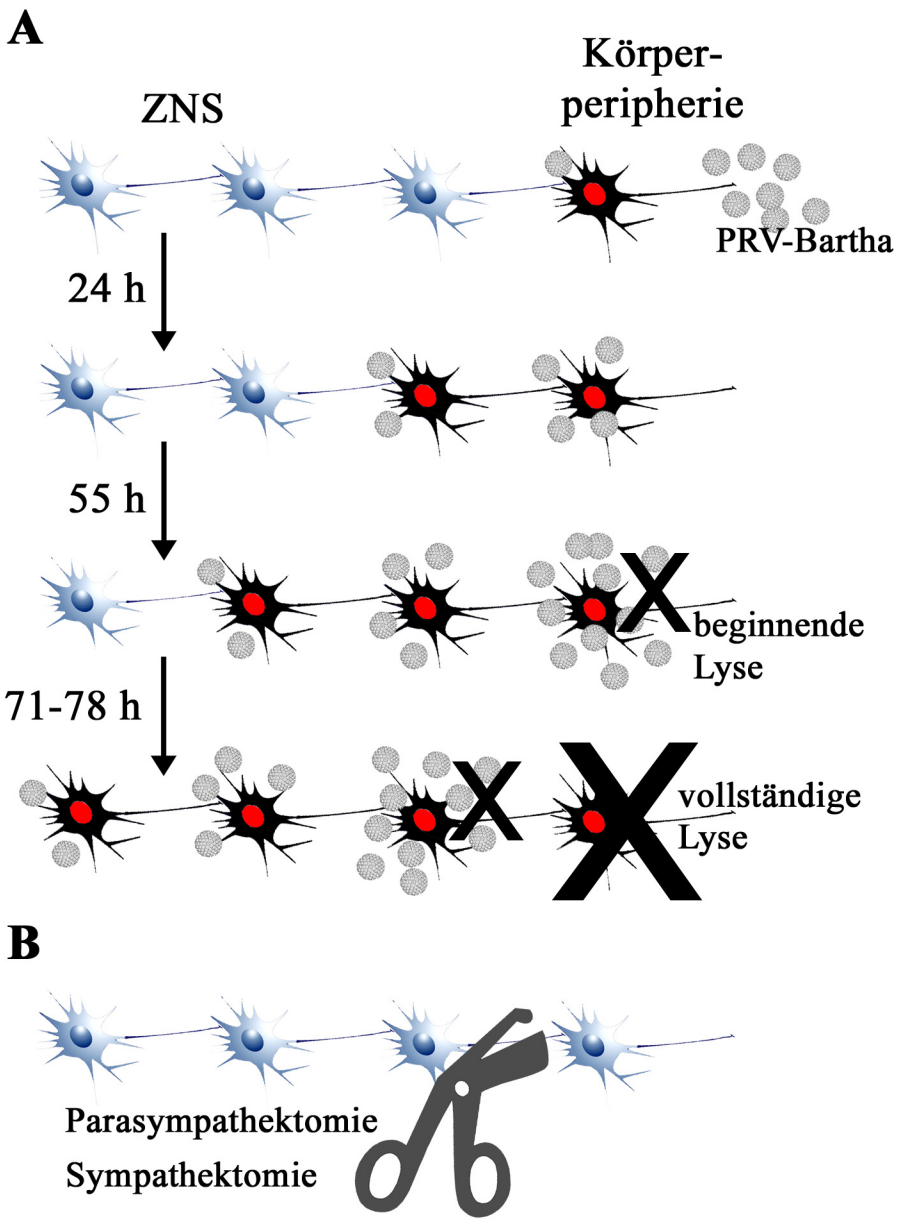

Abbildung 10
(A) Zeitabhängigkeit und Nachteile der viralen Tracing-Methode
(B) Kombination des viralen transneuronalen Tracings mit Denervationsstudien (Erläuterungen insbesondere zu Nachteilen der viralen Tracing-Methode im Text).

Der nächste Schritt ist die transneuronale, transsynaptische Infektion der vorgeschalteten Nervenzelle zweiter Ordnung. Nun beginnt der zuvor beschriebene Prozess von neuem, und so kann letztendlich eine ganze Kette von hintereinander geschalteten Nervenzellen vom ZNS zur Körperperipherie nachgewiesen werden. Der eigentliche neuroanatomische Nachweis der

Viruspartikel im Gehirnschnitt erfolgt immunhistochemisch, d.h. mittels spezifischer Antikörper gegen virale Glykoproteine.

Wie in Abbildung 10 gezeigt, ist das transneuronale „Wandern“ der Viruspartikel ein zeitabhängiger Prozess. So ist es möglich, durch Analyse der Gehirnschnitte zu unterschiedlichen Zeitpunkten die Hierarchie und damit die Abfolge der hintereinander geschalteten Nervenzellen von der Körperperipherie zum ZNS (vgl. Abb. 9, Neurone 1. bis 4. Ordnung) zu ermitteln. Ein entscheidender Nachteil dabei ist jedoch die Virus-induzierte Lyse der Wirtszelle, die nach etwa 2 Tagen in den zuerst infizierten Nervenzellen zu verzeichnen ist. Mit Beginn der Zelllyse werden Viruspartikel nicht nur in Bereichen von Synapsen, sondern überall an der Zelloberfläche der infizierten Nervenzelle in den Extrazellulärraum abgegeben. Der Transport der Viruspartikel erfolgt jetzt nicht mehr transsynaptisch und damit auch nicht mehr in spezifisch hintereinandergeschalteten Neuronenketten. Geht man allerdings zum Zeitpunkt solch einer beginnenden Lyse der Neurone 1. Ordnung zu hierarchisch höheren ZNS-Regionen, so stellt man fest, dass bereits Neurone 2. und 3. Ordnung infiziert wurden und dies noch zu einem Zeitpunkt, an der keine Zelllyse in der Peripherie auftrat.

Trotz des Nachteils der Virus-induzierten Lyse der Wirtszelle hat man also ein Zeitfenster zur Verfügung, in welchem spezifische Untersuchungen zur efferenten Kontrolle peripherer Organe durchgeführt werden können. Der Experimentator wird versuchen, den Zeitpunkt mit substantieller, jedoch früher Infektion eines bestimmten Hirngebietes zu ermitteln, und dazu sind unterschiedliche Tracing-Zeiten nach peripherer Inokulation unabdingbare Voraussetzung.

Die virale Tracing-Methode kann mit chirurgischen Denervationsstudien kombiniert werden (Abb. 10B), um spezifisch die sympathische bzw. parasympathische Innervation eines Organs X darstellen zu können. Unterbricht man die Neuronenkette der efferenten Innervation etwa durch (Para-)Sympathektomie, so sollten virale Infektionen hierarchisch übergeordneter Gehirnstrukturen bzw. der Nachweis viralen Proteins in diesen negativ ausfallen. Dies kann bei totaler Denervation beider Äste des vegetativen Nervensystems am Beispiel der Submandibulardrüse der Ratte nachgewiesen werden [Hübschle et al. 2001a]. Zudem ist es möglich, durch die Kombination von viralem Tracing mit (Para-)Sympathektomie nachzuweisen, ob zu untersuchende Hirnregionen spezifisch sympathisch oder parasympathisch innerviert sind. Dies ist vor allem bei Organen mit gemischter Innervation von großem Interesse.

3.2.2. Immunhistochemischer Nachweis der nukleären Translokation der Transkriptionsfaktoren Fos und STAT3

Bereits 1988 beschrieb Sagar et al. eine „metabolische Kartierungsmethode“, die es erlaubt, Effekte auf das Gehirn funktionell und auf zellulärer Ebene zu lokalisieren. Auf einen externen Stimuli hin kommt es zu veränderten Aktivitätszuständen neuronaler Strukturen. Diese Veränderung kann durch den Nachweis des Proteinproduktes eines sogenannten „immediate-early genes“ wie z.B. c-fos erfasst werden. Das Gen c-fos gehört zur Familie der Protoonkogene. Das Protein Fos fungiert als Transkriptionsfaktor, indem es in heteromerer Form an spezifischen Promotorregionen (AP1-Bindungsdomäne) nachgeschalteter Gene bin-

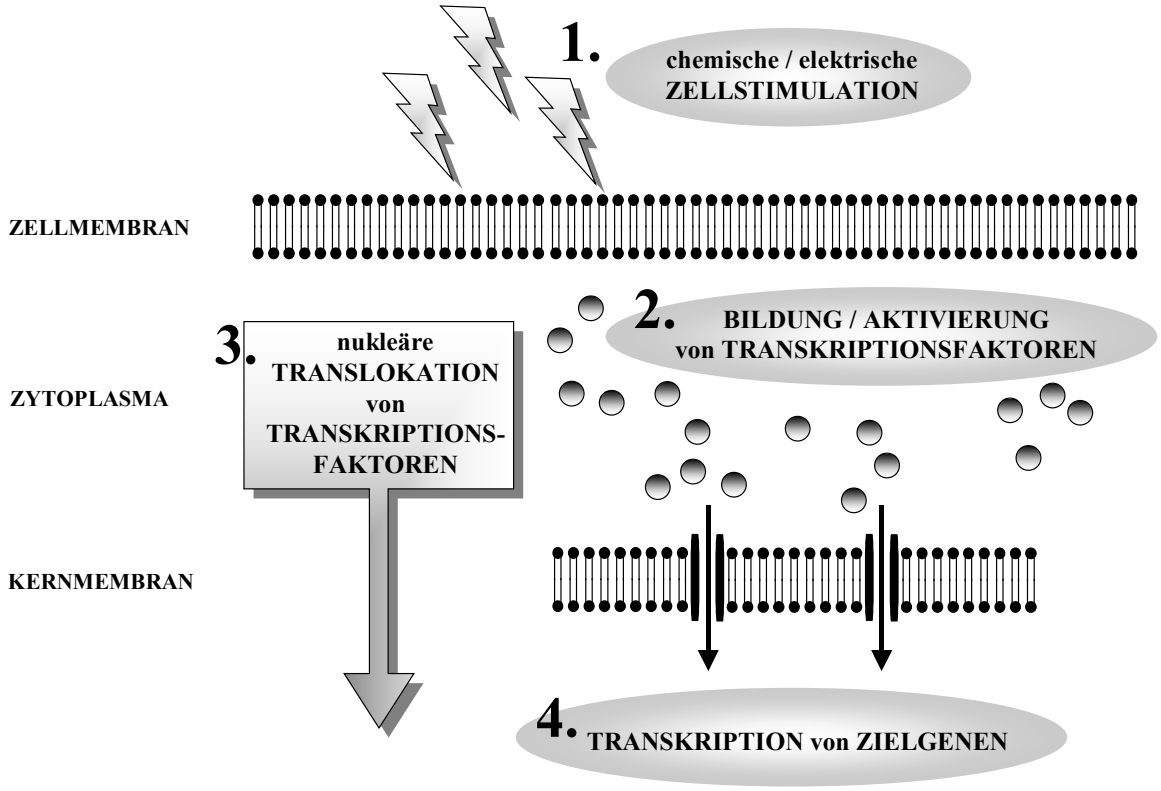

Abbildung 11
Prinzip der durch *in vivo* Zellstimulation induzierten nukleären Translokation von Transkriptionsfaktoren als funktionelle, neuroanatomische Untersuchungsmethode.
Dieses Schema zeigt in stark vereinfachter Form den methodischen Ansatz, der in 7 von 10 für diese Habilitationsschrift relevanten Originalpublikationen angewandt wurde. Chemische und/oder elektrische Stimulation von Zellen des ZNS (1.) induziert die Bildung/Aktivierung (2.) und anschließende nukleäre Translokation (3.) der Transkriptionsfaktoren Fos oder STAT3. Die Transkriptionsfaktoren binden an Promotor-Regionen und modulieren damit die Transkription von Zielgenen (4.).

det („late genes“) und dadurch deren Transkription induziert bzw. reprimiert. Somit kann der Transkriptionsfaktor Fos durch Regulation der Genexpression externe Stimuli in Langzeitreaktionen umwandeln.

Die vorliegende Arbeit ist primär nicht an der Beschreibung von potenziellen Zielgenen interessiert. Von viel größerem Interesse ist die topographische Charakterisierung entsprechender Hirnstrukturen und der Phänotyp einzelner Zellen, die nach externer Stimulation eine Genregulation vermuten lassen. Solch eine Analyse der Orte der sogenannten Stimulus-Transkriptions-Kopplung kann über den immunhistochemischen Nachweis von Transkriptionsfaktoren durchgeführt werden. Abbildung 11 zeigt das Prinzip der durch Zellstimulation *in vivo* induzierten nukleären Translokation von Transkriptionsfaktoren als funktionelle, neuroanatomische Untersuchungsmethode. Es soll darauf hingewiesen werden, dass dieses Schema stark vereinfacht und generalisiert ist. Nicht die Beschreibung der Zielgene (Punkt 4 in Abb. 11), sondern vielmehr der immunhistochemische Nachweis der nukleären Translokation der Transkriptionsfaktoren (Punkt 3 in Abb. 11) ist das primäre Ziel der vorliegenden Untersuchungen.

Der immunhistochemische Nachweis des Fos-Proteins wird inzwischen als Standardmethode angewendet, um nach einem distinkten Stimulus aktivierte Nervenzellen im ZNS zu identifizieren. Diese Methode wurde in Gerstberger et al. [2001] und Hübschle et al. [2001a, 2001b] angewandt.

Erst in jüngster Zeit wurde der immunhistochemische Nachweis der nukleären Translokation des Transkriptionsfaktors STAT3 zur funktionellen Kartierung Zytokin-aktivierter Zellen des ZNS etabliert. Unsere Arbeitsgruppe (AG Gerstberger, Veterinär-Physiologie in Giessen) hat hierzu entscheidende Beiträge geliefert. So wurde von uns zum ersten Mal eine Kartierung hypothalamischer Zielstrukturen von zentral bzw. systemisch verabreichtem Leptin und Interleukin-6 gezeigt [Hübschle et al. 2001b, 2001c, Harré et al. 2002, 2003).

4. Ergebnisse und Diskussion

4.1. Hypothalamische Kontrolle des thermo- und osmoregulatorischen Effektororgans Submandibulardrüse der Ratte bei Hitzestress

4.1.1. Efferente Regulation der Speichelsekretion (Ergebnisse der Anlage 5.1.)

In einer klinischen Fallstudie beschreibt Penfield [1929] am Menschen das erste Beispiel einer dienzephalischen, autonomen Epilepsie, welche durch einen Hirntumor in der Nähe der anterodorsalen Wand des dritten Ventrikels ausgelöst wurde. Die auftretende epileptische Aktivität ist von mehreren autonom-nervösen Phänomenen, unter anderen auch von massivem Speichelfluß, begleitet. Neuere Läsionsstudien in der Ratte bestätigen die Beteiligung dieser im vorderen Hypothalamus gelegenen Hirnregion - der *Lamina terminalis* - an der efferenten Kontrolle der Speichelsekretion [Renzi et al. 1990, Whyte und Johnson 2002].

Zur Identifikation zentralnervöser Hirnzentren, die an der efferenten Regulation der Submandibulardrüse der Ratte beteiligt sind, ist die Methode des viralen transneuronalen Tracings erstmals 1992 eingesetzt worden [Jansen et al.]. Die Studie beschreibt eine Vielzahl von ZNS Regionen, die polysynaptisch mit der autonomen Innervation dieser Speicheldrüse verbunden sind. Jedoch sind in dieser Arbeit keine neuronalen Verbindungen der *Lamina terminalis* oder der angrenzenden präoptischen Region mit der Submandibulardrüse aufgezeigt. Dies ist insofern verwunderlich, als die Submandibulardrüse der Ratte unter Hitzestress ein wichtiges, thermoregulatorisches Effektororgan zur evaporativen Hitzeabgabe darstellt und gerade die präoptische Region eine entscheidende Rolle bei der Regulation der Körpertemperatur spielt [Kanosue et al. 1990] (siehe auch 2.1.3.). Diese Diskrepanz zwischen den beschriebenen (patho-)physiologischen Funktionen und den nicht nachgewiesenen neuroanatomischen Konnektivitäten ansonsten dafür wichtiger hypothalamischer Hirnstrukturen soll unter erneutem Einsatz der viralen transneuronalen Tracing-Methode analysiert werden.

In der Tat stellt sich heraus, dass PRV-infizierte Neurone in allen Teilkomponenten der *Lamina terminalis* und der umgebenden präoptischen Region zu finden sind. Dies ist in der ersten PRV-Studie über die zentralnervöse Innervation der Submandibulardrüse der Ratte übersehen worden [Jansen et al. 1992], obwohl die identifizierte PRV-Infektion in anderen Hirngebieten ansonsten nahezu identisch zu der hier vorliegenden Studie ist. Damit ist zu

vermuten, dass nun zum erstem Mal das neuroanatomische Korrelat für die efferente Regulation der Speicheldrüse unter Hitzestress beschrieben wurde.

Die Ergebnisse der Anlage 5.1. lassen sich folgendermaßen zusammenfassen und diskutieren:

- An der zentralen Regulation der Speicheldrüsensekretion sind eine Vielzahl von ZNS-Strukturen beteiligt. Eine bemerkenswerte Häufung von Kerngebieten, die efferent mit der Innervation der Submandibulardrüse verbunden sind, ist im Hypothalamus zu finden. Hypothalamische Neurone sind als Kontrollneurone dritter, vierter und fünfter Ordnung für die Aktivität der Submandibulardrüse einzustufen.
- Zu den hypothalamischen Kerngebieten zählen auch die *Lamina terminalis* und die sie umgebende präoptische Region. Es ist anzunehmen, dass diesen Hirnzentren eine wichtige Bedeutung bei der thermoregulatorischen Kontrolle der Speichelsekretion unter Hitzestress zukommt.
- Für die meisten Hirnstrukturen kann eine ipsilaterale Dominanz bei der zentralnervösen Kontrolle der Submandibulardrüse aufgezeigt werden. Eine Ausnahme bilden kortikale Strukturen.

4.1.2. Zentrale Blockade des AT1-Rezeptorsubtyps hemmt Wärmeabgabemechanismen unabhängig von der Speichelsekretion (Ergebnisse der Anlage 5.2.)

Ratten, die einer heißen Umgebungstemperatur ausgesetzt werden, aktivieren im wesentlichen zwei Mechanismen der physiologischen Wärmeabgabe (Abb. 12).

(1) Evaporative Wärmeabgabe durch Verdunstungskälte, die z.B. beim Auftragen von Speichel der Submandibulardrüse auf die Körperoberfläche entsteht [Hainsworth und Stricker 1971].

(2) Nicht-evaporative, konvektive Wärmeabgabe z.B. durch Umverteilung von warmem Blut aus dem Körperkern hin zur Körperoberfläche.

In beiden Fällen handelt es sich um autonom ablaufende Prozesse, die vom ZNS gesteuert werden. Wenn nun unter Hitzestress kein Wasser zur Verfügung steht, tritt einerseits schnell ein Konflikt zwischen osmoregulatorischem Bedarf an freiem Wasser zur Aufrechterhaltung basaler Zellfunktionen und andererseits der Notwendigkeit der Wasserabgabe zur evaporativen Wärmeabgabe ein (Abb. 12). Speichelproduktion der Ratte unter Hitzestress hat folglich erheblichen Einfluss auf den Wasserhaushalt und trägt zur Dehydrierung und Erzeugung eines Durstgefühls bei [Hainsworth et al. 1968, Ritter und Epstein 1974]. Unter diesen Bedingun-

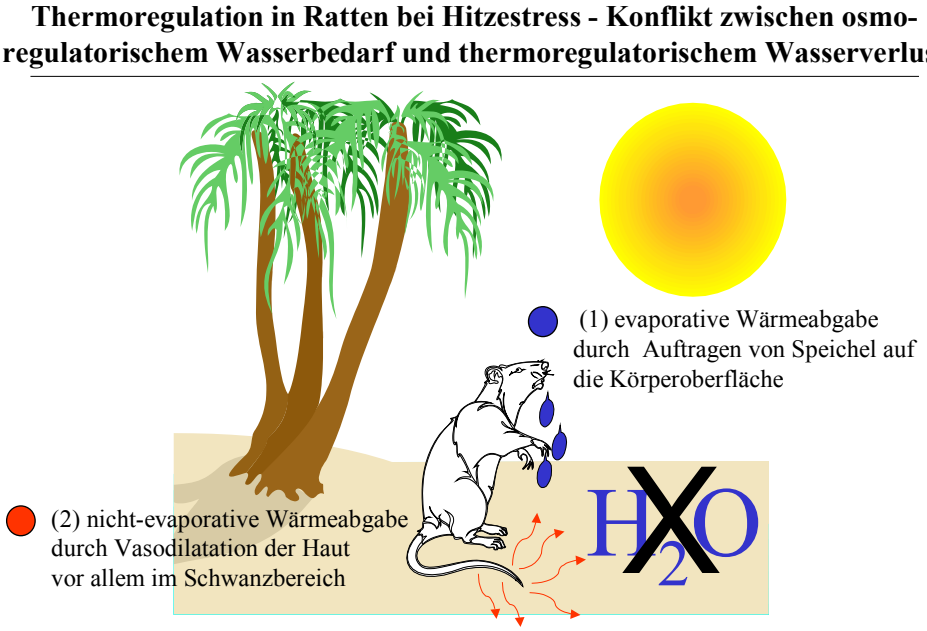

Abbildung 12
Wärmeabgabemechanismen der Ratte bei experimentell induziertem Hitzestress (Erläuterungen siehe Text).

gen muss also eine Regulation erfolgen, die sowohl thermo- als auch osmoregulatorischen Ansprüchen genügt.

Die *Lamina terminalis* des vorderen Hypothalamus repräsentiert eine wichtige Hirnregion für die zentralnervöse Regulation des Wasserhaushaltes. So löst z.B. das unter hypovolämischen Bedingungen gebildete Hormon Angiotensin II über Wechselwirkung mit Angiotensin II-Rezeptoren des Subtyps AT1 an den beiden Teilkomponenten der *Lamina terminalis* mit offener Blut-Hirn-Schranke, dem OVLT und SFO, Trinkverhalten aus [McKinley et al. 1992, 1996]. Dies lässt vermuten, dass die hypothalamische Integration thermo- und osmoregulatorischer Signale bei hitzeinduzierter evaporativer Wärmeabgabe der Ratte in der *Lamina terminalis* erfolgt. Die ausgeprägte Expression hochaffiner AT1-Rezeptoren entlang der *Lamina terminalis* könnte zudem auf eine Bedeutung zentraler angiotensinerger Mechanismen hinweisen. Dies soll in physiologischen Studien unter zentraler Blockade der AT1-Rezeptoren durch Losartan ermittelt werden.

Losartan-behandelte Ratten zeigen im Vergleich zur Kontrollgruppe einen erhöhten hitzeinduzierten (1 Stunde Aufenthalt in einer Umgebungstemperatur von 39°C) Anstieg der Körpertemperatur bei signifikant reduzierter Wasseraufnahme. Folglich könnten zentrale angiotensinerge Mechanismen für die niedrigere Körpertemperatur in der Kontrollgruppe verantwortlich sein. Dies wiederum würde bedeuten, dass die Aktivierung zentraler AT1-Rezeptoren Wärmeabgabemechanismen auslösen kann. Um nun zu überprüfen, inwieweit

Speichelbildung und damit evaporative Wärmeabgabemechanismen in diesen Versuchen involviert sein kann, ist unter identischen Versuchsbedingungen die Speichelsekretion Losartan-behandelter Ratten mit Kontrolltieren verglichen worden. Es ist jedoch kein Unterschied bei der hitzeinduzierten Speichelsekretion festgestellt worden. Dies lässt vermuten, dass es nicht evaporative, sondern nicht-evaporative, konvektive Wärmeabgabemechanismen sind, die bei dem gewählten Versuchsansatz zur niedrigeren Körpertemperatur der Kontrolltiere beitragen. In der Tat haben Fregly und Rowland [1996] bereits gezeigt, dass zentrale Gabe von Angiotensin II nicht-evaporative Wärmeabgabe-mechanismen, wie Vasodilatation des Rattenschwanzes, über *Lamina terminalis* abhängige Mechanismen auslöst.

Einschränkend soll allerdings erwähnt werden, dass die *in vivo* Messung der Speichelsekretion über die sogenannte nicht-invasive Speichel-Indikator-Messmethode [Hainsworth und Epstein 1966] mit einigen methodischen Schwierigkeiten verbunden ist. Daher werden zur endgültigen Klärung angiotensinerger Mechanismen bei hitzeinduzierter Speichelsekretion weiterführende Untersuchungen nötig sein.

Die Ergebnisse der Anlage 5.2. lassen sich folgendermaßen zusammenfassen und diskutieren:

- Unter Hitzestress vermitteln zentrale AT1-Rezeptoren Wärmeabgabemechanismen und initiieren Wasseraufnahme.
- Nicht-evaporative Wärmeabgabemechanismen, wie z.B. die Umverteilung von warmem Blut vom Körperkern hin zur Körperperipherie, leisten unter Hitzestress nach zentraler Aktivierung der AT1-Rezeptoren den überwiegenden Anteil der Körperkühlung.
- Die evaporative Wärmeabgabe durch hitzeinduzierte Speichelbildung steht scheinbar nicht unter zentraler angiotensinerger Kontrolle.

4.1.3. Die *Lamina terminalis*, ein hypothalamisches Kontrollzentrum der Speichelsekretion unter Hitzestress (Ergebnisse der Anlage 5.3.)

Die im vorherigen Kapitel unter Hitzestress beschriebenen physiologischen Veränderungen werden, wie bereits erwähnt, zentralnervös kontrolliert und ein mögliches hypothalamisches Kontrollzentrum könnte die *Lamina terminalis* sein. Die Wichtigkeit dieses Hirngebietes für die zentralnervöse Regulation des Wasserhaushaltes ist ausführlich dokumentiert [McKinley et al. 1992, 1996]. Die in den vorherigen Kapiteln beschriebenen Ergebnisse lassen nun zusätzlich vermuten, dass die *Lamina terminalis* auch in der zentralnervösen Kontrolle der

Körpertemperatur unter Hitzestress von Bedeutung ist [Hübschle et al. 1998, Mathai et al. 2000]. In diesem Kapitel wird deshalb die Hypothese einer Beteiligung der *Lamina terminalis* an der hypothalamischen Kontrolle einerseits osmo- und andererseits thermoregulatorischer Funktionen formuliert. Unter Einsatz funktioneller neuroanatomischer Methoden (virales Tracing kombiniert mit Denervationsstudien und Fos-Immunhistochemie) soll insbesondere die Bedeutung dieser Hirnregion an der zentralnervösen Kontrolle hitzeinduzierter Speichelsekretion zur evaporativen Wärmeabgabe erörtert werden. Die dabei beteiligten Innervationswege sollen neuroanatomisch näher charakterisiert werden.

Akuter Hitzestress (2 Stunden Aufenthalt in einer Umgebungstemperatur von 40°C) induziert die nukleäre Translokation des Transkriptionsfaktors Fos (neuronaler Aktivitätsmarker, siehe auch 3.2.2.) in den gleichen Teilstrukturen der *Lamina terminalis*, die mittels viralen Tracings nachgewiesenermaßen Efferenzen zur Innervation der Submandibulardrüse der Ratte besitzen. Die efferenten Informationsbahnen, die von der *Lamina terminalis* ausgehen, scheinen hauptsächlich zur parasympathischen Seite der autonomen Innervation zu ziehen, da Parasympathektomie, nicht aber Sympathektomie virale Infektion in allen Teilkomponenten der *Lamina terminalis* unterbindet. Eine hypothalamische Umschaltstation der efferenten Information scheint dabei der laterale Hypothalamus zu sein. Aus einer Vielzahl von unter Hitzestress aktivierten hypothalamischen und extrahypothalamischen Hirngebieten scheint insbesondere eine dorsale Komponente des OVLT sowie der MnPO stark aktiviert zu sein. Dies steht im Einklang mit Fos-Untersuchungen, welche die differentielle thermisch- und osmotisch-induzierte neuronale Aktivität im ZNS der Ratte charakterisieren [Patronas et al. 1998]. Auch in dieser Studie scheint insbesondere der MnPO bei experimentell induzierten Veränderungen (kurzzeitige Hitzeakklimatisation und milde Dehydrierung) eine wichtige Rolle bei der Interaktion thermo- und osmoregulatorischer Signale auszuüben.

Angesichts der Notwendigkeit, bei hitzeinduzierter Speichelsekretion osmo- und thermoregulatorische Belange gegeneinander abzugleichen, scheint die *Lamina terminalis* etliche Voraussetzungen zur Ausübung dieser Kontrolle zu besitzen. Sie hat über die beiden sensorischen CVOs, OVLT und SFO, direkten Kontakt zu zirkulierenden Botenstoffen und besitzt vielfältige reziproke Konnektivitäten zu hypothalamischen und extrahypothalamischen Hirngebieten, die an der zentralen Kontrolle autonomer Funktionen beteiligt sind. Zudem macht die unmittelbare Nähe zu der für die Thermoregulation so wichtigen präoptischen Region die *Lamina terminalis* zu einem idealen Kandidaten, als „vermittelnde Schaltstelle“ zwischen Thermo- und Osmoregulation wirksam zu sein. Die bereits erwähnten

Läsionsversuche unterstützen diese Hypothese [McKinley et al. 1992, 1996, Whyte und Johnson 2002].

Zusammenfassend lässt sich aus den Ergebnissen der Anlage 5.3. folgende Hypothese ableiten, die in Abbildung 13 zusätzlich schematisch dargestellt ist:

- Die zentrale Kontrolle hitzeinduzierter Speichelsekretion wird durch die integrative Verrechnung thermo- und osmoregulatorischer Signale in der *Lamina terminalis* ausgeübt. Der innerhalb der Blut-Hirn-Schranke gelegene MnPO scheint von den 3 Teilkomponenten die am stärksten interaktiv wirksame zu sein.
- Die efferente Regulation der *Lamina terminalis* scheint vornehmlich die parasympathisch modulierte Speicheldrüsenaktivität zu beeinflussen.
- Die *Lamina terminalis* scheint an der hypothalamischen Kontrolle sowohl osmo- als auch thermoregulatorischer Funktionen beteiligt zu sein.

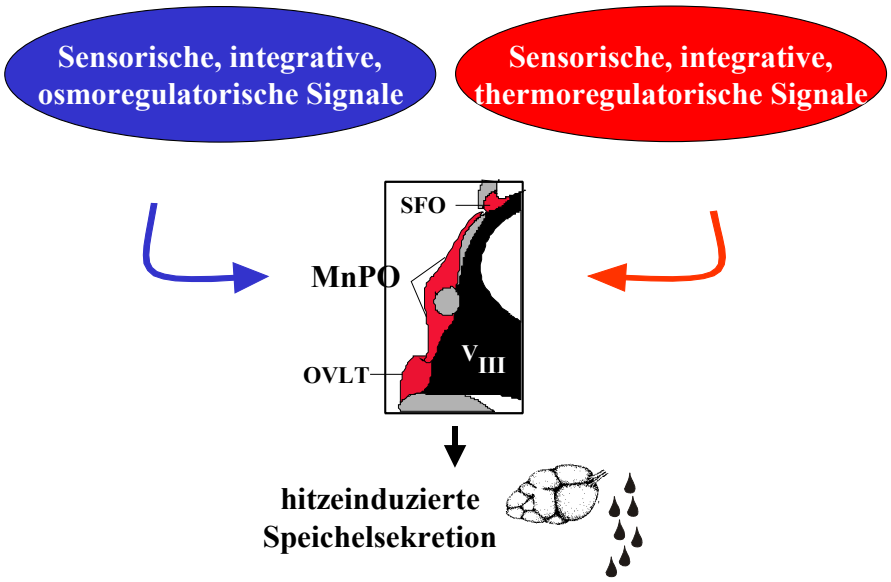

Abbildung 13
Hypothese zur Interaktion thermo- und osmoregulatorischer Signale in der *Lamina terminalis* bei hitzeinduzierter Speichelsekretion. Die *Lamina terminalis* und ihre 3 Teilkomponenten, das *organum vasculosum laminae terminalis* (OVLT), der *Nucleus praeopticus medianus* (MnPO) und das Subfornikalorgan (SFO), sind schematisch als rostrale Begrenzung des dritten Hirnventrikels (V_{III}) gezeigt. (weitere Erläuterungen siehe Text).

4.1.4. Die Interaktion thermo- und osmoregulatorischer Signale im MnPO steht unter Einfluss des Neuromodulators Stickstoffmonoxid (Ergebnisse der Anlage 5.4.)

Die neuroanatomische Grundlage der hypothalamischen Kontrolle des Salz- und Wasserhaushaltes ist in ihren Strukturen bereits sehr gut beschrieben [McKinley et al. 1992, 1996]. Die hypothalamische Zytoarchitektur der Thermoregulation bei Hitzestress ist jedoch nur sehr lückenhaft bekannt, wobei u.a. die in den Vorkapiteln beschriebenen Ergebnisse [Hübschle et al. 1998, 2001a, Mathai et al. 2000] Beiträge zum besseren neuroanatomischen Verständnis, insbesondere der Regulation hitzeinduzierter Speichelsekretion, liefern. Eine wichtige Rolle in der Interaktion thermo- und osmoregulatorischer Signale kommt offenbar den MnPO-intrinsischen Neuronenpopulationen zu, die sowohl von osmotischen als auch von thermischen Stimuli aktiviert werden, wie aufgrund elektrophysiologischer und molekular-neuroanatomischer Studien zu fordern ist [Travis und Johnson 1993, Patronas et al. 1998, Hübschle et al. 2001a]. Enzym- und immunhistochemische Untersuchungen zur hypothalamischen Expression der neuronalen Stickstoffmonoxidsynthase (nNOS) zeigen, dass gerade Strukturen der *Lamina terminalis*, insbesondere der MnPO, eine ausgeprägte konstitutive Expression dieses Enzyms zeigt [Jurzak et al. 1994, Gerstberger et al. 2001, eigene Beobachtung]. Daher kann vermutet werden, dass NO als Neuromodulator bzw. Neurotransmitter bei der Interaktion thermo- und osmoregulatorischer Signale im Bereich des MnPO dient. Osmotisch und thermisch induzierte regulative Aktivitätsänderungen im MnPO sollen durch den enzymhistochemischen Nachweis der NADPH-Diaphoraseaktivität (Marker für nitrerge, nNOS-exprimierende Neurone im ZNS), die Bindung eines radioaktiv markierten L-Arginin-Analogs und durch Fos-Immunhistochemie näher charakterisiert werden.

Der MnPO weist als einzige hypothalamische Hirnstruktur sowohl nach osmotischer (Wasserentzug für 24 Stunden) als auch nach thermischer Belastung (Wärmeexposition für 48 Stunden bei 34°C) eine vergleichbar starke Zunahme Fos-positiver Zellen auf. Zudem zeigen sich additive Effekte bei der Kombination beider Einzelbelastungen. Dies könnte auf eine Koexistenz zweier unterschiedlicher MnPO-Zellpopulationen hinweisen, die funktionell entweder dem osmo- oder dem thermoregulatorischen System zugerechnet werden können. Sowohl osmotische als auch thermische Belastung induzieren eine Zunahme der NADPH-Diaphoraseaktivität und der [^{3}H]-Nitro-Arginin-Bindung exklusiv im MnPO. Die Kombination beider neuroanatomischer Nachweismethoden zeigt, dass Wasserentzug nitrerge MnPO-Neurone aktiviert, während im Gegensatz dazu bei Wärmeexposition keine Aktivierung nitrerger Neurone nachzuweisen ist.

Die experimentelle Nachahmung der hypothalamischen NO-Freisetzung mittels Mikroapplikation von NO freisetzenden Trägersubstanzen (NO-Donoren) in den dritten Hirnventrikel induziert einen Abfall der Körpertemperatur durch gesteigerte evaporative und nicht-evaporative Wärmeabgabemechanismen [Eriksson et al. 1997, Gerstberger 1999]. Unter Hitzebelastung könnte also hypothalamisch gebildetes NO Wärmeabgabemechanismen stimulieren. Auf Grundlage der oben genannten Ergebnisse unter milder Hitzebelastung ist weiterhin anzunehmen, dass die hypothalamische Expression der nNOS unter starkem Hitzestress (1 bis 2 Stunden bei 39-40°C) vergleichsweise noch stärker zunimmt. Somit könnte die lokale Bildung von NO innerhalb der *Lamina terminalis* und insbesondere im MnPO Wärmeabgabemechanismen unter Hitzestress, wie z.B. die Speichelsekretion der Ratte, auslösen [Hainsworth und Stricker 1971, Hübschle et al. 2001a]. Andererseits zeigen direkte Mikroapplikationen von NO-Donoren in den MnPO bei thermoneutraler Umgebungstemperatur, dass die durch Pilokarpin pharmakologisch stimulierte Speichelsekretion der Ratte durch NO gehemmt wird [Saad et al. 2003]. Unter Einfluss der Aktivierung zentraler Warmrezeptoren könnte folglich eine Umkehr in der NO-kontrollierten Regulation der Speicheldrüsensekretion stattfinden. Weiterführende tierphysiologische Untersuchungen sind offensichtlich notwendig, um die Rolle von NO als Neuromodulator in der durch die *Lamina terminalis* vermittelten Senkung der Körpertemperatur unter Hitzestress zu etablieren.

Die Ergebnisse der Anlage 5.4. lassen sich folgendermaßen zusammenfassen und diskutieren:

- Sowohl moderater Wasserentzug als auch moderate Wärmeexposition aktivieren unterschiedliche Subpopulationen MnPO-intrinsischer Neurone. Die Kombination beider Stimuli zeigt additive Effekte.
- Nur die osmotische Belastung induziert eine Aktivierung nitrerger Zellen, während bei thermischer Belastung nitrerge Neurone nicht vermehrt aktiviert werden. Auf Ebene des MnPO könnten somit zwei unterschiedliche Zellpopulationen etabliert sein, die funktionell entweder dem osmo- oder dem thermoregulatorischen System zuzuordnen wären.
- Moderater Wasserentzug sowie moderate Wärmeexposition steigern die Expression der nNOS im MnPO.

4.2. Hypothalamische Kontrolle der Ruhethermogenese und der Fieber begleitenden Thermogenese

4.2.1. Hypothalamische Verteilungsmuster der nukleären STAT3-Translokation nach zentraler Applikation von Leptin bzw. Interleukin-6 (Ergebnisse der Anlage 5.5.)

Wichtige Regelleistungen des Hypothalamus sind unter anderen die zentrale Kontrolle des Energiehaushaltes sowie die Regulation der Körpertemperatur bei Fieber. Zwei Mitglieder der Zytokin-Familie mit vergleichbarer intrazellulärer Signaltransduktion spielen dabei eine wichtige Rolle. Das von Adipozyten gebildete Hormon Leptin sowie das von aktivierten Immunzellen gebildete proinflammatorische Zytokin Interleukin-6 aktivieren nach Bindung an ihren Zielzellen im Hypothalamus die sogenannte Jak-STAT-Signalkaskade (Abb. 14).

Leptin und Interleukin-6 aktivieren die Jak2-STAT3 Signalkaskade

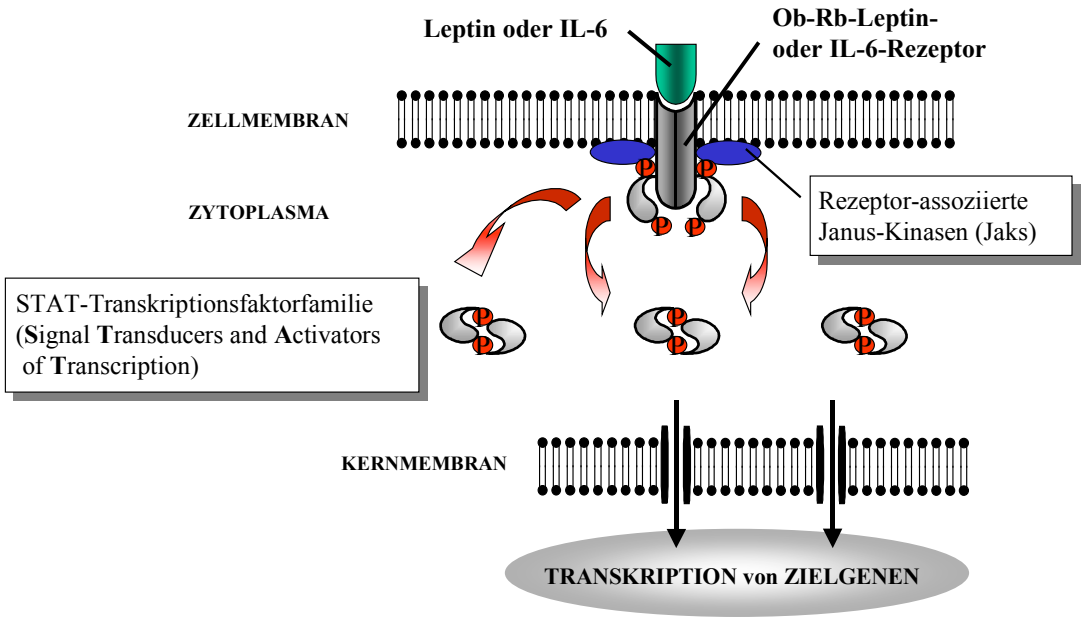

Abbildung 14
Prinzip der Zytokin-induzierten nukleären Translokation des Transkriptionsfaktors STAT3 nach Aktivierung der langen Form des Leptin-Rezeptors (Ob-Rb) oder des Interleukin-6-Rezeptors. Der immunhistochemische Nachweis der nukleären STAT3-Translokation erlaubt es, eine funktionell neuroanatomische Kartierung derjenigen hypothalamischen Strukturen und Zellen vorzunehmen, die spezifisch durch das entsprechende Zytokin genomisch aktiviert werden. Dieser methodische Ansatz wurde zum ersten Mal von unserer Arbeitsgruppe beschrieben [Hübschle et al. 2001b] und in insgesamt 5 von 10 für diese Habilitationsschrift relevanten Originalpublikationen angewandt.

In dieser Signalkaskade ist STAT3 die entscheidende Isoform der STAT-Transkriptionsfaktorfamilie, die für die Regulation der Zielgene des entsprechenden Zytokins verantwortlich ist. Nach Bindung des Zytokins am Rezeptor werden STAT3-Monomere durch rezeptorassoziierte Janus-Kinasen phosphoryliert and damit aktiviert. Zwei derartig aktivierte STAT3-Monomere dimerisieren, und erst dieses STAT3-Dimer ist die eigentlich aktive Form des Transkriptionsfaktors. STAT3-Dimere wandern in den Zellkern, binden an Promotorregionen bestimmter Zielgene und modulieren damit die Zytokin-abhängige Genexpression. Unser Interesse gilt nicht der Beschreibung solcher Zytokin-abhängiger Zielgene, sondern vielmehr dem funktionellen Nachweis der Lokalisation hypothalamischer Kerngebiete, die durch ein bestimmtes Zytokin direkt aktiviert werden. Vor dem Hintergrund dieser Zytokin-abhängigen intrazellulären Signalkaskade soll die Hypothese überprüft werden, ob der immunhistochemische Nachweis der nukleären STAT3-Translokation eine funktionell neuroanatomische Kartierung erlaubt.

Nach zentraler Applikation beider Zytokine in den Lateralventrikel der Ratte kann eine nukleäre STAT3-Translokation in einer Vielzahl (extra-)hypothalamischer Strukturen mit allerdings deutlich unterschiedlichem Verteilungsmuster für das jeweilige Zytokin nachgewiesen werden. So induziert Leptin eine ausgeprägte nukleäre STAT3-Translokation überwiegend in mehreren Kerngebieten des caudobasalen Hypothalamus, die wichtig für die Kontrolle der Nahrungsaufnahme und der Körpergewichtsregulation sind [Friedman 1998, Elmquist et al. 1999, Meister 2000], während IL-6 einen starken Effekt in medialen und vor allem rostralen hypothalamischen Regionen zeigt, die als „pyrogene Zonen“ bekannt sind [Saper 1998, Zhang et al. 2000]. Für die Spezifität der etablierten Methode spricht sowohl die differentielle Aktivierung ganz unterschiedlicher hypothalamischer Strukturen durch beide Zytokine, als auch die extrem gute Übereinstimmung mit der ZNS-Rezeptorexpression für das jeweilige Zytokin [Schöbitz et al. 1993, Vallières und Rivest 1997, Friedman 1998]. Der Nachweis der Lokalisation des Transkriptionsfaktors STAT3 im Kern der Zelle wird in Kolokalisationsstudien mit dem nukleären Marker DAPI geführt. Dabei zeigt sich, dass die nukleäre STAT3-Translokation ein zeitabhängiger Prozess ist, der sein Maximum ca. 15-30 Minuten nach zentraler Zytokinstimulation erreicht. Bereits eine Stunde später können nur noch wenige nukleäre STAT3-Signale detektiert werden.

Unter Einsatz von Mehrfachmarkierungen kann zusätzlich der Phänotyp der Zellen näher charakterisiert werden, die eine nukleäre STAT3-Translokation nach Leptin-Stimulation zeigen. Hierbei kann nachgewiesen werden, dass es sich nur bei einer kleinen Subpopulation der aktivierten hypothalamischen Zellen, die mit der nukleären Translokation des

Transkriptionsfaktors STAT3 reagieren, um Neurone handelte. Leptin-aktivierte Neurone sind insbesondere im lateralen *Nucleus arcuatus* zu finden. Die überwiegende Mehrzahl an STAT3-positiven Zellen zeigt keine Kolokalisation mit dem neuronalen Aktivitätsmarker Fos und mehreren glialen Zellmarkern. Damit ist zu vermuten, dass es sich bei diesen Zellen um Neurone handelt, die nicht aktiviert werden. Inzwischen können weiterführende immunhistochemische Untersuchungen unter Einsatz neuronaler Marker (Neuronspezifischer nukleärer Faktor (NeuN) und eines neuronalen Zilienmarkers) klar zeigen, dass es sich bei einigen dieser Zellen in der Tat um Neurone handelt [Stepanyan et al. 2003, eigene Beobachtung].

Die Ergebnisse der Anlage 5.5. lassen sich folgendermaßen zusammenfassen und diskutieren:

- Leptin und Interleukin-6 induzieren eine zeitabhängige und Zytokin-spezifische nukleäre Translokation des Transkriptionsfaktors STAT3.
- Mehrfachmarkierungen erlauben die Ermittlung des Phänotyps der hypothalamischen Zellen, die einen direkten Zytokineffekt zeigen.
- Leptin-induzierte nukleäre STAT3-Signale sind sowohl in Fos-positiven („aktivierten“) Neuronen als auch in Fos-negativen („nicht-aktivierten“) Neuronen zu finden. Solch eine neuroanatomische STAT3-Kartierung von Zytokineffekten ist deshalb verglichen mit der Fos-Methode deutlich umfassender und spezifischer.
- Die immunhistochemische STAT3-Methode trägt zum besseren Verständnis der Regulation des Energiehaushaltes und Interleukin-6-abhängiger Fieberentstehungs-mechanismen auf Ebene hypothalamischer Kerngebiete bei. Sie stellt quasi das neuroanatomische Korrelat zur zentralnervös kontrollierten Physiologie her.
- STAT3-Immunhistochemie stellt daher, wie auch in den Folgekapiteln gezeigt, eine geeignete Methode zur funktionellen neuroanatomischen Charakterisierung von Zytokineffekten auf das Gehirn dar.

4.2.2. Hypothalamische Leptin-Zielneurone exprimieren unterschiedliche Somatostatin-Rezeptorsubtypen (Ergebnisse der Anlage 5.6.)

Die hypothalamische Regulation des Energiehaushaltes ist ein komplexes, multifaktoriell kontrolliertes System. Leptin scheint dabei auf Ebene des Hypothalamus mit anderen Kofaktoren, wie z.B. dem Neuropeptid Y, Grehlin, Pro-Opiomelanocortin (POMC), Cocain-Amphetamin-verwandten Transkript (CART), Orexinen und dem Agouti-verwandten Peptid

(AgRP) zu interagieren. Die Bedeutung des hypothalamisch produzierten Neuropeptids Somatostatin ist in diesem Zusammenhang nur sehr lückenhaft untersucht. Es kann jedoch neuroanatomisch beim Schaf gezeigt werden, dass insbesondere Somatostatin-produzierende Zellen des caudobasalen Hypothalamus die lange Form des Leptinrezeptors exprimieren [Iqbal et al. 2000]. Ob umgekehrt Leptin-responsive Zellen des Hypothalamus einen der sechs Subtypen der Somatostatin-Rezeptoren (sst1-sst5) exprimieren, war *dato* unbekannt. Daher soll die neuroanatomische Basis einer potenziellen Somatostatin-Leptin-Wechselwirkung intensiver untersucht werden. Dazu soll die hypothalamische Lokalisation von Somatostatin und Somatostatin-Rezeptor-exprimierenden Zellen mit der Lage hypothalamischer Leptin-Zielneurone verglichen werden.

Nur in wenigen Fällen kann eine Kolokalisation des Neuropeptids Somatostatin in Zellen mit nukleärer STAT3-Immunreaktivität als Marker für Leptin-responsive Zellen nachgewiesen werden. Dies ist insofern erstaunlich, als beim Schaf eine signifikante Kolokalisation Somatostatin-produzierender Zellen mit der zur Signaltransduktion befähigten langen Leptinrezeptorform beschrieben ist [Iqbal et al. 2000]. Diese Unterschiede könnten durch unterschiedliche neuroendokrinologische Gegebenheiten bei Nagern und kleinen Wiederkäuern wie dem Schaf erklärt werden. Anders verhält es sich bei der Analyse Somatostatin-Rezeptor-exprimierender Zellen im Vergleich zu Leptin-Zielneuronen. Für die einzelnen Rezeptorsubtypen kann hierbei eine starke, teilweise sehr starke Kolokalisation einzelner Rezeptorsubtypen mit Leptin-Zielzellen ermittelt werden. Beeindruckend ist dies für Neurone des ventromedialen Hypothalamus gezeigt worden, die den Rezeptorsubtyp sst3 spezifisch auf ihren neuronalen Zilien exprimieren. Über mögliche physiologische Funktionen der hypothalamischen Somatostatin-Rezeptoren, insbesondere im Hinblick auf die Interaktion mit dem Leptinsystem, kann beim derzeitigen Wissensstand nur spekuliert werden. Es ist jedoch wahrscheinlich, dass solch eine Interaktion an der neuroendokrinen Kontrolle des Energiehaushaltes und des Wachstums beteiligt ist.

Die Ergebnisse der Anlage 5.6. lassen sich folgendermaßen zusammenfassen und diskutieren:

- Nur eine geringe Zahl Leptin-responsiver Zellen des Hypothalamus ist in der Lage Somatostatin selbst zu produzieren.
- In unterschiedlichen hypothalamischen Kerngebieten exprimieren Leptin-Zielneurone unterschiedliche Subtypen des Somatostatin-Rezeptors.
- Diese neuroanatomischen Daten sprechen für eine Somatostatin-Leptin-Wechselwirkung auf Ebene des Hypothalamus. Über die dadurch kontrollierten Regelleistungen kann momentan nur spekuliert werden.

4.2.3. Die anteroventrale präoptische Region, ein hypothalamisches Kontrollzentrum der Interleukin-6-vermittelten Fieberentstehung (Ergebnisse der Anlage 5.7.)

Die lokal intrahypothalamische bzw. intracerebroventrikuläre Applikation des Zytokins und endogenen Pyrogens IL-6 induziert eine Vielzahl zentralnervös kontrollierter Begleiterscheinungen von Krankheiten, wie z.B. Fieber, Anorexie, Reduktion der motorischen Aktivität und Aktivierung der hypothalamo-hypophysär-adrenalen Achse [LeMay et al. 1990, Chai et al. 19996, Plata-Salaman 1996, Lenczowski et al. 1999]. Die neuroanatomische Analyse IL-6-spezifischer Zielstrukturen des Gehirns ist erstmals mittels Detektion des Transkriptionsfaktors und neuronalen Aktivitätsmarkers Fos durchgeführt worden [Callahan und Piekut 1997, Niimi et al. 1997, Vallières et al. 1997]. In der Liste aktivierter Gehirnstrukturen finden sich auch einige hypothalamische Kerngebiete, insbesondere Teilbereiche der für die Kontrolle der Körpertemperatur so wichtigen präoptischen Region und der *Lamina terminalis*. Vor dem Hintergrund der bereits in Abbildung 14 gezeigten IL-6-abhängigen Signalkaskade soll nun in der Ratte überprüft werden, ob der immunhistochemische Nachweis der IL-6-induzierten nukleären STAT3-Translokation in solchen hypothalamischen Strukturen geführt werden kann, die nachgewiesenermaßen als „pyrogene Zonen“ im Gehirn beschrieben sind. Der entscheidende Vorteil dieses neuen neuroanatomischen Versuchsansatzes soll darin liegen, dass bei der nukleären Translokation des Transkriptionsfaktors STAT3 nur direkte Effekte auf die Zielzelle getestet werden und im Falle von neuronalen Zielzellen die Kartierung unabhängig von einer neuronalen Aktivierung oder Hemmung derselben ist [Hübschle et al. 2001b].
Die zentrale Applikation von rekombinantem, rattenspezifischen IL-6 induziert über einen Zeitraum von ca. 6 Stunden eine deutliche Fieberantwort, die durch einen Anstieg der Körpertemperatur von 37,0°C auf 38,4°C (100 ng IL-6 pro Tier) bzw. 39,2°C (200 ng IL-6 pro Tier) gekennzeichnet ist. Bereits 15-30 Minuten nach der icv-Applikation von IL-6 kann eine nukleäre STAT3-Translokation in einigen hypothalamischen und extrahypothalamischen Hirnstrukturen nachgewiesen werden. Ausgeprägte Effekte sind für den Hypothalamus in der ventromedialen präoptischen Region (VMPO), dem *Nucleus supraopticus* (SON) und einer Region im caudobasalen Hypothalamus, die den *Nucleus arcuatus* umgibt, zu finden. Zudem zeigen ventral gelegene Hirnhäute und Ependymzellen der Ventrikel starke nukleäre STAT3-Signale. Der direkte Nachweis der IL-6-induzierten STAT3-Translokation in den Kern einer Zelle kann mittels Doppelmarkierung und dem Einsatz des Kernmarkers DAPI geführt werden.

Die Vielzahl der ermittelten hypothalamischen IL-6-Zielstrukturen sind insofern nicht erstaunlich, als IL-6, wie bereits anfangs erwähnt, an der Regulation mehrerer zentralnervös kontrollierter Begleiterscheinungen von Krankheiten beteiligt ist. Eine für die Fieberentstehung entscheidende hypothalamische Hirnstruktur, die eine starke IL-6-induzierte nukleäre STAT3-Translokation zeigt, ist die VMPO. Dies steht im Einklang zur beschriebenen Expression von IL-6-Rezeptoren in der präoptischen Region, die unter basalen Bedingungen mittels *in situ* Hybridisierung vor allem in ventromedialen Anteilen in unmittelbarer Nähe zum dritten Ventrikel zu finden sind [Schöbitz et al. 1993]. Nach derzeitigem Wissensstand werden Prostaglandine und insbesondere PGE2 als die letzten Vermittler einer ganzen Kaskade fieberauslösender Botenstoffe angesehen. Dies trifft für fieberauslösende Signalwege zu, die im Gehirn aber auch in der Körperperipherie ihren Ursprung haben (Abb. 15). Allerdings kann das endogene Pyrogen IL-6 die Synthese und Freisetzung von Prostaglandinen nur im Gehirn und nicht in der Körperperipherie induzieren [Dinarello et al. 1991, Bishai und Coceani 1996]. Interessanterweise scheint gerade die VMPO-Region in PGE2-abhängige Fiebersignalwege stark involviert zu sein [Scammel et al. 1996, Zhang et al. 2003]. Inwieweit die IL-6-induzierte genomische Aktivierung von VMPO-Zellen durch den Transkriptionsfaktor STAT3 mit einer Regulation des für die PGE2-Bildung verantwortlichen Enzyms COX2 gekoppelt ist, bleibt künftigen Untersuchungen vorbehalten.
Frühere Fos-Untersuchungen zeigen im Verlauf der Fieberentstehung eine Aktivierung von VMPO-Neuronen, während ansonsten die restlichen Anteile der präoptischen Region nicht oder nur gering aktiviert werden [Scammel et al. 1996, Saper 1998, Zhang et al. 2003]. Dies ist insofern nicht verwunderlich, als, wie in der Einleitung bereits vorgestellt, die Hemmung warmsensitiver Neurone der präoptischen Region ein entscheidender Mechanismus ist, Fieber zu initiieren (Abb. 6). Der prozentuale Anteil der warmsensitiven Neurone, die durch den finalen Fiebermediator PGE2 gehemmt wurden, ist deutlich höher als der Anteil warmsensitiver Neurone, die erregt wurden [Matsuda et al. 1992, Ranels und Griffin 2003]. Daher ist es kaum vorstellbar, dass aktivierte Neurone der VMPO-Region allein verantwortlich für die Fieberentstehung sein sollen, während andere Teilstrukturen der präoptischen Region unbedeutend sind. Wie wir in der Diskussion zur Anlage 5.10. sehen werden, kann offenbar die Ausstattung der Zellen mit unterschiedlichen Subtypen der PGE2-Rezeptoren entscheidend für die Aktivierung bzw. Nicht-Aktivierung und damit wiederum für potenzielle Fieberentstehungsmechanismen sein [Yoshida et al. 2003]. Das dort vorgestellte Konzept erlaubt neben der Integration der VMPO auch die Integration anderer Teilbereiche der präoptischen Region als neuroanatomische Basis zur Fieberregulation.

Die Ergebnisse der Anlage 5.7. lassen sich folgendermaßen zusammenfassen und diskutieren:

- Zentral appliziertes Interleukin-6 induziert eine robuste Fieberantwort und eine zeitabhängige nukleäre Translokation des Transkriptionsfaktors STAT3 in mehreren hypothalamischen Kerngebieten
- Ausgeprägte IL-6-induzierte STAT3-Effekte waren in der VMPO zu finden, einer für die Fieberentstehung wichtigen hypothalamischen Hirnregion. Damit können wir die mit dem neuronalen Aktivitätsmarker Fos durchgeführten neuroanatomischen Kartierungen früherer Studien bestätigen.
- Allerdings zeigen Überlegungen zur Zytokin- und PGE2-vermittelten Fieberentstehung, dass dieses Teilgebiet der präoptischen Region nicht allein verantwortlich für die hypothalamische Initiierung von Fieber sein kann. Auf alternative Mechanismen, die in der Anlage 5.10 untersucht werden, wird daher hingewiesen [Yoshida et al. 2003].

4.2.4. Die Bedeutung der circumventrikulären Organe in der durch zirkulierendes Interleukin-6 vermittelten Fieberentstehung (Ergebnisse der Anlage 5.8.)

Bei den sensorischen CVOs der *Lamina terminalis* handelt es sich um neurogliale Einheiten mit multipler reziproker Verbindung zu anderen Zentren des Dienzephalon, des limbischen Systems sowie des Hirnstamms. Auf Grund des Fehlens einer charakteristischen endothelialen Blut-Hirn-Schranke haben zirkulierende Botenstoffe ungehinderten Zutritt zum Parenchym des SFO oder des OVLT. Von Makrophagen freigesetzte proinflammatorische Zytokine, wie z.B. Interleukin-6, können somit im Rahmen immunologischer Reaktionsvorgänge als afferente, humorale Signale auf diese hypothalamischen Zentren wirken und zentrale Komponenten der Akute-Phase-Reaktion auslösen (Abb. 8, 15).
Die wichtige Bedeutung des OVLT und SFO bei Fieberentstehungsmechanismen kann in Läsionsversuchen gezeigt werden [Blatteis et al. 1983, 1987, Hunter et al. 1994, Takahashi et al. 1997]. Allerdings weist eine erst kürzlich veröffentlichte Arbeit darauf hin, dass solche Studien mit elektrolytischen OVLT-Läsionen mit Vorsicht zu genießen sind, da die Läsion selbst eine Erhöhung der Körpertemperatur über etliche Tage verursacht [Romanovsky et al. 2003]. Neue Methoden mit weniger invasiven Manipulationen am Tier werden gefordert. In dieser Teilstudie soll deshalb die Bedeutung der CVOs bei der Interleukin-6-vermittelten Fieberentstehung möglichst „physiologisch“, d.h. ohne Manipulation am ZNS selbst untersucht werden.

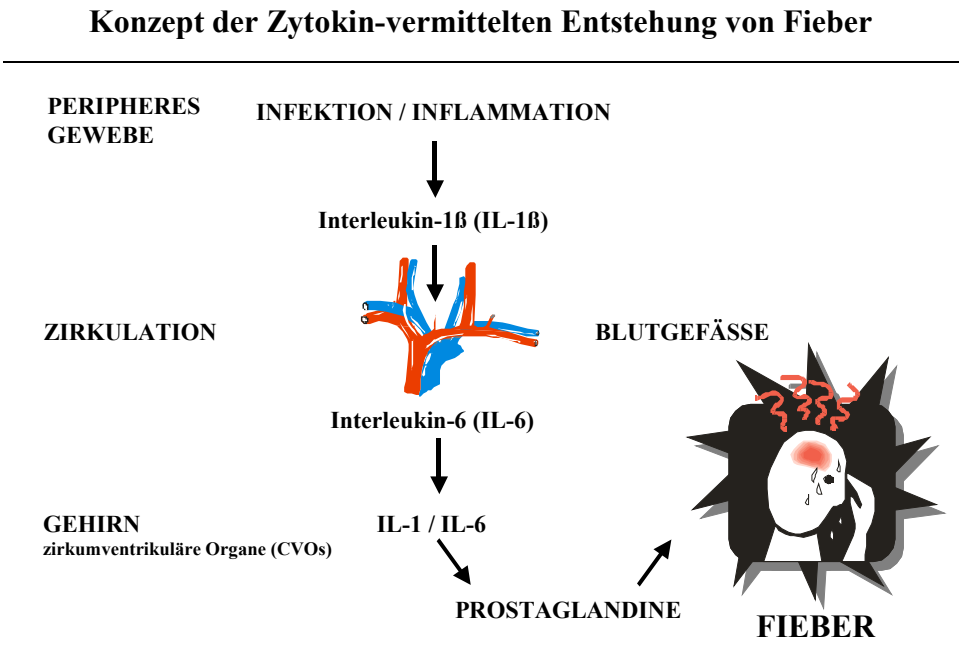

Abbildung 15
Konzept der Entstehung von Fieber unter Beteiligung des humoralen, proinflammatorischen Zytokins Interleukin-6 und des finalen Fiebermediators Prostaglandin-E2 (Erläuterungen siehe Text).

Die systemische Gabe des exogenen Pyrogens Lipopolysaccharid (LPS) Gram-negativer Bakterien ist ein häufig benutztes Experimentalmodell zur Induktion peripherer Entzündungen. Als Folge der Behandlung mit LPS produzieren immunkompetente Zellen proinflammatorische Zytokine. Interessanterweise ist IL-6 nach systemischer LPS-Applikation das einzige potenziell fiebererzeugende Zytokin, welches in stark erhöhter Konzentration in der systemischen Zirkulation über einen längeren Zeitraum nachweisbar ist [Roth et al. 1994, 2004]. Allein aus diesem Grund wird IL-6 eine entscheidende Rolle bei der zentralnervös vermittelten Fieberentstehung zugesprochen. Interessant ist zudem, dass es offenbar von entscheidender Bedeutung ist, ob IL-6 als zirkulierender Faktor oder aber als Pyrogen auftritt, welches gehirnintrinsisch gebildet wird [Vallières et al. 1997]. Die zweite Situation ist ja bereits im vorherigen Teilprojekt untersucht worden [Hübschle et al. 2001c]. Daher soll nun insbesondere untersucht werden, ob die LPS-induzierte IL-6-Freisetzung ins Blut von einer nukleären STAT3-Translokation in den CVOs begleitet wird. Zudem sollen die Wirkungen der systemischen Applikation des exogenen Pyrogens LPS mit Effekten des endogenen Pyrogens Interleukin-6 (rekombinantes, rattenspezifisches IL-6) verglichen werden. Die dabei gemessenen Parameter sind Körpertemperatur, IL-6-Plasmawerte und der immunhistochemische Nachweis der nukleären STAT3-Translokation im Gehirnschnitt.

Wie aus früheren Studien bereits bekannt, führt die systemische LPS-Applikation zunächst zu einem moderaten (1 Stunde) und danach über einen Zeitraum von mehreren Stunden zu einem starken Anstieg der IL-6-Plasmawerte. Gleichzeitig kommt es zu einer robusten biphasischen Fieberantwort und zu einem Maximum der nukleären Translokation des Transkriptionsfaktors STAT3 in Zellen der beiden sensorischen CVOs der *Lamina terminalis*, OVLT und SFO, zwei Stunden nach systemischer LPS-Applikation. Auch die systemische Applikation von IL-6 selbst induziert hohe Konzentrationen an zirkulierendem Zytokin mit einem Maximum bereits 1 Stunde nach der Behandlung. Dies wird allerdings erst in einer Folgestudie gezeigt [Harré et al. 2003]. Dieser Anstieg des IL-6 im Plasma ist jedoch von einer eher moderaten Fieberreaktion begleitet. Andererseits induziert IL-6 eine nukleäre STAT3-Translokation mit nahezu identischer Verteilung in exakt den gleichen Hirnstrukturen (OVLT und SFO) und mit etwas schwächerem Ausmaß wie die LPS-Applikation. Erneut tritt dieser IL-6-induzierte Effekt 1 Stunde nach der Applikation des Zytokins selbst und damit 1 Stunde vor dem LPS-induzierten Maximum der nukleären STAT3-Translokation auf. Die Einheitlichkeit der durch Pyrogenapplikation betroffenen ZNS-Regionen ist umso mehr erstaunlich, als im gesamten Rattengehirn und damit auch in anderen Hirnstrukturen mit offener bzw. teilweise offener Blut-Hirn-Schranke keine solch starke Pyrogen-induzierte nukleäre STAT3-Translokation auftrat.

Die Ergebnisse der Anlage 5.8. lassen sich folgendermaßen zusammenfassen und diskutieren:

- Die systemische Applikation von IL-6 bzw. LPS induziert moderates bzw. robustes Fieber, einen Anstieg der IL-6-Plasmawerte in vergleichbarer Höhe mit einem Maximum nach 1 Stunde bzw. 2 Stunden und eine nukleäre STAT3-Translokation in den beiden hypothalamischen CVOs, dem OVLT und dem SFO.
- Die sensorischen CVOs der *Lamina terminalis* sind daher für die Fieberentstehung vor allem dann wichtig, wenn pyrogene Botenstoffe im Blut zirkulieren. Erstmals wird mittels immunhistochemischem Nachweis eine direkte Beeinflussung von Gehirnzellen durch zirkulierendes IL-6 gezeigt.
- IL-6 vermittelt folglich einen Teil der LPS-induzierten nukleären Translokation des Transkriptionsfaktors STAT3. Während dieser genomischen Aktivierung der CVOs spielt zirkulierendes IL-6 offenbar eine Schlüsselrolle als Mediator der LPS-induzierten Fieberantwort. Weitere für die Fieberentstehung notwendige Mechanismen könnten durch die IL-6-vermittelte Genregulation ausgelöst werden.

- Welche IL-6-abhängigen Zielgene an der Initiierung und Aufrechterhaltung von Fieber beteiligt sind, kann momentan nur spekulativ beantwortet werden. Ein möglicher Kandidat ist die induzierbare Cyclooxygenase 2 (COX2), die für die Bildung von Prostaglandin E2 (PGE2) verantwortlich ist, welches wiederum nach dem derzeitigen Wissensstand als finaler Fiebermediator angesehen wird. In der Tat können bei einer Sequenzanalyse in der Promotorregion des COX2-Gens der Ratte STAT3-Bindungsstellen gezeigt werden [Harré et al. 2002].

4.2.5. Astrozyten der circumventrikulären Organe sind Zielzellen bei der durch zirkulierendes Interleukin-6 vermittelten Fieberentstehung (Ergebnisse der Anlage 5.9.)

Dieses Teilstudie ist eine direkte Weiterführung des vorherigen Teilprojektes. Nachdem die Bedeutung des Pyrogens IL-6 als Mediator der LPS-induzierten nukleären STAT3-Translokation im OVLT und SFO etabliert ist [Harré et al. 2002], stellt sich die Frage, in welchem Zelltyp der sensorischen CVOs diese genomische Aktivierung stattfindet. CVO-intrinsische Zellen mit LPS- bzw. IL-6-induzierter nukleärer Translokation sollen mittels zellspezifischer Markerproteine in Mehrfachmarkierungen immunzytochemisch näher charakterisiert werden. Dazu werden gliale (Astrozyten, Oligodendrozyten, Mikroglia), endothelilale und neuronale Marker eingesetzt.
Nach Pyrogen-Applikation kann zu Zeitpunkten mit hohen IL-6-Plasmawerten eine nukleäre STAT3-Translokation in Astrozyten der beiden sensorischen CVOs gefunden werden. Zusätzlich können Zellen mit nukleären STAT3-Signalen dargestellt werden, deren Zuordnung zu einem bestimmten Phänotyp trotz Einsatz mehrerer anderer Zellmarker nicht gelingt. Diese Zellpopulation macht immerhin ca. 60 % der Zellen aus, die mit einer Pyrogen-induzierten nukleären STAT3-Translokation reagieren (persönliche Mitteilung Dr. Harré).
Die Ergebnisse der Anlage 5.9. lassen sich folgendermaßen zusammenfassen und diskutieren:

- Die Astrozyten der beiden CVOs, OVLT und SFO, sind in der Ratte offenbar Zielzellen bei der durch zirkulierendes Interleukin-6 vermittelten Fieberentstehung.
- Welche funktionelle Relevanz die Genregulation astrozytärer Zielgene an der Initiierung und Aufrechterhaltung von Fieber haben, muss in weiterführenden Studien geklärt werden.

4.2.6. Efferente Regulation der Fieber begleitenden zitterfreien Thermogenese (Ergebnisse der Anlage 5.10.)

Wärmeproduktion durch das interskapuläre braune Fettgewebe der Ratte wird durch mehrere (patho-)physiologische Stimuli ausgelöst. Dazu zählen Kälteexposition, eine überhöhte Nahrungsaufnahme oder auch übermäßig positive Bilanz des Energiehaushaltes und Fieber. In allen drei Fällen ist das braune Fettgewebe als wärmeproduzierendes Effektororgan entscheidend an einer Erhöhung der Körpertemperatur beteiligt. Da diese Wärmebildung anders als bei der Wärmeproduktion im Muskel zitterfrei abläuft, spricht man von zitterfreier Thermogenese. Dieses Teilprojekt soll die hypothalamische Regulation der Fieber begleitenden zitterfreien Thermogenese untersuchen.

Bei Nagern ist die Bedeutung des interskapulären braunen Fettgewebes als wichtiges thermoregulatorisches Effektororgan bei Fieberprozessen gut etabliert [Rothwell 1992]. Wie bereits in den vorherigen Kapiteln erwähnt, wird Prostaglandin E2 als finaler Fiebermediator angesehen (Abb. 15), der eine Sollwertverstellung zu höheren Körpertemperaturen unter Mitwirkung warmsensitiver Neurone und nachgeschalteter thermointegrativer Strukturen im Hypothalamus auslöst (Abb. 6). Die ZNS-Struktur mit der höchsten Prostaglandin-E2-Sensitivität ist die präoptische Region. Lokale PGE2-Mikroapplikationen in die präoptische Region führt zu Fieber [Feldberg und Saxena 1971, Stitt 1973, Williams et al. 1977, Blatteis und Sehic 1997]. Dies wird auch durch neuroanatomische Fos-Kartierungen für einen Teilbereich der präoptischen Region, der VMPO, bestätigt [Scammel et al. 1996, Saper 1998]. Die methodisch bedingte Problematik, die hinter diesen Fos-Studien steht, wurde bereits in 4.2.3. diskutiert, und es muss daher vermutet werden, dass neben der VMPO-Region auch andere Teilgebiete der präoptischen Region mit Prostaglandin-E-abhängigen Mechanismen ebenso für die hypothalamische Initiierung von Fieber verantwortlich sein können.

Aus mehreren Gründen scheint in diesem Zusammenhang der Subtyp 3 der PGE2-Rezeptoren von besonderer Bedeutung zu sein. Transgene Mäuse, in denen das Gen für den EP3R ausgeschaltet wurde, zeigen keine Fieberreaktion nach Pyrogen- oder Zytokinbehandlung [Ushikubi et al. 1998]. Weiterhin ist verglichen mit anderen Strukturen des ZNS gerade der EP3R in Neuronen medialer Anteile der präoptischen Region stark exprimiert [Nakamura et al. 1999, 2000]. Diese Neurone scheinen zudem Ausgangspunkt für efferente, EP3R-abhängige pyrogene Signalwege zur Körperperipherie zu sein, die im Hirnstamm im sogenannten *Nucleus raphé pallidus* zur autonomen Innervation des braunen Fettgewebes umgeschaltet werden [Nakamura et al. 2002, Morrison et al. 1999]. Folglich scheinen unter

Fieberbedingungen Prostaglandin-sensitive Neurone der medialen präoptischen Region mittels EP3R die efferente Kontrolle der zitterfreien Thermogenese des braunen Fettgewebes mit zu regulieren.

Der Nachweis der Existenz einer efferenten Neuronenkette von der präoptischen Region zum braunen Fettgewebe wurde neuroanatomisch nur teilweise, ansonsten rein physiologisch geführt [Nakamura et al. 2002]. Zur kompletten neuroanatomischen Darstellung dieses pyrogenen Signalweges sollen deshalb potenziell PGE2-sensitive Neurone der präoptischen Region, die den EP3R exprimieren, auf ihre efferente Verschaltung zur sympathischen Innervation des braunen Fettgewebes untersucht werden. Dazu wird die virale, transneuronale Tracing-Methode (siehe 3.2.1.) mit dem immunhistochemischen Nachweis für den EP3R kombiniert.

Viral infizierte Neurone, die den EP3R exprimieren, sind besonders zahlreich in zwei Gehirnregionen vertreten, der medialen präoptischen Region und dem *Nucleus raphé pallidus*. In Tieren, die 71 h nach PRV-Injektion in das braune Fettgewebe neuroanatomisch untersucht werden, sind ca. 40 % aller in der medialen präoptischen Region viral infizierten Neurone mit dem EP3R ausgestattet. Damit ist der Nachweis einer EP3R-abhängigen, Prostaglandin-sensitiven, efferenten Neuronenkette von der präoptischen Region zum wärmebildenden thermoregulatorischen Effektororgan erbracht. Interessanterweise zeigen auch die beiden benachbarten Teilstrukturen der *Lamina terminalis*, der MnPO und das OVLT (siehe Abb. 7 und Abb. 13), eine substantiell hohe Anzahl solch doppelt markierter Neurone. Dies unterstützt erneut die Hypothese, dass die im vorderen Hypothalamus gelegene *Lamina terminalis* an der Regulation der Körpertemperatur beteiligt ist. Offensichtlich kann die *Lamina terminalis* einerseits Wärmebildungsmechanismen (zitterfreie Thermogenese) und andererseits Wärmeabgabemechanismen (siehe 4.1.3. und 4.1.4.) steuern.

Die Weiterleitung der pyrogenen Information aus dem vorderen Hypothalamus zum braunen Fettgewebe scheint über Hirnstammneurone im *Nucleus raphé pallidus* abzulaufen [Nakamura et al. 2002, Morrison et al. 1999]. Diese Neurone können in der vorliegenden Teilstudie als Neurone dritter Ordnung (siehe Abb. 9) in der efferenten Kontrolle des interskapulären, braunen Fettgewebes charakterisiert werden. Zudem zeigt sich, dass etwa zwei Drittel der viral infizierten Neurone des *Nucleus raphé pallidus* den EP3R exprimieren. Dies lässt vermuten, dass dieses Kerngebiet selbst EP3R-abhängige Prostaglandinsensitivität besitzt, die unter Fieberbedingungen zur Regulation der zitterfreien Thermogenese beiträgt. Allerdings ist dies bislang mit physiologischen Methoden noch nicht untersucht worden.

Die Ergebnisse der Anlage 5.10. lassen sich folgendermaßen zusammenfassen und diskutieren:

- Unter Fieberbedingungen scheint eine starke EP3R-abhängige Prostaglandin-sensitivität, insbesondere in Neuronen der medialen präoptischen Region und des *Nucleus raphé pallidus*, an der zentralnervösen Kontrolle der zitterfreien Thermogenese im interskapulären braunen Fettgewebe beteiligt zu sein.
- Die mediale präoptische Region und die benachbarten Teilstrukturen der *Lamina terminalis*, der MnPO und das OVLT, sind Ausgangspunkte eines efferenten Signalweges, der EP3R-abhängige, pyrogene Information zum wärmebildenden thermoregulatorischen Effektororgan transportiert. Diese neuroanatomische Analyse ergänzt bereits publizierte physiologische Studien und bekräftigt die wichtige Bedeutung des vorderen Hypothalamus in der Kontrolle der zitterfreien Thermogenese nach pyrogener Stimulation.
- Eine Subpopulation der Neurone des *Nucleus raphé pallidus*, welche die Sympathikusaktivität zum braunen Fettgewebe regulieren, könnte eigene EP3R-abhängige Prostaglandinsensitivität besitzen. Diese auf neuroanatomischen Daten basierende Vermutung ist in physiologischen Studien noch nicht untersucht.

5. Anlagen

5.1.

5.1. HÜBSCHLE, T., McKINLEY, M.J. & OLDFIELD, B.J. (1998)

Efferent connections of the lamina terminalis, the preoptic area and the insular cortex to submandibular and sublingual gland of the rat traced with pseudorabies virus.
Brain Res. **806** (2): 219-231.

Eigener Anteil an der Publikation:

- Beteiligung an der Versuchsplanung (100 %)
- Durchführung der Versuche (100 %)
- Beteiligung an der Zusammenfassung und Veröffentlichung der Ergebnisse (90 %)

ELSEVIER

Brain Research 806 (1998) 219–231

BRAIN RESEARCH

Research report

Efferent connections of the lamina terminalis, the preoptic area and the insular cortex to submandibular and sublingual gland of the rat traced with pseudorabies virus

Thomas Hübschle [a,b,*], Michael J. McKinley [a], Brian J. Oldfield [a]

[a] *The Howard Florey Institute of Experimental Physiology and Medicine, University of Melbourne, Parkville, Victoria 3052, Australia*
[b] *Max-Planck-Institute for Physiological and Clinical Research, W.G. Kerckhoff-Institute, Parkstr. 1, D-61231 Bad Nauheim, Germany*

Accepted 21 July 1998

Abstract

Neurones situated in the lamina terminalis (organum vasculosum of the lamina terminalis, median preoptic nucleus and subfornical organ) as well as within medial and lateral parts of the preoptic area and in the insular cortex become transneuronally labelled following pseudorabies virus injections into the submandibular or the sublingual gland. These neurones are efferently connected to a chain of central neurones directed to secretory or vascular tissue of the submandibular or the sublingual gland. By varying the postinoculation time a stepwise infection of different forebrain nuclei was registered, with the hypothalamic paraventricular nucleus and the lateral hypothalamic area being the first forebrain structures labelled. Such early infected neurones within these hypothalamic nuclei are in all likelihood third order neurones regulating salivary secretion and might have functioned as relays transmitting virus to other forebrain structures. The above mentioned forebrain areas together with several other hypothalamic nuclei as well as the bed nucleus of the stria terminalis, the central nucleus of the amygdala and the substantia innominata, seem to be the widespread anatomical basis for the central regulation of salivary gland function.

Keywords: Central regulation of salivation; Salivary gland; Viral tracing; Organum vasculosum of the lamina terminalis; Subfornical organ; Median preoptic nucleus; Preoptic area; Insular cortex

1. Introduction

The nerves supplying the salivary glands consist of afferent and efferent nerve fibres innervating various types of secretory, myoepithelial and vascular cells and it is well established that these various effector cells are supplied by both the parasympathetic and the sympathetic nervous system [10]. Glandular function depends on complex integration of secretory, motor and vasomotor actions regulated by nerves. Polysynaptic chains of neurones innervating the glands have been intensively investigated using electrophysiological and neuronal tracing techniques. The parasympathetic nervous system seems to play a dominant role in activating and maintaining salivary secretion and the transneuronal viral tracing technique has been successfully used in a recent study to investigate central connections to the parasympathetic innervation of the rat's submandibular gland [14]. Unilateral injections of a pseudorabies virus mutant (Bartha strain with inserted *lacZ* gene) into the submandibular gland of sympathectomized rats resulted in retrograde labelling of neurones across a number of widespread regions of the central nervous system. The most rostral amongst them was detected in the bed nucleus of the stria terminalis. However, other regions of the forebrain, not described in that study, are known from a number of previous clinical, physiological and lesion studies to be involved in the central regulation of salivation.

In a clinical case report, Penfield (1929) [33] described the first example of diencephalic autonomic epilepsy in a patient who showed epileptic discharges accompanied by various autonomic motor phenomena, amongst them salivation. Centrifugal neuronal pathways were probably activated under those conditions. A brain tumor, located in the anterodorsal part of the wall of the third ventricle near to the anterior commissure, was the possible origin of the episodes. This is suggestive of an involvement of this brain

* Corresponding author. Fax: +49-6032-705-211; E-mail: huebschle@kerckhoff.mpg.de

0006-8993/98/$ - see front matter
PII: S0006-8993(98)00765-3

region in salivary control. In addition, lesions of the anteroventral wall of the third ventricle influenced submandibular morphology [34] or diminished salivary secretion induced by intracerebroventricular injections of the cholinergic agonist pilocarpine [35], thereby supporting the concept of salivary control mediated through the anterior wall of the third ventricle, also known as the lamina terminalis.

The function of the submandibular and sublingual glands as thermoregulatory effector organs in the rat during extreme heat stress has been clearly established [13]. The preoptic area, a region in close vicinity to the organum vasculosum of the lamina terminalis (OVLT), has been repeatedly implicated in the efferent control of thermoregulatory salivation [18,47]. Furthermore, cortical areas within the insular cortex in the rat may mediate heterogenous autonomic functions including salivation [6,19,50]. Possible neuronal connections of this cortical structure to both parasympathetic and sympathetic preganglionic neurones controlling salivary glands have been described in the rat either electrophysiologically [50] or neuroanatomically [51]. Finally, the insular cortex, the preoptic area and the lamina terminalis may form, together with other central nervous system structures, a central network regulating autonomic functions such as salivation [6,14,17,23]. In view of the apparent discrepancy between the data supporting a forebrain involvement in salivary control, and the lack of labelling of some structures in the already existing viral tracing study [14], we have investigated a potentially more extensive forebrain salivary gland innervation using pseudorabies virus.

2. Materials and methods

2.1. Details on neurotropic virus

Pseudorabies virus is not endemic to Australia, therefore the inoculations of the rats were performed in a microbiologically secure environment at the CSIRO Australian Animal Health Laboratory in Geelong, Australia (Biosafety level 2 laboratory). The Bartha strain of the pseudorabies virus imported to Australia under an Australian Quarantine Inspection Service Permit was propagated in porcine kidney fibroblasts (PK15) cell culture and the titer measured. Virus pools grown from purified stock were shown to be authentic pseudorabies virus by neutrali-

Table 1
Time-dependent infection of forebrain structures after pseudorabies virus (PRV) injection into the submandibular or the sublingual gland

Survival time	24 h		55 h	66 h	71–78 h				96 h			
Animal number	SM4	SL4	SM17	SM21	SM5	SM6	SM8	SL6	SM1	SL1	SL2	SL5
Third order hypothalamic structures												
Hypothalamic paraventricular nucleus	−/−	−/−	+/−	+/C	+/C	+/C	+/C	+/C	+/C	+/C	+/C	+/C
Lateral hypothalamic area	−/−	−/−	+/−	+/C	+/C	+/C	+/C	+/C	+/C	+/C	+/C	+/C
Lamina terminalis structures[a]												
Organum vasculosum of the lamina terminalis	−	−	−	2	+	4	+	3	+	+	+	+
Median preoptic nucleus	−	−	−	+	+	+	+	3	+	+	+	+
Subfornical organ	−	−	−	1	+	3	+	4	+	+	+	+
Preoptic area												
Medial preoptic area	−/−	−/−	−/−	−/−	+/2	4/2	+/C	−/−	+/C	+/4	+/C	+/C
Lateral preoptic area	−/−	−/−	−/−	3/1	3/1	3/2	+/C	1/−	+/C	+/C	+/C	+/C
Cortical structures												
Insular cortex	−/−	−/−	−/−	2/1	+/3	2/2	+/C	2/1	+/C	+/C	+/C	+/C
Primary and secondary motor cortex	−/−	−/−	−/−	−/−	−/−	1/−	2/4	−/−	3/−	−/−	4/3	−/−
Primary and secondary somatosensory cortex	−/−	−/−	−/−	−/−	1/1	−/−	2/C	−/−	−/−	−/−	3/1	−/−
Other forebrain structures												
Bed nucleus of the stria terminalis	−/−	−/−	−/−	+/−	+/3	+/C	+/C	+/3	+/C	+/C	+/C	+/C
Central nucleus of the amygdala	−/−	−/−	−/−	+/2	+/1	+/C	+/C	+/2	+/C	+/C	+/C	+/C
Arcuate nucleus and periarquate area	−/−	−/−	−/−	3/1	+/C	+/C	+/C	+/3	+/C	+/C	+/C	+/C
Retrochiasmatic area	−/−	−/−	−/−	4/3	+/C	+/C	+/C	+/C	+/C	+/C	+/C	+/C
Substantia inominata	−/−	−/−	−/−	3/2	3/3	+/C	+/C	−/−	+/C	+/C	+/C	+/C
Zona incerta	−/−	−/−	−/−	4/2	3/4	3/3	4/4	1/−	+/C	+/C	+/C	+/C

SM = animal with PRV injections into the left submandibular gland.
SL = animal with PRV injection into the left sublingual gland.
+ = 5 cells or more on the ipsilateral side of PRV injection.
C = 5 cells or more on the contralateral side of PRV injection.
1–4 = cell number on the ipsi- or contralateral side of PRV injection.
[a] Midline Lamina terminalis structures with no separation of the ipsi- or contralateral side of PRV injection.

sation. The average titer of the pseudorabies virus stocks was 2.8×10^6 plaque-forming units per millilitre.

2.2. Inoculation procedure

Sixteen male Sprague–Dawley rats (250–350 g) were anaesthetised with sodium pentobarbitone (60 mg/kg body weight). The left submandibular and sublingual gland were surgically exposed and three injections (0.5 μl) of pseudorabies virus were made into the submandibular gland ($n = 10$) or one injection (1–2 μl) into the center of the sublingual lobe ($n = 6$). The injections of pseudorabies virus were made with a 30 gauge needle attached to a 5 μl syringe (SGE Australia, Ringwood, Australia). The injection was administered during a one minute period and the needle was kept in place for at least another minute. Any efflux from the point of puncture of the gland was immediately absorbed with sterile cotton buds. The wound was closed and the rats were allowed to survive up to 4 days.

2.3. Immunocytochemistry

The rats were then anaesthetised (100 mg/kg sodium pentobarbitone) and transcardially perfused with 0.9% saline followed by 300–400 ml of 4% paraformaldehyde/phosphate buffer (pH 7.2). Brains and spinal cords were removed, postfixed for 2 h in 4% paraformaldehyde/phosphate buffer and then transferred into a 20% sucrose solution overnight. The next day the tissue was cut at 40 μm sections on a Leitz freezing microtome. Coronal or sagittal (submandibular gland injections, $n = 2$) sections of the forebrain, coronal midbrain or medullary sections and horizontal sections of the thoracic segments (T1 to T6) were processed. Immunocytochemical processing of free floating sections was performed with an avidin biotin horseradish peroxidase complex (Vector Elite, Burlingame, CA, USA) and visualised by diaminobenzidine hydrochloride reaction in the presence of hydrogen peroxide. Neurones infected by pseudorabies virus were detected using overnight incubations at 4°C with two specific antisera raised in rabbit (Rb 134, 1:10 000) and goat (Gtα-PRV, 1:2000) against acetone inactivated pseudorabies virus. These antisera have been shown previously to recognize all major viral envelope glycoproteins [3,4]. Sections were mounted onto glass slides, examined using a Leica DMV microscope and photographed with Kodak TMAX 400 pro negative films.

2.4. Analysis

Brain tissue was analysed with computer-based mapping and drawings [45] using Corel Draw as graphics computer program. Detailed quantitative analysis of pseudorabies virus infected forebrain neurones was performed on forebrain structures using a representative animal with submandibular pseudorabies virus injections (SM 8), which was allowed to survive for 78 h (survival time). Brain levels 0.0, −0.3, −0.8 and −2.0 mm caudal to bregma were selected and all coronal sections at those levels (0.0 ± 220 μm, -0.3 ± 180 μm, -0.8 ± 360 μm and -2.0 ± 160 μm) were analysed. Data are represented as average number of pseudorabies virus infected neurones per section within the investigated forebrain structure. For the semiquantitative analysis (Table 1), serial coronal sections were investigated from various animals of the different survival time groups within the same bregma levels as described for animal SM8. When the average number of infected neurones in any structure exceeded five, this was indicated by + on the ipsi- or C on the contralateral side of injection. An attempt was made to standardise the comparison between groups which were based on the relative degree of labelling within the paraventricular nucleus of the hypothalamus. This approach has been used effectively by others utilising viral tracing techniques [14,37,46]. The terminology used to describe brain structures was modified from the rat brain map atlas of Swanson [45].

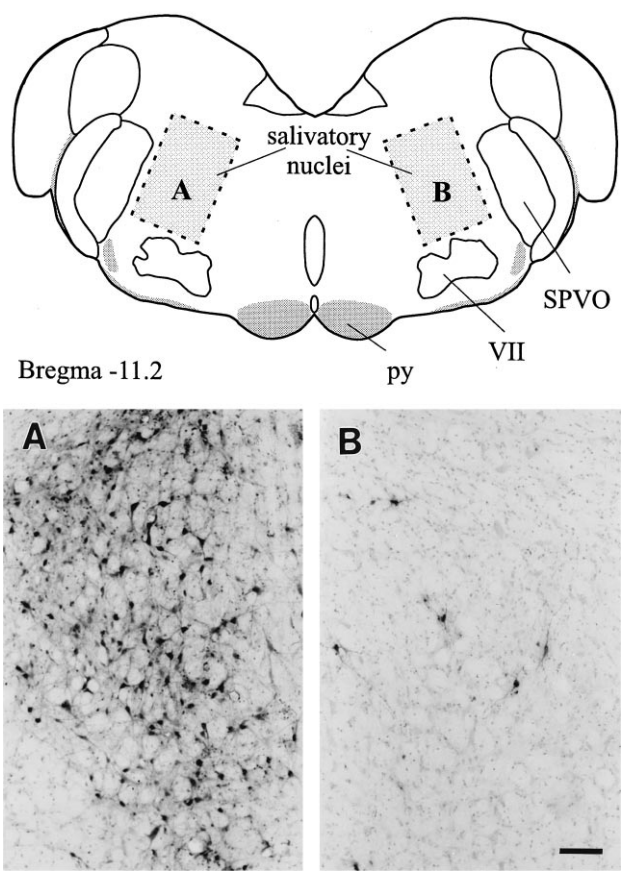

Fig. 1. Retrogradely traced cell bodies and nerve fibres in the salivatory nuclei after pseudorabies virus injections into the left submandibular gland (rat SM5). The brainmap (upper panel) indicates the location of the two photomicrographs A and B (lower panel) within the rostral, lateral medulla oblongata, which show viral infection for the ipsi- (A) and contralateral side (B). Bar = 100 μm. Drawing and abbreviations (see list) were modified from Swanson [45].

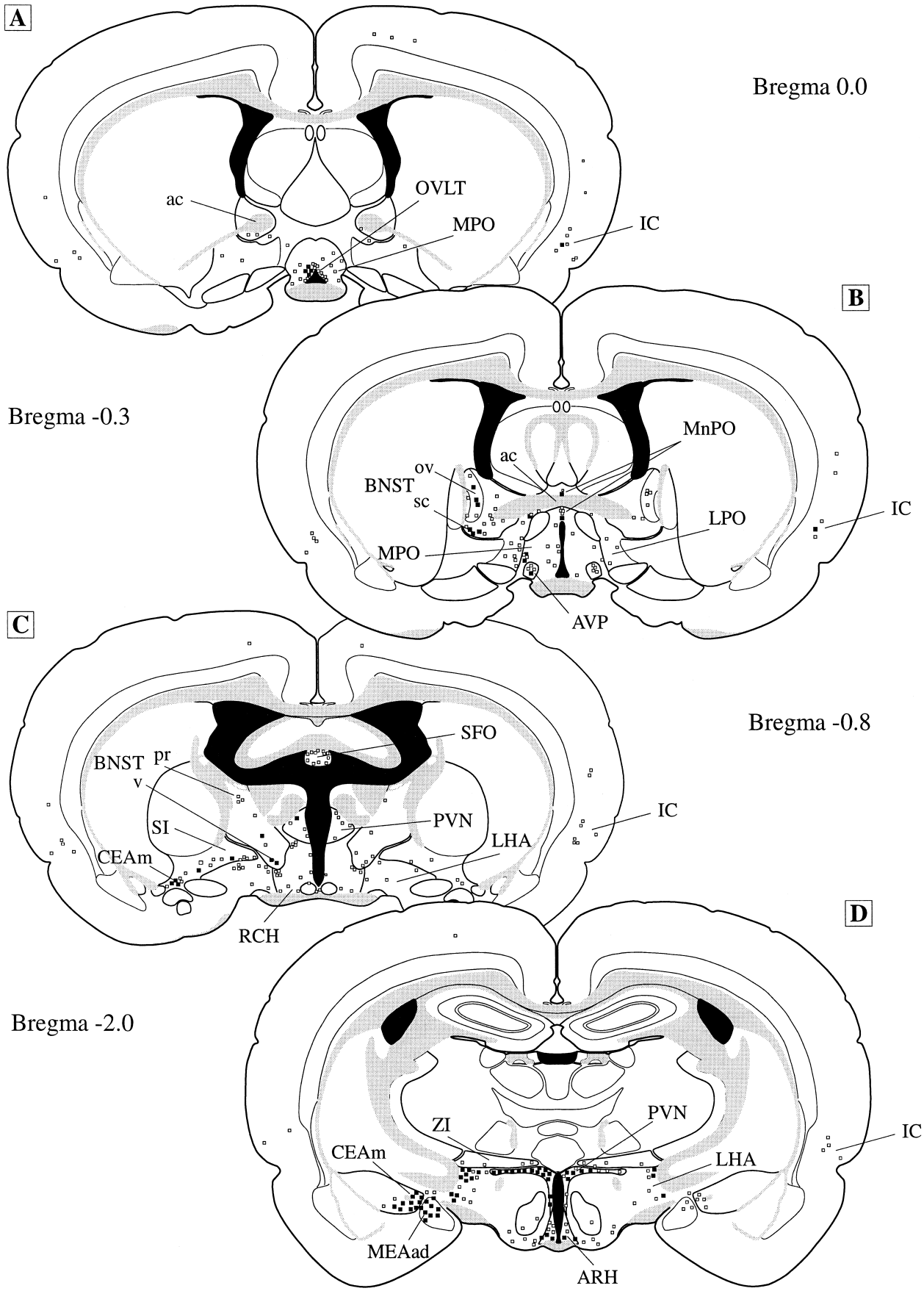
A
Bregma 0.0
ac
OVLT
MPO
IC
B
Bregma -0.3
MnPO
ac
ov
BNST
sc
LPO
IC
MPO
AVP
C
Bregma -0.8
SFO
BNST
pr
v
IC
PVN
SI
LHA
CEAm
RCH
D
Bregma -2.0
ZI
PVN
IC
CEAm
LHA
MEAad
ARH

3. Results

3.1. Pseudorabies virus infection in the medullary salivatory nuclei and thoracic spinal cord

In order to assess whether the virus entered the central nervous system via the known efferent preganglionic autonomic pathways innervating the submandibular or the sublingual gland, sections of the medulla and spinal cord were examined. The infection in the rostral medulla, at the level of the salivatory nuclei, 3 days after inoculation (71 h, animal SM5) was mainly restricted to the ipsilateral side (Fig. 1A). Labelled cells were seen extending from the dorsolateral to the ventrolateral regions of the rostral medulla with no clearcut separation of the inferior or superior salivatory nuclei. On the contralateral side, after this survival time, only a few neurones were infected and these were scattered within the entire lateral area of the rostral medulla next to the oral part of the spinal trigeminal nucleus (Fig. 1B). The infection in the animal with a 55 h survival period (SM17) was quite similar in distribution, although the degree of infection was less advanced and infection was restricted to the ipsilateral side only. Again, infected neurones were found within the entire lateral area of the rostral medulla with no concentration in the dorsal or ventral part. This distribution of labelling was the same in animals which received injections of virus into the sublingual gland.

After a survival time of 55 h, infected neurones were restricted to the ipsilateral thoracic (T1–T6) intermediolateral cell column. There was no evidence of infection in other spinal cord areas. After 3 (71–78 h) or 4 days (96 h) survival, horizontal sections of the thoracic spinal cord (T1–T6) revealed infection in preganglionic sympathetic neurones within the ipsi- or contralateral intermediolateral cell column following injection of virus into the submandibular or sublingual gland. In addition, other spinal cord layers (laminae I, II, V, VII, X) occasionally showed viral infection.

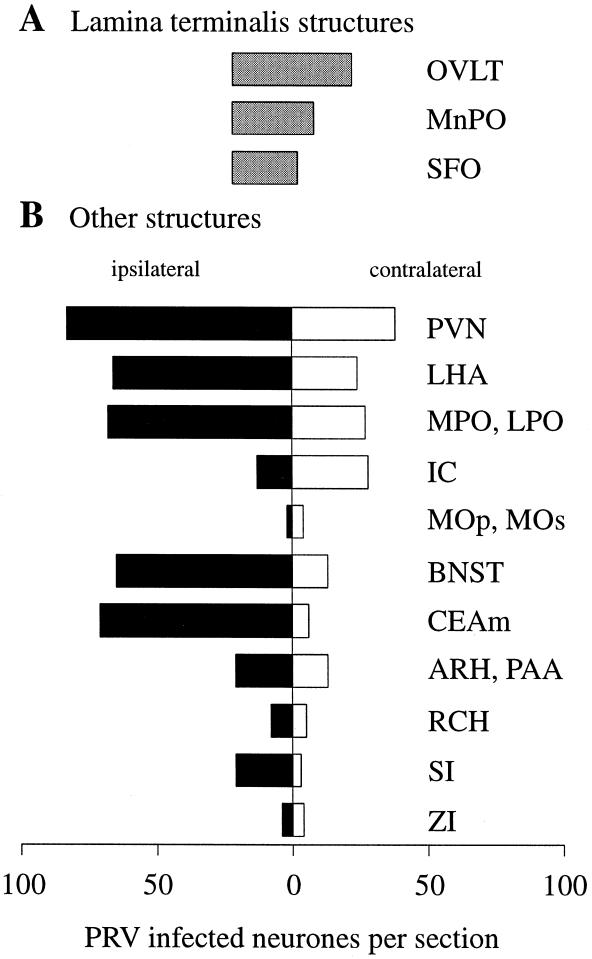

Fig. 3. Number of virally infected neurones in lamina terminalis (A) and other forebrain structures (B) after pseudorabies virus (PRV) injections into the left submandibular gland (rat SM8). Neurones were counted for the ipsilateral side (black bars) and the contralateral side (white bars) of virus injection in between the Bregma levels 0.0 and −2.0. Infected cells within midline lamina terminalis structures were determined without separation of the ipsi- or contralateral side of virus injections (grey bars). Bars represent an average cell count per section of virally infected neurones within a particular forebrain nucleus. Abbreviations (see list) were modified from Swanson [45].

3.2. Pseudorabies virus infection in forebrain structures

In rats surviving between 71–78 h after inoculation of the submandibular or sublingual gland, the same forebrain structures were consistently infected in the telencephalon and diencephalon. (Table 1, Fig. 2). These included the bed nucleus of the stria terminalis, the central nucleus of the amygdala, the substantia innominata, the hypothalamic paraventricular nucleus, the lateral hypothalamic area, the zona incerta, the retrochiasmatic area, the arcuate nucleus and the periarcuate area. The labelling in these structures, as quantified for the representative case SM8, was predominantly on the ipsilateral side of the viral injection (Fig. 3B), an observation consistent for all longer survival times examined (Table 1, 55 to 96 h). The lateral hypothalamic area and the hypothalamic paraventricular nucleus were the only forebrain nuclei ipsilaterally infected after a survival time of 55 h and these were considered to be third order forebrain sites projecting in all likelihood to the

Fig. 2. Location of virally infected neurones after pseudorabies virus injections into the left submandibular gland (rat SM8) mapped at four different forebrain levels (Bregma 0.0 to −2.0, A–D). The distribution of infected neurones is taken from a representative experiment with a survival time of 78 h. Open squares represent single infected neurones, a cluster of five infected neurones is given by the filled squares. Drawings and abbreviations (see list) were modified from Swanson [45].

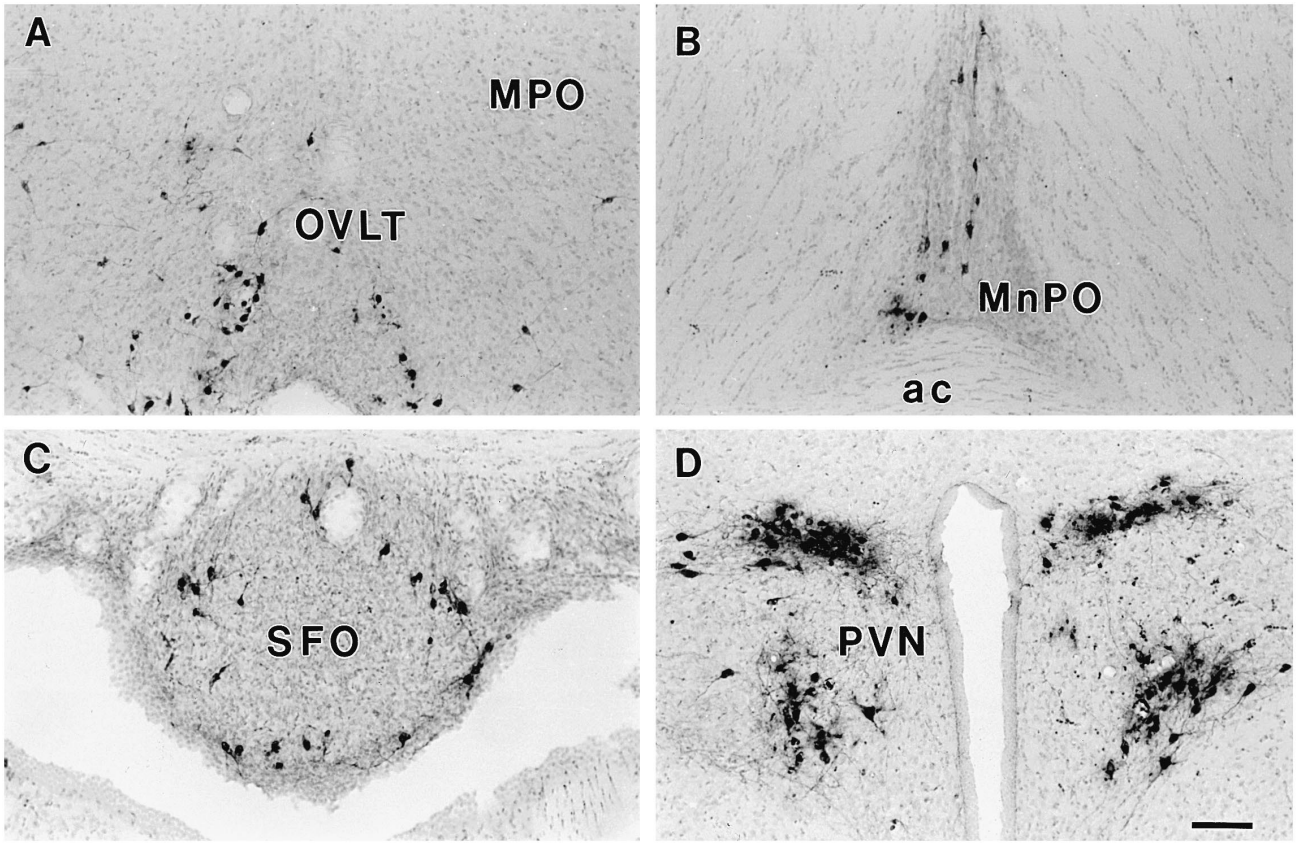

Fig. 4. Retrogradely traced cell bodies and nerve fibres in the lamina terminalis and the hypothalamic paraventricular nucleus after pseudorabies virus injections into the left submandibular gland (rat SM8). Virally infected neurones are shown after a survival time of 78 h. The first wave of viral infection appeared in the OVLT (A), MnPO (B) and SFO (C), however, within the PVN (D) infection was already more advanced. Bars = 100 μm. Abbreviations (see list) were modified from Swanson [45].

submandibular gland (Table 1). The initial ipsilateral labelling in the lateral hypothalamic area at 55 h survival time was first detected in the caudal dorsolateral part of this region and extended to the equivalent contralateral side after a 3–4 day survival time (Table 1, Fig. 2D). In the hypothalamic paraventricular nucleus, the viral infection was first apparent in the ipsilateral dorsal parvocellular division (55 h), although after 71–78 h survival time it extended to include the dorsal, medial and lateral parvocellular subnuclei on both sides (Fig. 2C, D, Fig. 4D). Rat SM8 was chosen as representative of the rats which survived 71–78 h. Data of this representative animal are given in Figs. 2–5 and compared below.

3.3. Virally infected neurones in cortical areas

Cells labelled with pseudorabies virus after injections into the submandibular or the sublingual gland were found in three cortical areas. By far the largest number of infected neurones was found in the insular cortex just dorsal to the rhinal fissure (Fig. 2A–D, Fig. 5). The first infection within the insular cortex appeared after 3 days (Table 1, 66–78 h). Longer survival times led to a greater degree of infection, but remained restricted to the same cortical areas. In some rats (e.g. SM8) there was a tendency towards more infection on the contralateral side (Fig. 3B), however this was slight and in most animals labelled neurones were found in more or less equal numbers bilaterally. There were no cases observed of ipsilateral dominance of cortical labelling, a feature seen for many other labelled forebrain nuclei. Labelled cortical neurones were found mainly in layer 5, although layer 2 occasionally exhibited viral infection (Fig. 5). Highest infection was prominent in the anterior part of the insular cortex at 0 to −0.3 mm caudal to bregma. The proportion of infection in the other two cortical areas, the primary and secondary motor cortex, and the primary and secondary somatosensory cortex, was minor compared to the labelling of the insular cortex. Only a few neurones (1 to 6) scattered within cortex layer 5 were found. Clusters of labelled cells were observed in the insular cortex (Fig. 5C) but never in the other cortical areas. Even with the longest survival time (96 h), when infection in the insular cortex was more advanced, an increase in the numbers of infected neurones in the motor or somatosensory cortical regions was not found. In addition, three out of eight animals with longer

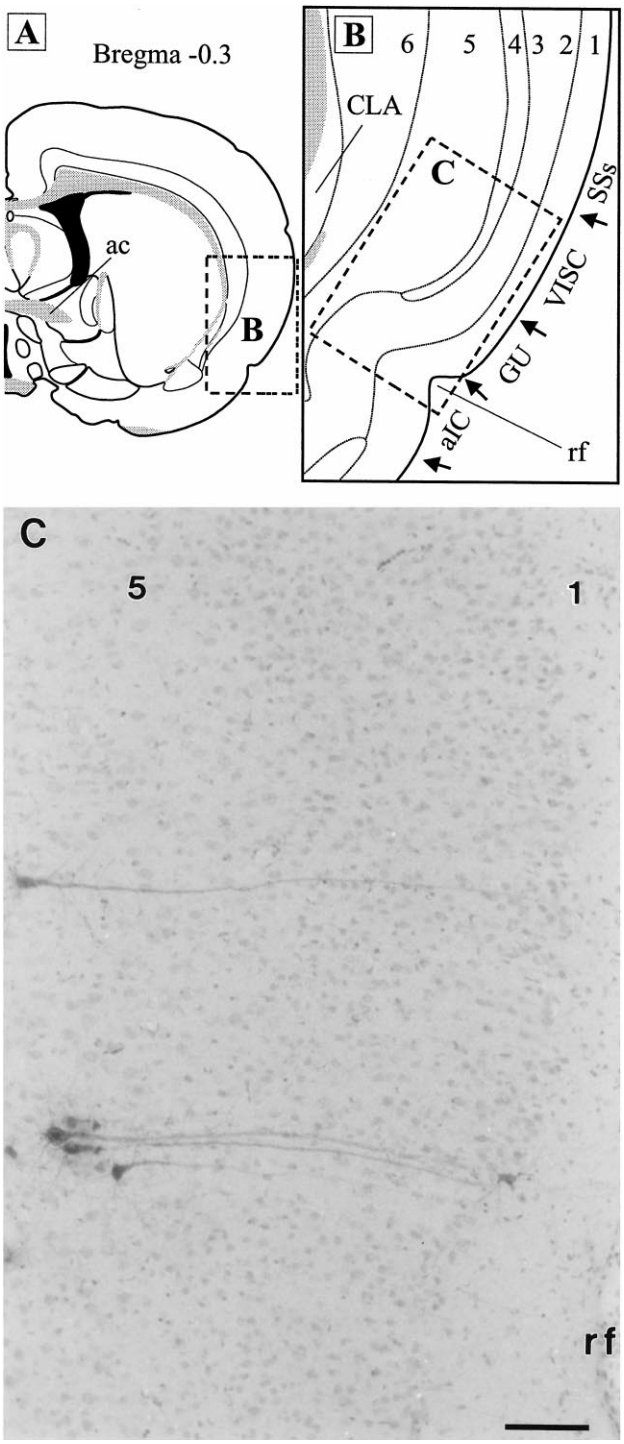

Fig. 5. Retrogradely traced cell bodies and nerve fibres in the insular cortex (IC) after pseudorabies virus injections into the left submandibular gland (rat SM8). Virally infected neurones are shown after a survival time of 78 h. The brainmaps (upper panel, A and B) indicate the location of the photomicrograph C (lower panel) within the IC. Cortical labelling is mainly restricted to pyramidal cells in cortex layer 5, as shown in C for the contralateral side of virus injection. Bar = 100 μm. Drawings and abbreviations (see list) were modified from Swanson [45].

survival periods (71–96 h) did not show any viral infection in these cortical regions, although the insular cortex was consistently labelled in all cases (Table 1).

3.4. Virally infected neurones in the preoptic area

The preoptic area also showed infected neurones after pseudorabies virus injection into the submandibular or the sublingual gland with a dominance on the side ipsilateral to the virus injection (Fig. 2A,B, Fig. 3B, Fig. 4A, Fig. 6). A few infected cells were labelled at approximately the same time as the first appearance of neurones within cortical areas and the lamina terminalis (see below), however, the lateral preoptic area received this initial infection and not the medial preoptic area (Table 1, 66 h). The first wave of infection in the medial preoptic area occurred at slightly longer survival times (Table 1, 71–78 h). After a survival time of 71–78 h following injection of virus into the submandibular gland (Fig. 2A,B, Fig. 4A) infected neurones were primarily located in two ipsilateral sites within the preoptic area. One infected site within the rostral medial preoptic area was situated just lateral to the caudal OVLT, the second area was more caudal, extending dorsolaterally from the anteroventral preoptic nucleus through the medial preoptic area to the lateral part of the

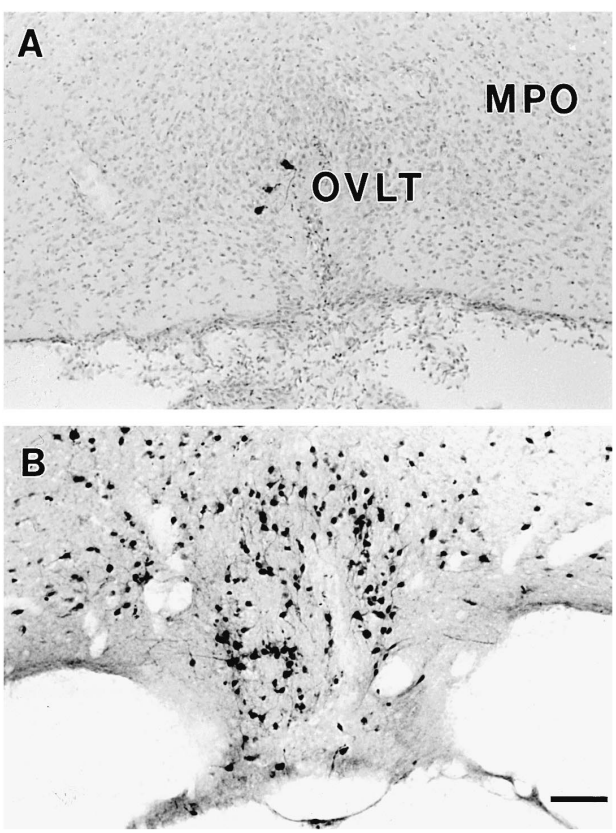

Fig. 6. Retrogradely traced cell bodies and nerve fibres in the OVLT and preoptic area after pseudorabies virus injections into the left sublingual gland. Virally infected neurones are shown after a survival time of 71 h (A, rat SL6) and 95 h (B, rat SL2). The influence of the survival time, but also the influence of a twofold higher volume of virus injection (2 μl) is demonstrated by the more advanced viral infection in the OVLT and the adjacent MPO (B). Bar = 100 μm. Abbreviations (see list) were modified from Swanson [45].

preoptic area (Fig. 2A,B). Cell counts revealed that the total numbers of infected neurones in both the medial and lateral aspects of the preoptic area were comparable to the magnitude of the infection seen within the hypothalamic paraventricular nucleus, the bed nucleus of the stria terminalis, the medial part of the central nucleus of the amygdala or the lateral hypothalamic area after a 71–78 h survival time (Fig. 3B). The strongest viral infection observed in this study was in animal SL2 from the 96 h survival time group (Table 1). A coronal section of the rostral medial preoptic area from this rat is shown in Fig. 6B and is compared with the degree of forebrain infection seen in animals from the 71–78 h survival time period having received sublingual (Fig. 6A, SL6) or submandibular pseudorabies virus injections (Fig. 4A, SM8). The differences detected in the degree of viral infection and in particular the absence of infection in the medial preoptic area in animal SL6 is most likely related to the shorter period of survival (71 h) and/or the smallest volume of virus injected (1 μl). However this difference was not reflected in the degree of infection observed in the hypothalamic paraventricular nucleus in these animals.

3.5. Virally infected neurones in the lamina terminalis

The first virally infected neurones in the lamina terminalis were detected after 3 days of survival (Table 1, 66–78 h). Longer survival times led to a more advanced degree of infection in each of its components, the OVLT, the median preoptic nucleus and the subfornical organ. The first wave of infection reliably appeared within 71–78 h of survival. Within the OVLT the labelling was primarily restricted to the lateral parts with only a few labelled neurones in the dorsal cap (Fig. 4A, Fig. 6). Virally infected neurones were scattered throughout all parts of the median preoptic nucleus (Fig. 4B). In the subfornical organ, a clear annular distribution of virally infected cells was found in coronal sections (Fig. 4C). Midline sagittal sections of two animals with pseudorabies virus injections into the submandibular gland and a survival time period of 73 and 76 h showed labelled cells along the entire lamina terminalis. The quantitative analysis performed in animal SM8 showed that the OVLT had the highest number of infected neurones followed by the median preoptic nucleus and the subfornical organ (Fig. 3A).

4. Discussion

The present study showed for the first time that viral infection occurred in central nervous system structures such as the lamina terminalis, the preoptic area and the insular cortex following virus injection into either the submandibular or the sublingual gland. Furthermore, by varying the period of survival, we were able to demonstrate a time dependent, stepwise infection of different forebrain nuclei efferently connected to the innervation of both glands. Consistent with previous findings, injections of pseudorabies virus into the submandibular or sublingual gland resulted in the infection of a number of forebrain regions. Some of these sites have already been demonstrated following virus injection into the submandibular gland of unilaterally sympathectomized animals using a 4 days tracing period [14]. However, the multisynaptic efferent projections of the lamina terminalis, the preoptic area and the insular cortex to the submandibular gland demonstrated in the present investigation were not detected in the previous viral tracing study. This discrepancy could simply be due to the use of different pseudorabies virus mutants and this is strengthened by the finding that two different pseudorabies virus strains are transported with different speed within the same pathways [5]. While in the present study the Bartha strain was used, the previous investigation from Jansen et al. [14] worked with a genetically engineered mutant of the Bartha strain which contained a *lacZ* gene insert. This alone could account for the different neurotropism and/or transneuronal transport time required to miss the labelling in the lamina terminalis, the preoptic area and the insular cortex.

4.1. Neuroanatomical aspects of viral infection in the lamina terminalis and the preoptic area

Pseudorabies virus injections into the submandibular or the sublingual gland revealed virally infected neurones in the lamina terminalis and the preoptic area. Viral infections in these forebrain structures have also been reported in the rat after pseudorabies virus injections in various other organs of the rat such as the heart [46], the esophagus, stomach and cecum [27], the urinary bladder [28] and the urethral sphincter [29]. The hypothesis has been put forward that central regulation of autonomic functions might be controlled by a 'visceral neuraxis' involving these anterior forebrain nuclei [27].

One of the concerns that has been raised particularly in relation to viral labelling in brain regions that lack a blood–brain barrier such as the circumventricular organs OVLT and the subfornical organ within the lamina terminalis after injection of virus into a peripheral organ is that some virus may have entered the blood stream and thereby led to infection of the central nervous system from the circulation. In the present study viral infection within these structures via direct polysynaptic pathways is more likely to be the case because the time taken for the first wave of viral infection to occur (3 days) is consistent with passage through neurones rather than a vascular route. Furthermore, direct injections of the virus into the circulation made by us (unpublished observation) and others [46] never led to viral infection within circumventricular organs or any other brain structures, precluding the possibility of uptake into other organs or tissues and subsequent transport to the central nervous system via this route.

The typical labelling pattern observed in the circumventricular organs was mainly restricted to the lateral parts of the OVLT and the outer rim of the subfornical organ. Although a variety of efferent projections from these circumventricular organs are known [17,26,31], a likely source for retrograde viral infection is from the hypothalamic paraventricular nucleus and/or the lateral hypothalamic area. These two forebrain structures contained the first wave of infected neurones after a 55 h tracing period and were therefore considered as third order neurones. Conventional tracing studies have already confirmed that neurones in the subfornical organ (originating in its perimeter) have efferent projections to the hypothalamic paraventricular nucleus or to the lateral hypothalamic area. In regard to the efferent neural connections of the OVLT, a recent study showed that microinjections of the retrogradely transported tracer cholera toxin B into the paraventricular nucleus led to labelling of neurones in the lateral parts of the OVLT [22]. This is similar to the distribution of virally infected neurones within the OVLT following virus injection into the salivary glands and suggests that this infection may have taken place via this third order relay. The first wave of infection coincidentally appeared within the entire lamina terminalis after a 3 day survival period (66–78 h). Therefore it is unlikely that the viral infection within the OVLT, subfornical organ or median preoptic nucleus resulted from the heavy reciprocal interconnection between the component structures within the lamina terminalis [17,26,31].

Similar to what is known about the efferent projections of the subfornical organ and the OVLT there is no evidence for a direct connection between the median preoptic nucleus and preganglionic (para-)sympathetic salivary centers. However the median preoptic nucleus has efferent projections to the hypothalamic paraventricular nucleus with terminals mainly restricted to the parvocellular parts [52], where viral infection was observed in the present study. We cannot exclude the possibility that viral infection of neurones in the median preoptic nucleus occurred via efferents to noradrenergic and serotonergic relay nuclei in the upper brainstem [53], especially from neurones of the locus coeruleus where virus has been detected simultaneously with the first forebrain labelling in the hypothalamic paraventricular nucleus and lateral hypothalamic area.

Injections of pseudorabies virus into the submandibular or sublingual gland led to viral infection within the preoptic area. Preoptic area labelling was also reported using the viral tracing technique after injections into the heart [46], the esophagus, stomach and cecum [27], the urinary bladder [28], the urethral sphincter [29], the kidney [41] and into the sympathetic stellate ganglion [15]. Many brain areas have been reported to receive efferent projections from the preoptic area [7,8,21,40,44], including the lateral hypothalamic area and the hypothalamic paraventricular nucleus. Due to the rich efferent connectivity of the preoptic area, not only could these hypothalamic areas have contributed to the infection seen in the preoptic area but also additional mesencephalic or brainstem third order neurones may have been involved (present study) [14]. Among likely possibilities are relay neurones in the dorsorostral mesencephalic periaqueductual gray which showed viral infection at the same postinoculation time as early third order labelling within the hypothalamus. The possibility exists that there are direct connections from preoptic neurones to parasympathetic preganglionic neurones controlling salivary function, however, as shown by Simerly and Swanson [40], the efferent projections from the medial preoptic area to this region are sparse.

4.2. Viral infection in the insular cortex

The viral labelling of neurones in the cerebral cortex following virus injection into the submandibular or sublingual gland is consistent with early clinical and experimental studies showing altered salivary function resulting from cortical stimulation [9,50]. Direct polysynaptic efferent connections to salivary glands from cortical pyramidal cells within particular parts of the cerebral cortex have been shown here for the first time at the cellular level. Three cortical regions are known to be linked to autonomic functions, the insular cortex, the frontal cortex and the sensorimotor cortex [6]. Each of these contained virally infected neurones after glandular virus injections, however, the most specific and consistent labelling was found in the insular cortex. Injections of pseudorabies virus into other peripheral organs such as the heart [46], the esophagus, stomach and cecum [27], the urinary bladder [28] and the urethral sphincter [29] also led to viral infection of cortical areas e.g. within the insular cortex. There is evidence in the literature that the insular cortex might be organized topographically [6,51] and that specific functions are controlled from distinct subareas. An interesting finding in this regard is that cortical retrograde labelling from the heart was mainly found in caudal parts of the insular cortex [46], whereas viral infection after submandibular or sublingual gland injection was predominantly present in rostral regions of the insular cortex, which would further support the topographical parcellation of this cortical structure. The first wave of viral infection in the insular cortex appeared after 3 days of survival. An anterograde tracing study described few fibre projections to the parvocellular reticular nucleus in the rostral medulla after tracer injection into the insular cortex [51], which would favour the idea of monosynaptic insular cortex projections to preganglionic parasympathetic salivatory centers in the rostral medulla. In addition to intercortical projections, major sites of efferent projections from the insular cortex are the central nucleus of the amygdala, the bed nucleus of the stria terminalis and the lateral hypothalamic area [6,51]. Of these, only the lateral hypothalamus showed viral infection after two days survival and might therefore account as

third order relay of virus to the insular cortex. Additional cortical output to potentially sympathetic outflow centers might be represented by the viral infection seen in the frontal and sensorimotor cortex after glandular pseudorabies virus injections. This is supported by the finding that conventional retrograde tracer injections into the rostroventrolateral medulla labelled cells within these cortical regions [1] and pseudorabies virus injections into the sympathetic stellate ganglia led to viral infection of the frontal cortex [15].

4.3. Viral infection in other forebrain structures

The degree of infection after 4 days in many of the forebrain areas (e.g. the hypothalamic paraventricular nucleus, the lateral hypothalamic area, the bed nucleus of the stria terminalis, and the central nucleus of the amygdala) resulting from inoculation of the submandibular gland with pseudorabies virus in sympathectomized animals [14], seemed to be comparable to the present findings reported after 3 days but with an intact innervation. Indeed this distinct set of labelled forebrain nuclei identified in these and other viral studies [15,27–29,39,41,46] are thought to be part of a central autonomic network with numerous interconnected central nervous system nuclei at various brain levels [23]. The additional structures found in the present study (e.g. the lamina terminalis, the preoptic area and the insular cortex) are likely to represent a rostral extension of this 'visceral neuraxis' [27]. It should be considered however that the set of forebrain regions labelled after injection of pseudorabies virus into a range of different peripheral end points is remarkably similar. This raises the question as to whether the nature of the infection in this forebrain autonomic network might be the neuronal innervation of the blood vessels common to all injected organs. Future studies will be required to specifically address this question.

4.4. Technical and general considerations

All neuronal retrograde tracing studies face the problem of distinguishing the type of innervation traced from the periphery and in the present study it is likely that the viral infection detected in the central nervous system reflects the diversity of the glandular effector cell innervation, e.g. efferent innervation of different secretory, myoepithelial or vascular cells [10]. Nevertheless the attenuated pseudorabies virus mutant (Bartha strain) appears to be the method of choice for investigating command lines involved in central regulation of autonomic functions [20,24] and much effort has been applied to demonstrate the specificity of this method in retrograde labelling of synaptic autonomic circuits within the central nervous system [3].

Previous studies investigating a possible anterograde transport of pseudorabies virus which would reflect sensory innervation of end organs, showed no or minor infection of dorsal root ganglia after viral injections into kidney, adrenal gland or muscle, which led the authors to the conclusion that viral infection seen in central sensory nuclei happened indirectly and retrogradely via the efferent system [16,37,39]. However, reports in the literature, and our own experimental experience, clearly showed viral infection in first order sensory neurones within dorsal root ganglia [28,49] or the trigeminal ganglia (data not shown), which led us to the point of view that the attenuated Bartha strain might have, though less, affinity for peripheral sensory systems and that anterograde viral transport is slower compared to the retrograde transport within the efferent innervation. Although such an anterograde transport might exist there would be still 'a window of opportunity' during which the first appearance of viral labelling within central structures is not influenced by transport within sensory pathways. If qualitative or quantitative analysis is then restricted to survival times after pseudorabies virus injections which show early neuronal infection, only backtraced efferent pathways should be involved. Furthermore this would be the period of primary infection, which is characterized by lack of neuronal lysis and therefore lack of potential nonspecific viral spread within neurones [3]. The survival times in this study were consequently varied in order to register the specific initial wave of efferent infection in distinct forebrain structures.

The order attributed to particular groups of neurones has been based on the timing of first appearance of successive, virally labelled populations. This is dependent on the assumption that the timing of transport and replication is comparable in all central neurones. The exceptions that have been recognized to date relate to the different transport time of alpha-herpes virus in sensory vs. efferent pathways [48] and in other investigations to situations where the central nervous system has been compromised, for example, by spinal transection [42]. In all other cases, the only determinant of the extent of infectivity has been the titer and the volume of virus injected [32]. In addition to the timing of transport as described above, our estimates of the hierarchical separation of forebrain efferents have taken into account data from tracing studies using conventional markers. For example, the description of neurones in the lamina terminalis as fourth order is an assumption consistent with known projections from this region to the paraventricular nucleus and lateral hypothalamic area [17,26,31] (see above).

Injections of virus into the sublingual gland showed in most cases a similar distribution of infected cells in forebrain structures as occurred in animals which received submandibular gland injections. The sublingual gland has been shown to have only minor sympathetic innervation [9] and therefore differences in viral forebrain infection might have been expected. However, this did not prove to be the case. A possible explanation might be the fact that the main secretory driving force of salivary glands is

thought to be the parasympathetic nervous system with only a modulatory role for the sympathetic nerves controlling the composition of saliva [9]. Therefore the results from pseudorabies virus injections to either gland may reflect mainly the central connections to the parasympathetic autonomic innervation. We are aware of the possibility that subdistributions of viral infection may occur in particular forebrain structures following submandibular or sublingual gland injections of virus, however, these remain undefined.

4.5. Functional aspects of viral infection in the lamina terminalis and the preoptic area

Saliva lost under heat stress has severe implications for the rat's body fluid economy and has been described as a factor contributing to thermal dehydration and subsequent thirst [2,12,36]. Thermo- as well as osmoresponsive neurones, characterised at the cellular level, are located in parts of the lamina terminalis and adjacent preoptic area [30,38]. Integration within these structures is likely to result in efferent control of both, osmoregulatory and thermoregulatory behaviour, and those neurones traced retrogradely from the submandibular or sublingual gland might influence salivary secretion under hyperthermic or hyperosmolar conditions. Indeed, an intact neuronal connectivity of the anteroventral wall of the third ventricle, involving lamina terminalis structures as well as medial parts of the preoptic area, is of particular importance for the control of body fluid homeostasis [17,25]. On the other hand, lesions of the anteroventral wall of the third ventricle, the preoptic area or the anterior hypothalamus in the rat led to severe deficits in regulating body temperature under heat stress and affected the secretory function of salivary glands [34,35,43,47]. During heat stress efferent thermoregulatory signals from the preoptic area are most likely to be transferred via the medial forebrain bundle system to the lateral hypothalamic area and/or the mesencephalic periaqueductual gray [11,18,43,54], finally inducing reflex salivation by activation of preganglionic parasympathetic salivary neurones in the rostral medulla connected to the submandibular or the sublingual gland (present study) [14]. This functional thermoregulatory pathway based in the past on physiological data now seems to have the neuroanatomical correlation, which shows the full polysynaptic efferent chain.

5. Abbreviations

ac	Anterior commissure
aIC	Agranular insular cortex
ARH	Arcuate nucleus
AVP	Anteroventral preoptic nucleus
BNSTov	Bed nucleus of the stria terminalis, anterior division, oval nucleus
BNSTpr	Bed nucleus of the stria terminalis, posterior division, principal nucleus
BNSTsc	Bed nucleus of the stria terminalis, anterior division, subcommissural zone
BNSTv	Bed nucleus of the stria terminalis, anterior division, ventral nucleus
CEAm	Central nucleus of the amygdala, medial part
CLA	Claustrum
GU	Gustatory cortex
IC	Insular cortex
LHA	Lateral hypothalamic area
LPO	Lateral preoptic area
MEAad	Medial nucleus amygdala, anterodorsal part
MnPO	Median preoptic nucleus
MOp	Primary motor cortex
MOs	Secondary motor cortex
MPO	Medial preoptic area
OVLT	Organum vasculosum of the lamina terminalis
PAA	Periarquate area
PVN	Hypothalamic paraventricular nucleus
py	Pyramidal tract
RCH	Retrochiasmatic area
rf	Rhinal fissure
SFO	Subfornical organ
SI	Substantia innominata
SPVO	Spinal trigeminal nucleus, oral part
SSs	Supplemental somatosensory cortex
VISC	Viscero-autonomic cortex
ZI	Zona incerta
VII	Facial nucleus
1–6	Cortex layers

Acknowledgements

This manuscript is dedicated to Ayse and Liana.

We would like to thank the CSIRO Australian Animal Health Laboratory in Geelong, Australia. The authors greatly appreciated the help and excellent technical assistance of L. Colvill and P. Davern. We would like to particularly thank Prof. Dr. E. Simon for his support. Dr. T. Hübschle was supported by a postdoctoral fellowship grant for the Advancement of Science by the Max–Planck-Society, Germany. The work was supported by an Institute Block Grant to the Howard Florey Institute by the National Health and Medical Research Council of Australia.

References

[1] S. Ba-M'Hamed, H. Sequeira, P. Poulain, M. Bennis, J.C. Roy, Sensorimotor cortex projections to the ventrolateral and the dorsomedial medulla oblongata in the rat, Neurosci. Lett. 164 (1993) 195–198.

[2] C.C. Barney, J.S. Williams, D.H. Kuiper, Thermal dehydration-induced thirst in rats: role of angiotensin II, Am. J. Physiol. 261 (1991) R1171–R1175.
[3] J.P. Card, L. Rinaman, R.B. Lynn, B.H. Lee, R.P. Meade, R.R. Miselis, L.W. Enquist, Pseudorabies virus infection of the rat central nervous system: ultrastructural characterization of viral replication transport and pathogenesis, J. Neurosci. 13 (1993) 2515–2539.
[4] J.P. Card, L.W. Enquist, Use of pseudorabies virus for definition of synaptically linked populations of neurons, Methods in Molecular Genetics, Academic Press, San Diego, 1994, pp. 363–382.
[5] J.P. Card, L.W. Enquist, Neurovirulence of pseudorabies virus, Crit. Rev. Neurobiol. 9 (1995) 137–162.
[6] D.F. Cechetto, C.B. Saper, Role of the cerebral cortex in autonomic function, in: A.D. Loewy, K.M. Spyer (Eds.), Central Regulation of Autonomic Function, Oxford Univ. Press, New York, 1990, pp. 208–223.
[7] T. Chiba, Y. Murata, Afferent and efferent connections of the medial preoptic area in the rat: a WGA-HRP study, Brain Res. Bull. 14 (1985) 261–272.
[8] L.C. Conrad, D.W. Pfaff, Efferents from medial basal forebrain and hypothalamus in the rat: I. An autoradiographic study of the medial preoptic area, J. Comp. Neurol. 169 (1976) 185–219.
[9] N. Emmelin, Nervous control of salivary glands, in: C.F. Code, W. Heidel (Eds.), Handbook of Physiology, Williams and Wilkins, Baltimore, MD, 1967, pp. 595–632.
[10] N. Emmelin, Nerve interactions in salivary glands, J. Dent. Res. 66 (1987) 509–517.
[11] F.R. Hainsworth, A.N. Epstein, Severe impairment of heat-induced saliva-spreading in rats recovered from lateral hypothalamic lesions, Science 153 (1966) 1255–1257.
[12] F.R. Hainsworth, E.M. Stricker, A.N. Epstein, Water metabolism of rats in the heat: dehydration and drinking, Am. J. Physiol. 214 (1968) 983–989.
[13] F.R. Hainsworth, E.M. Stricker, Evaporative cooling in the rat: differences between salivary glands as thermoregulatory effectors, Can. J. Physiol. Pharmacol. 49 (1971) 573–580.
[14] A.S.P. Jansen, G.J. Ter Horst, T.C. Mettenleiter, A.D. Loewy, CNS cell groups projecting to the submandibular parasympathetic preganglionic neurons in the rat: a retrograde transneuronal viral cell body labeling study, Brain Res. 572 (1992) 253–260.
[15] A.S.P. Jansen, M.W. Wessendorf, A.D. Loewy, Transneuronal labeling of CNS neuropeptide and monoamine neurons after pseudorabies virus injections into the stellate ganglion, Brain Res. 683 (1995) 1–24.
[16] L. Jasmin, E. Carstens, A.I. Basbaum, Interneurons presynaptic to rat tail-flick motoneurons as mapped by transneuronal transport of pseudorabies virus: few have long ascending collaterals, Neuroscience 76 (1997) 859–876.
[17] A.K. Johnson, A.D. Loewy, Circumventricular organs and their role in visceral functions, in: A.D. Loewy, K.M. Spyer (Eds.), Central Regulation of Autonomic Function, Oxford Univ. Press, New York, 1990, pp. 247–267.
[18] K. Kanosue, T. Nakayama, H. Tanaka, M. Yanase, H. Yasuda, Modes of action of local hypothalamic and skin thermal stimulation on salivary secretion in rats, J. Physiol. (London) 424 (1990) 459–471.
[19] E. Kosar, H.J. Grill, R. Norgren, Gustatory cortex in the rat: I. Physiological properties and cytoarchitecture, Brain Res. 379 (1986) 329–341.
[20] H.G. Kuypers, G. Ugolini, Viruses as transneuronal tracers, Trends Neurosci. 13 (1990) 71–75.
[21] P.J. Larsen, A. Hay-Schmidt, J.D. Mikkelsen, Efferent connections from the lateral hypothalamic region and the lateral preoptic area to the hypothalamic paraventricular nucleus of the rat, J. Comp. Neurol. 342 (1994) 299–319.
[22] P.J. Larsen, J.D. Mikkelsen, Functional identification of central afferent projections conveying information of acute 'stress' to the hypothalamic paraventricular nucleus, J. Neurosci. 15 (1995) 2609–2627.
[23] A.D. Loewy, Central autonomic pathways, in: A.D. Loewy, K.M. Spyer (Eds.), Central Regulation of Autonomic Functions, Oxford Univ. Press, New York, 1990, pp. 88–103.
[24] A.D. Loewy, Pseudorabies virus: a transneuronal tracer for neuroanatomical studies, in: M.G. Kaplitt, A.D. Loewy (Eds.), Viral Vectors—Gene Therapy and Neuroscience Applications, Academic Press, San Diego, 1995, pp. 349–366.
[25] M.J. McKinley, R.J. Bicknell, D.K. Hards, R.M. McAllen, L. Vivas, R.S. Weisinger, B.J. Oldfield, Efferent neural pathways of the lamina terminalis subserving osmoregulation, Prog. Brain Res. 91 (1992) 395–402.
[26] R.R. Miselis, The efferent projections of the subfornical organ of the rat: a circumventricular organ within a neural network subserving fluid balance, Brain Res. 230 (1981) 1–23.
[27] R.R. Miselis, B.H. Lee, L.W. Enquist, J.P. Card, Characterization of the visceral neuroaxis by transneuronal passage of pseudorabies virus, Soc. Neurosci. 17 (1991) 545.13, (Abstract).
[28] I. Nadelhaft, P.L. Vera, J.P. Card, R.R. Miselis, Central nervous system neurons labelled following the injection of pseudorabies virus into the rat urinary bladder, Neurosci. Lett. 143 (1992) 271–274.
[29] I. Nadelhaft, P.L. Vera, Neurons in the rat brain and spinal cord labeled after pseudorabies virus injected into the external urethral sphincter, J. Comp. Neurol. 375 (1996) 502–517.
[30] B.J. Oldfield, E. Badoer, D.K. Hards, M.J. McKinley, Fos production in retrogradely labelled neurons of the lamina terminalis following intravenous infusion of either hypertonic saline or angiotensin II, Neuroscience 60 (1994) 255–262.
[31] B.J. Oldfield, M.J. McKinley, Circumventricular organs, in: G. Paxinos (Ed.), The Rat Nervous System, Academic Press, San Diego, 1995, pp. 391–403.
[32] J. Park, L.W. Enquist, R.Y. Moore, J.P. Card, The effect of viral concentration upon invasiveness, replication and transynaptic passage of pseudorabies virus injected into striatum, Soc. Neurosci. 22 (1996) 683.2, (Abstract).
[33] W. Penfield, Diencephalic autonomic epilepsy, Arch. Neurol. Psychiatr. 22 (1929) 358–374.
[34] A. Renzi, R.A. Lopes, M.A. Sala, L.A. Camargo, J.V. Menani, W.A. Saad, G.M. Campos, Morphological, morphometric and stereological study of submandibular glands in rats with lesion of the anteroventral region of the third ventricle (AV3V), Exp. Pathol. 38 (1990) 177–187.
[35] A. Renzi, E. Colombari, T.R. Mattos-Filho, J.E. Silveira, W.A. Saad, L.A. Camargo, L.A. De-Luca-Junior, J.G. Derobio, J.V. Menani, Involvement of the central nervous system in the salivary secretion induced by pilocarpine in rats, J. Dent. Res. 72 (1993) 1481–1484.
[36] R.C. Ritter, A.N. Epstein, Saliva lost by grooming: a major item in the rat's water economy, Behav. Biol. 11 (1974) 581–585.
[37] D.M. Rotto-Percelay, J.G. Wheeler, F.A. Osorio, K.B. Platt, A.D. Loewy, Transneuronal labeling of spinal interneurons and sympathetic preganglionic neurons after pseudorabies virus injections in the rat medial gastrocnemius muscle, Brain Res. 574 (1992) 291–306.
[38] T.E. Scammell, K.J. Price, S.M. Sagar, Hyperthermia induces c-*fos* expression in the preoptic area, Brain Res. 618 (1993) 303–307.
[39] L.P. Schramm, A.M. Strack, K.B. Platt, A.D. Loewy, Peripheral and central pathways regulating the kidney: a study using pseudorabies virus, Brain Res. 616 (1993) 251–262.
[40] R.B. Simerly, L.W. Swanson, Projections of the medial preoptic nucleus: a Phaseolus vulgaris leucoagglutinin anterograde tract-tracing study in the rat, J. Comp. Neurol. 270 (1988) 209–242.
[41] D.J. Sly, B.J. Oldfield, Identification of neural pathways to the kidney using the neurotropic virus pseudorabies (PRV), Proc. Aust. Neurosci. Soc. 8 (1997) 32, (Abstract).

[42] A. Standish, L.W. Enquist, J.A. Escardo, J.S. Schwaber, Central neuronal circuit innervating the rat heart defined by transneuronal transport of pseudorabies virus, J. Neurosci. 15 (1995) 1998–2012.
[43] E.M. Stricker, F.R. Hainsworth, Evaporative cooling in the rat: effects of hypothalamic lesions and chorda tympani damage, Can. J. Physiol. Pharmacol. 48 (1970) 11–17.
[44] L.W. Swanson, An autoradiographic study of the efferent connections of the preoptic region in the rat, J. Comp. Neurol. 167 (1976) 227–256.
[45] L.W. Swanson, Brain Maps: Structure of the Brain, Elsevier, Amsterdam, The Netherlands, 1992.
[46] G.J. Ter Horst, R.W.M. Hautvast, M.J.L. De-Jongste, J. Korf, Neuroanatomy of cardiac activity-regulating circuitry: a transneuronal retrograde viral labelling study in the rat, Eur. J. Neurosci. 8 (1996) 2029–2041.
[47] D.M. Toth, Temperature regulation and salivation following preoptic lesions in the rat, J. Comp. Physiol. Psychol. 82 (1973) 480–488.
[48] G. Ugolini, Transneuronal tracing with alpha-herpesviruses: a review of the methodology, in: M.G. Kaplitt, A.D. Loewy (Eds.), Viral Vectors—Gene Therapy and Neuroscience Applications, Academic Press, San Diego, 1995, pp. 293–317.
[49] M.L. Weiss, G.K. Fitch, Renal afferent circuitry: complementary results from c-FOS and virus studies, Soc. Neurosci. 22 (1996) 707.4, (Abstract).
[50] T. Yamamoto, Role of the cortical gustatory area in taste discrimination, in: R.H. Cagan (Ed.), Neural Mechanisms in Taste, CRC Press, Boca Raton, FL, USA, 1989, pp. 197–219.
[51] Y. Yasui, C.D. Breder, C.B. Saper, D.F. Cechetto, Autonomic responses and efferent pathways from the insular cortex in the rat, J. Comp. Neurol. 303 (1991) 355–374.
[52] A.M. Zardetto-Smith, R.L. Thunhorst, M.Z. Cicha, A.K. Johnson, Afferent signalling and forebrain mechanisms in the behavioral control of extracellular fluid volume, Ann. N.Y. Acad. Sci. U.S.A. 689 (1993) 161–176.
[53] A.M. Zardetto-Smith, A.K. Johnson, Chemical topography of efferent projections from the median preoptic nucleus to pontine monoaminergic cell groups in the rat, Neurosci. Lett. 199 (1995) 215–219.
[54] Y.H. Zhang, K. Yamada, T. Hosono, X.M. Chen, S. Shiosaka, K. Kanosue, Efferent neuronal organization of thermoregulatory vasomotor control, Ann. N.Y. Acad. Sci. U.S.A. 813 (1997) 117–122.

5.2.

5.2. MATHAI, M.L., HÜBSCHLE, T. & McKINLEY, M.J. (2000)

Central angiotensin receptor blockade impairs thermolytic and dipsogenic responses to heat exposure in rats.

Am. J. Physiol. **279** (5): R1821-R1826.

Eigener Anteil an der Publikation:

- Beteiligung an der Versuchsplanung (30 %)
- Durchführung der Versuche (50 %)
- Beteiligung an der Zusammenfassung und Veröffentlichung der Ergebnisse (20 %)

Am J Physiol Regulatory Integrative Comp Physiol
279: R1821–R1826, 2000.

Central angiotensin receptor blockade impairs thermolytic and dipsogenic responses to heat exposure in rats

M. L. MATHAI, T. HÜBSCHLE, AND M. J. McKINLEY
Howard Florey Institute, University of Melbourne, Parkville, Victoria 3052, Australia

Received 18 October 1999; accepted in final form 13 July 2000

Mathai, M. L., T. Hübschle, and M. J. McKinley. Central angiotensin receptor blockade impairs thermolytic and dipsogenic responses to heat exposure in rats. *Am J Physiol Regulatory Integrative Comp Physiol* 279: R1821–R1826, 2000.—The effect of central angiotensin AT_1 receptor blockade on thermoregulation and water intake after heat exposure was investigated. Rats were placed in a chamber heated to 39 ± 1°C for 60 min and then returned to their normal cage (at 22°C), and water intake was measured for 120 min. Artificial cerebrospinal fluid (5 μl) was injected intracerebroventricularly 60 min before heat exposure in five control rats. Colonic temperature increased from 37.22 ± 0.21 to 40.68 ± 0.31°C after 60 min. In six rats injected intracerebroventricularly with 10 μg of the AT_1 antagonist losartan, colonic temperature increased from 37.41 ± 0.27 to 41.72 ± 0.28°C after 60 min. This increase was significantly greater than controls ($P < 0.03$). Losartan-treated rats drank 1.1 ± 0.4 ml of water compared with 5.9 ± 0.77 ml ($P < 0.002$) drank by control animals, despite a similar body weight loss in the two groups. Central losartan did not inhibit the drinking response to intracerebroventricular carbachol in heated rats, suggesting that losartan treatment did not nonspecifically depress behavior. We conclude that central angiotensinergic mechanisms have a role in both thermoregulatory cooling in response to heat exposure and also the ensuing water intake.

thirst; saliva; heat defense

DURING EXPOSURE to a hot environment, mammals regulate their core temperature by a number of mechanisms that include increased circulation of warm blood from the body core to the surface and evaporative cooling from the body surface. In the rat, cutaneous vasodilation redirects heat to the body surface and evaporative cooling is achieved by spreading of saliva onto the skin and fur. If drinking water is not available during heat exposure, the rats become dehydrated over time (27). There is evidence that the water drinking response to thermal dehydration is correlated with the increase in plasma sodium and osmolality (3). The major forebrain sites regulating these body functions are in the preoptic and hypothalamic regions (7, 15, 25). Different inputs from thermal and osmotic sensors are integrated there with the subsequent neural output modulating autonomic and neuroendocrine pathways influencing thermoregulatory and osmoregulatory effector organs (9, 13, 22, 23).

The role of angiotensin has been investigated as a signaling molecule for both thermoregulatory and fluid balancing effector pathways. In the rat, there is evidence that ANG II may be a central transmitter inducing heat-loss mechanisms (29, 31). Fregly and Rowland (10) showed that central administration of the AT_1-receptor antagonist losartan inhibited the hypothermic effect of intracerebroventricular ANG II. Brain structures in the lamina terminalis, such as the subfornical organ (which lacks a blood-brain barrier) and the median preoptic nucleus, may have a role in this function (9). ANG II receptors of the AT_1 subtype are present in these regions, and blockade of AT_1 receptors with systemically administered losartan prevented tail vasodilation induced by systemic administration of ANG II (10). However, Horowitz et al. (14) showed that neither systemic nor central AT_1 receptor blockade had any effect on the tail vasodilatory response to heat exposure or the onset of salivation in naive rats. These investigators suggested rather that ANG II signaling is directed at acclimatization to a hot environment by accelerating the onset of evaporative heat loss.

The lamina terminalis also has a crucial role in regulating angiotensin-induced drinking behavior and other aspects of body fluid homeostasis (22, 23, 30). Thermogenic drinking induced in cold-acclimated rats transferred back to room temperature has been partly attributed to the central action of circulating ANG II (9). Barney et al. (4) used captopril-induced blockade of systemic ANG II to investigate a role for ANG II in drinking after thermal dehydration. However, they found no difference in the drinking response, suggesting that peripherally formed ANG II is not involved in thermogenic drinking. The aim of the present study was twofold: to investigate the possible involvement of ANG II in the drinking response to thermally induced dehydration, concentrating in particular on angiotensinergic mechanisms within the brain, and second, to investigate a role for central angiotensinergic mechanisms in heat-defense pathways during exposure to a hot environment.

Address for reprint requests and other correspondence: M. McKinley, Howard Florey Institute, Univ. of Melbourne, Parkville 3052, Australia (E-mail: mmck@hfi.unimelb.edu.au).

The costs of publication of this article were defrayed in part by the payment of page charges. The article must therefore be hereby marked "*advertisement*" in accordance with 18 U.S.C. Section 1734 solely to indicate this fact.

EXPERIMENTAL PROCEDURES

All experimental protocols received prior approval from the Animal Ethics Committee of the Howard Florey Institute, which adheres to the Australian code of practice for the care and use of animals for scientific purposes.

Animal preparation. Male Sprague-Dawley rats (315–355 g body wt) were used in this study. Animals were anesthetized with Nembutal (60 mg/kg ip) and underwent surgical implantation of a metal cannula (23 gauge) into the right lateral cerebral ventricle. The cannula was anchored to the skull with screws embedded into dental acrylic. Two weeks later, the patency of the ventricular probe was established by a positive drinking response to an injection of 10 ng ANG II in 2 μl of artificial cerebrospinal fluid (aCSF). Experiments involving heat exposure commenced 3 days after the drinking test.

In preliminary experiments, all rats treated with intracerebroventricular aCSF survived heat exposure (39°C) for up to 120 min, but some unexpected deaths occurred in the intracerebroventricular losartan-treated group when the dosage of losartan was 100 μg and the period of heat exposure was 90 min. Consequently, the dose of losartan was decreased 10-fold and the time of exposure to heat exposure was reduced to 60 min for both experimental groups. In addition, we imposed a condition based on ethical considerations that heat exposure was stopped if colonic temperature reached 42°C. After these changes to the protocol, all animals survived the procedure in good condition, displaying alert responses and free movement.

Plasma data. To provide data on changes that occur in plasma ions and protein concentration during heat exposure, a blood sample (300 μl) was collected from rats treated with either losartan (10 μg in 5 μl aCSF; $n = 5$) or aCSF (5 μl; $n = 5$) by cutting the distal tip of the tail (0.5–1 mm). Once bleeding had stopped, the rats were returned to their home box without food or water access and placed in a chamber with an ambient temperature of 39 ± 1°C. After 1 h, the rats were removed from the heated chamber and another blood sample was collected. These rats were not used in the experiments that monitored body temperature and drinking responses to heat exposure. Plasma ion and protein concentrations were measured using a Beckman Synchron CX-5 (Beckman-Coulter). Plasma osmolality was measured using a Fiske one-ten osmometer (Fiske Associates).

Central AT_1 receptor blockade and short-term heat exposure. On the day of the experiment at 1100, rats were given an injection into the lateral ventricle of either 5 μl aCSF or 10 μg of the ANG II AT_1 receptor antagonist losartan (DuPont-Merck) in 5 μl of aCSF. Temperature was measured by K-type thermocouples connected to a dual channel Fluke 52 (John Fluke MFG) electronic thermometer that was calibrated to two decimal places against a conventional glass mercury thermometer. To measure deep body temperature, a thermocouple (coated in silicon at the tip) was inserted 5 cm into the anal sphincter of each rat. The tip of the thermocouple and connecting wires were coated with 5% lidocaine gel (Xylocaine, Astra Pharmaceuticals) as a local anesthetic and lubricant. To indirectly measure active cutaneous vasodilation via temperature changes of the tail skin, a second thermocouple was attached to the skin 3 cm distal to the root of the tail. The insulated wires from both thermocouples were secured to the tail using cloth tape, taking care to further insulate the tail skin thermocouple. The thermocouple wires were very flexible and light (0.5-mm diameter), allowing the rat free movement around its home cage. The body weights of the rats were measured, and they were returned for the next hour to their home cages. Recording of rectal and tail skin temperature began 10 min before the rat (while in its home cage) was put into the heat chamber for baseline measurements. The floor of the cage was lined with blotting paper that had been treated with cresyl red (11). This paper stained pink on contact with saliva (compared with yellow-brown on contact with urine), and this indicator, together with spreading of the saliva on the skin and fur, allowed visual confirmation that evaporative cooling behavior was intact. After transfer into the preheated heating chamber, the wires connected to the thermocouples were brought out of the chamber through a small hatch in the top cover. This experimental procedure was well tolerated by all animals. The temperature of the heat chamber was maintained at 39 ± 1°C by a thermostat connected to a ceramic-coated heating element. Air was circulated around the chamber by a fan situated underneath the heating element to provide an even distribution of heat.

During heat exposure (1 h), colonic and tail skin temperature were continuously monitored and recorded at 2-min intervals for 60 min. At the end of this period, the rat was taken from the heat chamber and the thermocouples were removed before it was weighed again and then returned to a fresh cage at room temperature (22°C). Each rat was then given access to water using a 20-ml graduated glass cylinder connected to a drinking spout, and water intake was monitored at 15-min intervals for a total of 120 min.

Effect of losartan on intracerebroventricular carbachol-induced drinking. In another set of experiments, the specificity of the effect of losartan on the drinking response to short-term heat exposure was tested using intracerebroventricular injection of carbachol (carbamylcholine chloride, Sigma-Aldrich), a cholinergic agonist, that is known to induce drinking via a central mechanism that is independent of angiotensin (5). As in the first set of experiments, rats were treated with intracerebroventricular injections of either losartan (10 μg in 5 μl of aCSF) or 5 μl of aCSF vehicle alone 1 h before heat exposure. However, after 1 h of heat exposure, animals were given an additional intracerebroventricular injection of carbachol (300 ng or 1.25 μg in 2 μl of aCSF) and water intake was measured for 120 min.

Statistical analysis. Plasma ionic and protein data in animals treated with losartan or aCSF before and after heat exposure were analyzed by a paired *t*-test.

In animals where body temperatures were continuously measured, colon and tail skin temperatures were collated for each 2-min interval and expressed as means ± SE. Data for the aCSF-treated and the losartan-treated groups of animals were then tested by repeated-measures analysis of variance with a post hoc Bonferroni correction (SigmaStat, Jandel Scientific). Similarly, water-intake data were compared between aCSF- and losartan-treated groups, with and without the intracerebroventricular injection of carbachol after heat exposure.

For each animal, the volume of saliva that was collected on the cresyl red-treated paper was determined by calculating the total surface area of the stains over 1 h and dividing the total area by a known volume-to-surface area constant (200 μl = 12.5 cm^2). These data were collected for both aCSF- and losartan-treated groups, and statistical significance was determined by a Student's *t*-test (SigmaStat, Jandel Scientific).

RESULTS

Table 1 shows plasma measurements in rats that received an intracerebroventricular injection of either aCSF ($n = 5$) or losartan ($n = 5$) before and after they

Table 1. *Plasma sodium, chloride, osmolality and protein concentration in rats treated with either aCSF (5 μl) or losartan (10 μg in 5 μl of aCSF)*

	aCSF		Losartan	
	Baseline	60 min	Baseline	60 min
Na, mmol/l	146.0 ± 0.3	148.0 ± 0.4*	145.1 ± 0.5	147.0 ± 0.3*
Cl, mmol/l	107.4 ± 1.5	113.8 ± 1.5*	105.3 ± 0.9	111.4 ± 1.6*
Osm, mosmol/ kgH_2O	306.2 ± 2.5	311.2 ± 2.3*	307.2 ± 1.6	312.6 ± 1.5*
Protein, g/l	60.6 ± 2.5	62.6 ± 2.8	64.5 ± 1.6	65.6 ± 1.2

Values are means ± SE (n = 5 rats). Rats were compared before and after 60 min exposure to a 39°C environment. Data were compared before and after heat exposure for each group of animals (*$P < 0.01$). aCSF, artificial cerebrospinal fluid.

were exposed to a 39°C environment. In both groups, equivalent increases in plasma sodium, chloride, and osmolality were measured after 1 h of heat exposure. Changes in plasma protein were not statistically significant in either group.

Effect of central AT_1 receptor blockade on temperature regulation and body weight loss during short-term heat exposure. In the control group that received intracerebroventricular aCSF, colonic temperature increased steadily during heat exposure from 37.22 ± 0.21 to 40.68 ± 0.31°C (Fig. 1). In the intracerebroventricular losartan-treated group, colonic temperature increased to a significantly higher level compared with the controls, rising from 37.41 ± 0.27 to 41.72 ± 0.28°C ($P < 0.03$) by the end of the period of heat exposure (Fig. 1). Tail skin temperature increased rapidly in both groups of animals during heat exposure, rising from 25.40 ± 0.41°C to a maximum of 39.45 ± 0.37°C at the end of heat exposure in the control group. In losartan-treated animals, tail temperature increased from 26.4 ± 0.47 to a maximum of 41.12 ± 0.37°C, which was significantly higher than in the control group ($P < 0.05$). This result was consistent with the higher rectal temperature that was observed in losartan-treated animals relative to controls.

Both losartan- and aCSF-treated groups lost 13.0 ± 2 g of body weight during exposure to heat exposure. Grooming and licking behavior was observed in all animals exposed to the heat. In addition, increased salivation was present in both experimental groups as shown by the saliva records (cresyl red-incubated filter papers). Area analysis of the saliva records revealed that an equivalent of 2.7 ± 0.3 ml of saliva was collected in the group treated with intracerebroventricular losartan compared with 2.2 ± 0.2 ml (not significantly different) in the group treated with intracerebroventricular aCSF. These values are only approximations, because all the rats intermittently spread the saliva from their mouths onto their skin during grooming. Furthermore, the spread of the saliva spots would have been inhibited by the high rate of evaporation in the heat chamber. Although this method substantially underestimates the actual volume of saliva produced, it does provide an indication of the relative rate of salivation between the two experimental groups.

Effect of central AT_1 receptor blockade on water intake after short-term heat exposure. In the control group, rats initiated water drinking within 30 min after the end of the period of heat exposure. They drank a total of 5.9 ± 0.7 ml by 120 min after heat exposure (Fig. 2). In rats treated with losartan, the drinking response to heat exposure was inhibited and the volume of water drunk was reduced to 1.1 ± 0.3 ml ($P < 0.002$) at the end of the 120-min observation period.

To test whether the blockade of the drinking response to heat exposure was specific to the pharmacological antagonism of central angiotensin rather than a consequence of the rats being debilitated, an additional experiment was performed. Both aCSF- and losartan-pretreated rats initiated drinking within 8 min after having received an intracerebroventricular injection of carbachol (300 ng or 1.25 μg in 2 μl). Both groups of rats also drank similar volumes of water during the 120-min period after the carbachol injection in a dose-dependent manner (Fig. 3).

DISCUSSION

The major finding of this study is that a central angiotensin AT_1 receptor-dependent pathway is involved in thermoregulatory cooling mechanisms and in the drinking response after heat exposure. Previous studies in the rat and rabbit have suggested that central injection of ANG II can reduce core temperature (19, 28, 29, 31) and have cited evidence of decreased metabolic rate and increased cutaneous heat loss. These reports are consistent with the current observation that core temperature of rats increases at a faster rate during pharmacological blockade of central AT_1

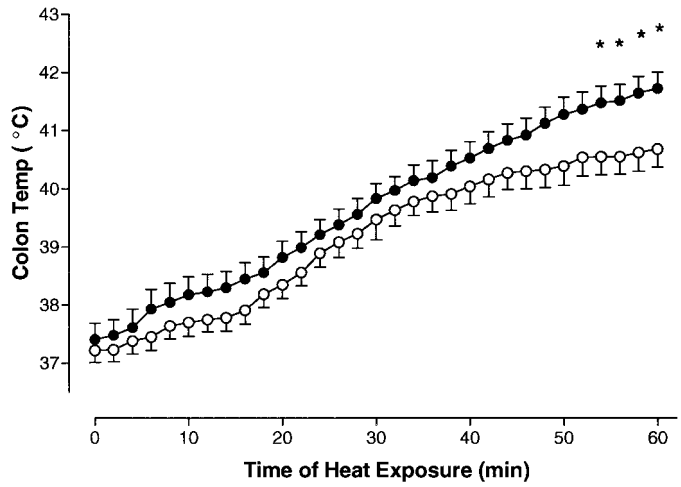

Fig. 1. Core temperature during heat exposure in conscious rats. During 1-h exposure to a 39°C environment, colonic temperature (T_c) was measured at 2-min intervals in 5 rats treated with intracerebroventricular injection of 5 μl of artificial cerebrospinal fluid (aCSF; ○) and 6 rats treated with intracerebroventricular injection of losartan (10 μg in 5 μl aCSF, ●). T_c was observed to increase to a higher level in losartan-treated rats (*$P < 0.05$).

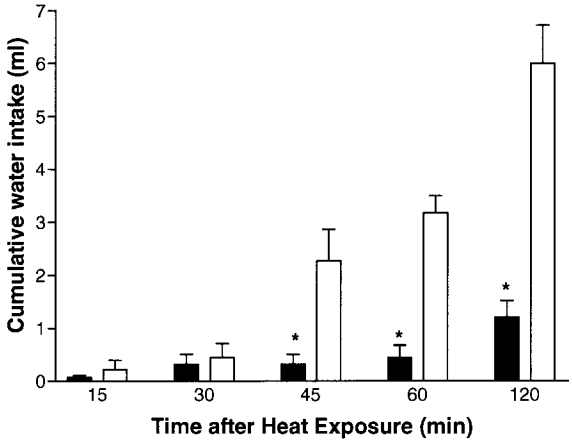

Fig. 2. Cumulative water intake in rats after 1-h exposure to a 39°C environment. Losartan-treated rats (black bars, $n = 6$) initiated water drinking later and drank significantly less than control rats injected intracerebroventricularly with aCSF (open bars, $n = 5$, $^*P < 0.05$).

receptors during short-term heat exposure. The exact location and the precise mode of this central disruption to normal thermoregulation remains to be elucidated; however, hypothalamic sites expressing AT_1 receptors, such as the lamina terminalis or the hypothalamic paraventricular nucleus, are possible sites of losartan influences on thermoregulation (1).

There was no difference in body weight loss between the control and losartan-treated groups and also no difference in grooming behavior, suggesting that there was no change in evaporative heat loss arising from the spreading of saliva on the skin and fur. Indeed, area analysis of stains on saliva records did not reveal a difference between the two experimental groups, confirming that this aspect of thermoregulation was not disrupted by centrally administered losartan. Similarly, tail skin vasodilation during heat exposure was not inhibited by losartan treatment, in agreement with previously reported data in the rat (17). The data in the present study show ostensibly that despite the activation of major thermoregulatory cooling mechanisms (such as cutaneous vasodilation and/or saliva spreading), core temperature increased to a higher level in losartan-treated rats compared with control animals. An increase in core temperature has been shown to be associated with increases in lumbar, renal, and splanchnic sympathetic nerve activity (16). Thus, during heat exposure, sympathetically mediated vasoconstriction might be important for blood flow redistribution to areas with a high surface area-to-volume ratio (such as the tail) and also to the vascular bed of the salivary glands to facilitate heat-loss mechanisms. In rats subjected to a similar heating protocol, Kregel et al. (17) showed that central AT_1 receptor blockade causes a reduction in blood pressure. In addition, by measuring regional nerve activity, these workers demonstrated that losartan treatment prevented the usual increase in splanchnic nerve activity and they suggest that this would reduce the redistribution of blood flow to the skin during heat exposure. These results fit well with our data during short-term heat exposure that show that central losartan treatment resulted in an increased core temperature. It is possible that when splanchnic vasoconstriction is attenuated (17) during heat exposure, pooling of blood in the viscera might reduce the efficacy of cutaneous heat-loss mechanisms, eventually leading to the observed increase in colonic temperature.

During heat exposure, water is lost during evaporative cooling, which leads to thermal dehydration and consequent thirst (2, 12, 27). Our experimental protocol increased plasma sodium and osmolality without significantly changing the protein concentration. Thus it is more likely that thirst arising from heat exposure is driven by osmotic signaling rather than by hypovo-

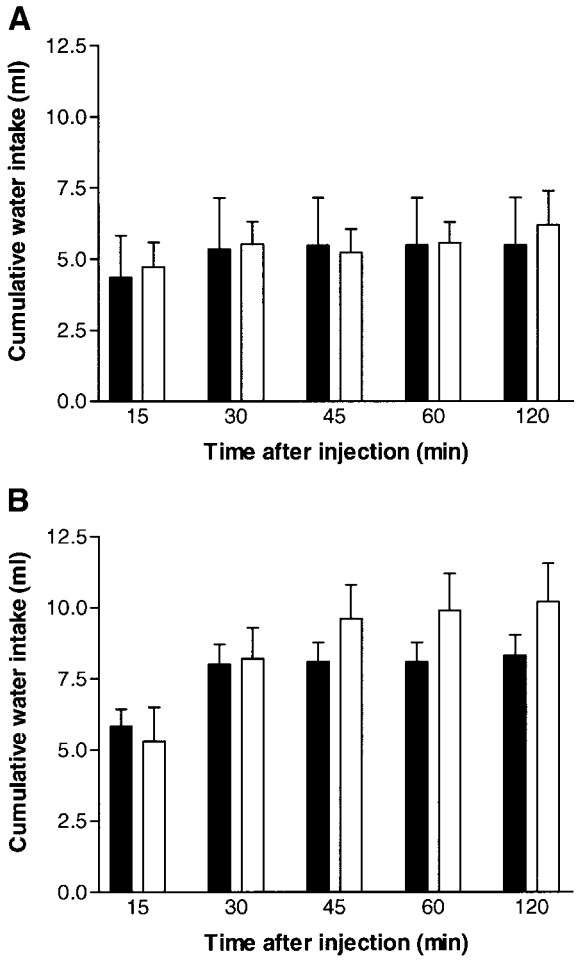

Fig. 3. Cumulative water drinking in response to intracerebroventricular carbachol after 1 h of heat exposure in rats treated with either intracerebroventricular aCSF (open bars) or losartan (10 μg, black bars). Two doses of carbachol were tested: 300 ng (*A*) and 1.25 μg (*B*). *A*: losartan ($n = 4$)- and aCSF-treated ($n = 4$) rats were exposed to a 39°C temperature for 1 h. After heat exposure, rats were given an intracerebroventricular bolus injection of carbachol (300 ng in 2 μl aCSF) and cumulative water intake was measured. Similar volumes were drunk by both groups. *B*: losartan ($n = 5$)- and aCSF-treated ($n = 5$) rats were exposed to the same thermal stimulus and then injected with a higher dose of intracerebroventricular carbachol (1.25 μg in 2 μl aCSF). Both groups of rats drank similar volumes, which were greater than at the lower dose of carbachol.

lemia. Other studies have also shown that thermogenic thirst in rats has a smaller volemic component than water deprivation-induced thirst (3, 24, 26), and, therefore, plasma ANG II levels should also be less elevated. In agreement, systemic blockade of ANG II formation with captopril failed to significantly alter thermogenic water intake after heat exposure (4). The present study demonstrated, however, that water intake after heat-induced fluid loss is attenuated by blockade of central AT_1 receptors. This is a novel finding that has several parallels in the literature relating to central angiotensinergic influences on water drinking in response to intracerebroventricular hypertonic NaCl (6, 20) and feeding (21) in a number of mammals. Therefore, we hypothesize that thermal dehydration does not activate water drinking via the peripheral renin-angiotensin system, but that neural pathways, using centrally generated ANG II, are involved in drinking after heat exposure.

The experiment using carbachol as a central dipsogen after a 1-h period of heat exposure was performed to eliminate the possibility that the inhibitory effect of losartan on water intake might have been due to the rats feeling unwell. This possibility was investigated because of our observations in preliminary experiments, which showed that a 10-fold higher dose of losartan increased the mortality rate of rats subjected to a twofold longer period of heat exposure. Barney and West (3) also reported that rats sometimes appeared "semi-comatose" after a long-term period (3–4 h) of heat exposure at 40°C, which delayed their drinking response. Because of the higher rectal temperature observed in the present study in losartan-treated rats, we were careful to check that all rats were alert and exhibited free movement after heat exposure. This experiment clearly showed that even with the combined treatment of heat exposure and losartan, rats responded to intracerebroventricular carbachol with appropriate drinking behavior, suggesting that this combination of higher body temperature and central losartan treatment did not nonspecifically depress drinking behavior. In addition, the fact that losartan treatment did not inhibit the dipsogenic response to intracerebroventricular injection of carbachol after heat exposure is consistent with earlier studies showing that carbachol-induced drinking is independent of neurochemical pathways using angiotensin (5, 8).

Perspectives

Central blockade of ANG II AT_1 receptors not only significantly reduced the drinking response to short-term heat exposure, but also led to a significantly higher body temperature. Therefore, a central angiotensinergic pathway appears to be important in mediating thermogenic drinking and the thermoregulatory response to heat exposure in the rat. Barney and West (3) reported a 13.6% mortality rate for rats subjected to long-term heat exposure (3–4 h, 40°C), with no deaths occurring before this time period. It is likely that pharmacological blockade of central angiotensin inhibits thermoregulatory cooling and may eventually increase mortality as well as disrupt fluid replacement in response to thermal dehydration. Whether this general impairment of heat defense is a specific effect on central body temperature control or secondary to alterations of body fluid distribution has yet to be clarified.

We thank Prof. Eckhart Simon for critical reading of the manuscript and Craig Thomson for excellent technical assistance.

This study was supported by Institute Block Grant Key Number 983001 from the National Health and Medical Research Council of Australia and the G. Harold and Leila Y. Mathers Charitable Foundation. Dr. Thomas Hübschle was supported by a postdoctoral fellowship grant for the Advancement of Science by the Max-Planck Society, Germany.

Present address of T. Hübschle: Dept. of Veterinary Physiology, Justus Liebig University, Frankfurter Str. 100, D-35392 Giessen, Germany.

REFERENCES

1. **Allen AM, Paxinos G, Song KF, and Mendelsohn FAO.** Localization of angiotensin receptor binding sites in the rat brain. In: *Handbook of Chemical Neuroanatomy: Neuropeptide Receptors in the CNS*, edited by Björklund A, Hökfelt T, and Kuhar MJ. Amsterdam: Elsevier, 1992, vol. 11, p. 1–37.
2. **Barney CC.** Effects of preloads of water and saline on thermal dehydration-induced thirst. *Physiol Behav* 61: 763–769, 1997.
3. **Barney CC and West DR.** Control of water intake in thermally dehydrated rats. *Physiol Behav* 48: 387–395, 1990.
4. **Barney CC, Williams JS, and Kuiper DH.** Thermal dehydration-induced thirst in rats: role of angiotensin II. *Am J Physiol Regulatory Integrative Comp Physiol* 261: R1171–R1175, 1991.
5. **Beresford MJ and Fitzsimons JT.** Intracerebroventricular angiotensin II-induced thirst and sodium appetite in rat are blocked by the AT1 receptor antagonist, losartan (DuP 753), but not by the AT2 antagonist, CGP42112B. *Exp Physiol* 77: 761–764, 1992.
6. **Blair-West JR, Burns P, Senton DA, Ferraro T, McBurnie MI, Tarjan E, and Weisinger RS.** Thirst induced by increasing brain sodium concentration is mediated by brain angiotensin. *Brain Res* 637: 335–338, 1994.
7. **Crawshaw L, Grahn D, Wollmuth L, and Simpson L.** Central nervous regulation of body temperature in vertebrates: comparative aspects. *Pharmacol Ther* 30: 19–30, 1985.
8. **Fitzsimons JT.** Angiotensin, thirst and sodium appetite. *Physiol Rev* 78: 583–685, 1998.
9. **Fregly MJ.** Thermogenic drinking: mediation by osmoreceptor and angiotensin II pathways. *Fed Proc* 41: 2515–2519, 1982.
10. **Fregly MJ and Rowland NE.** Centrally mediated vasodilation of the rat's tail by angiotensin II. *Physiol Behav* 60: 861–865, 1996.
11. **Hainsworth FR and Epstein AN.** Severe impairment of heat-induced saliva-spreading in rats recovered from lateral hypothalamic lesions. *Science* 153: 1255–1257, 1966.
12. **Hainsworth FR, Stricker EM, and Epstein AN.** Water metabolism of rats in the heat: dehydration and drinking. *Am J Physiol* 214: 983–989, 1968.
13. **Horowitz M and Meiri U.** Thermoregulatory activity in the rat: effects of hypohydration, hypovolemia and hypertonicity and their interaction with short-term heat acclimation. *Comp Biochem Physiol A Physiol* 82: 577–582, 1985.
14. **Horowitz M, Kaspler P, Simon E, and Gerstberger R.** Heat acclimation and hypohydration: involvement of central angiotensin II receptors in thermoregulation. *Am J Physiol Regulatory Integrative Comp Physiol* 277: R47–R55, 1999.
15. **Keil R, Gerstberger R, and Simon E.** Hypothalamic thermal stimulation modulates vasopressin release in hyperosmotically stimulated rabbits. *Am J Physiol Regulatory Integrative Comp Physiol* 267: R1089–R1097, 1994.
16. **Kenney MJ, Claassen DE, Bishop MR, and Fels RJ.** Regulation of the sympathetic nerve discharge bursting pattern dur-

ing heat stress. *Am J Physiol Regulatory Integrative Comp Physiol* 275: R1992–R2001, 1998.
17. **Kregel KC, Stauss H, and Unger T.** Modulation of autonomic nervous system adjustments to heat stress by central ANG II receptor antagonism. *Am J Physiol Regulatory Integrative Comp Physiol* 266: R1985–R1991, 1994.
18. **Lin MT.** Effects of angiotensin II on metabolic, respiratory and vasomotor activities as well as body temperature in the rabbit. *J Neural Transm* 49: 197–204, 1980.
19. **Lin MT, Chandra A, and Jou JJ.** Angiotensin II inhibits both heat production and heat loss mechanisms in the rat. *Can J Physiol Pharmacol* 58: 909–914, 1980.
20. **Mathai ML, Evered MD, and McKinley MJ.** Central losartan blocks natriuretic, vasopressin and pressor response to central hypertonic NaCl in sheep. *Am J Physiol Regulatory Integrative Comp Physiol* 275: R548–R554, 1998.
21. **Mathai M, Evered MD, and McKinley MJ.** Intracerebroventricular losartan inhibits postprandial drinking in sheep. *Am J Physiol Regulatory Integrative Comp Physiol* 272: R1055–R1059, 1997.
22. **McKinley MJ, Bicknell RJ, Hards DK, McAllen RM, Vivas L, Weisinger RS, and Oldfield BJ.** Efferent neural pathways of the lamina terminalis subserving osmoregulation. *Prog Brain Res* 91: 395–402, 1992.
23. **McKinley MJ, Pennington GL, and Oldfield BJ.** Anteroventral wall of the third ventricle and dorsal lamina terminalis: headquarters for control of body fluid homeostasis? *Clin Exp Pharmacol Physiol* 23: 271–281, 1996.
24. **Nose H, Morita M, Yawata T, and Morimoto T.** Recovery of blood volume and osmolality after thermal dehydration in rats. *Am J Physiol Regulatory Integrative Comp Physiol* 251: R492–R498, 1986.
25. **Patronas P, Horowitz M, Simon E, and Gerstberger R.** Differential stimulation of c-fos expression in hypothalamic nuclei of the rat brain during short-term heat acclimation and mild dehydration. *Brain Res* 798: 127–139, 1998.
26. **Ramsay DJ, Rolls BJ, and Wood RJ.** Body fluid changes which influence drinking in the water deprived rat. *J Physiol (Lond)* 266: 453–469, 1977.
27. **Ritter RC and Epstein AN.** Saliva lost by grooming: a major item in the rat's water economy. *Behav Biol* 11: 581–585, 1974.
28. **Sharpe LG, Garnatt JE, and Olsen NS.** Thermoregulatory changes to cholinomimetics and angiotensin II, but not to the monoamines microinjected into the brain stem of the rabbit. *Neuropharmacology* 18: 117–125, 1978.
29. **Shido O and Nagasaka T.** Effects of intraventricular angiotensin II on heat balance at various ambient temperatures in rats. *Jpn J Physiol* 35: 163–167, 1985.
30. **Simpson JB.** The circumventricular organs and the central actions of angiotensin. *Neuroendocrinology* 32: 248–256, 1981.
31. **Wilson KM and Fregly MJ.** Angiotensin II-induced hypothermia in rats. *J Appl Physiol* 58: 534–554, 1985.

5.3.

5.3. HÜBSCHLE, T., MATHAI, M.L., McKINLEY, M.J. & OLDFIELD, B.J. (2001a)
Multisynaptic neuronal pathways from the submandibular and sublingual gland to the lamina terminalis in the rat - A model for the role of the lamina terminalis in the control of osmo- and thermoregulatory behaviour.
Clin. Exp. Pharmacol. Physiol. **28** (7): 558-569.

Eigener Anteil an der Publikation:

- Beteiligung an der Versuchsplanung (100 %)
- Durchführung der Versuche (100 %)
- Beteiligung an der Zusammenfassung und Veröffentlichung der Ergebnisse (90 %)

Clinical and Experimental Pharmacology and Physiology (2001) **28**, 558–569

Circumventricular Organs: Gateways to the Brain

MULTISYNAPTIC NEURONAL PATHWAYS FROM THE SUBMANDIBULAR AND SUBLINGUAL GLANDS TO THE LAMINA TERMINALIS IN THE RAT: A MODEL FOR THE ROLE OF THE LAMINA TERMINALIS IN THE CONTROL OF OSMO- AND THERMOREGULATORY BEHAVIOUR

Thomas Hübschle,* Michael L Mathai,* Michael J McKinley* and Brian J Oldfield*

**The Howard Florey Institute of Experimental Physiology and Medicine, University of Melbourne, Parkville, Victoria, Australia and Institute of Veterinary Physiology, Justus-Liebig-University, Giessen, Germany*

SUMMARY

1. The putative regulatory role of the lamina terminalis in the central control of salivation was investigated in the rat using the viral-tracing technique and Fos-immunohistochemistry.

2. Neurons situated in the lamina terminalis, such as the vascular organ of the lamina terminalis (OVLT), median preoptic nucleus (MnPO) and subfornical organ (SFO), were retrogradely labelled after pseudorabies virus injections into the submandibular or sublingual gland.

3. Viral tracing combined with glandular denervation showed that lamina terminalis structures sent efferents, in particular, to the parasympathetic side of submandibular gland innervation.

4. Saliva lost under heat stress has severe implications for the body fluid economy of rats and a key to the understanding of the central regulation of heat-induced salivation may be the integrative role of the lamina terminalis processing thermoregulatory and osmoregulatory information.

Key words: lamina terminalis, osmoregulation, pseudorabies virus, salivary glands, thermoregulation, viral tracing.

INTRODUCTION

Rats exposed to extreme heat stress (40°C) neither sweat nor pant. Instead, they activate other heat loss mechanisms, such as skin vasodilation, especially of the tail, and they also salivate and spread the saliva on their skin and fur to remove heat by evaporation. For saliva spreading, the submandibular and the sublingual glands are primary thermoregulatory effector organs under such conditions.[1] Saliva lost under heat stress has implications for the body fluid economy of the rat and contributes to thermal dehydration and subsequent thirst.[2–4] The importance of the lamina terminalis in the control of body fluid homeostasis has been intensively demonstrated and reviewed in the past.[5–7] Far less data are available concerning a possible role of the lamina terminalis in the control of body temperature. However, lesioning studies of the anteroventral wall of the third ventricle (AV3V) in the rat, which also included parts of the preoptic area or the anterior hypothalamus, led to severe deficits in regulating body temperature under heat stress and clearly affected the thermoregulatory secretory function of salivary glands.[8–11]

Recently, a powerful neuroanatomical tool has been established using trans-synaptic retrograde transport of an attenuated strain of pseudorabies virus (PRV-Bartha) for neuronal tract tracing.[12–17] It is clear that a prerequisite for a putative regulatory role of the lamina terminalis in the central control of salivation is the presence of neuronal connections to salivary gland innervation. Therefore, we used the viral tracing technique in our experiments, performing unilateral injections of PRV-Bartha into the left submandibular or sublingual gland, to address this question. Indeed, inoculation of the glands revealed multisynaptic neuronal pathways from these salivary glands to the entire lamina terminalis (Fig. 1) and also various other forebrain regions (Fig. 2).[18,19] A key to the understanding of the central regulation of heat-induced salivation in the rat may be the integrative role of the lamina terminalis processing thermoregulatory and osmoregulatory information.

PSEUDORABIES VIRUS INFECTION IN FOREBRAIN STRUCTURES AFTER SALIVARY GLAND INOCULATION

Lamina terminalis

Viral-infected neurons within the lamina terminalis were first detected 3 days (66–78 h) after unilateral inoculation of the submandibular or sublingual gland (Fig. 1). Longer postinoculation times led to a more advanced degree of infection in each of its components: the organum vasculosum of the lamina terminalis (OVLT), the median preoptic nucleus and the subfornical organ.

Correspondence: Thomas Hübschle, Institute of Veterinary Physiology, Justus Liebig University, Frankfurter Str. 100, D-35392 Giessen, Germany. Email: Thomas.Huebschle@vetmed.uni-giessen.de

Based on a paper originally presented at a meeting on the structure and function of the brain circumventricular organs, held in Port Douglas, Australia, 1997.

Received 7 February 2001; accepted 14 March 2001.

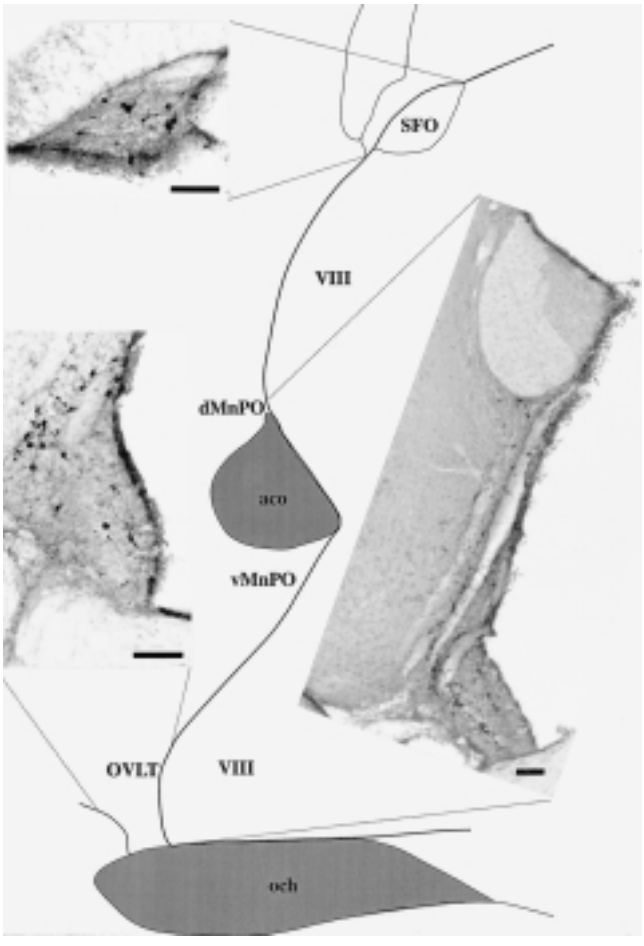

Fig. 1 Retrogradely traced cell bodies and nerve fibres in the lamina terminalis after pseudorabies virus (PRV) injection into the left submandibular gland. Viral-infected cells were found along the entire lamina terminalis in mid-sagittal brain sections. The brain map indicates the location of the three photomicrographs. For the two circumventricular organs (CVO), namely the organum vasculosum of the lamina terminalis (OVLT; lower left photomicrograph) and the subfornical organ (SFO; upper left photomicrograph), labelled cells and fibres were detected. Within the median preoptic nucleus (MnPO), here shown for its ventral component (v), virally infected cells and fibres could also be demonstrated (right photomicrograph). VIII, third ventricle; dMnPO, dorsal MnPO; aco, anterior commissure; och, optic chiasm. Bar, 100 µm. Drawing nomenclature modified from Swanson.[71]

A typical topographic labelling pattern was observed within the two circumventricular organs (CVO), namely the OVLT and the subfornical organ (SFO).[18] Infected cells within the OVLT were primarily restricted to the lateral parts, with only a few labelled neurons in the dorsal cap. In the SFO, a clear annular distribution of viral-infected cells was found. Although a variety of efferent projections from these CVO are known,[5,20,21] a likely source for retrograde viral infection is via relay neurons within the hypothalamic paraventricular nucleus (PVN) and/or the lateral hypothalamic area (see also later). Conventional tracing studies have already confirmed that neurons in the OVLT (originating in the lateral parts) and neurons in the SFO (originating in its outer rim) have efferent projections to magno- and parvocellular components of the hypothalamic PVN and/or to the lateral hypothalamic area.[20–26] Infected cells within the median preoptic nucleus were scattered within the ventral and the dorsal subnuclei. Sagittal sections near the midline clearly revealed infection along the entire lamina terminalis and, furthermore, that infected cells in the median preoptic nucleus not only bypassed the anterior commissure rostrally, but also caudally (between the ventricular ependym and the fibre tracts of the anterior commissure), connecting the ventral with the dorsal subnuclei. The first wave of infection coincidentally appeared within the entire lamina terminalis after a 3 day survival period. This eliminates the possibility that viral infection may have resulted from the marked reciprocal interconnection of those areas.[5,20,21] The number of infected neurons within the lamina terminalis 71–78 h postinoculation was highest in the OVLT followed by the median preoptic nucleus and the SFO.[18]

Other forebrain areas

With 71–78 h postinoculation time, unilateral PRV-Bartha injections into the submandibular or sublingual gland led to additional infection in other telencephalic and diencephalic forebrain structures, such as infection in cortical areas, the medial and lateral preoptic area, the bed nucleus of the stria terminalis, the central amygdaloid nucleus, the substantia innominata, the hypothalamic PVN, the dorsomedial hypothalamic nucleus, the lateral hypothalamic area, the zona incerta, the retrochiasmatic area, the arcuate nucleus and the periarcuate area (Fig. 2a). In most cases of sublingual gland inoculation, a similar distribution of forebrain infection was seen as for animals that received submandibular gland injections. Infection in the brain areas mentioned above was predominantly noticed on the ipsilateral side of PRV-Bartha injection, an observation consistent for all longer survival times examined. Using 55 h postinoculation time only, the lateral hypothalamic area and the hypothalamic PVN were ipsilaterally infected within the forebrain and may, therefore, be regarded as relay nuclei transmitting virus further rostrally. Labelled neurons within these nuclei were considered to be third-order neurons projecting, in all likelihood, to the preganglionic autonomic neurons in the rostral medulla or the thoracic spinal cord (second-order neurons) in the central command line supplying the salivary glands.

A complex central control of salivation is indicated by the many different forebrain nuclei labelled after virus injection into the salivary glands; however, this diverse set of nuclei may also reflect the fact that salivation is induced in response to a variety of different physiological demands (e.g. ingestive behaviour, immuneprotective functions within the oral cavity and the gastrointestinal tract, evaporative heat loss mechanism) and it is known that salivation may even be influenced by emotional state. In addition to a discussion about viral transport in the afferent innervation of a peripheral organ,[12–14,16,17] all neuronal retrograde tracing studies face the problem of distinguishing from each other the local functional diversity of the autonomic efferents traced from the periphery. Therefore, it is likely that the distributed forebrain infection detected after salivary gland inoculation also reflects the diversity of efferent glandular innervation; for example, secretory, myoepithelial or vascular smooth muscle cells.[27]

Effect of parasympathetic, sympathetic or total denervation on lamina terminalis infection

In a series of denervation experiments with ipsilateral chorda tympani destruction (parasympathectomy), removal of the superior cervical ganglion (sympathectomy) and total efferent denervation

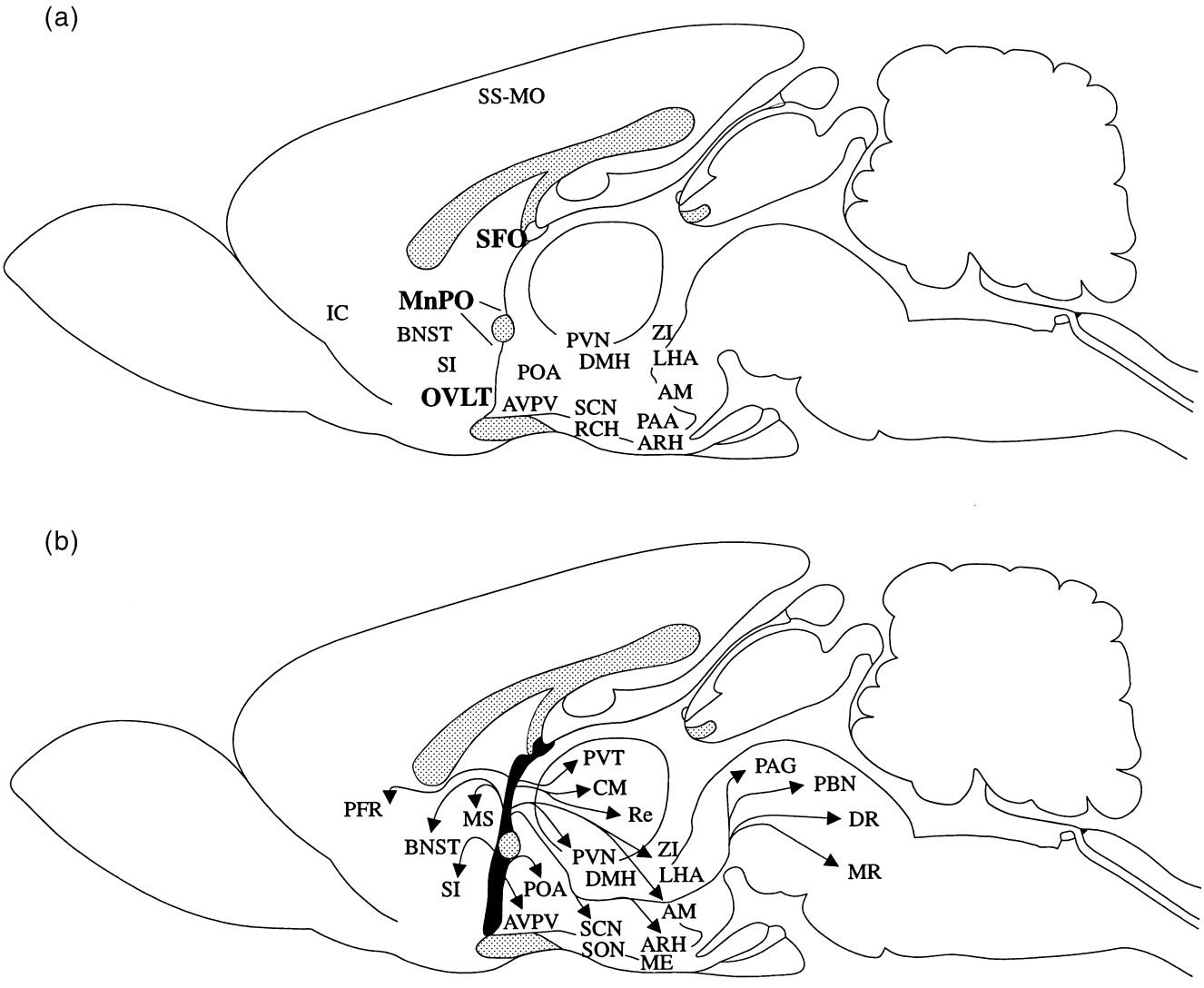

Fig. 2 Forebrain nuclei efferently connected to autonomic submandibular or sublingual gland innervation as revealed by the viral-tracing technique (a) compared with the efferent projections of the lamina terminalis characterized via conventional tracers (b). Retrogradely infected cells were detected in various forebrain nuclei 71–78 h after inoculation (a). At this time, all lamina terminalis structures (e.g. the organum vasculosum of the lamina terminalis (OVLT), the median preoptic nucleus (MnPO) and the subfornical organ (SFO)) showed the first wave of viral infection and were labelled coincidentally. Forebrain relay nuclei, where viral infection could have been transferred to lamina terminalis components, are depicted by the comparison of the viral-tracing results (a) with the already known efferent projections originating in the lamina terminalis (shown in the scheme as a thin black tissue layer of the anterior wall of the third ventricle; b). Two likely hypothalamic relay nuclei are the lateral hypothalamic area (LHA) and the hypothalamic paraventricular nuclei (PVN), which revealed the first wave of viral infection 55 h postinoculation (see also Table 1). However, it should be mentioned that viral transport time may differ in different neurons and, therefore, a clear-cut neuronal hierarchy is difficult to establish. PVT, thalamic paraventricular nucleus; CM, thalamic central medial nucleus; Re, nucleus reuniens; ZI, zona incerta; AM, amygdala; PAG, periaqueductal grey; PBN, parabrachial nucleus; DR, MR, dorsal and median raphe nucleus, respectively; ARH, DMH, hypothalamic arcuate and dorsomedial nucleus, respecitvely; ME, median eminence; SCN, suprachiasmatic nucleus; SON, supraoptic nuclei; POA, preoptic area; AVPV, hypothalamic anteroventral periventricular nucleus; SI, substantia innominata; MS, medial septal nucleus; BNST, bed nucleus of the stria terminalis; PFR, prefrontal cortex; SS-MO, somatosensory and motor cortex; IC, insular cortex; RCH, retrochiasmatic area; PAA, periarcuate area. Drawing nomenclature modified from Swanson.[71]

(parasympathectomy and sympathectomy) of the left submandibular gland, the influence of the denervation on forebrain infection induced by PRV-Bartha inoculation was investigated and compared with control animals (Fig. 3;Table 1). In order to assess the success of surgical denervation, the entry of the virus into the central nervous system (CNS) or its blockade was determined in each animal within the preganglionic autonomic neurons of the medullary salivatory nuclei (parasympathetic) and in the intermediolateral column of the thoracic spinal cord segments T1–T6 (sympathetic). Table 1 shows the infection determined in representative animals of all groups in the preganglionic autonomic neurons (second-order neurons) within the lateral hypothalamic area and the hypothalamic PVN (neurons labelled in those two hypothalamic nuclei 55 h after inoculation are, in all likelihood, third-order neurons) and within the lamina terminalis (putative fourth-order neurons). In the controls, the first wave of infection appeared coincidentally in all lamina terminalis structures after 3 days (66–78 h). Using the same postinoculation period, animals with total denervation and parasympathectomy did

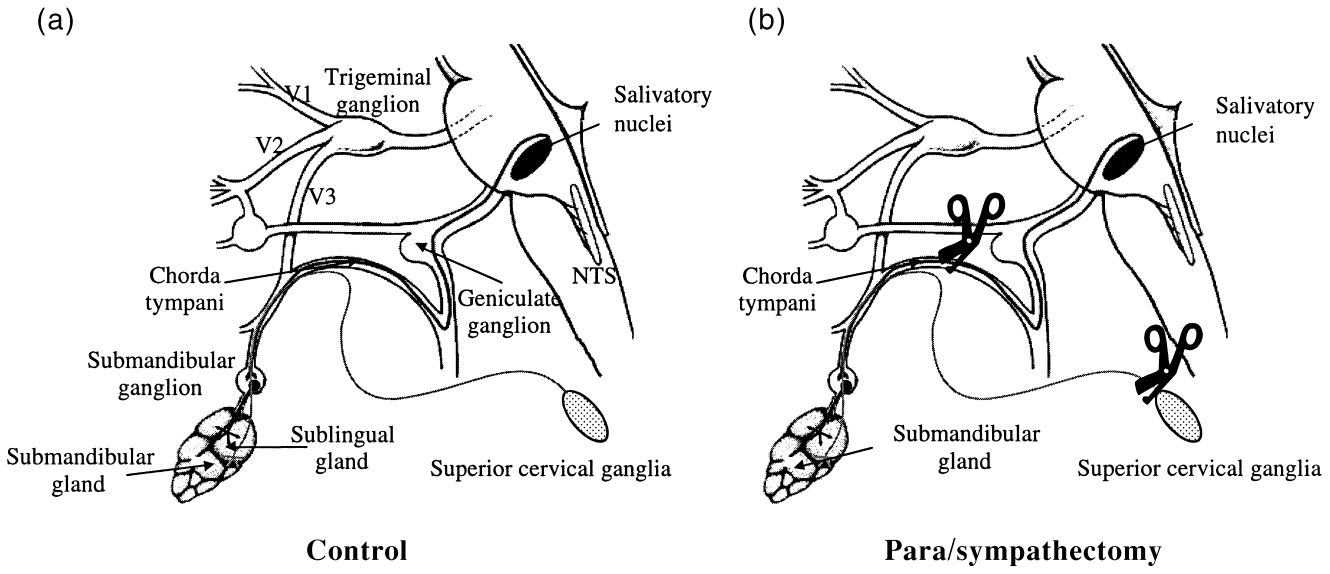

Fig. 3 Schemes of the efferent autonomic innervation of the rat submandibular and sublingual glands (a) and the specific location of denervation along the sympathetic and/or parasympathetic pathways (b). Unilateral sympathectomy (S), parasympathectomy (PS) and total unilateral efferent denervation (PS + S) on the left body side were combined with pseudorabies virus (PRV) injection into the left submandibular gland. In addition, denervated animals were compared with controls. Viral infection within the central nervous system was detected at three different postinoculation times (55, 66 and 71–78 h) and is listed in Table 1 for preganglionic autonomic neurons, hypothalamic nuclei and the lamina terminalis. One main result of these set of experiments is the fact that neurons showing the first wave of viral infection within the lamina terminalis are specifically connected to the parasympathetic innervation of the submandibular gland. V1, V2, V3, first, second and third branches of the trigeminal nerve, respectively; NTS, nucleus tractus solitarius.

Table 1 Effect of unilateral denervation on viral infection detected in second- (preganglionic autonomic neurons), putative third- (hypothalamic nuclei) and putative fourth-order (lamina terminalis) neurons after pseudorabies virus injection into the submandibular gland

	Postinoculation time (h)											
	55				66				71–78			
	Control	PS	S	PS + S	Control	PS	S	PS + S	Control	PS	S	PS + S
Preganglionic autonomic neurons												
Thoracic intermediolateral column (T1–T6)	+/–	+/–	–/–	–/–	+/C	+/C	–/–	–/–	+/C	+/C	–/–	–/–
Salivatory nuclei	+/–	–/–	+/–	–/–	+/C	–/–	+/2	–/–	+/C	–/–	+/C	–/–
Hypothalamic nuclei												
Lateral hypothalamic area	+/–	–/–	+/2	–/–	+/C	+/C	+/3	–/–	+/C	+/C	+/C	4/–
Paraventricular hypothalamic nucleus	+/–	+/–	1/1	–/–	+/C	+/C	1/–	–/–	+/C	+/C	+/C	1/–
Lamina terminalis structures*												
Subfornical organ	–	–	–	–	+	–	–	–	+	–	+	–
Median preoptic nucleus	–	–	–	–	+	–	–	–	+	–	+	–
Organum vasculosum lamina terminalis	–	–	–	–	+	–	–	–	+	–	+	–

+, five cells or more on the ipsilateral side of pseudorabies virus (PRV) injection; C, five cells of more on the contralateral side of PRV injection; 1–4, cell number on the ipsi- or contralateral side of PRV injection; S, unilateral sympathectomy; PS, parasympathectomy; PS + S, and total unilateral efferent denervation.

*Midline lamina terminalis structures with no separation of the ipsi- or contralateral side of PRV injection.

not show any viral infection in the lamina terminalis. However, infection was still present in selectively sympathectomized animals 71–78 h after virus injection. In a further control, the question of whether the surgical procedure itself may have influenced viral transport to the lamina terminalis was addressed by performing parasympathectomy on the side contralateral to virus injection. A comparison with controls showed no difference in the extent and distribution of forebrain infection 71–78 h after inoculation. This clearly indicates that the first wave of infection in the lamina terminalis is due to multisynaptic connections directed towards the parasympathetic innervation of the submandibular gland. This means, specifically, that neurons in the outer rim of the SFO, in the lateral OVLT and neurons scattered throughout the median preoptic nucleus do project to preganglionic parasympathetic neurons of the salivatory nuclei (superior and inferior) in the rostrolateral medulla along a pathway that becomes essentially unilateral at the mid-hypothalamic level.[28,29]

LAMINA TERMINALIS AS A FOREBRAIN SITE WITH VISCERAL MOTOR OUTPUT

Following submandibular or sublingual gland PRV injections, viral-infected neurons were seen in the lamina terminalis and the adjacent preoptic area. Viral infections in these forebrain structures

have also been reported in the rat after PRV injections in various other organs, such as the heart,[30] the oesophagus, stomach and caecum,[31] the urinary bladder[32] and the urethral sphincter.[33] The hypothesis was put forward that central regulation of autonomic functions may be controlled by a 'visceral neuraxis' involving these anterior forebrain nuclei.[31] Indeed, a distinct set of labelled forebrain nuclei identified in the present and other viral studies[19,30–37] is thought to be part of a central autonomic network with numerous interconnected CNS nuclei at various brain levels.[5,38] The lamina terminalis is likely to represent a rostral extension of this 'visceral neuraxis'.[5,25,31]

Lamina terminalis and efferent control of exocrine gland function

Direct functional evidence in the rat for the presumed involvement of lamina terminalis efferents in the control of salivary function is limited and data are mainly based on lesioning experiments in which destruction of the AV3V, including the OVLT, the ventral median preoptic nucleus and parts of the medial preoptic area or preoptic area lesions influenced submandibular gland morphology and secretion.[8,9,11,39] Now, the neural pathways to the salivary glands postulated on the basis of these functional studies to exist in the rat have been clearly identified by viral tracing (Figs 1,2a).[18]

The primary constituent of saliva is water and, indeed, in various mammalian species a link between body water homeostasis and salivary function has been suggested. In humans, for example, it is known that elderly people have a greater prevalence of dehydration and also often show salivary gland dysfunction (xerostomia). This knowledge led to a series of experiments in differently aged groups of healthy subjects testing the influence of 24 h dehydration on parotid salivary gland flow rates. The results showed that body dehydration led to decreased parotid gland salivation, thereby implying that salivary glands could be involved in the control of water balance as an accessory osmoregulatory effector organ.[40] Having in mind the outstanding importance of the lamina terminalis in integrative control of body water and electrolyte homeostasis and the above-presented viral tracing studies, one could speculate that efferents originating in these brain structures modulate saliva production under such hyperosmolal conditions.[5–7,41]

Different to humans, who dissipate heat by sweating, but similar to animals (e.g. dogs using open-mouth panting), the salivary glands of rats, especially the submandibular and the sublingual glands, function under certain physiological conditions (e.g. heat stress) as thermoregulatory heat loss effector organs.[1] Salivation is the autonomically controlled component of otherwise complex thermoregulatory responses engaged in dissipating body heat by evaporative water loss used by several mammalian species. During activation of evaporative heat loss mechanisms, rats spread saliva onto their body surface;[1,42–45] however, heat- or excercise-induced salivation in dogs, cats and rabbits is combined with tachypnoea (thermal panting).[46–51] The interference of osmoregulatory with thermoregulatory control of saliva production[2–4] was demonstrated by showing that hydrated dogs performing heavy excercise lost a 10-fold higher amount of water by salivation than dehydrated animals. Therefore, in dehydrated, hypovolaemic dogs, mechanisms are activated that counteract water loss by reducing the rate of saliva secretion[48] and this seems to be comparable to the situation known for the rat[52] and, more generally, to the inhibition of any drive for salivation by dehydration as, for example, in humans.[40] A well-known signal during dehydration is the rise in angiotensin (Ang) II plasma hormone levels and, consequently, inhibition of saliva flow rate by AngII, irrespective of its direct or indirect action on electrolyte composition, would be a likely assumption. Indeed, data based on experiments in which AngII was systemically applied or its endogenous generation was blocked, argue for an inhibitory effect of AngII on spontaneous or stimulated saliva flow in sheep,[53] rats[54] and humans.[55] It is interesting to note that the avian salt gland, a parasympathectically activated exocrine gland, although serving a completely different function, is powerfully inhibited by systemic infusions of AngII.[56]

For the brain-intrinsic AngII system, further comparative physiological studies in vertebrates on the central control of two other exocrine glands, namely the parotid gland in the sheep and the salt gland in the Pekin duck, also suggest an inhibitory action on parasympathetically controlled exocrine glands which is, in a way, compatible with the recent evidence for efferent lamina terminalis projections to the exocrine salivary glands in the rat. Secretion by these exocrine glands was inhibited by intracerebroventricular infusions of AngII into the lateral or the third cerebral ventricle, most likely via interaction with AngII receptors of the lamina terminalis (cf. the situation in sheep (ML Mathai and MJ McKinley, unpubl. obs., 1999) and Pekin duck[57,58]) and, thus, with the subsequent neural transfer of information to the autonomic innervation of these glands.

Lamina terminalis and efferent control of heat loss mechanisms

When heat stress is applied to dehydrated animals, AngII becomes involved as a signal modulating heat loss mechanisms according to the requirements of body fluid homeostasis. When exposed to heat stress or excercise-induced heat loads, some animals will counteract dehydration by a reduction of evaporative heat loss mechanisms simply to save water.[45,48] Under dehydrated conditions, plasma AngII levels should be elevated and, therefore, should centrally inhibit evaporative heat loss mechanisms and, indeed, during dehydration, the control of body fluids overrides the control of body temperature.[45]

In contrast, systemically applied AngII (a potent vasoconstrictor) in euhydrated rats was shown to activate heat loss by tail vasodilation, thereby reducing body temperature.[59] Lesions of the SFO and the dorsal median preoptic nucleus significantly reduced AngII-induced tail vasodilation, which suggests that systemic infusion of AngII acts centrally via mechanisms involving AngII receptors of the lamina terminalis.[60,61] Indeed, a recent viral-tracing study demonstrated multisynaptic efferent connections of the median preoptic nucleus to the sympathetic innervation of the rat tail (e.g. the arteriovenous anastomoses of its skin).[37] In addition, central blockade of the AngII AT_1 receptors in conscious, freely moving rats by intracerebroventricular infusions of losartan not only significantly reduced the drinking response to heat stress, but also led to a significantly higher body temperature.[62] This shows that centrally regulated thermoregulatory heat loss mechanisms are impaired in losartan-treated rats.

The observation of a temporary tendency for the increase in threshold temperature for salivation in the condition of short-term, but not long-term, heat exposure in rats[63] would seem to be in accordance with the assumption of a general inhibitory effect of AngII on salivation. However, especially in the control of heat defense,

the need for water conservation may divide the drive for heat loss away from the evaporative (panting, salivation) and towards the conductive (tail skin vasodilation) or even more towards behavioural heat defence, as has been demonstrated in rats[64] and pigeons.[65] If AngII is involved, this would explain its opposing actions on evaporative and nonevaporative heat loss mechanisms. Whether the general impairment of heat defence after blockade of central AngII actions[62] is a specific effect on central body temperature control or secondary to alterations of circulatory and/or fluid input and output control has yet to be clarified.

Indeed, central AT_1 receptor blockade not only impaired heat loss responses, but also attenuated heat stress-induced rises in blood pressure and decreased splanchnic sympathetic neuronal activity.[66] This centrally induced vasodilation in the vascular beds of the internal organs may have reduced cooling capacity during intracerebroventricular losartan infusions simply by reducing the pool of blood available for cutaneous heat exchange or for salivary secretion. In the light of the viral-tracing experiments shown herein, one likely brain site of AT_1 receptor blockade is the lamina terminalis, with its projections to the submandibular and sublingual glands as heat loss organs involved in evaporative heat dissipation. Concerning lamina terminalis projections to effector organs involved in convective heat loss mechanisms, for example tail skin vasodilation in the rat, two recent viral-tracing studies have revealed multisynaptic efferent pathways to the tail also originating from the lamina terminalis, such as from the median preoptic nucleus,[37] as well as from the OVLT and the SFO (JA Rathner *et al.*, unpubl. obs., 1998).

Sufficient evidence has been provided to support the notion of a central modulatory role of the neurohormone AngII in heat loss regulation during hyperthermia in the rat (*vide supra*). However, the neuronal circuitry in general and the role of brain structures expressing AngII receptors in particular and, moreover, the exact multisynaptic central command line integrating sensory information and transferring it to the periphery, are presently not understood. The sympathetic nervous system is known to be engaged in thermoregulatory heat loss responses by action on sweat glands or cutaneous blood vessels, but salivation in response to increasing body temperatures in dogs and rats is essentially mediated by parasympathetic fibres and forebrain output to the preganglionic parasympathetic salivary neurons. Consequently, heat-induced salivation is abolished by parasympathetic denervation.[10,27] Interesting in this context is the specific prevention of early viral infection within the lamina terminalis in the parasympathectomized but not sympathectomized animals, indicative of multisynaptic efferent connections either exclusively to the parasympathetic side of the autonomic salivary gland innervation or of a presumambly longer viral transport time via the sympathetic salivary gland innervation. Lesions of the AV3V and the preoptic–anterior hypothalamic area in the rat led to severe deficits in regulating body temperature under heat stress and impaired the secretory function of salivary glands.[8–11] Two major centrifugal pathways emerging from this forebrain area have been described, one taking a midline and the other a more lateral route.[67–72] The midline pathway passes the posterior hypothalamus, the midbrain periaqueductal grey (PAG) area, and then further down to the dorsal vagal complex.[73,74] After knife cut experiments along this midline pathway, a disruption of forebrain outflow to the sympathetic nervous system regulating cold-induced cutaneous vasoconstriction has been reported.[75] However, a later knife cut study[76] concluded that the preoptic–anterior hypothalamic area is not essential for autonomic thermoregulatory responses, which indicates that other thermoregulatory circuits, for example within the brainstem, are important as well. The one pathway that is likely to transfer neuronal information involved in regulation of the evaporative heat loss mechanism salivation is not the midline, but the lateral, pathway. It originates in the lamina terminalis and/or adjacent preoptic area, passes via the medial forebrain bundle system to the lateral hypothalamus, the ventral tegmental area and the PAG and terminates in the rostral medulla (T Hübschle *et al.*, unpubl. obs., 1999).[10,18,19,28,77] Further evidence for the lateral route comes from lateral hypothalamic lesioning experiments that severely impaired heat-induced saliva spreading in rats.[78] This led us to the hypothesis that, during heat stress, an integration of osmoregulatory and thermoregulatory afferent signals within the lamina terminalis is likely to result in efferent control of both osmoregulatory and thermoregulatory behaviour and that integrated forebrain output activates the parasympathetic innervation of the thermoregulatory effector organs, the submandibular and sublingual glands. Indeed, recent cFOS studies in the rat investigating the competitive CNS interplay between requirements for body fluid balance and temperature regulation point to the lamina terminalis and, in particular, the median preoptic nucleus as putative integrative centres for both autonomic control circuits.[79] These findings are strengthened by the fact that median preoptic nucleus neurons do express sensitivity for both thermal and osmotic stimuli.[80]

LAMINA TERMINALIS INTRINSIC OSMO- AND THERMORESPONSIVENESS AND SENSORY INPUT

Under hyperthermic conditions, afferent information is likely to be transferred to the lamina terminalis to integrate body temperature signals with the osmoregulatory circuitry. Generally there would be three possible ways of information transfer:

1. Lamina terminalis intrinsic neuronal sensitivity to both thermal and osmotic stimuli.
2. Neuronal afferent transfer to lamina terminalis structures originating from different thermosensitive sites.
3. Humoral afferent transfer relayed via the sensory CVO OVLT and SFO.

Lamina terminalis neurons as generation sites for thermo- and osmoregulatory signals: Intrinsic versus synaptic responsiveness

Neurons influenced *in vivo* by thermo- as well as osmostimulation, as characterized at the cellular level using cFos immunocytochemistry, are located in parts of the lamina terminalis and the adjacent preoptic area.[79,81–83] Our own studies imposing heat stress (2 h, 40°C) on rats have also revealed cFos immunoreactive cells in the lamina terminalis. In particular, cells within the median preoptic nucleus seemed to be activated (Fig. 4). The osmotic challenge induced through intraperitoneal hypertonic sodium chloride injections specifically activated cells within the lamina terminalis.[82,84–87] However, there is the problem with short-term cFos responses that some neuronal activation in the lamina terminalis may be induced by the stress of the injection procedure *per se*.[23] However, such

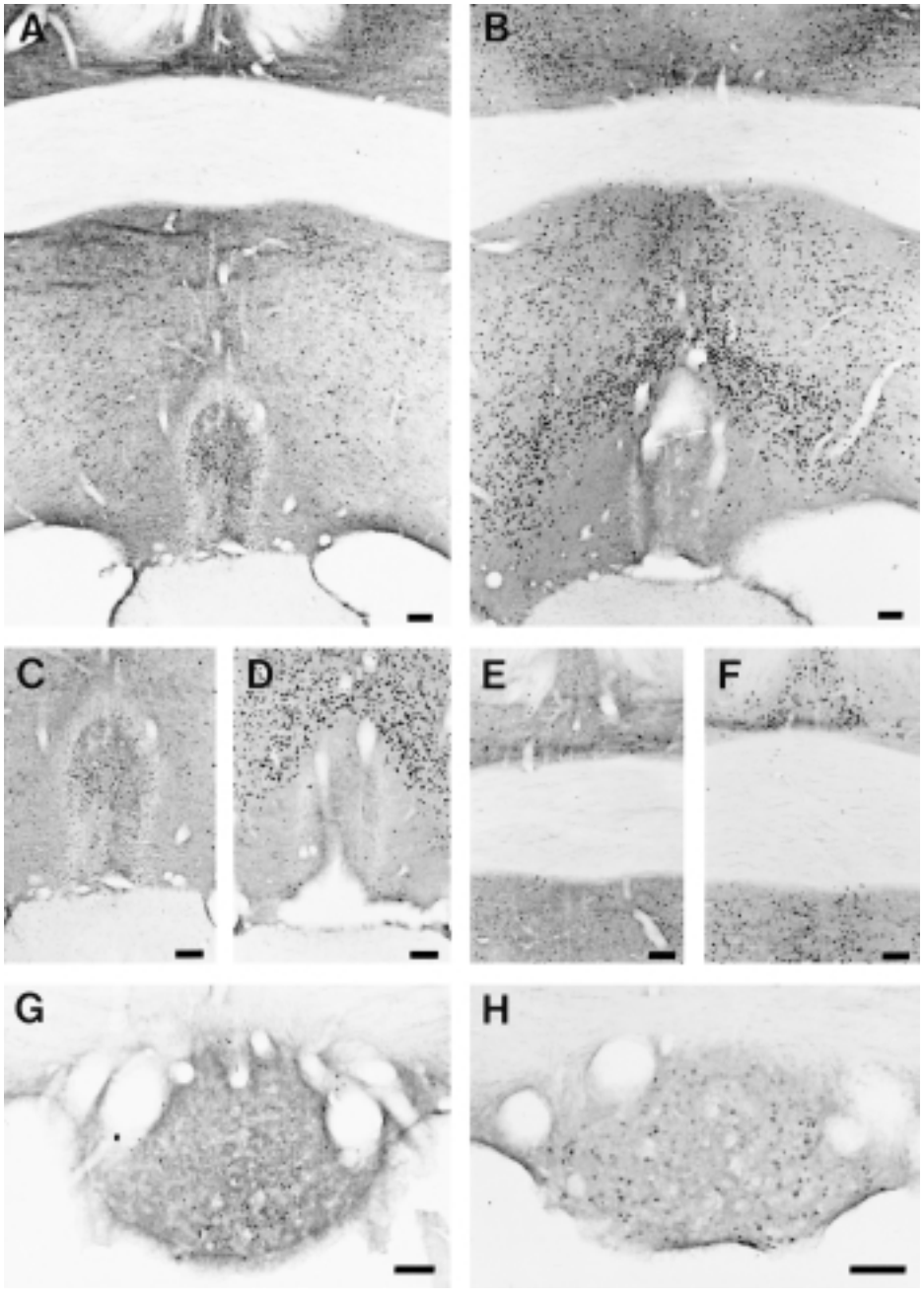

Fig. 4 Distribution of cFos-immunoreactive cell nuclei in coronal sections of the rat brain at the level of the organum vasculosum of the lamina terminalis (a–d), the median preoptic nucleus (a,b,e,f) and the subfornical organ (g,h). Representative sections for control rats (a,c,e,g) are compared with representative sections obtained from heat stressed (2 h, 40°C) animals (b,d,f,h). Cells that were activated during heat stress within the lamina terminalis are found, in particular, within the median preoptic nucleus (b,d,f). Bar, 100 µm.

a non-specific response component may be excluded for more sustained cFos activations, because they were shown to be induced by longer-lasting thermal and osmotic challenges.[79]

With regard to direct responsiveness, either intrinsic to the neuron under consideration or due to stimulation-induced changes of synaptic transmission in local neuronal circuitries, there is electrophysiological evidence for a population of neurons in the preoptic area that not only respond to local thermal but also osmotic stimuli.[88,89] This indicates an overlap of inputs, even at the single-unit level of the neuronal networks, by which thermo- and osmoregulatory neuronal circuitries are established. In addition, many of the recorded preoptic neurons displayed responsiveness to a variety of endogenous factors. Such multiresponsive neurons may serve as single-unit integrative structures on which the interdependence of the regulations of body fluid and temperature balance is based.[88,90,91] Multiresponsive neurons have also been characterized within the lamina terminalis, for example within the median preoptic nucleus of the rat[80] and within the OVLT and the SFO of the Pekin duck.[92] In addition, electrophysiological studies have proven neurons in the median preoptic nucleus and SFO of the rat and sheep to be osmosensitive.[93,94]

To our knowledge, there is no information about efferent projections of lamina terminalis neurons that are responsive to local or remote thermal stimuli. However, more data exist on the connectivity of lamina terminalis neurons that are osmoresponsive. The origin of local osmoresponsiveness within the lamina terminalis, whether cell intrinsic, for example transduced by stretch-sensitive cation channels as shown for magnocellular neurosecretory

neurons,[95,96] by other hitherto non-identified ionic mechanisms or synaptically generated, has not been identified. However, it is clear that mutual interconnections exist conveying information from the lamina terminalis to the neurosecretory supraoptic nuclues and PVN.[41,97–100] Osmosensitive neurons in the median preoptic nucleus and SFO are also efferently connected to a specific cell group in the lateral hypothalamic area and dehydration of rats induces peptidergic gene expression within this subarea of the lateral hypothalamus.[101] This result is analogous to that of our viral-tracing studies, in which we have found viral protein in the identical subarea of the lateral hypothalamus after PRV injections into the submandibular or sublingual glands of the rat.[18] Moreover, cFos activation in response to heat stress (2 h, 40°C) was also prominent in the same subarea (T Hübschle, unpubl. obs., 1999). Thus, each line of evidence independently supports the view that this brain area is a favourite relay station for osmo- and thermoregulatory information from the lamina terminalis to the salivary glands.

Lamina terminalis neurons as target sites for thermo- and osmoregulatory signals: Neuronal sensory inputs

The lamina terminalis and, in particular, its components located on the brain side of the blood–brain barrier (i.e. the median preoptic nucleus and the medial aspects of the ventromedial preoptic area) are brain structures from where humorally or neurally generated, integrated information originates and clearly affects autonomic as well as behavioural responses. The functional and neuroanatomical aspects of the connections to and from these brain regions have been extensively reviewed.[5–7] In the light of the angiotensinergic modulation of the state of thermoregulation under hyperthermic conditions, Kregel *et al*.[66] postulated that:

> '… although both osmoreceptors and cardiopulmonary volume receptors are likely to be involved in stimulating AngII release in the brain during hyperthermia, it is also possible that thermoreceptor inputs to the CNS may participate in modulating the central action of AngII and subsequent sympathetic nervous system and endocrine responses.'

It has to be added that, of course, thermoeffector activities controlled also by somatomotor and parasympathetic visceromotor efferents have to be included. Especially for the latter system, the role of the salivary glands as components of evaporative heat dissipating mechanisms have to be considered and our own studies have specified the underlying information pathway from the lamina terminalis to these glands.

Besides the interconnectivity of lamina terminalis structures,[20,21,102,103] several afferent inputs to this forebrain region have been described. Lamina terminalis afferents originate within the lateral hypothalamic area, the parvocellular PVN, the dorsomedial hypothalamic nucleus, the zona incerta, the nucleus reuniens of the thalamus, the dorsal and median raphe, the parabrachial nuleus, the nucleus tractus solitarius and the ventrolateral medulla.[24,25,104–106] In terms of thermoafferent information during hyperthermia, important afferents are assumed to originate from the adjacent preoptic and anterior hypothalamic areas that have been clearly identified as sites of deep-body temperature perception.[90] Corresponding morphological evidence has been provided for the preoptic region[67–69] and for the anteroventral preoptic area,[106] recently renamed as ventromedial preoptic area.[107,108] In addition, early and more recent electrophysiological *in vivo* studies have also demonstrated thermal inputs to neurons of the preoptic area, but also to anterior and more caudal hypothalamic regions that originate in the skin, in the spinal cord and in the lower brainstem.[109] These thermal inputs are conveyed by spinal anterolateral tract neurons and their brainstem homologues via interneurons directing information to the hypothalamus from the sensory pathways that ultimately terminate at cortical, via thalamic, neurons. Thus, preoptic area and adjacent lamina terminalis regions have to be considered as part of the thermosensory as well as thermointegrative brainstem network. With respect to the underlying cytoarchitecture, no functional organization on the basis of regional subnuclei has so far been elucidated for neural control of body temperature, a situation different from the rather well-defined cytoarchitecture of the osmoregulatory system. However, our viral-tracing studies have revealed two main topographically independent preoptic subareas traced retrogradely after PRV injections into the submandibular and sublingual glands of the rat[18] as organs involved in fluid excretion for the purpose of thermoregulatory evaporative heat dissipation. Indeed, in the lateral preoptic area, at a location similar to that reached retrogradely by the virus from the salivary glands, local thermal stimulation induced salivary secretion.[28] Whether these neurons project to or receive projections from the lamina terminalis, in particular the median preoptic nucleus, is presently not known.

Lamina terminalis neurons as target sites for thermo- and osmoregulatory signals: Humoral inputs

The two so-called 'sensory' CVO of the lamina terminalis, the OVLT and the SFO, are known as central receptive sites on the blood side of the blood–brain barrier, where hormones circulating in the blood can signal the physiological status of the body to the brain. This view is well established for AngII,[6,110] to some degree also for natriuretic peptides[110,111] and, most recently, also for hormones released in the process of digestion from the pancreas.[112] For the salivary glands, the concept has been put forward that the submandibular glands not only serve exocrine but also endocrine functions and this is well established for peptides like nerve growth factor,[113–115] epidermal growth factor[116] and kinins.[117–119] In view of the role of growth factors in tissue repair, it is hypothesized that the submandibular gland participates in the regulation of systemic homeostasis.[120–123] In addition, the submandibular gland is assumed to liberate a factor that regulates cardiovascular responses in the condition of shock induced by endotoxin, because it has been shown that bilateral removal of the superior cervical ganglia (sympathectomy) and/or the submandibular glands themselves (sialadenectomy) results in enhanced hypotension and suppressed adrenocorticotropic hormone release in response to the pyrogen lipopolysaccharide.[124] These authors have also suggested a functional unit that is established by the sympathetic superior cervical ganglion and the submandibular gland and is involved humorally in the modulation of body temperature and, in their opinion, this is due to the contribution of a particular endocrine factor (peptide T). Thus, if during hyperthermia the submandibular and sublingual glands are activated parasympathetically as thermoregulatory effector organs accomplishing evaporative heat loss, they may be simultaneously activated sympathetically to release a factor, such as peptide T, into the circulation as a feedback signal to the brain via the sensory CVO of the lamina terminalis. In this way, the OVLT and the SFO may serve as targets also within the thermoregulatory system in that they contribute specifically to the regulation of the forebrain autonomic outflow controlling evaporative

heat loss due to salivation. Knowing the importance of these CVO in body fluid balance, such a function in thermoregulation would add to the close functional interdependence of the two homeostatic systems.

HYPOTHESIS

A model for the role of the lamina terminalis in the control of osmo- and thermoregulatory behaviour

It is known that forebrain areas that are connected to the brainstem and spinal autonomic circuits modulate salivary secretion. Based on the presented data converging from multidisciplinary experiments, one efferent forebrain pathway influencing salivary secretion in the rat under heat stress may originate in the lamina terminalis and/or adjacent preoptic area and may be used especially under heat stress-induced hyperthermic and hyperosmolal conditions. Water loss during activation of evaporative heat loss mechanisms, such as salivation, needs to be balanced and integration within the lamina terminalis, a key structure in the control of body fluid homeostasis, is likely to contribute to this regulatory process. Indeed, as a prerequisite for a possible modulatory role of lamina terminalis neurons in this process, multisynaptic efferent projections from lamina terminalis structures to the autonomic innervation of the thermoregulatory effector organs, the submandibular and sublingual gland have been shown using the viral-tracing technique. Therefore, it is hypothesized that, during activation of the evaporative heat loss mechanism salivation, afferent neurohormonal signals carrying information about the physiological status of body temperature and body fluids are transferred to lamina terminalis neurons and consequent neuronal integration results in modulation of forebrain autonomic outflow to the submandibular and sublingual glands. Neuronal integration within the lamina terminalis may result in efferent control of both osmoregulatory and thermoregulatory behaviour.

ACKNOWLEDGEMENTS

This manuscript is dedicated to Ayse and Liana. We thank the CSIRO Australian Animal Health Laboratory (Geelong, Victoria, Australia). The authors are grateful for the constant support of Professors E Simon and R Gerstberger (Max-Planck-Institute for Physiological and Clinical Research, WG Kerckhoff-Institute, Bad Nauheim, Germany) and the time they spent in the critical reading of this manuscript. TH was supported by a postdoctoral fellowship grant for the Advancement of Science by the Max-Planck-Society, Germany. This work was supported by an Institute Block Grant to the Howard Florey Institute by the National Health and Medical Research Council of Australia.

REFERENCES

1. Hainsworth FR, Stricker EM. Evaporative cooling in the rat: Differences between salivary glands as thermoregulatory effectors. *Can. J. Physiol. Pharmacol.* 1971; **49**: 573–80.
2. Barney CC, Williams JS, Kuiper DH. Thermal dehydration-induced thirst in rats: Role of angiotensin II. *Am. J. Physiol.* 1991; **61**: R1171–5.
3. Hainsworth FR, Stricker EM, Epstein AN. Water metabolism of rats in the heat: Dehydration and drinking. *Am. J. Physiol.* 1968; **214**: 983–9.
4. Ritter RC, Epstein AN. Saliva lost by grooming: A major item in the rat's water economy. *Behav. Biol.* 1974; **11**: 581–5.
5. Johnson AK, Loewy AD. Circumventricular organs and their role in visceral functions. In: Loewy AD, Spyer KM (eds). *Central Regulation of Autonomic Function*. Oxford University Press, New York. 1990; 247–67.
6. McKinley MJ, Bicknell RJ, Hards DK *et al.* Efferent neural pathways of the lamina terminalis subserving osmoregulation. *Prog. Brain Res.* 1992; **91**: 395–402.
7. McKinley MJ, Pennington GL, Oldfield BJ. Anteroventral wall of the third ventricle and dorsal lamina terminalis: Headquarters for control of body fluid homeostasis? *Clin. Exp. Pharmacol. Physiol.* 1996; **23**: 271–81.
8. Renzi A, Lopes RA, Sala MA *et al.* Morphological, morphometric and stereological study of submandibular glands in rats with lesion of the anteroventral region of the third ventricle (AV3V). *Exp. Pathol.* 1990; **38**: 177–87.
9. Renzi A, Colombari E, Mattos-Filho TR *et al.* Involvement of the central nervous system in the salivary secretion induced by pilocarpine in rats. *J. Dent. Res.* 1993; **72**: 1481–4.
10. Stricker EM, Hainsworth FR. Evaporative cooling in the rat: Effects of hypothalamic lesions and chorda tympani damage. *Can. J. Physiol. Pharmacol.* 1970; **48**: 11–17.
11. Toth DM. Temperature regulation and salivation following preoptic lesions in the rat. *J. Comp. Physiol. Psychol.* 1973; **82**: 480–8.
12. Card JP, Rinaman L, Lynn RB *et al.* Pseudorabies virus infection of the rat central nervous system: Ultrastructural characterization of viral replication transport and pathogenesis. *J. Neurosci.* 1993; **13**: 2515–39.
13. Card JP, Enquist LW. Use of pseudorabies virus for definition of synaptically linked populations of neurons. In: Adolph KW (ed.). *Methods in Molecular Genetics*. Academic Press, San Diego. 1994; 363–82.
14. Card JP, Enquist LW. Neurovirulence of pseudorabies virus. *Crit. Rev. Neurobiol.* 1995; **9**: 137–62.
15. Kuypers HG, Ugolini G. Viruses as transneuronal tracers. *Trends. Neurosci.* 1990; **13**: 71–5.
16. Loewy AD. Pseudorabies virus: A transneuronal tracer for neuroanatomical studies. In: Kaplitt MG, Loewy AD (eds). *Viral Vectors: Gene Therapy and Neuroscience Applications*. Academic Press, San Diego. 1995; 349–66.
17. Ugolini G. Transneuronal tracing with alpha-herpesviruses: A review of the methodology. In: Kaplitt MG, Loewy AD (eds). *Viral Vectors: Gene Therapy and Neuroscience Applications*. Academic Press, San Diego. 1995; 293–317.
18. Hübschle T, McKinley MJ, Oldfield BJ. Efferent connections of the lamina terminalis, the preoptic area and the insular cortex to submandibular and sublingual gland of the rat traced with pseudorabies virus. *Brain Res.* 1998; **806**: 219–31.
19. Jansen ASP, Ter Horst GJ, Mettenleiter TC, Loewy AD. CNS cell groups projecting to the submandibular parasympathetic preganglionic neurons in the rat: A retrograde transneuronal viral cell body labeling study. *Brain Res.* 1992; **572**: 253–60.
20. Miselis RR. The efferent projections of the subfornical organ of the rat: A circumventricular organ within a neural network subserving water balance. *Brain Res.* 1981; **230**: 1–23.
21. Oldfield BJ, McKinley MJ. Circumventricular organs. In: Paxinos G (ed.). *The Rat Nervous System*. Academic Press, San Diego. 1995; 391–403.
22. Johnson AK, Wilkin LD. The lamina terminalis. In: Gross PM (ed.). *Circumventricular Organs and Body Fluids*. CRC, Boca Raton. 1987; 125–41.
23. Larsen PJ, Mikkelsen JD. Functional identification of central afferent projections conveying information of acute 'stress' to the hypothalamic paraventricular nucleus. *J. Neurosci.* 1995; **15**: 2609–27.
24. Lind RW. Neural connections. In: Gross PM (ed.). *Circumventricular Organs and Body Fluids*. CRC, Boca Raton. 1987; 27–42.
25. Miselis RR, Weiss ML, Shapiro RE. Modulation of the visceral neuraxis. In: Gross PM (ed.). *Circumventricular Organs and Body Fluids*. CRC, Boca Raton. 1987; 143–62.

26. Phillips MI, Camacho A. Neural connections of the OVLT. In: Gross PM (ed.). *Circumventricular Organs and Body Fluids*. CRC, Boca Raton. 1987; 157–69.
27. Emmelin N. Nervous control of salivary glands. In: Code CF, Heidel W (eds). *Handbook of Physiology*. Williams & Wilkins, Baltimore. 1967; 595–632.
28. Kanosue K, Nakayama T, Tanaka H, Yanase M, Yasuda H. Modes of action of local hypothalamic and skin thermal stimulation on salivary secretion in rats. *J. Physiol.* 1990; **424**: 459–71.
29. Kanosue K, Yanase-Fujiwara M, Hosono T, Zhang YH. Hypothalamic network for thermoregulation: Old but still unanswered question. In: Pleschka K, Gerstberger R (eds). *Integrative and Cellular Aspects of Autonomic Functions: Temperature and Osmoregulation*. John Libbey Eurotext, Paris. 1994; 253–7.
30. Ter Horst GJ, Hautvast RWM, De-Jongste MJL, Korf J. Neuroanatomy of cardiac activity-regulating circuitry: A transneuronal retrograde viral labelling study in the rat. *Eur. J. Neurosci.* 1996; **8**: 2029–41.
31. Miselis RR, Lee BH, Enquist LW, Card JP. Characterization of the visceral neuroaxis by transneuronal passage of pseudorabies virus. *Soc. Neurosci. Abstr.* 1991; **18**: 545.13 (Abstract).
32. Nadelhaft I, Vera PL, Card JP, Miselis RR. Central nervous system neurons labelled following the injection of pseudorabies virus into the rat urinary bladder. *Neurosci. Lett.* 1992; **143**: 271–4.
33. Nadelhaft I, Vera PL. Neurons in the rat brain and spinal cord labelled after pseudorabies virus injected into the external urethral sphincter. *J. Comp. Neurol.* 1996; **375**: 502–17.
34. Jansen ASP, Wessendorf MW, Loewy AD. Transneuronal labeling of CNS neuropeptide and monoamine neurons after pseudorabies virus injections into the stellate ganglion. *Brain Res.* 1995; **683**: 1–24.
35. Schramm LP, Strack AM, Platt KB, Loewy AD. Peripheral and central pathways regulating the kidney: A study using pseudorabies virus. *Brain Res.* 1993; **616**: 251–62.
36. Sly DJ, Colvill L, McKinley MJ, Oldfield BJ. Identification of neural projections from the forebrain to the kidney, using the virus pseudorabies. *J. Auton. Nerv. Syst.* 1999; **77**: 73–82.
37. Smith JE, Jansen ASP, Gilbey MP, Loewy AD. CNS cell groups projecting to sympathetic outflow of tail artery: Neural circuits involved in heat loss in the rat. *Brain Res.* 1998; **786**: 153–64.
38. Loewy AD. Central autonomic pathways. In: Loewy AD, Spyer KM (eds). *Central Regulation of Autonomic Functions*. Oxford University Press, New York. 1990; 88–103.
39. De Luca Jr LA, Menani JV. Preoptic–periventricular tissue (AV3V): Central cholinergic-induced hydromineral and cardiovascular responses, and salt intake. *Rev. Bras. Biol.* 1996; **56**: 233–8.
40. Ship JA, Fischer DJ. The relationship between dehydration and parotid salivary gland function in young and older healthy adults. *J. Gerontol. A Biol. Sci. Med. Sci.* 1997; **52**: M310–19.
41. Honda K, Negoro H, Dyball RE, Higuchi T, Takano S. The osmoreceptor complex in the rat: Evidence for interactions between the supraoptic and other diencephalic nuclei. *J. Physiol.* 1990; **431**: 225–41.
42. Elmer M, Ohlin P. Salivary glands of the rat in a hot environment. *Acta Physiol. Scand.* 1970; **79**: 129–32.
43. Hainsworth FR. Saliva spreading, activity, and body temperature regulation in the rat. *Am. J. Physiol.* 1967; **212**: 1288–92.
44. Hainsworth FR. Evaporative water loss from rats in the heat. *Am. J. Physiol.* 1968; **214**: 979–82.
45. Horowitz M, Meiri U. Thermoregulatory activity in the rat: Effects of hypohydration, hypovolemia and hypertonicity and their interaction with short-term heat acclimation. *Comp. Biochem. Physiol. A* 1985; **82**: 577–82.
46. Antal J, Kirilcuk V. Dynamics of polypneic salivation in a dog. *Pflügers Arch.* 1969; **308**: 25–35.
47. Baker MA, Doris PA. Control of evaporative heat loss during changes in plasma osmolality in the cat. *J. Physiol.* 1982; **328**: 535–45.
48. Baker MA, Doris PA, Hawkins MJ. Effect of dehydration and hyperosmolality on thermoregulatory water losses in exercising dogs. *Am. J. Physiol.* 1983; **244**: R516–21.
49. Hammel HT, Sharp F. Thermoregulatory salivation in the running dog in response to pre-optic heating and cooling. *J. Physiol.* 1971; **63**: 260–3.
50. Keil R, Gerstberger R, Simon E. Hypothalamic thermal stimulation modulates vasopressin release in hyperosmotically stimulated rabbits. *Am. J. Physiol.* 1994; **267**: R1089–97.
51. Sharp F, Smith D, Thompson M, Hammel HT. Thermoregulatory salivation proportional to hypothalamic temperature above threshold in the dog. *Life Sci.* 1969; **8**: 1069–76.
52. Stricker EM, Hainsworth FR. Evaporative cooling in the rat: Effects of dehydration. *Can. J. Physiol. Pharmacol.* 1970; **48**: 18–27.
53. McKinley MJ, Denton DA, Hatzikostas S, Weisinger RS. Effect of angiotensin II on parotid saliva secretion in conscious sheep. *Am. J. Physiol.* 1979; **237**: E56–60.
54. Liang T, Cascieri MA. Substance P stimulation of amylase release by isolated parotid cells and inhibition of substance P induction of salivation by vasoactive peptides. *Mol. Cell. Endocrinol.* 1979; **15**: 151–62.
55. Nederfors T, Dahlof C, Ericsson T, Twetman S. Effects of the antihypertensive drug captopril on human salivary secretion rate and composition. *Eur. J. Oral Sci.* 1995; **103**: 351–4.
56. Butler DG, Siwanowicz H, Puskas D. A re-evaluation of experimental evidence for the hormonal control of avian nasal salt glands. In: Hughes MR, Chadwick A (eds). *Progress in Avian Osmoregulation.* Leeds Philosophical and Literary Society, Leeds. 1989; 127–41.
57. Gerstberger R, Gray DA. Fine structural innervation and functional control of avian salt glands. *Int. Rev. Cytol.* 1993; **144**: 129–215.
58. Simon E, Gerstberger R, Gray DA. Central nervous angiotensin II responsiveness in birds. *Prog. Neurobiol.* 1992; **39**: 179–207.
59. Wilson KM, Fregly MJ. Angiotensin II-induced hypothermia in rats. *J. Appl. Physiol.* 1985; **58**: 534–43.
60. Fregly MJ, Rowland NE. Centrally mediated vasodilation of the rat's tail by angiotensin II. *Physiol. Behav.* 1996; **60**: 861–5.
61. Wilson KM, Fregly MJ. Factors affecting angiotensin II-induced hypothermia in rats. *Peptides* 1985b; **6**: 695–702.
62. Mathai ML, Hübschle T, McKinley MJ. Central angiotensin receptor blockade impairs thermolytic and dipsogenic responses to heat exposure in rats. *Am. J. Physiol.* 2000; **279**: R1821–6.
63. Horowitz M, Kaspler P, Simons E, Gerstberger R. Heat acclimation and hypohydration: Involvement of central angiotensin II receptors in thermoregulation. *Am. J. Physiol.* 1999; R47–55.
64. Epstein AN, Milestone R. Showering as a coolant for rats exposed to heat. *Science* 1968; **160**: 895–6.
65. Brummermann M, Rautenberg W. Interaction of autonomic and behavioral thermoregulation in osmotically stressed pigeons *Columba livia*. *Physiol. Zool.* 1989; **62**: 1102–16.
66. Kregel KC, Stauss H, Unger T. Modulation of autonomic nervous system adjustments to heat stress by central ANG II receptor antagonism. *Am. J. Physiol.* 1994; **266**: R1985–91.
67. Chiba T, Murata Y. Afferent and efferent connections of the medial preoptic area in the rat: A WGA-HRP study. *Brain Res. Bull.* 1985; **14**: 261–72.
68. Conrad LC, Pfaff DW. Efferents from medial basal forebrain and hypothalamus in the rat. I. An autoradiographic study of the medial preoptic area. *J. Comp. Neurol.* 1976; **169**: 185–219.
69. Simerly RB, Swanson LW. Projections of the medial preoptic nucleus: A *Phaseolus vulgaris* leucoagglutinin anterograde tract-tracing study in the rat. *J. Comp. Neurol.* 1988; **270**: 209–42.
70. Swanson LW. An autoradiographic study of the efferent connections of the preoptic region in the rat. *J. Comp. Neurol.* 1976; **167**: 227–56.
71. Swanson LW. *Brain Maps: Structure of the Brain*. Elsevier Science, Amsterdam. 1992.

72. Swanson LW, Kucharczyk J, Mogenson GJ. Autoradiographic evidence for pathways from the medial preoptic area to the midbrain involved in the drinking response to angiotensin II. *J. Comp. Neurol.* 1978; **178**: 645–59.
73. Knuepfer MM, Johnson AK, Brody MJ. Vasomotor projections from the anteroventral third ventricle (AV3V) region. *Am. J. Physiol.* 1984; **247**: H139–45.
74. Knuepfer MM, Johnson AK, Brody MJ. Identification of brainstem projections mediating hemodynamic responses to stimulation of the anteroventral third ventricle (AV3V) region. *Brain Res.* 1984; **294**: 305–14.
75. Gilbert TM, Blatteis CM. Hypothalamic thermoregulatory pathways in the rat. *J. Appl. Physiol.* 1977; **43**: 770–7.
76. Blatteis CM, Banet M. Autonomic thermoregulation after separation of the preoptic area from the hypothalamus in rats. *Pflügers Arch.* 1986; **406**: 480–4.
77. Zhang YH, Yamada K, Hosono T, Chen XM, Shiosaka S, Kanosue K. Efferent neuronal organization of thermoregulatory vasomotor control. *Ann. N.Y. Acad. Sci.* 1997; **813**: 117–22.
78. Hainsworth FR, Epstein AN. Severe impairment of heat-induced saliva-spreading in rats recovered from lateral hypothalamic lesions. *Science* 1966; **153**: 1255–7.
79. Patronas P, Horowitz M, Simon E, Gerstberger R. Differential stimulation of c-fos expression in hypothalamic nuclei of the rat brain during short-term heat acclimation and mild dehydration. *Brain Res.* 1998; **798**: 127–39.
80. Travis KA, Johnson AK. *In vitro* sensitivity of median preoptic neurons to angiotensin II, osmotic pressure, and temperature. *Am. J. Physiol.* 1993; **264**: R1200–5.
81. Kiyohara T, Miyata S, Nakamura T, Shido O, Nakashima T, Shibata M. Differences in Fos expression in the rat brains between cold and warm ambient exposures. *Brain Res. Bull.* 1995; **38**: 193–201.
82. Oldfield BJ, Bicknell RJ, McAllen RM, Weisinger RS, McKinley MJ. Intravenous hypertonic saline induces Fos immunoreactivity in neurons throughout the lamina terminalis. *Brain Res.* 1991a; **561**: 151–6.
83. Scammell TE, Price KJ, Sagar SM. Hyperthermia induces c-fos expression in the preoptic area. *Brain Res.* 1993; **618**: 303–7.
84. Bisley JW, Rees SM, McKinley MJ, Hards DK, Oldfield BJ. Identification of osmoresponsive neurons in the forebrain of the rat: A Fos study at the ultrastructural level. *Brain Res.* 1996; **720**: 25–34.
85. Guldenaar SE, Noctor SC, McCabe JT. Fos-like immunoreactivity in the brain of homozygous diabetes insipidus Brattleboro and normal Long-Evans rats. *J. Comp. Neurol.* 1992; **322**: 439–48.
86. Hamamura M, Nunez DJ, Leng G, Emson PC, Kiyama H. c-fos may code for a common transcription factor within the hypothalamic neural circuits involved in osmoregulation. *Brain Res.* 1992; **572**: 42–51.
87. Oldfield BJ, Badoer E, Hards DK, McKinley MJ. Fos production in retrogradely labelled neurons of the lamina terminalis following intravenous infusion of either hypertonic saline or angiotensin II. *Neuroscience* 1994; **60**: 255–62.
88. Nakashima T, Hori T, Kiyohara T, Shibata M. Osmosensitivity of preoptic thermosensitive neurons in hypothalamic slices *in vitro*. *Pflügers Arch.* 1985; **405**: 112–17.
89. Silva NL, Boulant JA. Effects of osmotic pressure, glucose, and temperature on neurons in preoptic tissue slices. *Am. J. Physiol.* 1984; **247**: R335–45.
90. Boulant JA, Dean JB. Temperature receptors in the central nervous system. *Annu. Rev. Physiol.* 1986; **48**: 639–54.
91. Boulant JA, Silva NL. Multisensory hypothalamic neurons may explain interactions among regulatory systems. *News Physiol. Sci.* 1989; **4**: 245–8.
92. Müller AR, Schäfer F, Schmid HA, Gerstberger R. Osmosensitive circumventricular structures connected to the paraventricular nucleus in the duck brain. In: Pleschka K, Gerstberger R (eds). *Integrative and Cellular Aspects of Autonomic Functions: Temperature and Osmoregulation*. John Libbey Eurotext, Paris. 1994; 439–49.
93. McAllen RM, Pennington GL, McKinley MJ. Osmoresponsive units in sheep median preoptic nucleus. *Am. J. Physiol.* 1990; **259**: R593–600.
94. Sibbald JR, Hubbard JI, Sirett NE. Responses from osmosensitive neurons of the rat subfornical organ *in vitro*. *Brain Res.* 1988; **461**: 205–14.
95. Oliet SH, Bourque CW. Mechanosensitive channels transduce osmosensitivity in supraoptic neurons. *Nature* 1993; **364**: 341–3.
96. Oliet SH, Bourque CW. Osmoreception in magnocellular neurosecretory cells: From single channels to secretion. *Trends Neurosci.* 1994; **17**: 340–4.
97. Aradachi H, Honda K, Negoro H, Kubota T. Median preoptic neurones projecting to the supraoptic nucleus are sensitive to haemodynamic changes as well as to rise in plasma osmolality in rats. *J. Neuroendocrinol.* 1996; **8**: 35–43.
98. Bourque CW, Oliet SH. Osmoreceptors in the central nervous system. *Annu. Rev. Physiol.* 1997; **59**: 601–19.
99. Honda K, Aradachi H, Higuchi T, Takano S, Negoro H. Activation of paraventricular neurosecretory cells by local osmotic stimulation of the median preoptic nucleus. *Brain Res.* 1992; **594**: 335–8.
100. Tanaka J, Ushigome A, Matsuda M, Saito H. Responses of median preoptic neurons projecting to the hypothalamic paraventricular nucleus to osmotic stimulation in Wistar-Kyoto and spontaneously hypertensive rats. *Neurosci. Lett.* 1995; **191**: 47–50.
101. Kelly AB, Watts AG. Mediation of dehydration-induced peptidergic gene expression in the rat lateral hypothalamic area by forebrain afferent projections. *J. Comp. Neurol.* 1996; **370**: 231–46.
102. Oldfield BJ, Hards DK, McKinley MJ. Projections from the subfornical organ to the supraoptic nucleus in the rat: Ultrastructural identification of an interposed synapse in the median preoptic nucleus using a combination of neuronal tracers. *Brain Res.* 1991; **558**: 13–19.
103. Oldfield BJ, Hards DK, McKinley MJ. Neurons in the median preoptic nucleus of the rat with collateral branches to the subfornical organ and supraoptic nucleus. *Brain Res.* 1992; **586**: 86–90.
104. McKellar S, Loewy AD. Efferent projections of the A1 catecholamine cell group in the rat: An autoradiographic study. *Brain Res.* 1982; **241**: 11–29.
105. Saper CB, Loewy AD, Swanson LW, Cowan WM. Direct hypothalamo-autonomic connections. *Brain Res.* 1976; **117**: 305–12.
106. Saper CB, Levisohn D. Afferent connections of the median preoptic nucleus in the rat: Anatomical evidence for a cardiovascular integrative mechanism in the anteroventral third ventricular (AV3V) region. *Brain Res.* 1983; **288**: 21–31.
107. Elmquist JK, Scammell TE, Jacobson CD, Saper CB. Distribution of Fos-like immunoreactivity in the rat brain following intravenous lipopolysaccharide administration. *J. Comp. Neurol.* 1996; **371**: 85–103.
108. Scammell TE, Elmquist JK, Griffin JD, Saper CB. Ventromedial preoptic prostaglandin E_2 activates fever-producing autonomic pathways. *J. Neurosci.* 1996; **16**: 6246–54.
109. Simon E, Pierau FK, Taylor DCM. Central and peripheral thermal control of effectors in homeothermic temperature regulation. *Physiol. Rev.* 1986; **66**: 235–89.
110. Ferguson AV, Bains JS. Electrophysiology of the circumventricular organs. *Front. Neuroendocrinol.* 1996; **17**: 440–75.
111. Ray PE, Saavedra JM. Selective chronic sodium or chloride depletion specifically modulates subfornical organ atrial natriuretic peptide receptor number in young rats. *Cell. Mol. Neurobiol.* 1997; **17**: 455–70.
112. Riediger T, Rauch M, Schmid HA. Actions of amylin on subfornical organ neurons and on drinking behavior in rats. *Am. J. Physiol.* 1999; **276**: R514–21.
113. Aloe L, Alleva E, Bohm A, Levi-Montalcini R. Aggressive behavior induces release of nerve growth factor from mouse salivary gland into the bloodstream. *Proc. Natl Acad. Sci. USA* 1986; **83**: 6184–7.
114. Maestripieri D, De Simone R, Aloe L, Alleva E. Social status and nerve growth factor serum levels after agonistic encounters in mice. *Physiol. Behav.* 1990; **47**: 161–4.

115. Murphy RA, Saide JD, Blanchard MH, Young M. Nerve growth factor in mouse serum and saliva: Role of the submandibular gland. *Proc. Natl Acad. Sci. USA* 1977; **74**: 2330–3.
116. Hwang DL, Wang S, Chen RC, Lev-Ran A. Trauma, especially of the submandibular glands, causes release of epidermal growth factor into bloodstream in mice. *Regul. Pept.* 1991; **34**: 133–9.
117. Berg T, Johansen L, Poulsen K. Exocrine and endocrine release of kallikrein after reflex-induced salivary secretion. *Acta Physiol. Scand.* 1990; **139**: 29–37.
118. Rabito SF, Orstavik TB, Scicli AG, Schork A, Carretero OA. Role of the autonomic nervous system in the release of rat submandibular gland kallikrein into the circulation. *Circ. Res.* 1983; **52**: 635–41.
119. Scicli AG, Orstavik TB, Rabito SF, Murray RD, Carretero OA. Blood kinins after sympathetic nerve stimulation of the rat submandibular gland. *Hypertension* 1983; **5**: I101–6.
120. Jones Jr DE, Tran-Patterson R, Cui DM, Davin D, Estell KP, Miller DM. Epidermal growth factor secreted from the salivary gland is necessary for liver regeneration. *Am. J. Physiol.* 1995; **268**: G872–8.
121. Mathison RD, Befus AD, Davison JS. A novel submandibular gland peptide protects against endotoxic and anaphylactic shock. *Am. J. Physiol.* 1997; **273**: R1017–23.
122. Mathison RD, Malkinson T, Cooper KE, Davison JS. Submandibular glands: Novel structures participating in thermoregulatory responses. *Can. J. Physiol. Pharmacol.* 1997; **75**: 407–13.
123. Mathison RD, Malkinson TJ, Davison JS, Cooper KE. Salivary glands, their hormones, and thermoregulation. *Ann. N.Y. Acad. Sci.* 1997; **813**: 338–43.
124. Mathison RD, Befus D, Davison JS. Removal of the submandibular glands increases the acute hypotensive response to endotoxin. *Circ. Shock* 1993; **39**: 52–8.

5.4.

5.4. GERSTBERGER, R., BARTH, S.W., HOROWITZ, M., HUDL, K., PATRONAS, P. & HÜBSCHLE, T. (2001)

Differential activation of nitrergic hypothalamic neurons by heat exposure and dehydration. In: Thermotherapy for Neoplasia, Inflammation, and Pain, Kosaka, M., Sugahara, T., Schmidt, K.L., Simon, E. (Eds.) Springer-Verlag, Tokyo. pp. 43-62.

Eigener Anteil an der Publikation:

- Beteiligung an der Versuchsplanung (20 %)
- Durchführung der Versuche (20 %)
- Beteiligung an der Zusammenfassung und Veröffentlichung der Ergebnisse (20 %)

Differential Activation of Nitrergic Hypothalamic Neurons by Heat Exposure and Dehydration

RÜDIGER GERSTBERGER[1], STEPHAN W. BARTH[2], MICHAL HOROWITZ[3], KRISTIANE HUDL[1], PANAGIOTIS PATRONAS[1], and THOMAS HÜBSCHLE[4]

Summary. Water is used both for evaporative cooling during external heat stress or exercise-induced heat load and for replenishment of the extracellular fluid (ECF) compartment under conditions of dehydration; thus, competing requirements for fluid or electrolyte balance and temperature regulation are well documented for homeothermic animals and humans. Hypothalamic control of salt and fluid balance is structurally well defined, whereas the neuronal cytoarchitecture for thermoregulation remains fragmentary. Employing classic and transsynaptic neuronal tracing techniques, diencephalic structures specifically involved in the perception and/or integration of thermoregulatory or osmoregulatory signals as well as the efferent pathways controlling respective effector systems could be determined. Stimulation of the osmoregulatory or thermoregulatory autonomic circuitries in the rat, using expression of c-*fos* as marker of neuronal activity, led to differential activation of specific neuronal populations in hypothalamic nuclei such as the SFO, OVLT, PVN, and SON for osmoregulation and MPA, VMPO, LHA, and LS for thermoregulation. The MnPO, activated by both thermal and osmotic stimuli, plays a major role as an integrative structure involved in both central control systems. The enzyme nNOS, generating NO as neuromodulatory agent involved in the centrally controlled homeostasis of body temperature and the ECF, was found to be upregulated in the respective hypothalamic structures during either heat exposure or osmotic stimuli. The latter induced coexpression of Fos protein with nNOS in the same neurons, whereas Fos-positive cells and nitrergic cells were found codistributed as a result of thermal stimulation, indicating NO-mediated neuronal activation in nearest-neighbor target neurons.

Keywords. Osmoregulation, Thermoregulation, Differential Fos activation, Neuronal nitric oxide synthase, Median preoptic nucleus, Transsynaptic tracing

Introduction

Homeostasis of body temperature as well as extracellular fluid (ECF) volume and tonicity in mammals, including humans, represents a necessary prerequisite for the functional control of life at the cellular, organ-specific, and organismic level. Under conditions of external heat stress or exercise-induced heat load, a human faces the challenge of suffering from heat stroke or severe dehydration. With water being used for both evaporative cooling and replenishment of the ECF compartment, competing requirements for fluid or electrolyte balance and temperature regulation are well documented for humans [1] and homeothermic animals [2–4]. Maintenance of the euhydration status allows adequate body temperature regulation and heat endurance, whereas reduction of ECF volume or a rise in its osmolality interferes with the ability to cope with thermal stress. The control of ECF volume and tonicity gains prevalence at the expense of reduced ability to dissipate heat. Thermoregulation under conditions of hypohydration is manifested by delayed and attenuated onset of water-consuming heat defense activities such as sweating in humans and horses [1,5], thermal panting in dogs and rabbits [3,6], and salivation in rats [7], finally leading to an upward shift of the regulated deep-body temperature. To compensate for reduced heat dissipation, basal metabolic rate (BMR) is often lowered to decrease the internal heat load. Despite these changes, however, heat endurance ultimately decreases. Observations such as an elevated temperature threshold for activation of heat-dissipating mechanisms [2,8,9], reduced sensitivity of the thermoregulatory center in converting temperature signals into heat loss activities

[1]Max-Planck-Institute for Physiological and Clinical Research, W.G. Kerckhoff-Institute, Parkstrasse 1, D-61231 Bad Nauheim, Germany
[2]Federal Research Center for Nutrition, Department of Physiology, Haid-und-Neu-Str. 9, D-76131 Karlsruhe, Germany
[3]Division of Physiology, Faculty of Dental Medicine, The Hebrew University, P.O.B. 12272, Jerusalem 91120, Israel
[4]German Institute of Human Nutrition, Arthur-Scheunert-Allee 114-116, D-14558 Potsdam-Rehbrücke, Germany

[4,6], and transition from sweating to the more economical panting in species that both pant and sweat [10] suggest that the elevated body temperature reflects central modulations of the thermoregulatory processes to enhance efficiency of the physical avenues for heat dissipation, rather than their failure [11].

Alterations in ECF osmotic pressure or volume, perceived by systemic and hypothalamic osmo- or volume-sensitive mechanisms [12,13], elevate the threshold temperature for evaporative cooling and lower BMR, whereas the combined stress produces an additive effect on these parameters [6,9,11,14,15]. Experimentally induced hypertonicity of the ECF therefore leads to reduced thermoregulatory panting in dogs or marked attenuation of thermal vasodilation in baboons [8,16]. The involvement of systemic volume receptors transmitting information to the hypothalamus via afferent fibers of the nervus vagus and brainstem neurons can be deduced from studies on rats showing inhibition of heat-induced skin vasodilation by lowered central venous pressure [17,18]. The delayed heat dissipation at reduced rate may be described as a rise in set point at the level of hypothalamic integration or reduced gain of heat defense mechanism [2,3,18–20].

With osmoregulatory modulation of the thermoregulatory circuit prevailing, temperature dependence of the osmoregulatory system, on the other hand, may be derived from thermally induced alterations in hypothalamo-neurohypophyseal vasopressin (AVP) secretion [6,21–24], including the phenomenon of cold-induced diuresis caused by an inhibition of AVP release in monkeys and pigs [22,23]. Studies in humans have clearly demonstrated that elevated body temperature due to external heat load results in augmented gain of the osmotically driven release of AVP into the circulation but also enhances both cumulative water intake and subjective thirst ratings during the rehydration period [24]. Despite all the physiological evidence of central interaction between the osmoregulatory and thermoregulatory systems, the underlying neuroanatomical topography and cellular transduction mechanisms remain largely unknown [20].

Hypothalamic Topography of Osmoregulatory and Thermoregulatory Circuits

The hypothalamus plays an eminent role in "assuring survival of both the individual and the species" [25] (see chapter by K. Kanosue et al., this volume). Its anterior component contains nuclei and regions involved in the perception and integration of systemic and central signals important for the maintenance of body temperature and ECF homeostasis. Schematic drawings of four coronal sections through the rat brain (Fig. 1A–D) delineate neuroglial structures important for osmo- or thermoregulation (colored in blue or yellow, respectively). Nuclei (presented in green) are notably involved in the interaction of both circuits.

Organization of the Osmoregulatory Circuitry

Hypothalamic control of salt and fluid balance is structurally well defined, with the magnocellular supraoptic and paraventricular nuclei (SON, mPVN) synthesizing the antidiuretic hormone AVP as the major neuroendocrine effector system [26]. The subfornical organ (SFO) and organum vasculosum laminae terminalis (OVLT) as circumventricular organs without a blood–brain barrier (BBB) serve as osmosensory structures and targets for circulating peptidergic factors such as angiotensin II (AngII) or AVP [27,28]. Neurons of both the SFO and OVLT send their efferents to the parvocellular PVN (pPVN) as a well-known integrative center, to the SON, and primarily to the median preoptic nucleus (MnPO) [29,30] (Fig. 1E). The MnPO of the lamina terminalis located inside the BBB serves as a major relay station within the central osmoregulatory circuit, and additionally receives afferent information regarding the volume status of the ECF from volume or stretch receptors located in major components of the low-pressure system such as the right superior vena cava. The signals are relayed to the MnPO via components of the cardiovascular control center located in the brainstem such as the nucleus tractus solitarius (NTS) [31,32] and the lateral parabrachial nucleus (LPBN). On the efferent side, the monosynaptic pathway of MnPO neurons to magnocellular neurons of the SON and PVN (mPVN) could be demonstrated by classical retrograde tracing techniques [33,34] (Fig. 1E) or local osmotic and electrical stimulations of MnPO neurons producing excitation in mPVN neurons [35].

Organization of the Thermoregulatory Circuitry

The neural organization of hypothalamic thermoregulation is less well defined. Important thermosensory and -integrative functions reside in the preoptic and anterior hypothalamic regions, with the medial preoptic area (MPA) including its substructures such as the ventromedial preoptic area (VMPO) being most thermosensitive [19,36]. The OVLT and the lateral septum

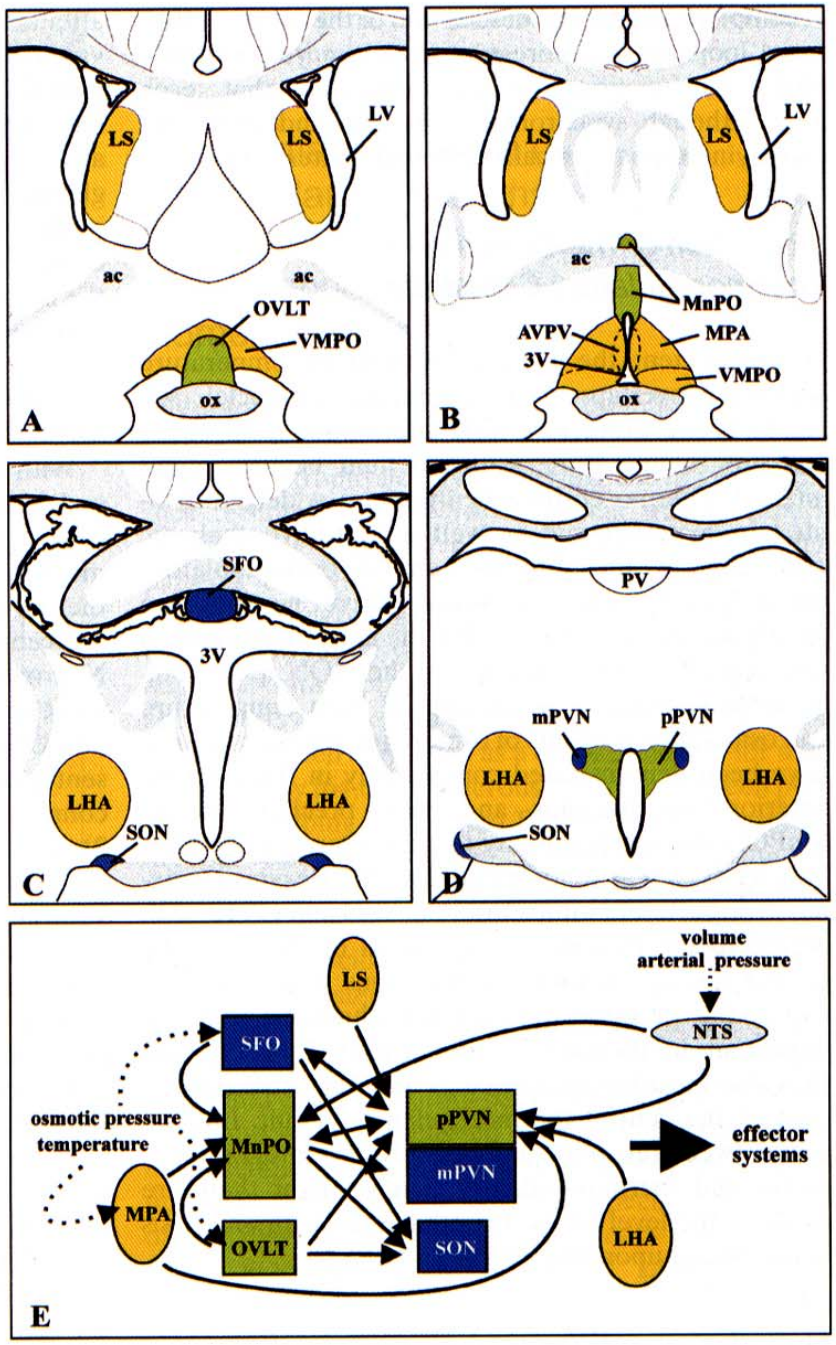

FIG. 1A–E. The hypothalamic cytoarchitecture of the circuitries underlaying thermo- and osmoregulatory control. **A–D** Schematic presentation of four coronal sections of the rat hypothalamus positioned at 200 µm (**A**), 300 µm (**B**), 1.3 mm (**C**), and 1.8 mm (**D**) caudally with regard to the bregma. **E** Schematic presentation of major efferent and afferent fiber connections (*arrows*) between (extra)hypothalamic nuclei and regions involved in the control of body fluid and temperature homeostasis, as revealed by conventional neural tracing techniques. The putative perception of osmotic, volume, or thermal stimuli by some structures is presented by *stippled lines*. Structures involved in the hypothalamic control of osmo- or thermoregulation are marked in *blue* or *yellow*, respectively; structures with sensory or integrative functions for both autonomic circuits are marked in *green*. *3V*, third ventricle; *ac*, anterior commissure; *LHA*, lateral hypothalamic area; *LS*, lateral septum; *LV*, lateral ventricle; *MnPO*, median preoptic nucleus; *MPA*, medial preoptic area; *mPVN*, magnocellular paraventricular nucleus; *NTS*, nucleus tractus solitarius; *OVLT*, organum vasculosum laminae terminalis; *ox*, optic chiasm; *pPVN*, parvocellular paraventricular nucleus; *PV*, paraventricular nucleus of the thalamus; *SFO*, subfornical organ; *SON*, supraoptic nucleus; *VMPO*, ventromedial preoptic area

(LS) were identified as initiating or modulating the fever response to endotoxin and circulating cytokines [37–39], with the pyrogenic factors either directly contacting OVLT neurons or indirectly activating anterior hypothalamic structures via stimulation of cyclooxygenase-2 in their vascular endothelium [40] (see chapter by K. Matsumura et al., this volume). Neurons in the posterior hypothalamus contribute to the control of thermoregulatory effectors, and the lateral hypothalamic area (LHA) is involved in energy balance linked to metabolic cold defense [2,41,42]. Conventional neuronal tracing methods could show that the MPA is reciprocally connected with the MnPO, LS, LHA, the periaqueductal gray of the mesencephalon, and the LPBN of the pons [43], and that most of its functionally important efferents are relayed via the medial forebrain bundle [44] (Fig. 1E). Through fiber passage in the medial forebrain bundle, the LHA receives the most abundant innervation originating in the lateral septum, as does the zona incerta [45], the latter being recognized as an important site of convergence of various signals related to drinking [46]. Retrograde tracing also led to the characterization of MnPO neurons, which are activated on systemic LPS injection, to evoke the fever-associated acute-phase response and finally project to the pPVN as a secondary integrative unit [47] (Fig. 1E).

A complete anatomical description of the various effectorial loops in thermoregulation is not yet available. However, functional studies indicated that each loop, although synchronized, operates independently employing topographically different centers [44,48].

Interaction of the Osmo- and Thermoregulatory Circuitries

To some extent, the neuronal network of temperature regulation overlaps with osmoregulatory nuclei (see Fig. 1). However, there is little information as to where and how temperature, salt, and fluid balance might interact. Thermosensitive neurons are widely distributed in hypothalamic as well as extrahypothalamic brain regions, including neurons in osmoregulatory nuclei [20,49], whereas osmosensitive neurons are mostly discussed for the MnPO, the anteroventral third ventricular (AV_3V) region, or the SON [32,35,50]. Neurons responding to changes of both temperature and osmolality or agents of osmoregulatory significance have been demonstrated convincingly in the preoptic anterior hypothalamus, and more precisely in the MnPO, with high sensitivity to both alterations in ECF tonicity as well as temperature [51–53]. Besides receiving strong afferent inputs from the SFO and OVLT with regard to the osmoregulatory status of the ECF, the MnPO reveals reciprocal connections with structures within the preoptic anterior hypothalamus that are important in thermoregulation (MPA, VMPO), and thus also must be considered as an integrative component of the central thermoregulatory circuit. Interaction between reception and possibly also integration of osmo- and thermoregulatory signals might therefore occur at the level of the hypothalamus, with emphasis being placed upon the MnPO and pPVN.

Hypothalamic Efferent Innervation of Thermo- and Osmoregulatory Effector Systems

Sensation and integration of signals with thermoregulatory or osmoregulatory importance at the level of hypothalamic nuclei is followed by the efferent modulation of respective effector organs such as—depending on the species—cutaneous blood vessels, sweat glands, the respiratory system, salivary glands, brown adipose tissue, the kidneys, and the neurohypophysis. The transsynaptic viral tracing method enables insights into the topographic arrangement of multisynaptic neuronal pathways from the hypothalamus to peripheral effector systems. Inoculation of rats (for the most part) with attenuated strains of pseudorabies virus into the tail vasculature [54], the submandibular and sublingual glands [55,56], the brown adipose tissue [57], or the kidney [58,59] led to viral infection in various forebrain and hindbrain structures. With sympathetic preganglionic neurons of the intermediolateral cell column in the spinal cord being labeled first, infected neurons could subsequently be located in brainstem nuclei and the periaqueductal gray of the midbrain. For the hypothalamus, third-order neurons proved to be labelled in distinct nuclei including LHA, PVN, and the anterior hypothalamus, fourth- to fifth-order neurons for the MPA and lateral preoptic area (Fig. 2).

With regard to preoptic control of salivary secretion and kidney function, the viral tracing studies are in good agreement with earlier reports using hypothalamic lesioning and physiological approaches to verify the involvement of the anterior hypothalamus in the central control of these effector systems [60–62]. Neurons infected in components of the lamina terminalis, including the MnPO inside and the sensory SFO and OVLT outside the blood–brain barrier, all represent putative fourth- or fifth-order neurons efferently connected to both the submandibular gland [55] (Fig. 2) and the kidney [58]. At a high degree of topographic codistribution of virally infected cells in the dorsal and ventral pPVN, a differential pattern could be obtained, for example, for the rat OVLT, with predominant cell infection of its dorsal cap finally projecting to the kidney and the majority of cells located laterally projecting to the submandibular gland (see Fig. 2).

In viral tracing studies performed from "pure" thermoregulatory effector organs, such as the sympathetically controlled vascular anastomoses in tail skin [54] or brown adipose tissue [57], the preoptic area including the MnPO was described as a major source of central fourth-order output to the respective effector organs. Labeled neurons were also found in the LHA, the zona incerta, pPVN, and the bed nucleus of the stria terminalis (Fig. 2). After 6 days of survival, PVN and MPA contained more than 60% of all neurons infected within the hypothalamus, whereas the two circumventricular organs did not reveal virus expression [57]. This finding is in agreement with the results obtained on fourth-order labeling after viral injections into various sympathetic ganglia including the superior cervical, stellate, and celiac ganglia of the rat to map sympathetic related neurons in the preoptic region [63]. Concerning a topographic classification of fourth-order preoptic anterior hypothalamic neurons, medial and lateral parts of the preoptic area, but also the MnPO, were preferentially infected after virus inoculation of thermoregulatory effector organs, whereas viral tracings from kidneys but also the salivary glands resulted in addi-

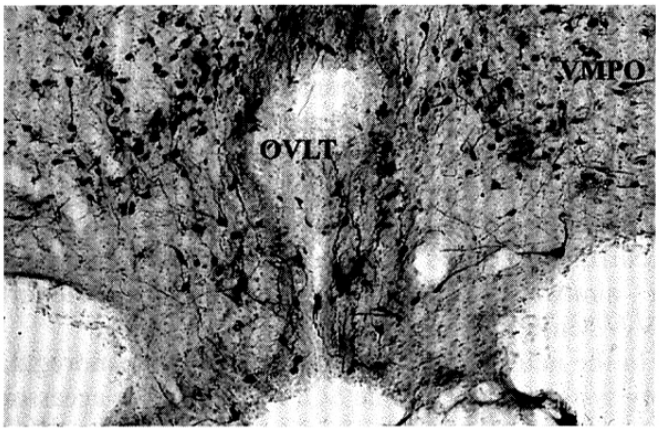

	PVN	LHA	MPA	MnPO	OVLT	SFO	BNST	LS
Tail anastomoses	+++	++	++	+			++	
Submandibular gland	+++	+++	++	+	+	+	++	
Brown adipose tissue	+++	++	+++				+	+
Kidney	++	+	++	+	+	+	++	

FIG. 2. Transsynaptic neuronal tracing techniques to mark efferent multisynaptic pathways for the differential hypothalamic control of effector systems involved in the maintenance of body fluid homeostasis and thermoregulation. Infection of putative third- and fourth-order neurons within rat hypothalamic nuclei after pseudorabies virus (PRV) infection into thermo- and osmoregulatory effector organs. *Top*: immunocytochemical detection of PRV protein in neurons at the level of the rat *OVLT* and ventromedial preoptic area detected 92 h after virus inoculation into the submandibular salivary gland. *Bottom*: extent of viral infection in hypothalamic structures involved in central autonomic control after PRV inoculation into effector organs of thermo- or osmoregulatory importance, such as vascular anastomoses of the tail skin, salivary glands, brown adipose tissue, or the kidneys [54–58]. The degree of PRV infection for each structure is presented as its percentage of total hypothalamic infection (+, 0%–5%; ++, 6%–25%; +++, 26%–50%) after 3–7 days of survival time and comparable infection at the level of the PVN. *BNST*, bed nucleus of the stria terminalis; *LHA*, lateral hypothalamic area; *LS*, lateral septum; *MnPO*, median preoptic nucleus; *MPA*, medial preoptic area; *PVN*, paraventricular nucleus; *OVLT*, organum vasculosum laminae terminalis; *SFO*, subfornical organ. (Modified from [55])

tional labeling of the lamina terminalis at reduced infection of the MPA region.

Differential Activation of Hypothalamic Neurons Involved in the Central Control of Body Temperature or Fluid Homeostasis

Physiological experiments in conscious and anesthetized animals including circumscribed lesioning studies, electrophysiology employing the in vitro brain slice technique, and (viral) neuronal tracing experiments point to partly congruent, partly differential patterns of activated hypothalamic nuclei and connectivites underlying the thermo- and osmoregulatory networks. In recent years, enhanced expression of some neuronal transcription factors such as Fos, Jun, or Crox as products of so-called immediate-early genes (IEGs) has widely been employed as a cellular marker for neuronal activity [64,65]. Numerous reports have been published describing augmented Fos expression in central nervous cell groups after appropriate systemic or central stimulations in conscious, regulating animals, and the histochemistry of IEGs is being increasingly used to also elucidate the cytoarchitecture of hypothalamic control systems like those responsible for thermo- or osmoregulation.

In an attempt to differentiate between thermoregulatory and osmoregulatory patterns of activation, it was made use of an established rat model for short-term heat acclimation (48 h at 34°C) and 24 h water deprivation [9,11,66]. Cellular activation in specific brain areas of the hypothalamus inside the blood–brain barrier (PVN, SON, MPA, VMPO, MnPO, LHA), sensory circumventricular organs of the lamina terminalis (SFO, OVLT), and the septal region (LS) were of importance in the perspective to differentiate hypothalamic targets of osmoregulatory versus thermoregulatory importance.

Activation of Specific Neuronal Groups by Osmoregulatory Stimuli

In dehydrated animals at slightly reduced ECF volume and elevated plasma sodium and AVP concentrations, cellular Fos-like immunoreactivity was consistently enhanced in hypothalamic structures involved in body fluid homeostasis. Numerous immunopositive cell nuclei were seen in the lamina terminalis (OVLT, SFO, and MnPO). The neuroglial portion of the OVLT

outside the BBB contained Fos-expressing cells, especially in its neuroglial lateral border and dorsal cap regions, with only a few neurons in the vascularized core being labeled [33]. The SFO represents another yet less prominent cell cluster exhibiting nuclear Fos-positive cells due to dehydration, with their highest densities located in the anterior and medial SFO at rather homogeneous distribution. In the caudal segments of the SFO, the number of immunopositive cell nuclei decreased continuously [66]. With the number of Fos-positive cells in the OVLT already markedly elevated after 5 h and maximal expression reached after 16 h of dehydration, neurons in the SFO proved to be significantly stimulated only after 24 h of water withdrawal [67].

Pronounced expression of c-*fos* caused by mild extracellular dehydration could also be verified for the MnPO located inside the BBB. With regard to its major subdivisions, the anterior (aMnPO), dorsal (dMnPO), and ventral (vMnPO) segments, all three entities proved to be equally and uniformly stimulated [33,66] (Fig. 3). Some 30% of the Fos-positive MnPO cells directly project to magnocellular neurons of the SON [33,68]. The strong Fos signal seen in the MnPO is consistent with the assumption that the AV_3V region represents a crossroad for the signals that are integrated to a large degree by the MnPO and mediate the distributed central neuronal responses to ECF hypertonicity, hypovolemia, or augmented circulating AngII, which all contribute to the regulatory activities induced by water deprivation. To support this notion, not only the drinking response but also the marked Fos expression occurring in the SON as a result of dehydration could be almost completely suppressed after bilateral AV_3V/MnPO lesioning [69].

In the neuroendocrine structures of the osmoregulatory system, including the SON, the adjacent accessory nuclei, and predominantly the mPVN, the numbers of Fos-immunopositive cells were also substantially increased by dehydration [66] (Fig. 3). Water deprivation for 5 to 48 h, leading to a rapid but mild rise in plasma osmolality, resulted in time-dependent Fos formation and nuclear transfer in the PVN and SON after 5 h with subsequent plateau formation [67].

Dehydration did not substantially enhance Fos-like immunoreactivity in several other structures not primarily involved in salt and fluid balance. With regard to neuroglial nuclei important for central temperature regulation, the number and distribution of immunopositive cell nuclei remained at low density and scattered,

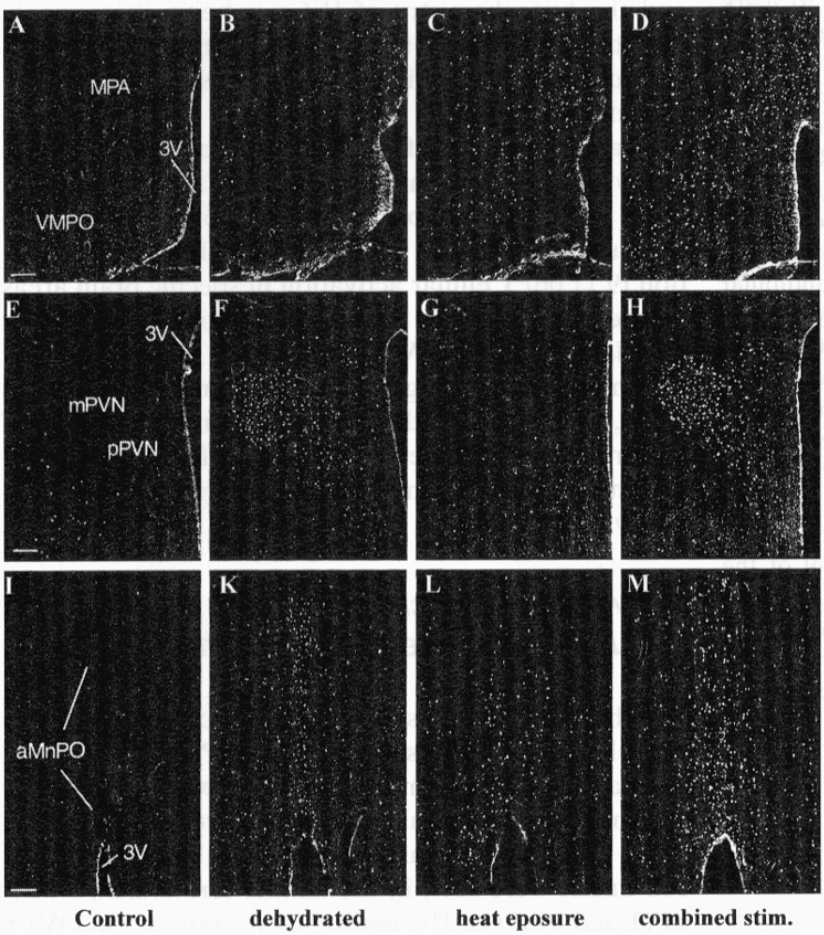

FIG. 3A–M. Differential activation of hypothalamic nuclei by thermal and osmotic stimulations of conscious rats. Spatial distribution of Fos immunoreactive cell nuclei in coronal sections of the rat brain at the level of the medial preoptic area including its ventromedial component (**A–D**), the magnocellular and parvocellular paraventricular nucleus (**E–H**) and the anterior component of the median preoptic nucleus (**I–M**). Representative sections for control euhydrated rats (**A**,**E**,**I**), rats dehydrated for 24 h (**B**,**F**,**K**), rats at short-term heat acclimation for 48 h (**C**,**G**,**L**), and of animals subjected to both stimuli (**D**,**H**,**M**). *3V*, third ventricle; *aMnPO*, anterior median preoptic nucleus; *MPA*, medial preoptic area; *mPVN*, magnocellular paraventricular nucleus; *pPVN*, parvocellular paraventricular nucleus; *VMPO*, ventromedial preoptic area. *Bar* 100 μm. (Modified from [66])

respectively, in the LS, VMPO, MPA, and LHA, with only a twofold increase in the VMPO (Fig. 3).

Looking at body fluid homeostasis, various physiological or pharmacological manipulations of the ECF ionic composition or volume represent the experimental paradigms most often used to elucidate the contribution of various medullary or hypothalamic structures or neurotransmitter systems in the central control mechanisms. Besides hypertonic hypovolemic dehydration or isotonic volume depletion, the application of hypertonic saline via the oral, intravenous (i.v.), intraperitoneal (i.p.), subcutaneous (s.c.), or intragastral route have all been employed to follow neuronal expression of IEGs in the hypothalamus [70].

Quite different from the pattern of Fos activation obtained after dehydration, the i.v. administration of hypertonic saline at low dosage caused marked stimulation of magnocellular cells in the SON, the PVN, and to a minor extent in neurons of the OVLT and lateral parabrachial nucleus. The MnPO, arcuate nucleus, and the SFO, however, showed only moderate Fos induction [71,72]. Many of the activated OVLT-intrinsic neurons directly projected to the magnocellular SON [33,68], and lesioning of the OVLT sigificantly reduced the number of Fos-positive cells in that nucleus [71]. A similar pattern could be observed in animals when the daily drinking water was exchanged for 2% NaCl solution for up to 10 days, resulting in pronounced stimulation of PVN and SON neurons, again diminished after AV_3V destruction [73,74]. Dehydration for as long as 48 h and short-term i.v. infusions of slightly hypertonic saline in most reports did not lead to an elevation of plasma sodium by more than 12 mEq/l and might therefore be termed physiological. The often used experimental approach of strongly hypertonic NaCl solutions injected i.p., on the other hand, resulted in a transient and pronounced rise in plasma sodium, and in most reports caused markedly enhanced Fos expression in all hypothalamic structures of osmoregulatory importance, namely PVN, SON, MnPO, SFO, and OVLT [75,76]. Even under these harsh conditions, however, the MPA of the anterior hypothalamus was devoid of Fos-positive cells [77]. Rather moderate expression of the transscription factor Fos in some structures of the lamina teminalis, at high neuronal activation in the PVN and SON, could also be demonstrated under conditions of isotonic hypovolemia introduced by hemorrhage, polyethylene glycol treatment, or cuffing of the vena cava in the rat or rabbit; this proved to be especially true for the MnPO [78,79]. The intragastric or hepatoportal instillation of hypertonic NaCl, causing mild elevation of the sodium concentration in the portal blood at unchanged general vascular tonicity, markedly augmented Fos immunoreactive cell numbers in the SON and PVN but also in the area postrema and LPBN [80,81]. The ineffectiveness of hypertonic LiCl or mannitol to stimulate both afferent hepatic nerve traffic and hypothalamic Fos expression as well as the full reduction of the NaCl-induced responses after hepatic nerve denervation allows elucidating the role of extracephalic, possibly hepatic, osmoreceptors in the induction of hypothalamic Fos expression [81].

Activation of Specific Neuronal Groups by Thermoregulatory Stimuli

External heat load up to heat stress, cold exposure, and the pharmacological induction of fever represent the experimental paradigms most often used to elucidate the contribution of various medullary or hypothalamic structures and/or neurotransmitter systems to the central control mechanisms underlying thermoregulation. To unravel putative differential activation of hypothalamic entities in conscious animals, exposure to a warm environment (34°C) for 2 days with free access to drinking water represents an almost pure thermoregulatory stimulus. This process of short-term heat acclimation (STHA) resulted in unaltered parameters of the ECF compartment including osmolality, volume, or plasma concentrations of AVP and AngII, at slightly elevated core temperature, and augmented nightly water intake [66].

Among the structures involved in the central perception and integration of thermoregulatory signals and the modulation of febrile phenomena, 2 days of heat exposure enhanced Fos-like immunoreactivity 5- to 10 fold in the MPA and in particular the VMPO as its ventromedial portion, and the LHA (see Fig. 3). With regard to the LS, only its portion located rostrally to the coronal plane with fully developed anterior commissure, and therefore closely associated with the medial septal nucleus, exhibited markedly enhanced activation of the IEG c-*fos*. An acute external heat load of comparable magnitude (33°–36°C) imposed for only 2–3 h also activated Fos expression in the MPA, the lateral preoptic area, and the LS in parallel to the increase in core temperature. Again, the anteromedial and ventromedial MPA revealed the most prominent staining [82,83]. Because most hypothalamic structures that were activated by acute heat load also exhibited enhanced Fos-like immunoreactivity in the rats having undergone STHA, these structures seem to be involved in acute heat defense as well as in the adaptive adjustments presumed to be initiated after the start of longer-lasting heat exposure.

Short exposure of rats to a cold environment (6°–10°C) did not alter Fos expression in the MPA, LHA, or LS in an early study by Scammell and

coworkers [82], whereas significantly augmented Fos expression has been reported for the preoptic area and the LS by Kiyohara and coworkers [83]. Based on the description of cold-sensitive neurons within the area of the MPA [36,49] and the pathways of signal transmission from the preoptic area to striated muscles involved in shivering, for example, [44,48], the latter description does not seem surprising. The potential role of the MPA in integration of peripherally or even centrally perceived cold signals may be deduced from the observation that rat pups at the age of 5–9 days, when transiently exposed to an ambient temperature of 15°C, responded with a drop in core temperature by 8°–10°C, whereas at the age of 10–14 days, it was only reduced by 3°–4°C, indicative of a thermogenic response [84]. Following the cold-induced expression of c-*fos* in various hypothalamic nuclei with age, Fos-positive neurons could first be detected at day 3 in the ventromedial hypothalamus, at day 8 in the PVN, and at day 10 in the preoptic-anterior hypothalamus. The appearance of a cellular response in the latter region to cold ambient temperature might represent a necessary prerequisite for the thermogenic response [84].

In conscious, unrestrained rats subjected to either STHA or acute heat loads in the presence of drinking water, thus not reaching the level of heat stress, neither the SON nor PVN showed increased expression of Fos [82,83]. Only under conditions of severe heat stress and anesthesia in combination with heat stress in rats [85,86], or physical restraint in prepubertal white boars accompanied by a small rise in body temperature [87,88], could augmented c-*fos* mRNA and Fos protein be detected in the SON and PVN of the hypothalamus. Interestingly, also during acute cold exposure numerous cells within the rat parvocellular PVN displayed distinct Fos-like immunoreactivity, which could, however, no longer be observed under conditions of chronic adaptation to a cold environment [82,83,89].

At the level of the CVOs, only a few cell nuclei within the outer zone of the rostral, neuroglial component of the OVLT revealed stimulated c-*fos* expression, whereas the SFO proved to be devoid of Fos protein induction resulting from 48-h heat exposure. The exclusion of the OVLT and the SFO as sensory structures of the osmoregulatory system from activation under STHA conditons is in agreement with the observations made after short-term heat exposure [82,83].

Among the hypothalamic structures also associated with osmoregulation, the number of cell nuclei exhibiting Fos-like immunoreactivity was increased only in the MnPO of the STHA and in rats exposed acutely to heat but not cold and having access to water, thus strengthening the importance of this nucleus for thermoregulatory signal perception or integration as a general phenomenon in mammals. With the aMnPO and vMnPO revealing scattered patterning of Fos expressing cell nuclei located near the dorsal edge of the third ventricle, the dMnPO situated above the anterior commissure showed uniform distribution of Fos-immunopositive cells [66,82] (see Fig. 3).

The pyrogen-induced phenomenon of fever represents a well-known pathophysiological situation at elevated set point of temperature regulation, and the altered expression of IEGs in (extra)hypothalamic structures after systemic or central induction of fever via LPS or cytokine application might substantially add to the understanding of central perception and integration of thermal signals. In agreement with this notion, enhanced Fos-like immunoreactivity was found in the MPA and MnPO in pigs treated intravenously with PGE_2 [88]. Fever induced by microinjection of PGE_2 into the preoptic area, especially along the ventromedial aspects lining the OVLT (VMPO region), is accompanied by the induction of Fos in the VMPO, the MnPO, the parvocellular areas of the PVN, and the NTS, suggestive of the MnPO and structures within the preoptic area such as the VMPO participating in thermoregulatory reception and integration [47]. In male piglets, systemic endotoxin administration led to a significant stimulation of c-*fos* gene expression in both the SON and PVN [90]. In a carefully performed study, Hare et al. [91] injected LPS i.v. at increasing doses into conscious, chronically implanted rats, subsequently followed by the determination of core temperature, plasma corticosterone and c-*fos* expression in (extra) hypothalamic structures. At the lowest LPS concentration inducing a mild rise in body temperature at unchanged plasma corticosteroid levels, Fos protein could be detected in the three sensory CVOs, the OVLT, SFO, and area postrema (AP), as well as the pPVN. At doses far below those necessary to modulate ACTH and corticosterone secretion, interleukin IL-1β also led to induction of c-*fos* mRNA in the OVLT, SFO, AP, and PVN [92]. Interestingly, cells became radiolabeled in two separate but related spatiotemporal patterns. A transient phase with c-*fos* mRNA expression in nonneuronal cells of the outer meninges, endothelial cells of various blood vessels, and choroid plexus cells is followed by a second phase in which endothelial cells, glial cells, and neurons are labeled in the CVOs, the arcuate nucleus, the PVN, or the MPA [92].

Superposition of Osmotic and Thermal Stimuli and Conclusion

When exposed to combined stress of hypohydration and heat exposure, Fos-like immunoreactivity was most

conspicuously enhanced in all neuroglial structures investigated (Figs. 3, 4). In the mPVN and SON, where dehydration alone had markedly increases the number of Fos-positive cells, there was a further significant enhancement when dehydration was combined with heat exposure. This increase proved to be particularly distinct in the MnPO, which had responded to osmotic but also elevated environmental temperature alone. The combined stress induced c-*fos* expression to an almost additive extent due to the activation of neuronal cell populations in all three subdivisions of the MnPO (Figs. 3, 4; see also Fig. 7, later in this chapter). In contrast, the two sensory CVOs outside the blood–brain barrier, which also were profoundly activated after 24 h of water deprivation, did not reveal further augmentation of Fos expression because of hypohydration superimposed upon heat acclimation (Fig. 4).

Among the structures implicated in temperature homeostasis, the intermediate division of the LS displayed intensely labeled cell nuclei along its dorsoventral extension after costimulation. For the MPA including the VMPO and the LHA, the spatial distribution patterns of Fos-immunopositive cell nuclei in costimulated animals were comparable to those seen in animals only exposed to heat. The counts of Fos-expressing cells in the LS and VMPO regions increased significantly when dehydration was superimposed on heat exposure, whereas in the MPA and LHA regions additional dehydration did not further augment the number of immunopositive cells in comparison to heat exposure alone.

When employing Fos immunocytchemistry to map hypothalamic neuronal activity during hypohydration or heat acclimation, only the MnPO responded to both heat and hypohydration stressors, suggesting that the MnPO, in addition to the pPVN, represents an important receptive and integrative hypothalamic structure in which the osmo- and thermoregulatory systems interact. Although early and transient c-*fos* responses seen after acute stimuli might direct cellular activities toward coping with the acute stress, the chronic c-*fos* response could promote cellular activities leading to adaptation of the control system as a whole.

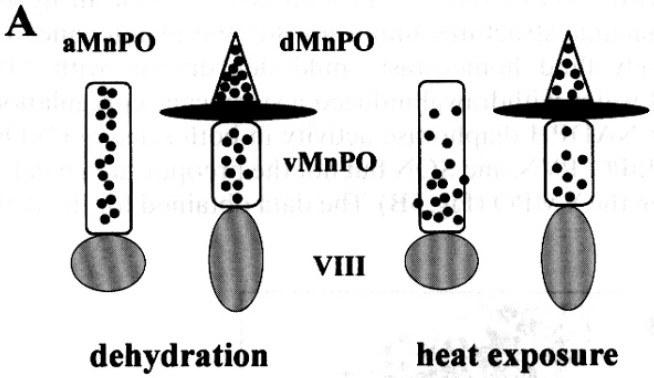

B

	dehydr.	heat exp.	Combin.
SFO	17 **	2	19 **
OVLT	24 **	3	26 **
MnPO	8 **	9 **	15 **
PVN	22 **	2	29 **
SON	24 **	2	36 **
MPA	1	5 **	6 **
VMPO	2	9 **	12 **
LHA	1	5 **	5 **
LS	1	6 **	8 **

FIG. 4A,B. Differential activation of neurons in the median preoptic nucleus by thermal and osmotic stimulation of conscious rats. **A** Schematic spatial distributions of Fos-positive cells in the anterior (*aMnPO*), dorsal (*dMnPO*), and ventral (*vMnPO*) components of the median preoptic nucleus after 24 h dehydration or 48 h heat exposure to 34°C. **B** Increases (x-fold) in the number of Fos-expressing neurons in various (extra)hypothalamic structures (cells per tissue section) involved in the central control of thermoregulation and body fluid homeostasis due to heat exposure, dehydration, or combined stimulation. $^{**}P < 0.01$ according to one-way ANOVA and post hoc Newman–Keuls's testing. *LHA*, lateral hypothalamic area; *LS*, lateral septum; *MnPO*, median preoptic nucleus; *MPA*, medial preoptic area; *PVN*, paraventricular nucleus; *OVLT*, organum vasculosum laminae terminalis; *SFO*, subfornical organ; *SON*, supraoptic nucleus; *VMPO*, ventromedial preoptic area. (Modified from [66])

Differential Activation of Nitrergic Neurons as a Result of Thermal and Osmotic Stimulations

With neurons of the lamina terminalis and the magnocellular nuclei primarily activated by osmotic and volume-driven stimuli, and neurons of the preoptic area, the MnPO, and the LHA activated by thermal stimuli, the question arises how these neurons, especially within the MnPO, could be characterized with regard to their transmitter systems conveying the signals locally for integration or further downstream the neuronal circuitries for efferent control functions. In recent years, neuronally formed nitric oxide (NO) has been postulated, among many other neuromodulators, to play a major role in both central osmo- and thermoregulation.

Numerous studies reported during the past decade have identified the radical gas NO as a widely distributed messenger molecule in the central nervous system. Being neither stored nor released from presynaptic vesicles, NO appears to be generated on demand with a range of action corresponding to its range of diffusion, which has been determined by theoretical kinetics and pharmacologial experiments to be of the order of 200–500 µm at an imposed biological half-life of less than 5 s [93,94]. Cells expressing the neuronal isoform of the generating enzyme nitric oxide synthase (nNOS) can easily be stained for nNOS-specific mRNA or nNOS-intrinsic NADPH diaphorase activity [94]. Using the rat as a model system, nNOS is expressed in neurons of all nuclei of the hypothalamus (the autonomic forebrain) involved in the perception or integration of osmoregulatory as well as thermoregulatory signals [95–98]. Although the nNOS protein itself may be detected in hypothalamic neurons using specific immuncytochemistry, its enzymatic activity can quantitatively be determined by (a) the conversion of tritiated L-[^{3}H]arginine to L-[^{3}H]citrulline, (b) binding of radiolabeled N^G-nitro-L-[^{3}H]arginine to the enzyme, or (c) the computerized optical evaluation of an intracellular, blue-colored formazan product of NADPH diaphorase action.

The Role of NO in the Hypothalamic Control of Body Fluid Homeostasis

With nNOS expressed in numerous cells of all hypothalamic structures important for the maintenance of body fluid homeostasis, mild dehydration with 24 h of water withdrawal induced a significant upregulation of NADPH diaphorase activity in both sensory CVOs, MnPO, PVN, and SON but not the preoptic area including the VMPO (Fig. 5B). The data obtained for the den-

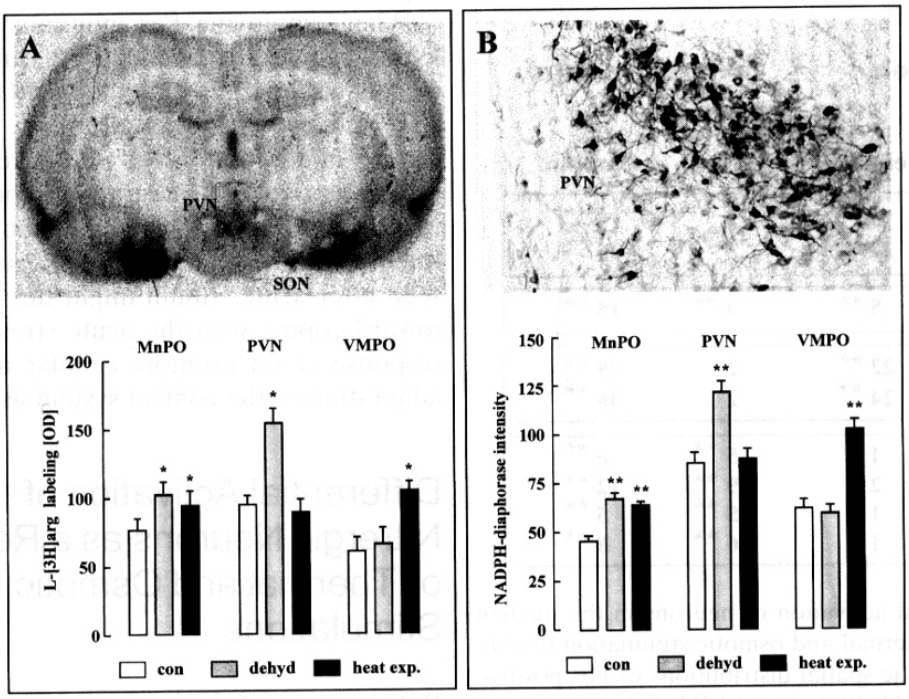

FIG. 5A,B. Differential upregulation of nNOS activity in the rat hypothalamus due to thermal and osmotic stimulation of conscious rats. Animals were either maintained under euthermic conditions with access to drinking water (con), dehydrated for 24 h at RT or exposed to 34°C for 48 h with water available. **A** Autoradiogram of specific in vitro N^G-nitro-L-[^{3}H]arginine binding to an unfixed coronal cryostat section (20 µm) of the rat brain (*top*). Computerized quantification (calibrated optical densities) of radioligand binding to consecutive brain tissue sections containing the median preoptic nucleus, paraventricular nucleus, and ventromedial preoptic area of control, dehydrated, and heat-exposed animals (*bottom*). **B** NADPH diaphorase staining of nitrergic neurons within the paraventricular nucleus of a hypothalamic tissue section (20 µm) obtained from a dehydrated rat after transcardial fixation (*top*). Computerized quantification (calibrated optical densities) of the NADPH diaphorase-specific formazan product in the median preoptic nucleus, paraventricular nucleus, and ventromedial preoptic area of control, dehydrated, and heat-exposed animals (*bottom*). For both approaches to quantify NOS activity in brain structures, values are presented as means ± SEM of four animals per treatment, with 5–10 consecutive tissue sections evaluated per structure and animal. $^*P < 0.05$ according to one-way ANOVA and post hoc Newman–Keuls's testing. *MnPO*, median preoptic nucleus; *PVN*, paraventricular nucleus; *SON*, supraoptic nucleus; *VMPO*, ventromedial preoptic area. (**A**, unpublished data, Gerstberger; **B**, from [114])

sitometric determination of the NADPH diaphorase reaction product were confirmed by quantitative autoradiography employing tritiated N^G-nitro-L-[^{3}H]arginine as radioligand and unfixed hypothalamic tissue sections: dehydration enhanced the ligand binding in the SFO, OVLT, PVN, SON, and MnPO but not the MPA/VMPO (Fig. 5A). Severe dehydration and acute or chronic salt loading additionally enhanced nNOS-specific mRNA expression and translation in both magnocellular nuclei of the rat hypothalamus [99–101], and the numbers of NADPH diaphorase-positive cells increased in PVN, SON, MnPO, and both sensory CVOs of the lamina terminalis, suggesting regulated recruitment of potentially nitrergic neurons [101,102]. At severe dehydration, NADPH diaphorase-positive cells were located primarily in the vascularized inner zone of the OVLT as compared to the localization of moderately stained neurons in the U-shaped neuroglial outer zone of this sensory CVO in euhydrated animals [101]. Within the boundaries of the anterior but not dorsal MnPO, the number of cells positively stained for NADPH diaphorase almost tripled. Adjacent structures such as the nucleus accumbens and the medial septal nucleus did not reveal upregulation of NADPH diaphorase staining [101]. Isotonic hypovolemia of the extracellular fluid compartment, achieved by intraperitoneal administration of polyethylene glycol, significantly enhanced the expression of nNOS mRNA in the SON and parvocellular as well as magnocellular PVN of the rat hypothalamus [103].

With regard to the central control of water intake, intrahypothalamic NO, otherwise acting in most cases as an inhibitory neuromodulator, appears to contribute as a stimulatory agent to drinking induced by dehydration, hypovolemia, salt, and also AngII, at least in the rat [104–106]. This statement is supported by findings that the intracerebroventricular pharmacological blockade of nNOS (Fig. 6D), as well as suppression of nNOS-specific mRNA translation caused by locally acting nNOS antisense oligodeoxynucleotides (Hudl and Gerstberger, unpublished) led to an inhibition of AngII-induced drinking. NO possibly acts via the stimulus–nNOS–NO–cGMP pathway, with cGMP representing the classical second messenger for NO-ergic cellular action. At the level of the SFO, the sensory CVO of the lamina terminalis outside the BBB, however, NO might act as an inhibitory neuromodulator, at least with regard to angiotensinergic stimulation of drinking [107–109].

A large amount of literature has accumulated describing modulatory effects of intrahypothalamic NO on the release of neurohypophyseal AVP, with rather contradictory results obtained depending on the preparation used (in vivo: degree of animal consciousness, osmo- and volume regulatory status of the animal, route of NO donor or NOS antagonist application; in vitro: hypothalamic or neurohypophyseal explants) [110]. Two examples are presented in Fig. 6E in which only in dehydrated rats with elevated plasma concentrations of AVP, but not euhydrated animals, the central application of the NOS antagonist L-NAME as a bolus [104] or continuous microinfusion [111] resulted in augmented release of neurohypophyseal AVP into the circulation, indicative of NO-mediated suppression of AVP secretion. Data obtained by central administration of potent NO donor substances in euhydrated animals, on the other hand, favor the idea of a NO-mediated enhancement of AVP secretion [112]. In humans subjected to mild hypoglycemia, resulting in increased plasma levels of vasopressin, NO might exert an inhibitory role in the glucoprivation-induced stimulation of posterior pituitary hormone release [113]. Summarizing all scientific reports available, a dual action of hypothalamic NO might present a plausible explanation for many of the discrepancies, with NO stimulating the basal release of AVP under conditions of euhydration, but inhibiting the vasopressinergic system under conditions of an activated AVP system.

The Role of NO in the Hypothalamic Control of Body Temperature

Exposing rats to an ambient temperature of 34°C for 2 days resulted in a marked increase in the enzymatic activity of nNOS in hypothalamic structures known to be involved in the central control of thermoregulation, such as the MPA, VMPO, MnPO, and to a limited extent also the OVLT of the lamina terminalis, but not the PVN, SON, or SFO. Enzymatic activity has been determined both as the NADPH diaphorase-specific formation of a dark blue formazan complex in hypothalamic neurons visualized in fixed sections of the rat brain and by quantitative autoradiography of N^G-nitro-L-[^{3}H]arginine binding to NOS in unfixed brain sections (see Fig. 5A,B). The unaltered level of nNOS-specific gene expression in all the hypothalamic structures mentioned, as revealed by quantitative in situ hybridization (Barth and Gerstberger, unpublished data), strongly indicates altered enzymatic nNOS activity as the prime aspect of heat-induced modulation of the hypothalamic nitrergic system. With regard to physiologically relevant thermal stimulations and possible regulation of the central nitrergic system, further histoneurochemical data are not available so far [114]. The systemic injection (i.p.) of LPS in rats with subsequent induction of a robust fever response, on the other hand, led to marked upregulation of mRNA coding for nNOS in the magnocellular and also parvocellular PVN, and the

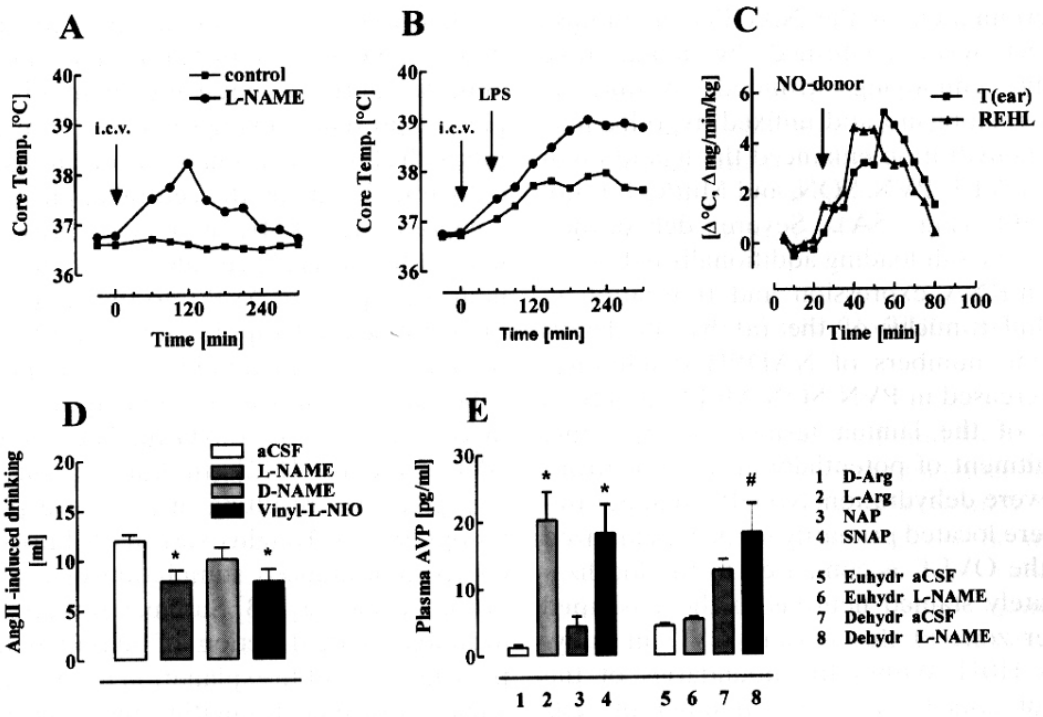

FIG. 6A–E. Nitric oxide (NO) plays a neuromodulatory role in the central control of thermoregulation (**A–C**) and osmoregulation (**D**,**E**). **A**,**B** The intracerebroventricular (*i.c.v.*) application of the general NOS antagonist *L-NAME* (250 µg in 1 µl artificial cerebrospinal fluid, *aCSF*) but not aCSF alone (*control*) caused a transient rise in core temperature of rats maintained at RT (**A**) and enhanced the pyrogenic response of these animals to an i.p. injection of *LPS* (**B**). (Modified from [122]). **C** Microapplication of the NO donor SIN-1 (5 µg in 2 µl aCSF per minute for 30 min) into the third cerebral ventricle of conscious rabbits resulted in a transient activation of cutaneous heat loss, measured as an increase in ear skin temperature (*T(ear)*), and respiratory evaporative heat loss (*REHL*). Modified from [114,117]. **D** The i.c.v. microapplication of the nNOS antagonists vinyl-L-NIO and L-NAME, but not D-NAME (125 µg in 5 µl aCSF) in the conscious rat significantly reduced the drinking response evoked by an immediately following i.c.v. injection of AngII (10 ng in 5 µl aCSF), indicative of NOergic stimulation of oral water intake. (Unpublished data of Hudl and Gerstberger). **E** Modulatory role of central NO on the secretion of AVP from the hypothalamo-neurohypophyseal system in the rat: i.c.v. microapplication of L-arginine (1 mg in 5 µl aCSF), but not D-arginine, and the NO donor SNAP (25 µg in 5 µl aCSF) but not NO-depleted NAP led to a marked release of AVP into the circulation of conscious, euhydrated rats (*left*). (Modified from [112]). In rats dehydrated for 24 h with elevated plasma AVP only, the preceeding long-term i.c.v. infusion (3-day osmotic mini pump; 10 µg L-NAME in 1 µl aCSF/h) caused augmented release of AVP into the circulation (*right*). (From [111])

number of NADPH diaphorase-positive cells in that nucleus was augmented [115].

Evidence for the involvement of centrally acting NO in the homeostatic control of body temperature in homeotherms is accumulating, and most of the available experimental data support the view that NO decreases body temperature if clearly acting at sites involved in thermointegration, for example, anterior hypothalamic structures inside the BBB [114,116]. The short-term local infusion of a potent NO donor substance into the third cerebral ventricle of rabbits at thermoneutral ambient temperature led to a transient reduction in core temperature due to enhanced respiratory and cutaneous heat dissipation, thus facilitating physiological heat loss activities in a coordinated manner [114,117] (see Fig. 6C). A comparable activation of heat-dissipating effector activities of NO has also been described after the systemic application of NO donors in rabbits [118] or indirectly after systemic treatment with NOS inhibitors in rabbits, horses, and rats [5,118,119]. Findings of reduced sweat rates in exercising horses [5] as well as ear skin vasodilation in rabbits [118,120] caused by systemic blockade of all NOS isoenzymes with L-NAME under conditions of external or exercise-driven heat load, however, have to be taken with caution because the effects observed might primarily have been caused by local vasoconstriction rather than central mechanisms. The potential contribution of hypothalamic NO to the effective control of enhanced heat dissipation under hyperthermic conditions, however, is strengthened by the recent finding that hypothalamic NOS blockade in conscious rats resulted in a transient rise of body temperature under euthermic conditions [121,122] (Fig. 6A).

Surveying the data available with regard to the central role of NO in the fever response evoked by either endotoxin, various cytokines, or prostaglandins in rats, rabbits, guinea pigs, and humans shows that rather contradictory observations have been reported so far [114,116,123]. The first conclusive results indicating an antipyretic action of NO released from hypothalamic neurons could be derived from observations that an i.c.v.-administered NO donor reduced the rise in core temperature caused by systemic LPS or intrahypothalamic PGE_2 application in rats [124,125]. In the same species, central nNOS blockade significantly enhanced the fever response to the systemic application of LPS [122] (Fig. 6B). An antipyretic action of NO is also discussed based on elaborate experiments in conscious rabbits as a perfect model for fever research [123] (also see chapter by W. Riedel, this volume). Bacterial LPS entering the bloodstream almost instantly leads to the reticuloendothelial formation of free oxygen radicals (FORs), which then through oxidation of vicinal thiol groups in subunits of the glutaminergic NMDA receptor (possibly in neurons of the preoptic region) appear to be responsible for the initiation of fever. Inhibition of FOR formation or reduction of vicinal thiol groups in the NMDA receptor, on the other hand, enables enhanced glutamate-induced NO formation by these neurons, which subsequently contributes to a downshift of the set point for temperature regulation with concomitant stimulation of heat defense mechanisms.

In disagreement with these reports are studies carried out in anesthetized animals where pharmacological blockade of NO-forming enzymes at the level of the preoptic area attenuated the hyperthermic effects of prostaglandin [126]. The febrile response resulting from direct LPS microinjection into the OVLT of rabbits could be mimicked by local injection of NO donors and reduced by local application of NOS inhibitors [127]. A pyrogenic rather than antipyrogenic effect of NO possibly acting at the level of thermoperception or fever induction within the OVLT and adjacent preoptic parenchyma, for example, becomes obvious from most studies employing the systemic route of NO donor or antagonist application. Thus, in the rat and guinea pig, systemic application of the NOS inhibitor L-NAME at a low concentration attenuated the temperature rise in the second phase of LPS-induced fever [38,128]. At higher concentrations of the NOS antagonist, the fever provoked in guinea pigs by i.p.-injected interleukin-1β also proved to be fully suppressed, despite the fact that the formation of cytokines such as interleukin-6 or TNF-α, two major endogenous pyrogens, was not diminished, suggesting that NO is mediating the fever response independent of the circulating LPS-induced cytokine network [129]. As discussed by Matsumura and coworkers (see chapter by K. Matsumura et al., this volume), diffusion of NO from cerebral capillary endothelium might act as a major mediator of cytokine receptor activation in the vascular endothelium and subsequent PGE_2 synthesis in preoptic hypothalamic structures including the OVLT or MPA, finally resulting in an elevation of the hypothalamic set point for body temperature regulation underlying the fever mechanism.

Cellular Colocalization or Codistribution of Fos and nNOS

Osmo- and thermoregulatory stimuli induced rather specific patterns of nuclear Fos protein and enhanced nNOS activity in hypothalamic structures involved in central homeostatic control. Thus, exposure to heat led to both stimulated Fos expression and augmented nNOS enzymatic activity in the MPA, VMPO, and MnPO, whereas mild dehydration caused both enhanced Fos immunoreactivity and increased nNOS activity in the PVN, SON, MnPO, and the sensory CVOs of the lamina terminalis. This finding fostered the prediction that cellular activation could be associated with alterations in nNOS activity. Combined NADPH diaphorase histochemistry and Fos immunocytochemistry were therefore applied to characterize putative Fos expression in identified nitrergic neurons [130].

After water deprivation with and without combined heat exposure, the IEG c-*fos* proved to be expressed in about 40% and 30% of all nitrergric neurons located within the OVLT and SFO, respectively. With some 15% of MnPO-intrinsic nitrergic neurons being colabeled for the Fos protein (Fig. 7A,B), high percentages of cells (60%) expressing both nuclear Fos and cytosolic nNOS could be evaluated for the magnocellular SON and PVN [131]. Within the MPA and VMPO as putative thermoreceptive structures, however, dehydration did not result in augmented activation of nitrergic neurons. When looking at the induction of Fos and the upregulation of nNOS activity in the same cell during dehydration, the physicochemical stimulus of sodium concentration may have activated certain hypothalamic neurons that subsequently express FOS and also show a higher activity of their own nNOS. The NO formed could then modulate neuronal activity in an autocrine or paracrine fashion.

The functional significance of specific activation of NOergic neurons for the central control of body fluid homeostasis is supported by enhanced Fos expression in some 30%–50% of the nitrergic neurons in the parvo- and magnocellular PVN, and to a minor extent the SON,

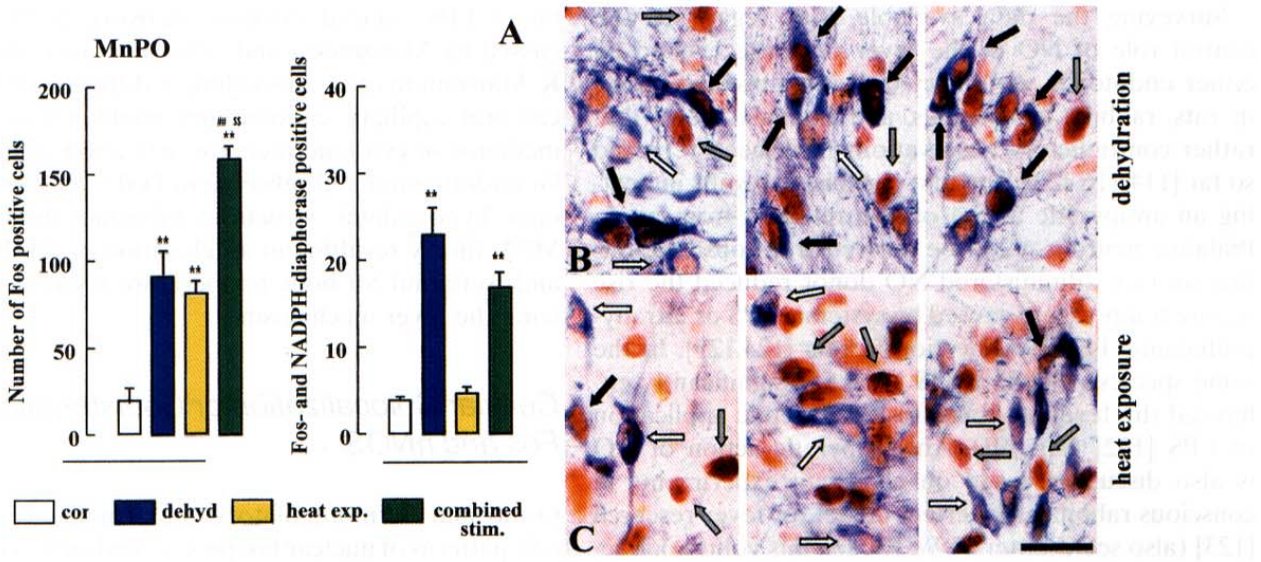

FIG. 7A–C. Activation of nitrergic neurons in the median preoptic nucleus (MnPO) due to both dehydration and heat exposure: differential colocalization or coexpression of Fos and nNOS. The marked stimulation of c-*fos* expression in MnPO cells caused by dehydration (24 h) (**A**,**B**) and heat exposure (34°C; 48 h) (**A**,**C**) proved to be additive under conditions of hypohydration superimposed upon heat acclimation (**A**). Only dehydration either alone or in combination with heat acclimation, but not heat exposure per se, caused an activation of cells also expressing nNOS, as indicated by NADPH diaphorase staining (**A**,**B**). Heat exposure alone led to distinct codistribution but not colocalization of Fos and nNOS proteins within the MnPO (**A**,**C**). *White arrows*, Fos-negative, NADPH diaphorase-positive cells; *gray arrows*, Fos-positive, NADPH diaphorase-negative cells; *black arrows*, cells expressing both Fos and nNOS. *Bar* in **B** 20 μm. (Unpublished data of Patronas and Gerstberger)

SFO, or MnPO, as the result of hemorrhage- and sodium nitroprusside-induced hypotension [132,133]. Primarily the Fos induction in nitrergic PVN neurons projecting to the NTS or the caudal ventrolateral medulla indicated NO as a key player in the hypotension-mediated hypothalamomedullary control system for cardiovascular homeostasis [130]. Under conditions of severe glucoprivation induced by systemic application of the antimetabolite 2-deoxy-glucose, for example, signals generated by glucose-sensitive neurons within the area postrema and NTS of the medulla or the ventromedial nucleus (VMN) of the posterior hypothalamus finally reach the PVN and other integrative hypothalamic units such as the MnPO. In these structures, then, glucoprivation caused pronounced expression of the c-*fos* gene in 40%–80% of all NADPH diaphorase-positive cells, whereas nNOS-containing cells proved not to be stimulated in the VMN and lateral hypothalamic area, major structures involved in the central regulation of energy balance [134].

Also, the peptide AngII, acting both as circulating factor and brain-intrinsic neuromodulator to stimulate thirst and enhance peripheral resistance during extracellular hypovolemia in mammals, caused distinct activation of 15%–25% of all NADPH diaphorase-positive neurons in SFO, MnPO, OVLT, SON, and parvo—and magnocellular PVN [106,135]. The eminent drinking response in animals receiving an i.c.v. injection of AngII, thus mimicking centrally formed AngII, could largely be inhibited by coapplication of the NOS inhibitor L-NAME, whereas the patterns of Fos induction in the lamina terminalis (SFO, MnPO, OVLT) as well as the magnocellular nuclei (PVN, SON) remained unaltered. The time sequence of the drinking response and enhanced Fos production indicated that "NO production might occur downstream of Fos production or that AngII-induced c-*fos* expression occurs via a parallel, NO-independent mechanism" [106].

Quite in contrast to the various osmoregulatory and volume regulatory stimuli, short-term heat acclimation induced Fos expression in less than 8% of all nNOS-containing cells within the MPA–VMPO complex and less than 3% of nitrergic neurons in any other hypothalamic structure investigated. At these low levels of cellular nNOS–Fos colocalization not different from unstimulated control conditions, cells expressing Fos as the result of heat exposure proved to be rather codistributed with nitrergic neurons, often in "nearest-neighbor" positions within the MnPO, including all its substructures, as well as the MPA–VMPO (Fig. 7C). This finding of a pronounced codistribution of Fos-positive neurons and NOergic neurons triggered the hypothesis that thermal stimulation might induce increased neuronal NO formation with subsequent nitrergic induction of c-*fos* expression in closely associated cells in an autocrine or paracrine fashion. Microscopic analysis revealed

the presence of basket-like fiber configurations originating from nitrergic neurons in close contact with Fos-positive cells in the MnPO of heat-exposed animals. In addition, nitrergic fibers could be localized in intimate vicinity to many hypothalamic Fos-positive cells activated by nitroglycerol-evoked systemic hypotension, thus providing a neuroanatomical basis for the autocrine and paracrine signal transduction between nNOS-positive cells and their nearest-neighbor target cells [136].

First indications that NO can induce the expression of c-*fos* in neurons or cells of neural crest origin, possibly through activation of the cyclic GMP pathway, could be derived from studies in cultured adrenal medullary pheochromocytoma PC12 cells [137]. In the central nervous system of the rat, primarily evidence for a functional significance of this pathway was demonstrated in several studies confirming a close relationship between NO and Fos expression. In the rat suprachiasmatic nucleus (SCN), NO appears to mediate the glutamate-induced phase resetting of the SCN pacemaker. The general NOS antagonist L-NAME, but not its stereoisomer D-NAME, significantly suppressed light-induced Fos expression, suggesting a light–glutamate–NO–Fos signal transduction cascade involving at least two neuronal populations [138]. Immobilization stress resulted in marked expression of the c-*fos* gene in the parvocellular but also the magnocellular PVN of the rat hypothalamus, and numerous Fos-positive neurons in the anterior and medial pPVN also contained nNOS. Pharmacological blockade of nNOS activity not only resulted in a reduction of Fos-positive cells but also the almost complete absence of cells double-stained for Fos and NADPH diaphorase [139].

Besides this obviously stimulatory action of neuronally released NO on the Fos expression of closely associated neurons, inhibitory nitregic neuromodulation has also been reported. Thus, the low expression of c-*fos* in the MPA of the female rat with suckling pups was markedly augmented after central pharmacological blockade of nNOS, indicative of NO-mediated attenuation of neuronal activation [140]. Also, the exogenous activation of NO–cGMP signaling within the PVN caused by i.c.v. administration of a NO donor inhibited Fos expression driven by glucodeprivation in vasopressinergic neurons of both PVN and SON, suggesting nitrergic modulation of neurosecretion through autocrine or paracrine mechanisms [141].

Concluding Remarks

Differential stimulation of the osmoregulatory and thermoregulatory autonomic circuitries, at least in the rat as an experimental model, results in differentiated activation of specific neuronal populations in various hypothalamic nuclei such as the SFO, OVLT, PVN, and SON for osmoregulation, and MPA, VMPO, LHA, and LS for thermoregulation. The MnPO, activated by thermal as well as osmotic stimuli, plays a major role as an integrative structure involved in both central control systems. The enzyme nNOS, generating NO as a neuromodulatory agent involved in the centrally controlled homeostasis of body temperature and the ECF compartment, is upregulated in the respective hypothalamic structures during either heat exposure or osmotic stimulation. Although the latter results in coexpression of the Fos protein as marker of neuronal activity with nNOS in the same neurons, Fos-positive cells and nitrergic cells are found codistributed following thermal stimulation, indicative of NO-mediated neuronal activation in nearest-neighbor target neurons.

References

1. Mack GW, Nadel E (1996) Body fluid balance during heat stress in humans. In: Fregly KJ, Blatteis CM (eds) Handbook of physiology: Environmental physiology, vol 1. Oxford University Press, New York, pp 187–214
2. Baker MA, Doris PA (1982) Effect of dehydration on hypothalamic control of evaporation in the cat. J Physiol (Lond) 322:131–142
3. Baker MA, Doris PA, Hawkins MJ (1983) Effect of dehydration and hyperosmolality on thermoregulatory water losses in exercising dogs. Am J Physiol 244:R516–R521
4. Turleska-Stelmasiak E (1974) The influence of dehydration on heat dissipation mechanisms in the rabbit. J Physiol (Paris) 68:5–15
5. Mills PC, Scott CM, Marlin DJ (1997) Effects of nitric oxide inhibition on thermoregulation during exercise in the horse. In: Blatteis CM (ed) Thermoregulation. Ann New York Acad Sci 813:591–599
6. Keil R, Gerstberger R, Simon E (1994) Hypothalamic thermal stimulation modulates vasopressin release in hyperosmotically stimulated rabbits. Am J Physiol 267:R1089–R1097
7. Horowitz M (1994) Heat stress and heat acclimation: the cellular response-modifier of autonomic control. In: Pleschka K, Gerstberger R (eds) Integrative and cellular aspects of autonomic functions: Temperature and osmoregulation. Libbey, Paris, pp 87–95
8. Baker MA, Dawson D (1985) Inhibition of thermal panting by intracarotid infusion of hypertonic saline in dogs. Am J Physiol 249:R787–R791
9. Horowitz M, Meiri U (1985) Thermoregulatory activity in the rat: effects of hypohydration, hypovolemia and hypertonicity and their interaction with short-term heat acclimation. Comp Biochem Physiol 82:577–582

10. Taylor CR (1970) Dehydration and heat: effects on temperature regulation of East African ungulates. Am J Physiol 219:1136–1139
11. Horowitz M, Samueloff S (1989) Dehydration, stress and heat acclimation. Prog Biometeorol 7:87–95
12. Bie P (1980) Osmoreceptors, vasopressin and control of renal water excretion. Physiol Rev 60:961–1048
13. Gerstberger R, Müller AR, Hübschle T (1997) Hypothalamic control of osmoregulation. In: Harvey S, Etches RJ (eds) Perspectives in avian endocrinology. Journal of Endocrinology, Bristol, pp 289–303
14. Baker MA (1984) Influence of dehydration on panting in mammals. In: Hales JRS (ed) Thermal physiology. Raven Press, New York, pp 407–412
15. Horowitz M, Nadel ER (1984) Effect of plasma volume on thermoregulation in dogs. Pflugers Arch 400:211–213
16. Thornton RM, Proppe DW (1988) Influence of dehydration on locally mediated hindlimb vasodilation in baboons. Am J Physiol 255:H266–H271
17. Takamata A, Nose H, Mack GW, et al (1990) Control of total peripheral resistance during hyperthermia in rats. J Appl Physiol 69:1087–1092
18. Morimoto T (1990) Thermoregulation and body fluids: role of blood volume and central venous pressure. Jpn J Physiol 40:165–179
19. Simon E, Pierau FK, Taylor DCM (1986) Central and peripheral thermal control of effectors in homeothermic temperature regulation. Physiol Rev 66:235–289
20. Simon E (1999) Thermoregulation as a switchboard of autonomic nervous and endocrine control. Jpn J Physiol 49:297–323
21. Sadowski J, Kruk B, Chwalbinska-Moneta J (1977) Renal function changes during preoptic-anterior hypothalamic heating in the rabbit. Pflugers Arch 370:51–57
22. Hayward JN, Baker MA (1968) Diuretic and thermoregulatory reponses to preoptic cooling in the monkey. Am J Physiol 214:843–850
23. Forsling ML, Ingram DL, Stanier MW (1976) Effects of various ambient temperatures and of heating and cooling the hypothalamus and cervical spinal cord on antidiuretic hormone secretion and urinary osmolality in pigs. J Physiol (Lond) 257:673–686
24. Takamata A, Mack GW, Stachenfeld NS, et al (1995) Body temperature modification of osmotically induced vasopressin secretion and thirst in humans. Am J Physiol 269:R874–R880
25. Swanson LW (1987) The hypothalamus. In: Björklund A, Hökfeld T, Swanson LW (eds) Handbook of chemical neuroanatomy, vol 5. Integrated systems of the CNS, part 1. Elsevier, Amsterdam, pp 1–120
26. Morris JF, Chapman DB, Sokol HW (1987) Anatomy and function of the classic vasopressin-secreting hypothalamus-neurohypophyseal system. In: Gash DN, Boer GJ (eds) Vasopressin: principles and properties. Plenum, New York, pp 1–89
27. McKinley MJ, McAllen AM, Mendelsohn FAO, et al (1990) Circumventricular organs: neuroendocrine interfaces between the brain and the hemal milieu. Front Neuroendocrinol 11:91–127
28. McKinley MJ, Gerstberger R, Mathai ML, et al (1999) The lamina terminalis and its role in fluid and electrolyte homeostasis. J Clin Neurosci 6:289–301
29. Miselis RR (1981) The efferent projections of the subfornical organ of the rat: a circumventricular organ within a neural network subserving water balance. Brain Res 230:1–23
30. Tanaka J, Hayashi Y, Watai T, et al (1997) Angiotensinergic modulation of osmotic activation of neurosecretory neurons. Neuroreport 8:2903–2906
31. Hartle DK, Brody MJ (1982) Hypothalamic vasomotor pathways mediating the development of hypertension in the rat. Hypertension 4(suppl III):68–71
32. Aradachi H, Honda K, Negoro H, et al (1996) Median preoptic neurones projecting to the supraoptic nucleus are sensitive to haemodynamic changes as well as to rise in plasma osmolality in rats. J Neuroendocrinol 8:35–43
33. McKinley MJ, Hards DK, Oldfield BJ (1994) Identification of neural pathways activated in dehydrated rats by means of Fos-immunohistochemistry and neural tracing. Brain Res 653:305–314
34. Voisin DL, Simonian SX, Herbison AE (1997) Identification of estrogen receptor-containing neurons projecting to the rat supraoptic nucleus. Neuroscience 78:215–228
35. Honda K, Aradachi H, Higuchi T, et al (1992) Activation of paraventricular neurosecretory cells by osmotic stimulation of the median preoptic nucleus. Brain Res 594:335–338
36. Pierau FK, Sann H, Yakimova KS, et al (1998) Plasticity of hypothalamic temperature-sensitive neurons. In: Sharma HS, Westman J (eds) Brain function in hot environment. Prog Brain Res 115:63–84
37. Zeisberger E (1990) The role of septal peptides in thermoregulation. In: Bligh JK, Voigt K (eds) Thermoreception and temperature regulation. Springer, Heidelberg, pp 273–284
38. Roth J, Störr B, Voigt K, et al (1998) Inhibition of nitric oxide synthase attenuates lipopolysaccharide-induced fever without reduction of circulating cytokines in guinea pigs. Pflugers Arch 436:858–862
39. Blatteis CM, Sehic E (1997) Fever: how may circulating pyrogens signal the brain? NIPS 14:1–9
40. Cao C, Matsumura K, Yamagata K, et al (1996) Endothelial cells of the rat brain vasculature express cyclooxygenase-2 mRNA in response to systemic interleukin-1 beta: a possible role of prostaglandin synthesis responsible for fever. Brain Res 733:262–272
41. Atrens DM, Williams MP, Brady CJ, et al (1982) Energy balance and hypothalamic self-stimulation. Behav Brain Res 5:131–142
42. Bernardi LL, Bellinger LL (1993) The lateral hypothalamic area revisited: neuroanatomy, body weight regulation, neuroendocrinology and metabolism. Neurosci Biobehav Rev 17:141–193
43. Chiba T, Murata Y (1985) Afferent and efferent connections of the medial preoptic area in the rat: a WGA-HRP study. Brain Res Bull 14:261–272

44. Kanosue K, Hosono T, Zhang YH, et al (1998) Neuronal networks controlling thermoregulatory effectors. In: Sharma HS, Westman J (eds) Brain function in hot environment. Prog Brain Res 115:49–62
45. Staiger JF, Nürnberger F (1991) The efferent connections of the lateral septal nucleus in the guinea pig: projections to the diencenphalon and brainstem. Cell Tissue Res 264:391–413
46. Tonelli L, Chiaraviglio E (1995) Dopaminergic neurons in the zona incerta modulate ingestive behavior in rats. Physiol Behav 58:725–729
47. Elmquist JK, Scammell TE, Jacobson CD, et al (1996) Distribution of Fos-like immunoreactivity in the rat brain following intravenous lipopolysaccharide administration. J Comp Neurol 371:85–103
48. Kanosue K, Zhang YH, Yanase-Fujiwara M, et al (1994) Hypothalamic network for thermoregulatory shivering. Am J Physiol 267:R275–R282
49. Boulant JA (1996) Hypothalamic neurons regulating body temperature. In: Fregly KJ, Blatteis CM (eds) Handbook of physiology: Environmental physiology, vol 1. Oxford University Press, New York, pp 105–126
50. Bourque CW, Oliet SHR (1997) Osmoreceptors in the central nervous system. Annu Rev Physiol 59:601–619
51. Hori T, Nakashima H, Koga H, et al (1988) Convergence of thermal, osmotic and cardiovascular signals on preoptic and anterior hypothalamic neurons in the rat. Brain Res Bull 20:879–885
52. Boulant JA, Silva NL (1989) Multisensory hypothalamic neurons may explain interactions among regulatory systems. NIPS 4:245–248
53. Travis K, Johnson AK (1993) In vitro sensitivity of median preoptic neurons to angiotensin II, osmotic pressure and temperature. Am J Physiol 264:R1200–R1205
54. Smith JE, Jansen AS, Gilbey MP, et al (1998) CNS cell groups projecting to sympathetic outflow of tail artery: neural circuits involved in heat loss in the rat. Brain Res 786:153–164
55. Hübschle T, McKinley MJ, Oldfield BJ (1998) Efferent connections of the lamina terminalis, the preoptic area and the insular cortex to submandibular and sublingual gland of the rat traced with pseudorabies virus. Brain Res 806:219–231
56. Jansen ASP, Ter Horst GJ, Mettenleiter TC, et al (1992) CNS cell groups projecting to the submandibular parasympathetic preganglionic neurons in the rat: a retrograde transneuronal viral cell body labeling study. Brain Res 572:253–260
57. Bamshad M, Song CK, Bartness TJ (1999) CNS origins of the sympathetic nervous system outflow to brown adipose tissue. Am J Physiol 276:R1569–R1578
58. Sly D, Colvill L, McKinley MJ, et al (1999) Identification of neural projections from the forebrain to the kidney using the virus pseudorabies. J Auton Nerv Syst 77:73–82
59. Huang J, Weiss ML (1999) Characterization of the central cell groups regulating the kidney in the rat. Brain Res 845:77–91
60. Kanosue K, Nakayama T, Tanaka H, et al (1990) Modes of action of local hypothalamic and skin thermal stimulation on salivary secretion in rats. J Physiol (Lond) 424:459–471
61. Weekley LB (1992) Renal secretion rate and norepinephrine secretion rate in response to centrally administered angiotensin II: role of the medial basal forebrain. Clin Exp Hypertens A 14:923–945
62. May CB, McAllen R, McKinley MJ (1997) Responses of renal sympathetic nerve activity to systemically and centrally administered angiotensin. J Auton Nerv Syst 65:81–82
63. Westerhaus MJ, Loewy AD (1999) Sympathetic-related neurons in the preoptic regions of the rat identified by viral transneuronal labeling. J Comp Neurol 414:361–378
64. Morgan JI, Curran T (1991) Stimulus-transcription coupling in the nervous system: involvement of the inducible proto-oncogenes fos and jun. Annu Rev Neurosci 14:421–451
65. Sagar M, Sharp FR, Curran T (1988) Expression of c-Fos protein in brain: metabolic mapping at the cellular level. Science 240:1328–1331
66. Patronas P, Horowitz M, Simon E, et al (1998) Differential stimulation of c-fos expression in hypothalamic nuclei of the rat brain during short-term heat acclimation and mild dehydration. Brain Res 798:127–139
67. Morien A, Garrard L, Rowland N (1999) Expression of Fos immunoreactivity in rat brain during dehydration: effect of duration and timing of water deprivation. Brain Res 816:1–7
68. Oldfield BJ, Badoer E, Hards DK, et al (1994) Fos production in retrogradely labelled neurons of the lamina terminalis following intravenous infusion of hypertonic saline or angiotensin II. Neuroscience 60:255–262
69. Xu Z, Herbert J (1996) Effects of unilateral or bilateral lesions within the anteroventral third ventricular region on c-fos expression induced by dehydration or angiotensin II in the supraoptic and paraventricular nuclei of the hypothalamus. Brain Res 713:36–43
70. Rowland NE (1998) Brain mechanisms of mammalian fluid homeostasis: insights from use of immediate early gene mapping. Neurosci Biobehav Rev 32:49–63
71. Hochstenbach SL, Ciriello J (1996) Effect of lesions of forebrain circumventricular organs on c-fos expression in the central nervous system to plasma hypernatremia. Brain Res 713:17–28
72. Han L, Rowland NE (1996) Dissociation of Fos-like immunoreactivity in lamina terminalis and magnocellular hypothalamic nuclei induced by hypernatremia. Brain Res 708:45–49
73. Miyata S, Nakashima T, Kiyohara T (1994) Expression of c-fos immunoreactivity in the hypothalamic magnocellular neurons during chronic osmotic stimulation. Neurosci Lett 175:63–66
74. Rocha MJA, Beltz TG, Dornelles RCM, et al (1999) Anteroventral third ventricle (AV3V) lesions alter *c-fos* expression induced by salt loading. Brain Res 829:197–200

75. Giovannelli L, Bloom FE (1992) c-Fos expression in the rat subfornical organ following osmotic stimulation. Neurosci Lett 139:1–6
76. Guldenaar SEF, Noctor SC, McCabe JT (1992) Fos-like immunoreactivity in the brain of homozygous diabetes insipidus Brattleboro and normal Long-Evans rats. J Comp Neurol 322:439–448
77. Hamamura M, Nunez DJR, Leng G, et al (1992) c-fos may code for a common transscription factor within the hypothalamic neural circuits involved in osmoregulation. Brain Res 572:42–51
78. Smith DW, Day TA (1995) Hypovolaemic and osmotic stimuli induce distinct patterns of c-fos expression in the rat subfornical organ. Brain Res 698:232–236
79. Potts PD, Ludbrook J, Gillman-Gaspari TA, et al (1999) Activation of brain neurons following central hypervolaemia and hypovolaemia: contribution of baroreceptor and non-baroreceptor inputs. Neuroscience 95:499–511
80. Carlson SH, Beitz A, Osborn JW (1997) Intragastric hypertonic saline increases vasopressin and central fos immunoreactivity in conscious rats. Am J Physiol 272:R750–R758
81. Morita H, Yamashita Y, Nishida, et al (1997) Fos induction in rat brain neurons after stimulation of the hepatoportal Na-sensitive mechanism. Am J Physiol 272:R913–R923
82. Scammell TE, Price KJ, Sagar SM (1993) Hyperthermia induces c-fos expression in the preoptic area. Brain Res 618:303–307
83. Kiyohara T, Miyata S, Nakamura T, et al (1995) Differences in Fos expression in the rat brain between cold and warm ambient exposures. Brain Res Bull 38:192–201
84. Joyce MP, Barr GA (1992) The appearance of Fos protein-like immunoreactivity in the hypothalamus of developing rats in response to cold ambient temperatures. Neuroscience 49:163–173
85. Hübschle T, Oldfield BJ, McKinley MJ, et al (1999) The median preoptic nucleus of the rat: a putative hypothalamic integration site of thermo- and osmoregulatory signals during heat stress. Pflugers Arch 437:P24–10
86. Lin MT, Yang YL, Tsay HJ (1999) C-fos expression in rat brain during heat stress. J Therm Biol 24:423–427
87. Vellucci SV, Parrott RF (1994) Hyperthermia-associated changes in Fos protein in the median preoptic and other hypothalamic nuclei of the pig following intravenous administration of prostaglandin E_2. Brain Res 646:165–169
88. Vellucci SV, Parrott RF (1995) Prostaglandin-dependent c-fos expression in the median peoptic nucleus of pigs subjected to restraint: correlation with hyperthermia. Neurosci Lett 198:49–51
89. Miyata S, Ishiyama M, Shido O, et al (1995) Central mechanism of neural activation with cold acclimation of rats using Fos immunocytochemistry. Neurosci Res 22:209–218
90. Velluci SV, Parrott RF, Mimmack ML, et al (1999) Endotoxin effects on hypothalamic gene expression in swine following sequencing of porcine c-fos mRNA. J Endotoxin Res 5:31–35
91. Hare AS, Calreke G, Tolchard S (1995) Bacterial lipopolysaccharide-induced changes in Fos protein expression in the rat brain—correlation with thermoregulatory changes and plasma corticosterone. J Neuroendocrinol 7:791–799
92. Herkenham M, Lee HY, Baker RA (1998) Temporal and spatial patterns of c-fos mRNA induced by intravenous interleukin-1: a cascade of non-neuronal cellular activation at the blood-brain barrier. J Comp Neurol 400:175–196
93. Wood J, Garthwaite J (1994) Models of diffusional spread of nitric oxide: implications for neural nitric oxide signalling and its pharmacological properties. Neuropharmacology 33:1235–1244
94. Vincent S (1995) Nitric oxide in the nervous system. Academic Press, London
95. Krukoff TL (1999) Central actions of nitric oxide in regulation of autonomic functions. Brain Res Rev 30:52–65
96. Iwase K, Iyama K, Akagi K, et al (1998) Precise distribution of neuronal nitric oxide synthase mRNA in the rat brain revealed by non-radioisotopic in situ hybridization. Mol Brain Res 53:1–12
97. Jurzak MR, Schmid HA, Gerstberger R (1994) NADPH-diaphorase staining and NO-synthase immunoreactivity in circumventricular organs of the rat brain. In: Pleschka K, Gerstberger R (eds) Integrative and cellular aspects of autonomic functions: temperature and osmoregulation. Libbey, Paris, pp 451–459
98. Wang F, Morris JF (1996) Constitutive nitric oxide synthase in hypothalami of normal and hereditary diabetes insipidus rats and mice: role of nitric oxide in osmotic regulation and its mechanisms. Endocrinology 137:1745–1751
99. Villar M, Ceccatelli S, Ronnqvist M, et al (1994) Nitric oxide synthase increases in hypothalamic magnocellular neurons after salt loading in the rat. An immunohistochemical and in situ hybridization study. Brain Res 644:273–281
100. Kadowaki K, Kishimoto J, Lang G, et al (1994) Upregulation of nitric oxide synthase (NOS) gene expression together with NOS activity in the rat hypothalamohypophysial system after chronic salt loading: evidence of a neuromodulatory role of nitric oxide in arginine vasopressin and oxytocin secretion. Endocrinology 134:1011–1017
101. Ciriello J, Hoechstenbach SL, Solano-Flores LP (1996) Changes in NADPH-diaphorase activity in forebrain structures of the lamina terminalis after chronic dehydration. Brain Res 708:167–172
102. Ueta Y, Levy A, Chowdrey HS, et al (1995) Water deprivation in the rat induces nitric oxide synthase (NOS) gene expression in the hypothalamic paraventricular and supraoptic nuclei. Neurosci Res 23:317–319
103. Ueta Y, Levy A, Lightman SL, et al (1998) Hypovolemia upregulates the expression of neuronal nitric oxide synthase gene expression in the paraventricular and supraoptic nuclei of rats. Brain Res 790:25–32

104. Liu H, Terrell ML, Bui V, et al (1998) Nitric oxide control of drinking, vasopressin and oxytocin release and blood pressure in dehydrated rats. Physiol Behav 63:763–769
105. Kadekaro M, Terrell ML, Harmann P, et al (1994) Central inhibition of nitric oxide synthase attenuates water intake but does not alter enhanced glucose utilization in the hypothalamo-neurohypophyseal system of dehydrated rats. Neurosci Lett 173:115–118
106. Zhu B, Herbert J (1997) Angiotensin II interacts with nitric oxide-cyclic GMP pathway in the central control of drinking behaviour: mapping with c-fos and NADPH-diaphorase. Neuroscience 79:543–553
107. Calapai G, Squadrito F, Altavilla D, et al (1992) Evidence that nitric oxide modulates drinking behaviour. Neuropharmacology 31:761–764
108. Nicolaidis S, Fitzsimons JT (1975) La dépendence de la prise d'eau induite par angiotensine II envers la fonction vasomotrice cérébrale locale chez le rat. CR Acad Sci Paris 281:1417–1420
109. Rauch M, Schmid HA, DeVente J, et al (1998) Electrophysiological and immunocytochemical evidence for a cGMP-mediated inhibition of subfornical organ neurons by nitric oxide. J Neurosci 17:363–371
110. Reïd IA (1994) Role of nitric oxide in the regulation of renin and vasopressin secretion. Front Neuroendocrinol 15:351–383
111. Gerstberger R, Seeman T, Rettig R (1996) Chronic central inhibition of neuronal nitric oxide synthase (nNOS) enhances NADPH-diaphorase activity in SON/PVN and vasopressin release in the conscious rat. Neuroforum 2(suppl):169
112. Ota M, Crofton JT, Festavan GT, et al (1993) Evidence that nitric oxide can act centrally to stimulate vasopressin release. Neuroendocrinology 57:955–959
113. Chipodera P, Volpi R, Coiro V (1994) Inhibitory control of nitric oxide on the arginine-vasopressin and oxytocin response to hypoglycemia in normal men. Neuroreport 5:1822–1824
114. Gerstberger R (1999) Nitric oxide and body temperature control. NIPS 14:30–36
115. Harada S, Imaki T, Chikada N, et al (1999) Distinct distribution and time-course changes in neuronal nitric oxide synthase and inducible NOS in the paraventricular nucleus following lipopolysaccharide injection. Brain Res 821:322–332
116. Simon E (1998) Nitric oxide as a peripheral and central mediator in temperature regulation. Amino Acids 14:87–93
117. Eriksson S, Hjelmqvist H, Keil R, et al (1997) Central application of a nitric oxide donor activates heat defense in the rabbit. Brain Res 774:269–273
118. Mathai ML, Hjelmquist H, Keil R, et al (1997) Nitric oxide increases cutaneous and respiratory heat dissipation in conscious rabbits. Am J Physiol 272:R1691–R1697
119. Gautier H, Murariu C (1999) Role of nitric oxide in hypoxic hypometabolism in rats. J Appl Physiol 87:104–110
120. Taylor WF, Bishop VS (1994) A role for nitric oxide in active thermoregulatory vasodilation. Am J Physiol 264:H1355–H1359
121. De Luca B, Monda M, Sullo A (1995) Changes in eating behaviour and thermogenic activity following inhibition of nitric oxide formation. Am J Physiol 268:R1533–R1538
122. Almeida MC, Trevisan FN, Barros RCH, et al (1999) Tolerance to lipopolysaccharide is related to the nitric oxide pathway. Neuroreport 10:3061–3065
123. Riedel W, Maulik G (1999) Fever: an integrated response of the central nervous system to oxidative stress. Mol Cell Biochem 196:125–132
124. Monda M, Amaro S, Sullo A, et al (1995) Nitric oxide reduces body temperature and sympathetic input to brown adipose tissue during PGE_2-hyperthermia. Brain Res Bull 38:489–493
125. Gourine AV (1995) Pharmacological evidence that nitric oxide can act as an endogenous antipyretic factor in endotoxin-induced fever in rabbits. Gen Pharmacol 26:835–841
126. Amir S, De Blasio E, English AM (1991) *NG*-Monomethyl-L-arginine co-injection attenuates the thermogenic and hyperthermic effects of E2 prostaglandin microinjection into the anterior hypothalamic preoptic area in rats. Brain Res 556:157–160
127. Lin JH, Lin MT (1997) Nitric oxide synthase–cyclic oxygenase pathway in organum vasculosum laminae terminalis: possible role in pyrogen fever in rabbits. Br J Pharmacol 118:179–185
128. Scammel TE, Elmquist JE, Saper CB (1996) Inhibition of nitric oxide synthase produces hypothermia and depresses lipopolysaccharide fever. Am J Physiol 271:R333–R338
129. Roth J, Störr B, Voigt K, et al (1998) Inhibition of nitric oxide synthase results in a suppression of interleukin-1β-induced fever in rats. Life Sci 62:345–350
130. Krukoff TL, MacTavish D, Jhamandas JH (1997) Activation by hypotension of neurons in the hypothalamic paraventricular nucleus that project to the brainstem. J Comp Neurol 385:285–296
131. Ying Z, Buggy J (1993) Nitric oxide neurons in hypothalamus and lamina terminalis express c-fos following dehydration treatments. Proc Soc Neurosci 19:93
132. Petrov T, Harris KH, MacTavish D, et al (1995) Hypotension induces Fos immunoreactivity in NADPH-diaphorase positive neurons in the paraventricular and supraoptic hypothalamic nuclei of the rat. Neuropharmacology 34:509–514
133. Tassorelli C, Joseph SA (1995) NADPH-diaphorase activity and Fos expression in brain nuclei following nitroglycerin administration. Brain Res 695:37–44
134. Briski KP, Sylvester PW (1999) Site-specific induction of Fos immunoreactivity in preoptic and hypothalamic NADPH-diaphorase positive neurons during glucoprivation. Neuroendocrinology 69:181–190
135. Dawson CA, Jhamandas JH, Krukoff TL (1998) Activation by systemic angiotensin II of neurochemically identified neurons in rat hypothalamic paraventricular nucleus. J Neuroendocrinol 10:453–459

136. Tassorelli C, Joseph SA, Buzzi MG, et al (1999) The effects on the central nervous system of nitroglycerin—putative mechanisms and mediators. Prog Neurobiol 57:607–624
137. Haby K, Lisovoski F, Aunis D, et al (1994) Stimulation of the cyclic GMP pathway by NO induces expression of the immediate early genes c-fos and junB in PC12 cell. J Neurochem 62:496–501
138. Amir S, Edelstein K (1997) A blocker of nitric oxide synthase, *NG*-nitro-L-arginine-methyl ester, attenuates light-induced Fos protein expression in rat suprachiasmatic nucleus. Neurosci Lett 224:29–32
139. Amir S, Rackover M, Funk D (1997) Blockers of nitric oxide synthase inhibit stress activation of c-fos expression in neurons of the hypothalamic paraventricular nucleus in the rat. Neuroscience 77:623–627
140. Okere CO, Kaba H, Seto K, et al (1999) Intracerebroventricular injection of a nitric oxide donor attenuates Fos expression in the paraventricular and supraoptic nuclei of lactating rats. Brain Res 828:101–114
141. Briski KP (1999) Pharmacological manipulation of central nitric oxide/guanylate cyclase activity alters Fos expression by rat hypothalamic vasopressinergic neurons during acute glucose deprivation. J Chem Neuroanat 17:13–19

5.5.

5.5. HÜBSCHLE, T., THOM, E., WATSON, A., ROTH, J., KLAUS, S. & MEYERHOF, W. (2001b)

Leptin-induced nuclear translocation of STAT3 immunoreactivity in hypothalamic nuclei involved in body weight regulation.

J. Neurosci. **21** (7): 2413-2424.

Eigener Anteil an der Publikation:

- Beteiligung an der Versuchsplanung (100 %)
- Durchführung der Versuche (80 %)
- Beteiligung an der Zusammenfassung und Veröffentlichung der Ergebnisse (90 %)

The Journal of Neuroscience, April 1, 2001, 21(7):2413–2424

Leptin-Induced Nuclear Translocation of STAT3 Immunoreactivity in Hypothalamic Nuclei Involved in Body Weight Regulation

Thomas Hübschle,[1] Elke Thom,[1] Anna Watson,[1] Joachim Roth,[2] Susanne Klaus,[1] and Wolfgang Meyerhof[1]

[1]*German Institute of Human Nutrition, Departments of Biochemistry and Physiology of Nutrition and Molecular Genetics, D-14558 Potsdam-Rehbrücke, Germany, and* [2]*Institute of Veterinary Physiology, Justus-Liebig-University, D-35392 Giessen, Germany*

Leptin is involved in the hypothalamic control of food intake and body weight. Fos immunohistochemistry has been used to functionally map leptin target neurons involved in these regulatory processes. However, only a subset of hypothalamic neurons expressing the long form of the leptin receptor (Ob-Rb) also coexpress the neuronal activation marker Fos after leptin stimulation. To functionally map all leptin target neurons, regardless of whether leptin-mediated neuronal activation or inhibition occurs, we immunohistochemically investigated the leptin-induced nuclear translocation of the signal transducer and activator of transcription molecule STAT3, which represents a crucial step in the regulation of leptin-dependent gene expression. As proven by colocalization studies with the nuclear 4′,6-diamidino-2-phenylindole dilactate stain, intracerebroventricular leptin treatment, but not intracerebroventricular application of pyrogen-free saline, induced a time-dependent nuclear translocation of STAT3 immunoreactivity in hypothalamic nuclei, with strong nuclear STAT3 signals detectable in the arcuate nucleus, the lateral hypothalamus, and the ventromedial and dorsomedial hypothalamic nuclei. This leptin-induced STAT3 translocation pattern proved to be distinct from that induced by interleukin-6, another cytokine using STAT3 in its signaling pathway. Combined immunohistochemical STAT3 and Fos detection after leptin treatment revealed a higher number of STAT3-positive than Fos-positive cell nuclei in the aforementioned hypothalamic structures and showed that Fos immunoreactivity colocalized only in a subset of all leptin-responsive STAT3 nuclei. These results suggest that the detection of nuclear STAT3 immunoreactivity represents a new neuroanatomical tool to functionally map central leptin actions. They further support the importance of ventrally located caudal hypothalamic structures representing the main leptin targets involved in body weight regulation.

Key words: hypothalamus; food intake; appetite control; leptin; interleukin-6; cytokines; transcription factors; signal transducers and activator of transcription; STAT3; c-Fos; immunohistochemistry; confocal microscopy

Leptin is a cytokine that acts in the hypothalamus as a hormone to regulate food intake and body weight (BW) (Friedman, 1998; Elmquist et al., 1999; Meister, 2000). Its discovery has raised questions on the mechanisms and locations of its receptive systems involved in these regulatory processes. Five receptor subtypes (Ob-Ra–Ob-Re) have been identified (Lee et al., 1996; Fei et al., 1997; Leibel et al., 1997; Friedman, 1998) with the second isoform, Ob-Rb, representing the only splice variant capable of full activation of the leptin receptor-specific signal transduction pathway, the Janus kinase signal transducer and activator of transcription (Jak–STAT) signaling cascade (Chen et al., 1996; Lee et al., 1996). Leptin acts through Jak2 and STAT3 isoforms of this signal transduction pathway (Bjorbaek et al., 1997; Ghilardi and Skoda, 1997). Leptin receptor activation *in vivo* resulted in a time-dependent stimulation of STAT3 tyrosine phosphorylation in the rodent hypothalamus (Vaisse et al., 1996; McCowen et al., 1998), suggesting the presence of functionally active Ob-Rb receptors there. Indeed, *in situ* hybridization analysis demonstrated the presence of Ob-Rb mRNA in various brain structures, with high levels in hypothalamic nuclei described previously to control body weight regulation, such as the arcuate nucleus (ARC), the paraventricular nucleus (PVN), the dorsomedial hypothalamic nucleus (DMH), the ventromedial hypothalamic nucleus (VMH), and the lateral hypothalamic area (LHA) (Hakansson et al., 1996; Mercer et al., 1996; Cheung et al., 1997; Fei et al., 1997; Guan et al., 1997; Elmquist et al., 1998a).

To functionally map the actions of leptin on the brain, Fos immunohistochemical studies were performed, revealing Fos induction in all of the aforementioned hypothalamic structures, but with a distinct activation pattern in some of their subnuclei (van Dijk et al., 1996; Woods and Stock, 1996; Elmquist et al., 1997, 1998b, 1999; Yokosuka et al., 1998; Niimi et al., 1999; Elias et al., 2000). Whereas ventrolateral parts of the ARC showed Fos activation, there was an almost complete lack of Fos immunoreactivity in ventromedial areas, an ARC subnucleus with intense Ob-Rb expression. This unexpected observation was explained by an inhibitory leptin action on these neurons not detectable by the neuronal activation marker c-Fos (Elmquist et al., 1998b). By studying the mRNA expression of SOCS-3, a member of the suppressors of cytokine signaling proteins and a leptin-induced inhibitor of the leptin signaling cascade, a neuroanatomical method that was useful as a marker of direct leptin actions regardless of whether leptin-mediated neuronal excitation or inhibition has occurred, was consequently established (Bjorbaek et al., 1998; Elias et al., 1999). This method proved to be helpful for the characterization of leptin effects in distinct ARC subnuclei;

Received Sept. 11, 2000; revised Dec. 14, 2000; accepted Dec. 22, 2000.

This work was supported in part by European Commission Grant QLG3-CT-1999–00908 to W.M. We thank Dr. E. Simon for critical reading of this manuscript.

Correspondence should be addressed to Dr. Thomas Hübschle, Institute of Veterinary Physiology, Justus-Liebig-University, Frankfurter Straße 100, D-35392 Giessen, Germany. E-mail: thomas.huebschle@vetmed.uni-giessen.de.

however, a comprehensive hypothalamic map of direct leptin actions is still missing.

We therefore hypothesized that the combination of central leptin treatment with the subsequent immunohistochemical detection of STAT3 should be a good tool to reveal direct leptin actions on the brain. Various studies examined the distribution of STAT3 immunoreactivity within the hypothalamus (Hakansson and Meister, 1998; Hakansson et al., 1999; Wilkinson et al., 2000) and the whole CNS (Strömberg et al., 2000). However, a functional analysis studying the leptin-induced nuclear STAT3 translocation within hypothalamic nuclei has not yet been performed. This study describes a new mapping procedure that is useful for the neuroanatomical characterization of the centrally mediated effects of leptin.

MATERIALS AND METHODS

Animals. Adult male Wistar rats (Tierzucht Schönwalde GmbH, Schönwalde, Germany), with an initial BW ranging from 180 to 210 gm, were housed in individual cages in the animal house (Max Rubner Laboratory, Bergholz-Rehbrücke, Germany) and used in accordance with ethics authorities and local regulations (ethics approval number 48-3560-1/2). Lights were on from 6:00 A.M. to 6:00 P.M., and room temperature (RT) was adjusted to 22 ± 1°C. Animals had constant access to water and were fed standard lab chow available *ad libitum*. BW was monitored daily, and thereby the rats were handled at least once a day.

Intracerebroventricular cannulation of the lateral ventricle. Animals were anesthetized with intraperitoneal injections of a ketamine–xylazine solution [100 mg/kg BW Ketamin Gräub (Albrecht, Aulendorf, Germany); 10 mg/kg BW Rompun (2%; Bayer Vital, Leverkusen, Germany)]. During surgery, body temperature was kept constant at ~37°C using a self-regulating heating pad (Fine Science Tools, Heidelberg, Germany). A modified 23 gauge cannula (Braun, Melsungen, Germany) attached to a PP30 tubing (Portex, Hythe, UK) and a 1 ml syringe (Braun) was filled with pyrogen-free saline (Sigma, Deisenhofen, Germany) and inserted stereotaxically (Ultra Precise Small Animal Stereotaxic Instrument, model 963; David Kopf Instruments, Tujunga, CA) into the left lateral ventricle of the brain. With a general +0.5 mm tooth bar adjustment, the coordinates used from bregma point were 0.4 mm posterior, 1.5 mm lateral, and 4 mm ventral (brain surface). Three small screws with a diameter of 1.4 mm (M1,4 V4A; Föhr Medical Instruments, Seeheim, Germany) were secured on the skull before the screws and the inserted cannula were embedded into dental cement. Finally, the cannula was sealed at the remaining opening with a plastic blocker, and the probe was checked daily during BW measurements to ensure that it remained sealed.

Accuracy of the cannula placement was tested by performing a drink test with a 50 ng intracerebroventricular bolus application of angiotensin II (Bachem Biochemica GmbH, Heidelberg, Germany) dissolved in 5 μl of 0.9% pyrogen-free saline (Sigma). The cumulative water intake was monitored for the following 60 min. Only those animals that showed an adequate drinking response of 9.8 ± 0.6 ml ($n = 35$; mean ± SEM) were used for additional studies. These drink tests were conducted 7–8 d after intracerebroventricular cannulation and 3–4 d before experimental stimulation.

Intracerebroventricular cytokine stimulation. On the day of experimental stimulation, BW of the rats reached 222.5 ± 3.4 gm compared with 198.5 ± 3.6 gm on the day of surgery ($n = 35$; mean ± SEM); hence, the rats had recovered from the surgical procedure and were gaining weight. *In vivo* cytokine stimulation was conducted in conscious animals with a 25 μl Hamilton syringe attached to the intracerebroventricular cannula via PP30 tubing. The central treatments consisted of an intracerebroventricular bolus injection of either 3.5 μg of recombinant murine leptin (kindly provided by Aventis Pharma, Frankfurt, Germany) or 200 ng of species homologous rat interleukin-6 (IL-6) (kindly provided by Dr. S. Poole, National Institute for Biological Standard and Control, Potters Bar, UK) (for details, see Rees et al., 1999), both diluted in 5 μl of pyrogen-free saline. The leptin and IL-6 doses used in this study were based on previous intracerebroventricular application experiments in which leptin proved to inhibit food intake by 40% at a dose of 4 μg per rat (Luheshi et al., 1999) and in which IL-6 caused a maximum febrile response at a dose of 200 ng per rat (Lenczowski et al., 1999; our unpublished observations). In control experiments, 5 μl of pyrogen-free saline alone was applied. Animals were then left 15–180 min before being deeply anesthetized with sodium pentobarbital (60 mg/kg BW Narcoren; Merial GmbH, Hallbergmoos, Germany) and transcardially perfused with 0.9% saline kept at RT, followed by ice-cold 4% paraformaldehyde in 0.1 M phosphate buffer, pH 7.2. The animal's brains were removed and post-fixed in the same fixative for 1 hr at RT, and then the tissue was cryoprotected in 20% sucrose in phosphate buffer overnight at 4°C. Tissue was cut the following day.

Catalyzed reporter deposition amplification protocol for STAT3 detection. Initially, standard immunohistochemical procedures were used for STAT3 detection (rabbit anti-STAT3 antibody, sc-482; Santa Cruz Biotechnology, Heidelberg, Germany), resulting in a very weak and nonsatisfying STAT3 signal. As shown in a recent publication investigating STAT3 distribution in the rat CNS, amplification procedures are a helpful tool to investigate STAT3 immunoreactivity (Strömberg et al., 2000). Therefore, to enhance basal as well as cytokine-induced STAT3 signals in brain sections, we used a commercial tyramide amplification kit (NEL700; NEN Life Science Products GmbH, Köln, Germany) based on the catalyzed reporter deposition method. The specificity of the Santa Cruz Biotechnology STAT3 antibody used in the present study was clearly proven in a recent publication (Strömberg et al., 2000). Our own preabsorption control experiments with the control STAT3 peptide (data not shown) confirmed these findings.

Coronal 20–40 μm free-floating hypothalamic sections (bregma levels, 0.00 to −4.80 mm) were cut on a freezing microtome (model 1205; Jung, Heidelberg, Germany) for double- and triple-labeling experiments, and 40 μm free-floating sections of the forebrain, midbrain, and hindbrain were used for STAT3 detection alone. Sections were placed into 10% fetal calf serum and 0.3% Triton X-100 in 0.1 M phosphate buffer, pH 7.2, for 1 hr at RT. For tyramide signal amplification, sections were then transferred to the blocking reagent provided in the kit for 30 min at RT. This was followed by the primary STAT3 antibody incubation (1:12000 diluted in 0.1 M phosphate buffer, 2% fetal calf serum, and 0.1% Triton X-100) for 24–48 hr at 4°C. The tyramide amplification protocol was continued according to the kit description but using a phosphate buffer system and not the suggested borate buffer. Primary STAT3 antibody was detected with a secondary biotinylated anti-rabbit antibody (Vector BA-1000; Linaris Biologische Produkte, Wertheim-Bettingen, Germany) for 1 hr at RT (diluted 1:200 in 0.1 M phosphate buffer and 2% fetal calf serum). The additional immunohistochemical processing was performed with an avidin–biotin–horseradish peroxidase complex (Vector Elite Kit; Linaris Biologische Produkte), which was visualized by either diaminobenzidine hydrochloride (Sigma) reaction in the presence of hydrogen peroxide or fluorescein (FITC)-conjugated avidin D (Vector A-200; Linaris Biologische Produkte).

Immunohistochemical colocalization studies and nuclear 4′,6-diamidino-2-phenylindole dilactate stain. In double-labeling experiments, coronal 20–40 μm free-floating hypothalamic sections already stained for STAT3 were coanalyzed using additional antibodies. A coincubation was performed with a 1:2000 mouse anti-glial fibrillary acidic protein (GFAP) antibody (MAB3402; Chemicon, Hofheim, Germany) and with a 1:200 mouse anti-adenomatous polyposis coli (APC) protein (OP80; Oncogene Research Products, Calbiochem, Bad Soden, Germany). Both antibodies are used as cytoskeletal and cytoplasmatic markers of glia cells in the CNS for either astrocytes (GFAP) or mature oligodendrocytes (APC).

STAT3 detection was also combined with the immunohistochemical analysis of the immediate early gene Fos. Fos-like immunoreactivity was detected with an anti-c-*fos* antibody (sc-52; Santa Cruz Biotechnology) at a 1:500–1:1000 dilution. In this experiment, both primary antisera were raised in rabbits, and therefore a consecutive detection of first STAT3 and then Fos was performed according to the method described previously by Shindler and Roth (1996). In detail, STAT3 was visualized using the catalyzed reporter deposition amplification protocol with FITC-conjugated avidin D as described above. With a STAT3 antibody dilution of 1:12000 that proved to be below the detection limit of a fluorescent-labeled secondary antibody, yet being still sufficient for detection with the catalyzed reporter deposition amplification system, the STAT3 primary antibody was effectively neglected during the visualization steps necessary to detect the second primary Fos antibody. Fos-like immunoreactivity was then localized using a Cy3-conjugated anti-rabbit (1:200–1:400) antibody (Sigma). All primary antibodies were diluted in 0.1 M phosphate buffer with 2% fetal calf serum and 0.1% Triton X-100, and the sections were incubated 12–48 hr at 4°C. The visualization for the monoclonal primary mouse antibodies were performed with a secondary Cy3-conjugated anti-mouse (1:2000) antibody (Sigma).

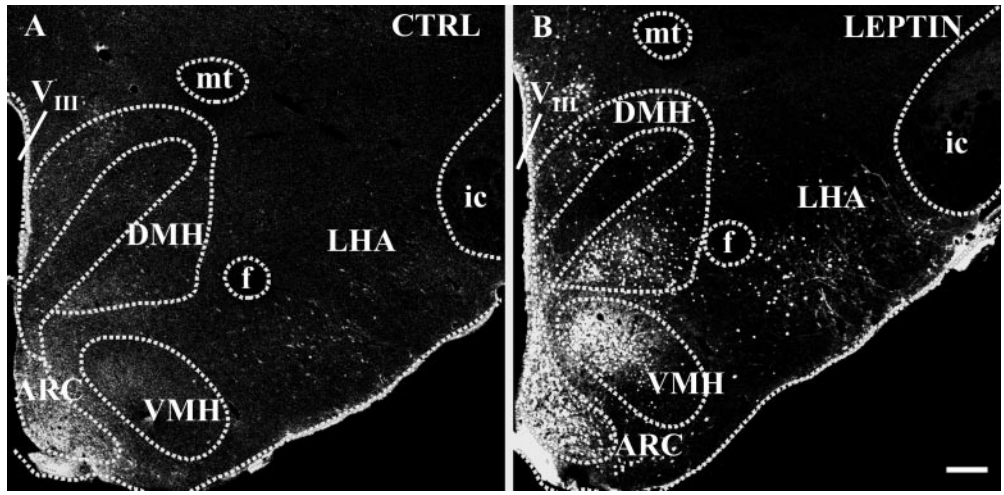

Figure 1. Hypothalamic leptin targets mapped by the detection of STAT3 immunoreactivity under control conditions (*A*) and after intracerebroventricular leptin application (*B*). Immunofluorescence photomicrographs show an overview at caudal hypothalamic levels approximately −3.3 mm posterior to bregma point under control conditions (*CTRL*; 30 min after 5 μl of pyrogen-free saline) and 30 min after central leptin treatment (3.5 μg of leptin in 5 μl of pyrogen-free saline). Note the massive increase of STAT3 immunoreactivity in various hypothalamic structures, such as within the ARC, the ventral parts of the DMH, the dorsal parts of the VMH, and the LHA, in the leptin-treated animal (*B*) compared with the basal STAT3 expression detected in the control (*A*). V_{III}, Third ventricle; *f*, fornix; *mt*, mamillothalamic tract; *ic*, internal capsule. Scale bar, 200 μm.

In a final step, all sections were stained for 5 min at RT with the nuclear stain 4′,6-diamidino-2-phenylindole dilactate (DAPI) (Molecular Probes Europe BV, Leiden, Netherlands), which was diluted 1:400 in phosphate buffer.

Microscopical analysis. The free-floating sections were mounted onto gelatin-coated slides and for the enzyme-histochemical detection coverslipped with Entellan (Merck, Darmstadt, Germany), whereas for fluorescent detection, slides were coverslipped with Crystal/Mount (Biomedia, Foster City, CA). The sections were analyzed using a conventional Zeiss (Jena, Germany) Axioplan light microscope and a Zeiss confocal microscope. Confocal images were taken with an inverted Zeiss Laser Scanning Microscope (model LSM 410) attached to an internal helium–neon ion laser and two external lasers, one argon ion and one argon UV laser with individual excitation outputs of 543, 488, and 364 nm, respectively. Images were individually processed for the color channel red, green, and blue (RGB) using a 570 long-pass emission filter for Cy3 detection (R), a 510–525 bandpass emission filter for FITC detection (G), and a 397 long-pass emission filter for DAPI detection (B). The images shown are the result of one optical section; the color images show individual color channels or the overlay of two of such individually taken RGB images. Image editing software (Adobe Photoshop; Adobe Systems, San Jose, CA) was used to change the graphic mode from RGB to CMYK (cyan, magenta, yellow, and black) and to combine the images into plates.

RESULTS

Intracerebroventricular leptin treatment induces a time-dependent nuclear translocation of STAT3 immunoreactivity within the hypothalamus

To investigate the basal and the leptin-induced hypothalamic STAT3 expression at the cellular level, immunohistochemical procedures were used. Basal STAT3 expression levels in the rat forebrain were evaluated in controls via intracerebroventricular pyrogen-free saline application and found to be highest in the caudal hypothalamus (Fig. 1*A*). In particular, ventrally located hypothalamic structures, such as the ARC (Figs. 1*A*, 2*A*), its adjacent periarcuate area (PAA), and areas ventral to the fornix in the LHA (Figs. 1*A*, 2*G*), were labeled. Weaker STAT3 immunoreactivity was observed in several other hypothalamic nuclei, such as the VMH, the DMH, the retrochiasmatic area (RCH), the PVN, the supraoptic nucleus (SON), and the medial preoptic area (MPO). By confocal microscopy and the nuclear DAPI stain, the subcellular distribution of the basal STAT3 expression was investigated. Under control conditions, STAT3 immunoreactivity was predominantly found in the cell cytoplasm and in nerve fibers (Fig. 2*A–C*, *G–I*, *insets* in *B*/*C*, *H*/*I*), with nuclear STAT3 labeling being rarely detectable in the aforementioned hypothalamic structures.

The subcellular distribution and the intensity of STAT3 signals within some of these hypothalamic structures dramatically changed after the intracerebroventricular leptin administration. As shown in overview in Figure 1*B*, leptin treatment led to a marked increase of STAT3 immunoreactivity in the caudal hypothalamus. Although all parts of the ARC seemed to be heavily labeled, a distinct subdistribution of the STAT3 signal became obvious for the VMH or the DMH, with dorsal (VMH) and ventral (DMH) parts being the most leptin-responsive hypothalamic targets besides the ARC. Within the PAA, the RCH, and the LHA, intense but more scattered labeling of individual medium- to large-sized neurons occurred. In addition, cells within the ependymal lining of the third ventricle, the adjacent periventricular nucleus, and in ventrally located meninges showed strong STAT3 immunoreactivity. A subcellular analysis of the leptin-induced STAT3 signals revealed that a massive shift of STAT3 immunoreactivity from the cytoplasm into the cell nucleus occurred 30 min after the intracerebroventricular leptin application, as shown for example within the ARC (Fig. 2*D–F*, *inset* in *E*/*F*) or the LHA (Fig. 2*J–L*, *inset* in *K*/*L*). Such a nuclear translocation of STAT3 was observed in various hypothalamic but also extrahypothalamic forebrain structures (Table 1). Besides the induction of this intense nuclear STAT3 signal, intracerebroventricular leptin treatment additionally induced a massive increase of the STAT3 signal in nerve fibers and axons, being most prominent within the ARC (Fig. 2*D*,*F*, *inset* in *E*/*F*) and the ventral LHA (Fig. 2*J*,*L*, *inset* in *K*/*L*).

The time dependency of this nuclear STAT3 translocation is demonstrated for the ARC using a post-application period ranging from 15 to 180 min (Fig. 3). Compared with the basal STAT3 expression in the control (Fig. 3*A*), intracerebroventricular leptin

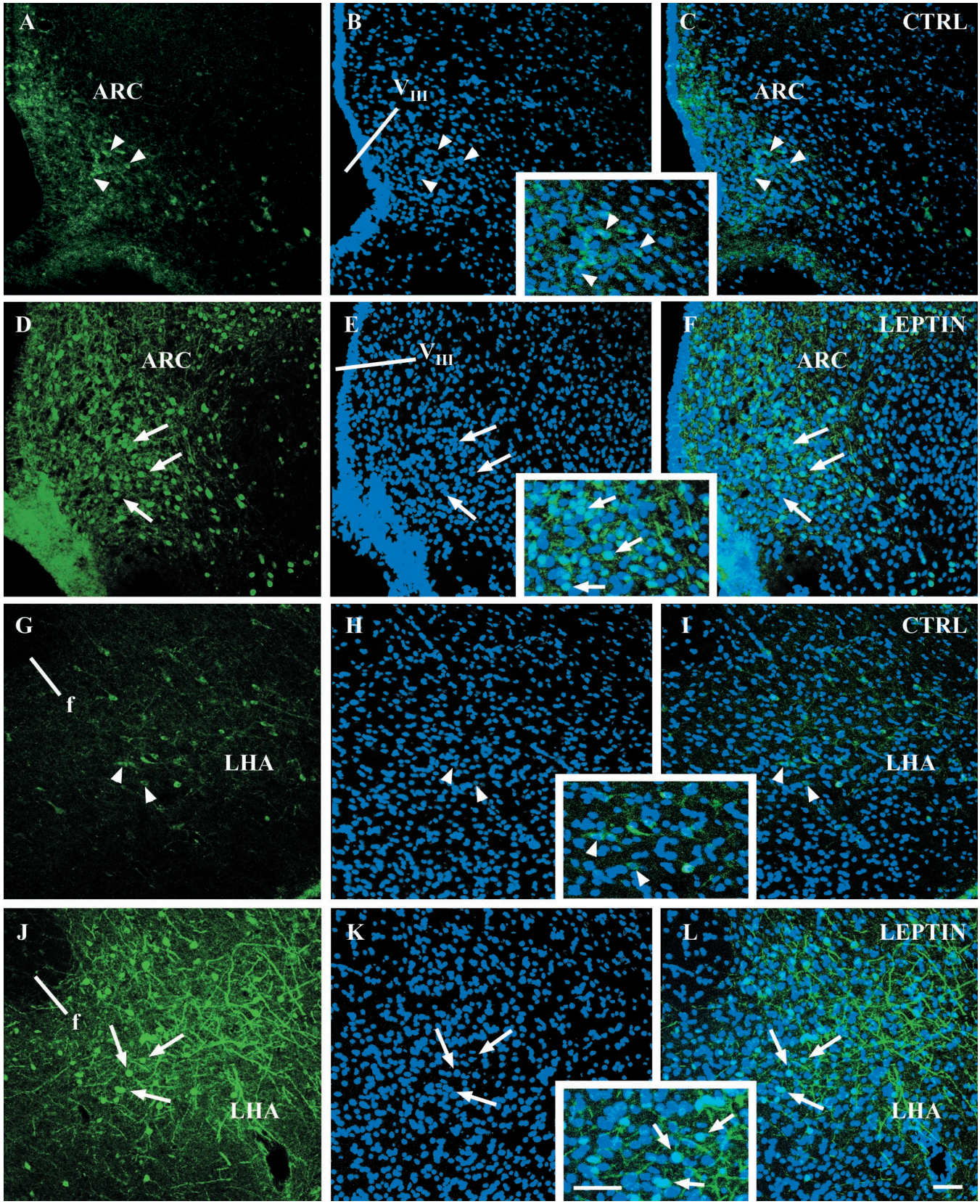

Figure 2. Leptin induces a nuclear translocation of STAT3 immunoreactivity in hypothalamic nuclei. Immunofluorescence photomicrographs of hypothalamic sections of the ARC (*A–F*) and ventral aspects of the LHA (*G–L*) are shown under control conditions (*CTRL*; *A–C*, *G–I*; 30 min after pyrogen-free saline) and leptin-stimulated conditions (*D–F*, *J–L*; 30 min after leptin). STAT3 immunoreactivity in *green* (*A*, *D*, *G*, *J*) is compared with the *blue* nuclear DAPI stain (*B*, *E*, *H*, *K*). The overlays of these individual confocal images are shown in *C*, *F*, *I*, and *L*. Note that, under basal control conditions, STAT3 immunoreactivity is predominantly located within the cytoplasm and also nerve fibers of ARC and LHA (*Figure legend continues.*)

Table 1. Forebrain[a] distribution of leptin- and interleukin-6 (IL-6)-induced nuclear STAT3 immunoreactivity[b] compared with basal nuclear STAT3 expression in the control

	Cytokine-induced nuclear STAT3 labeling[b]		
Forebrain[a] structures	i.c.v. Leptin	i.c.v. IL-6	Control
Hypothalamus			
Anterior hypothalamic area (AHA)	−	++	−
Arcuate nucleus (ARC)	+++	+	+
Dorsal hypothalamic area (DA)	+	++	+
Dorsomedial nucleus (DMH)	+++	+	−
Lateral hypothalamic area (LHA)	++	++	−
Mammillary body			
medial parts	+	+	−
lateral parts	+	++	−
Medial preoptic area (MPO)	+	++	−
Ventromedial preoptic nucleus (VMPO)	+	+++	−
Median preoptic nucleus (MnPO)	+	+	−
Paraventricular nucleus (PVN)	+	+	−
Periarcuate area (PAA)	++	+++	−
Perifornical area (PFA)	++	−	−
Periventricular nucleus (PE)	++	+	−
Posterior hypothalamic area (PA)	++	++	−
Retrochiasmatic area (RCH)	++	++	−
Subfornical organ (SFO)	−		−
near to the big lateral vessels		+	
Suprachiasmatic nucleus (SCN)	+	+	−
Supraoptic nucleus (SON)	−	+++	−
Vascular organ of the lamina terminalis (OVLT)	−		−
lateral parts		++	
Ventromedial nucleus (VMH)	+++	+	−
Septal and basal telencephalic regions			
Bed nucleus of the stria terminalis (BNST)	−	−	−
Lateral preoptic area (LPO)	−		−
only ventral parts		++	
Lateral septum (LS)	−	++	−
Substantia innominata (SI)	−	−	−
Others			
Ependymal lining of all ventricles	+++	+++	+
Meninges, in particular at ventral sites	++	+++	−
Periventricular			
lateral ventricles (cannula side)	+(+)	++(+++)	−(−)
third ventricle	+	+++	−
aqueduct	+	+	−
fourth ventricle	−	++	−
Piriform cortex, layer I+II	+++	+	−
Probe site	+++	+++	+++
Thalamic nuclei	−		−
medial and lateral habenular nucleus		++	
mediodorsal thalamic nuclei		+++	
Cerebellum	−	−	−

[a] The nomenclature used is modified from that used by Paxinos and Watson (1997) and Swanson (1992).

[b] Relative values are given as qualitative estimates of the densities of nuclear STAT3 labeling. A four-point scale was used to rate the data: +++, high density; ++, moderate density; +, low density; −, no nuclear signal. The data are based on the light microscopical analysis of representative animals treated with 30 min intracerebroventicular (i.c.v.) application of leptin, IL-6, or pyrogen-free saline (Control).

←

neurons, whereas most of the cell nuclei seem to be devoid of STAT3 labeling (see *arrowheads* in *A–C* and *G–I* and also the *insets* in *B*/*C* and *H*/*I* showing this at higher magnification). Leptin treatment (30 min) not only led to a nuclear translocation of STAT3 immunoreactivity in both hypothalamic structures the ARC and the LHA (see *arrows* showing the *light blue* double-labeled cell nuclei in *F* and *L* and also the *insets* in *E*/*F* and *K*/*L* showing this at higher magnification) but also to a general increase of STAT3 labeling (compare *A* with *D* and *G* with *J*). V_{III}, Third ventricle; *f*, fornix. Scale bars, 50 μm.

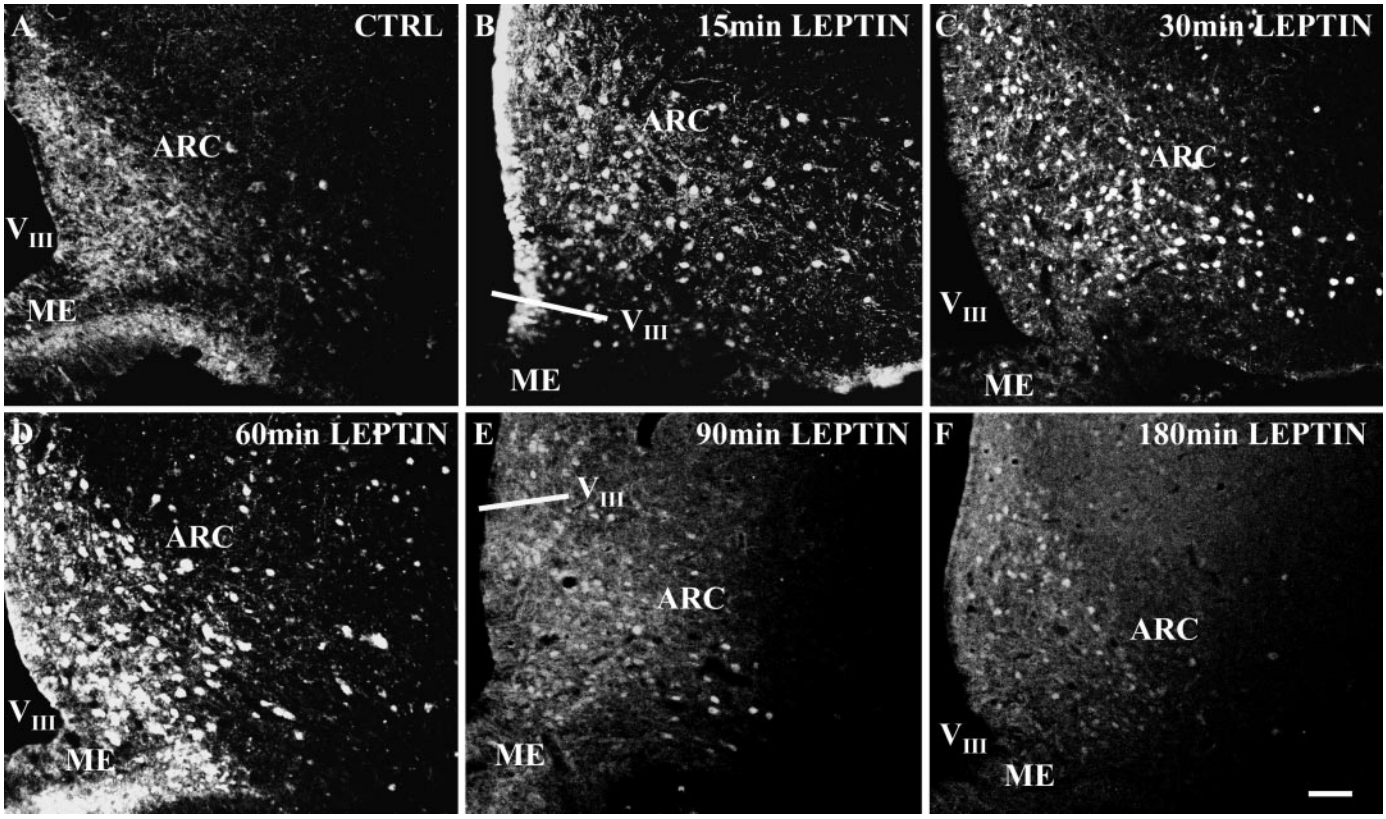

Figure 3. Leptin induces a time-dependent nuclear translocation of STAT3 immunoreactivity in the ARC. Immunofluorescence photomicrographs of STAT3 immunoreactivity in ARC sections are shown under control conditions (*A*, *CTRL*; 30 min pyrogen-free saline) and under leptin-stimulated conditions (*B–F*). Under basal control conditions, STAT3 immunoreactivity is detectable in all subnuclei of the ARC and is predominantly located in the cytoplasm and nerve fibers of ARC neurons (*A*). As soon as 15 min after leptin application, a massive increase in nuclear STAT3 labeling is detectable in all parts of the ARC (*B*), which becomes even more pronounced after 30 min (*C*). However, 60–180 min after leptin application (*D–F*), the nuclear STAT3 signal slowly starts to decrease again, which is indicated by the shift from a sharp-edged round-shaped STAT3 signal in the nucleus (*B*, *C*) to a more blurred and less defined nuclear labeling and a decrease in the intensity of STAT3 immunoreactivity (*D–F*). V_{III}, Third ventricle; *ME*, median eminence. Scale bar, 50 μm.

application rapidly induced a nuclear translocation of STAT3 immunoreactivity already present at 15 min (Fig. 3*B*), which became even more pronounced at 30 min (Fig. 3*C*). When using post-application periods longer than 30 min, the high intensity of the STAT3 signal present at 30 min slowly decreased (Fig. 3*D–F*), with only a small number of STAT3-positive cell nuclei being left 180 min after leptin treatment (Fig. 3*F*).

Intracerebroventricular leptin treatment shows a nuclear STAT3 translocation pattern distinct from that induced by intracerebroventricular interleukin-6 application

The specificity of the leptin-induced nuclear STAT3 translocation in distinct forebrain structures was additionally checked using IL-6, another cytokine also capable of activating the Jak–STAT3 signal transduction pathway. Indeed, for both cytokines, a specific pattern of nuclear STAT3 translocation became obvious within the rat forebrain (Fig. 4, Table 1). Whereas in controls most (extra)hypothalamic structures proved to be devoid of nuclear STAT3 labeling, both intracerebroventricular leptin and intracerebroventricular IL-6 induced a shift of the STAT3 signal into the cell nucleus (Table 1). However, the densities of nuclear STAT3 labeling and the brain sites affected were different for the two cytokines. Whereas leptin seemed to predominantly target ventral parts of the caudal hypothalamus, IL-6 additionally induced a massive STAT3 translocation in the rostral hypothalamus, in particular within the MPO and its ventromedial part, the VMPO (Fig. 4*B*, *inset* in *A*/*B*), which was not detectable in the leptin-treated animals (Fig. 4*A*). When looking at other forebrain structures, the two cytokine stimuli expressed a differing pattern of nuclear STAT3 translocations. This included the anterior piriform cortex (PIR), which showed a high density of nuclear STAT3-labeled layer II neurons in the intracerebroventricular leptin but not in the intracerebroventricular IL-6-treated animals (Fig. 4*C*,*D*), and also the SON (Fig. 4*E*,*F*) and some thalamic nuclei (Table 1) in which IL-6 but not leptin induced a nuclear translocation of STAT3 immunoreactivity. In the caudal hypothalamus, the overall pattern of STAT3 immunoreactivity induced by leptin or IL-6 again proved to be different (Fig. 4*G*,*H*). Whereas leptin induced nuclear STAT3 translocation in medial and lateral parts of the ARC as well as in dorsal parts of the VMH, IL-6 did not lead to STAT3 translocation in the medial ARC and only to a minor nuclear labeling in the dorsal VMH.

Leptin-induced nuclear STAT3 immunoreactivity within the piriform cortex and the hypothalamus does not colocalize with glial cell markers

For the light microscopic analysis, the enzyme immunohistochemical STAT3 detection was combined with cresyl violet counterstaining, indicating a predominant neuronal location of the STAT3 immunoreactivity under both basal and leptin-stimulated conditions within the hypothalamus (data not shown). However,

non-neuronal, nuclear STAT3 labeling was also detected, e.g., in ependymal and meningeal cells, and also near to the probe site in small, noncircular-shaped cell nuclei, which presumably belonged to glial cells (Table 1). Former electron microscopic investigations have shown that, within the brain tissue, leptin receptors are located on both neurons and glia. It was therefore of importance to analyze the cell types in which intracerebroventricular administration of leptin induced nuclear translocation of STAT3. To demonstrate the cellular origin of the STAT3 signals, double-labeling experiments combining the STAT3 detection with the immunohistochemical localization of the cytoskeletal and cytoplasmatic glial cell markers GFAP (Fig. 5*A–E*) and APC (Fig. 5*F*) were performed after intracerebroventricular leptin application. The size and shape of the STAT3-stained nuclei within most cells of the PIR (Fig. 5*A*) and the hypothalamus (Fig. 5*B–F*) again indicated a predominant neuronal cell origin. Indeed, no cellular colocalization of the nuclear STAT3 signal was found within the astrocytes in layer II of the anterior PIR (Fig. 5*A*) or within the astrocytes in the main hypothalamic leptin targets, such as the ARC (Fig. 5*B*), the LHA (Fig. 5*C*), and the DMH and VMH (Fig. 5*D*,*E*). In addition, leptin-induced nuclear STAT3 signals within the VMH did not colocalize with the cytoplasmatic labeling of oligodendrocytes (Fig. 5*F*). Within the most intense nuclear STAT3-labeled hypothalamic regions, in no single case did a colocalization occur, suggesting that glia cells in these areas may express a leptin receptor isoform that is not capable to activate the full cytokine specific Jak–STAT pathway.

Nuclear STAT3 and Fos immunoreactivity colocalizes only in a subset of leptin-responsive forebrain neurons

In double-labeling experiments, the leptin-induced nuclear STAT3 immunoreactivity within the forebrain was compared with the Fos response 60 min after intracerebroventricular leptin application. The time point used in these experiments was chosen as a compromise between the time necessary for nuclear translocation of STAT3 (15–30 min) (Fig. 3) and the time known to show the first peak of the nuclear Fos signal (90 min) in neurons. A clear difference between the number of STAT3-stained (*green* nuclei) versus Fos-stained (*red* nuclei) nuclei could be detected, with more STAT3-stained than Fos-stained nuclei after central leptin treatment (Fig. 6*A–G*,*I*,*J*). Individual detection of STAT3 and Fos immunoreactivity (Fig. 6*A–D*) showed a similar distribution of nuclear signals in layer II of the PIR (Fig. 6*A*,*B*) but distribution differences within the caudal hypothalamus. STAT3 was predominantly induced in medial parts of the ARC and dorsal aspects of the VMH (Fig. 6*C*), whereas nuclear Fos was mainly detectable in the ventrolateral ARC and the adjacent periarcuate area (Fig. 6*D*). At higher magnification, nuclear STAT3 and Fos immunoreactivity proved to be colocalized (*yellow* nuclei) only in a subset of neurons of the anterior PIR (Fig. 6*E*), the ventrolateral ARC (Fig. 6*F*), and ventral parts of the DMH (Fig. 6*I*). Minor colocalization of the two nuclear signals was detected within the LHA (Fig. 6*G*) and the dorsal part of the VMH (Fig. 6*J*).

DISCUSSION

The ventrobasal hypothalamus has been described as the primary central leptin target involved in the control of food intake and energy balance. Many physiological responses regulated by leptin, such as the inhibition of appetite via intracerebroventricular leptin treatment in rats, characteristically start with some delay and show long-lasting effects (Cusin et al., 1996; Woods et al., 1998). This is in agreement with the long-duration intracellular genomic mode of the Jak–STAT signaling pathway downstream to Ob-Rb receptor activation (Schindler and Darnell, 1995; Darnell, 1997). Thus, it is likely that the weight-reducing effects of leptin are mediated via the Jak–STAT signal transduction of hypothalamic Ob-Rb receptors.

The leptin-induced nuclear STAT3 pattern matches with Ob-Rb receptor expression in the ventrobasal hypothalamus

One open question in the past was whether the extensive distribution of the Ob-Rb receptor within the rodent hypothalamus, detected via *in situ* hybridization techniques (Mercer et al., 1996; Fei et al., 1997; Guan et al., 1997; Elmquist et al., 1998a) or immunohistochemistry (Hakansson et al., 1998; Baskin et al., 1999), really represents the active leptin receptor isoform. With the Ob-Rb receptor being the major brain-intrinsic leptin receptor isoform capable of full activation of the Jak–STAT signaling cascade, (Chen et al., 1996; Lee et al., 1996) the characterization of the leptin-induced nuclear STAT3 translocation could be a functional proof of active Ob-Rb expression. Indeed, our results demonstrate a leptin-induced nuclear STAT3 translocation in the rat hypothalamus. The hypothalamic location of strong Ob-Rb receptor expression on both mRNA and protein level described in the literature (Mercer et al., 1996; Elmquist et al., 1998a; Hakansson et al., 1998; Baskin et al., 1999) matches with the most intense nuclear STAT3 signals detected in the present study, and this overlap becomes even more evident in distinct subnuclei of the ventrobasal hypothalamus. In detail, all ARC subnuclei, a caudal DMH subnucleus located ventrolaterally to its compact formation and the dorsomedial part of the VMH, can be regarded as functionally active major hypothalamic leptin targets. Hypothalamic structures described to express less intense Ob-Rb mRNA levels, such as the LHA, the perifornical area, the periventricular nucleus, the parvocellular part of the paraventricular nucleus, the posterior hypothalamic nucleus, and the medial mammillary body (Elmquist et al., 1998a), showed an individual spread and/or a weaker nuclear STAT3 response in our study. Although for the above mentioned structures a relative clear-cut match of nuclear STAT3 signals and Ob-Rb expression was demonstrated, discrepant cases also existed. Strong leptin receptor immunoreactivity was found in the SON (Hakansson et al., 1998); however, leptin treatment failed to induce a nuclear STAT3 translocation there. This suggests that these immunohistochemically identified SON leptin receptors are not able to induce leptin-dependent signaling because they do not represent the active full-length receptor variant.

The present data also neuroanatomically confirm the finding of Vaisse et al. (1996) and McCowen et al. (1998) that leptin induces STAT3 phosphorylation in the rodent hypothalamus *in vivo*. Furthermore, the time course evaluated in the present study with nuclear STAT3 translocation already present at 15 min and being maximal at 30 min is identical to that reported with biochemical and molecular–biological approaches (Vaisse et al., 1996; McCowen et al., 1998). So in summary, our experiments further extend these studies by mapping the functionally active hypothalamic leptin targets, with their exact neuroanatomical localization being essential for the understanding of leptin-induced physiological responses.

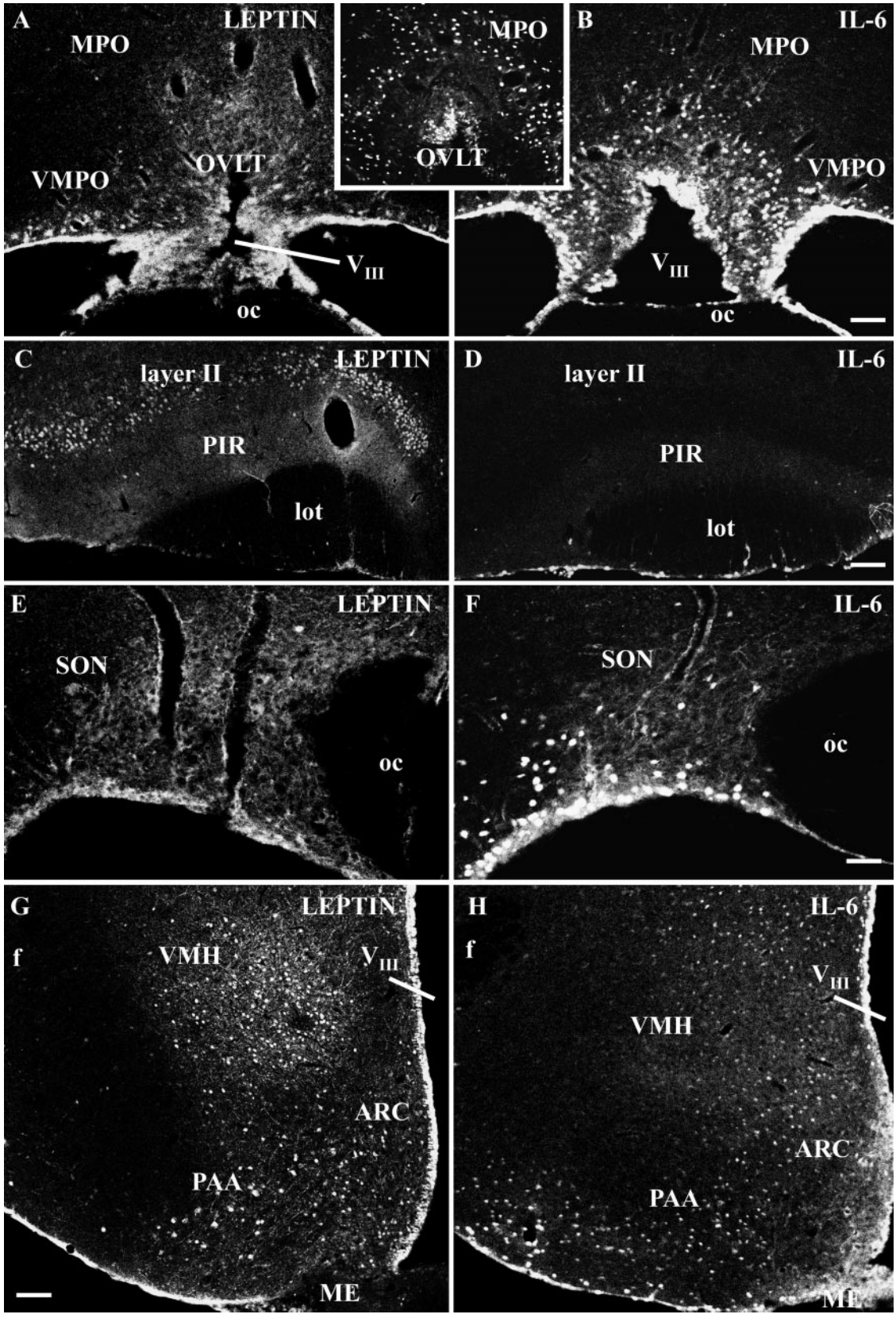

Figure 4. Distinct cytokine-induced nuclear STAT3 translocation patterns in forebrain structures induced by intracerebroventricular leptin or by intracerebroventricular IL-6 treatment. Immunofluorescence photomicrographs of STAT3 immunoreactivity are shown at rostral (*A–D*), medial (*E*, *F*), and caudal (*G*, *H*) hypothalamic levels under leptin-stimulated (*A*, *C*, *E*, *G*) or IL-6-stimulated (*B*, *D*, *F*, *H*, *inset* in *A*/*B*) conditions. Only basal, predominantly non-nuclear STAT3 signals are expressed in the 30 min leptin-treated animal within lateral parts of the organum vasculosum of the lamina terminalis (*OVLT*) and the adjacent ventromedial preoptic area (*VMPO*) (*A*). IL-6 treatment on the other hand induced an increase and shift of STAT3 immunoreactivity into cell nuclei, particularly in the MPO, including the ventromedial preoptic area, as well as in the lateral (*Figure legend continues.*)

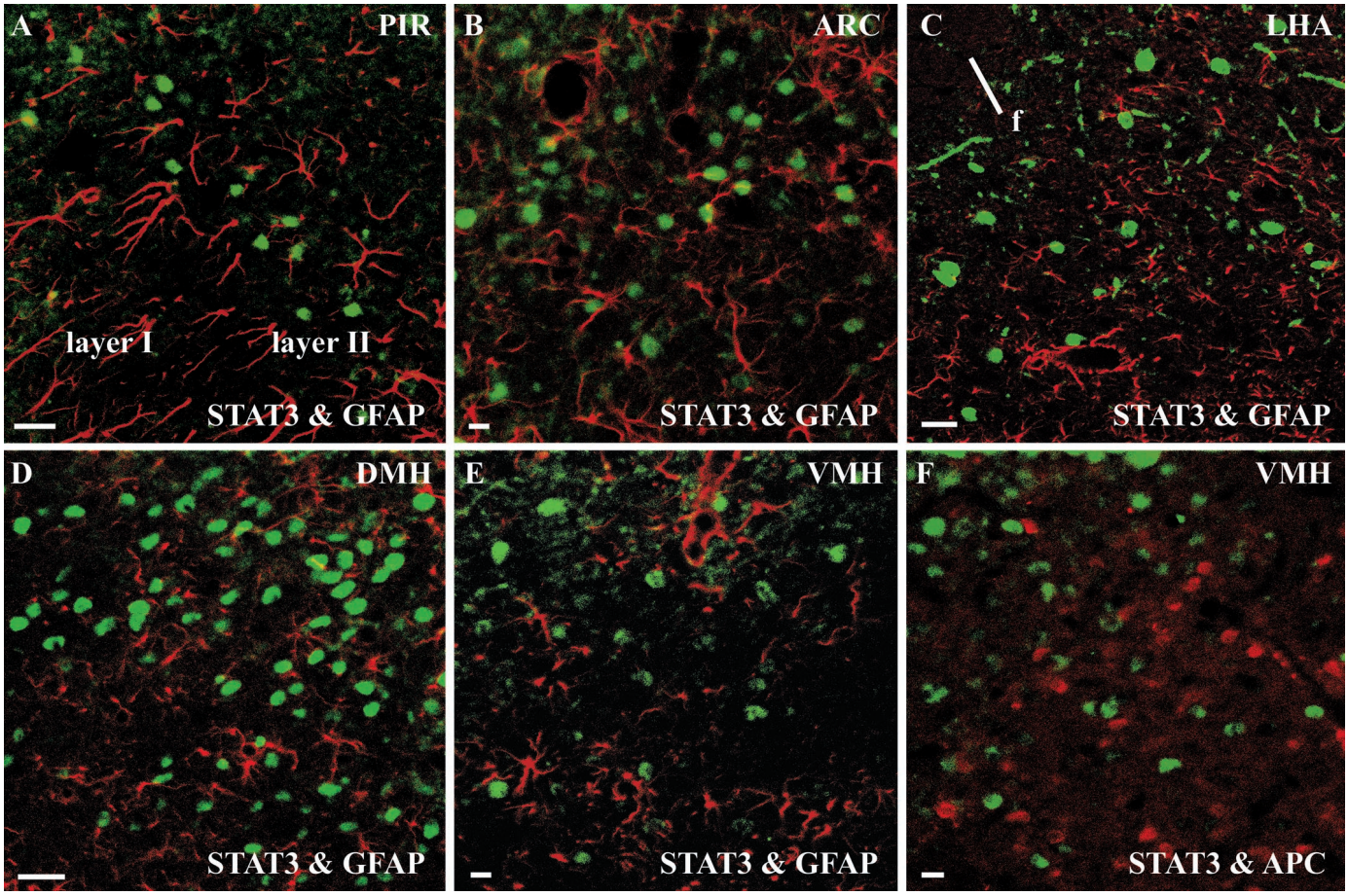

Figure 5. Leptin-translocated nuclear STAT3 immunoreactivity does not colocalize with the glial cell markers GFAP (*A–E*) and APC (*F*) in forebrain structures. Immunofluorescence photomicrographs of leptin responsive-forebrain structures, such as the PIR (*layer II*, *A*), the ARC (*B*), ventral aspects of the LHA (*C*), the DMH (*D*), and the VMH (*E*, *F*) are shown 30 min after intracerebroventricular leptin stimulation. Nuclear STAT3 immunoreactivity (*green*) is compared with the cellular location of glial cells (*red*). Note that the STAT3-labeled nuclei do not colocalize with the cytoplasm or cytoskeletal structures of labeled astrocytes or oligodendrocytes, thereby indicating that within these forebrain structures the leptin-induced nuclear STAT3-translocation has occurred in neurons. *f*, Fornix. Scale bars: *A*, *C*, *D*, 25 μm; *B*, *E*, *F*, 10 μm.

The leptin-induced nuclear STAT3 pattern is distinct from that induced by interleukin-6

The specificity of the leptin-induced STAT3 translocation was verified with intracerebroventricular treatment of the endogenous pyrogen IL-6. Central IL-6 administration elicits a variety of (patho)physiological functions, such as the reduction of food intake and locomotor activity, the activation of the hypothalamic–pituitary–adrenocortical axis, and the mediation of fever responses (Lenczowski et al., 1999). The IL-6 receptor has been described to act through similar signaling pathways as the Ob-Rb receptor, that is by altering gene expression via STAT3 binding to gene promoter regions (Darnell, 1997; Takeda and Akira, 2000). Indeed, intracerebroventricular IL-6 application also induced nuclear STAT3 translocation but with a pattern clearly different from that induced by leptin treatment. Whereas leptin proved to be almost ineffective in rostral hypothalamic regions such as the preoptic area, IL-6 induced a strong nuclear STAT3 translocation in the MPO, especially in its ventromedial part. Not surprisingly, these brain regions have been reported previously to participate in the central control of body temperature and fever regulation (Saper, 1998). Within the MPO, the observed IL-6-induced nuclear STAT3 staining pattern 15–30 min after intracerebroventricular application was similar to that seen with Fos analysis 2 hr after endotoxin (lipopolysaccharide) treatment (Elmquist et al., 1996), suggesting a STAT3 action upstream of Fos induction in those neurons.

STAT3 immunohistochemistry: a novel tool to map neurons responding to leptin

Leptin binding to the Ob-Rb receptor leads to nuclear translocation of the activated STAT3 isoform and finally induces transcrip-

←

and dorsal aspects of the organum vasculosum of the lamina terminalis (*B*, *inset A/B*). Intracerebroventricular leptin (*C*) but not IL-6 application (*D*) induced nuclear STAT3 labeling in neurons of layer II of the PIR. For orientation, note that *C* and *D* have been rotated. Within the hypothalamic SON, IL-6 (*F*) but not leptin treatment (*E*) led to nuclear STAT3 labeling. Note that the basal expression of STAT3 immunoreactivity depicted from the leptin-treated animal (*E*) is almost completely located within the cytoplasm of magnocellular SON neurons. In caudal hypothalamic aspects shown in overview for leptin (*G*) and IL-6 treatment (*H*), a distinct cytokine-induced pattern of nuclear STAT3 immunoreactivity could be detected in the ARC, the PAA, and the VMH. V_{III}, Third ventricle; *oc*, optic chiasm; *lot*, lateral olfactory tract; *f*, fornix; *ME*, median eminence. Scale bars: *A–D*, *G*, *H*, 100 μm; *E*, *F*, *inset* in *A/B*, 50 μm.

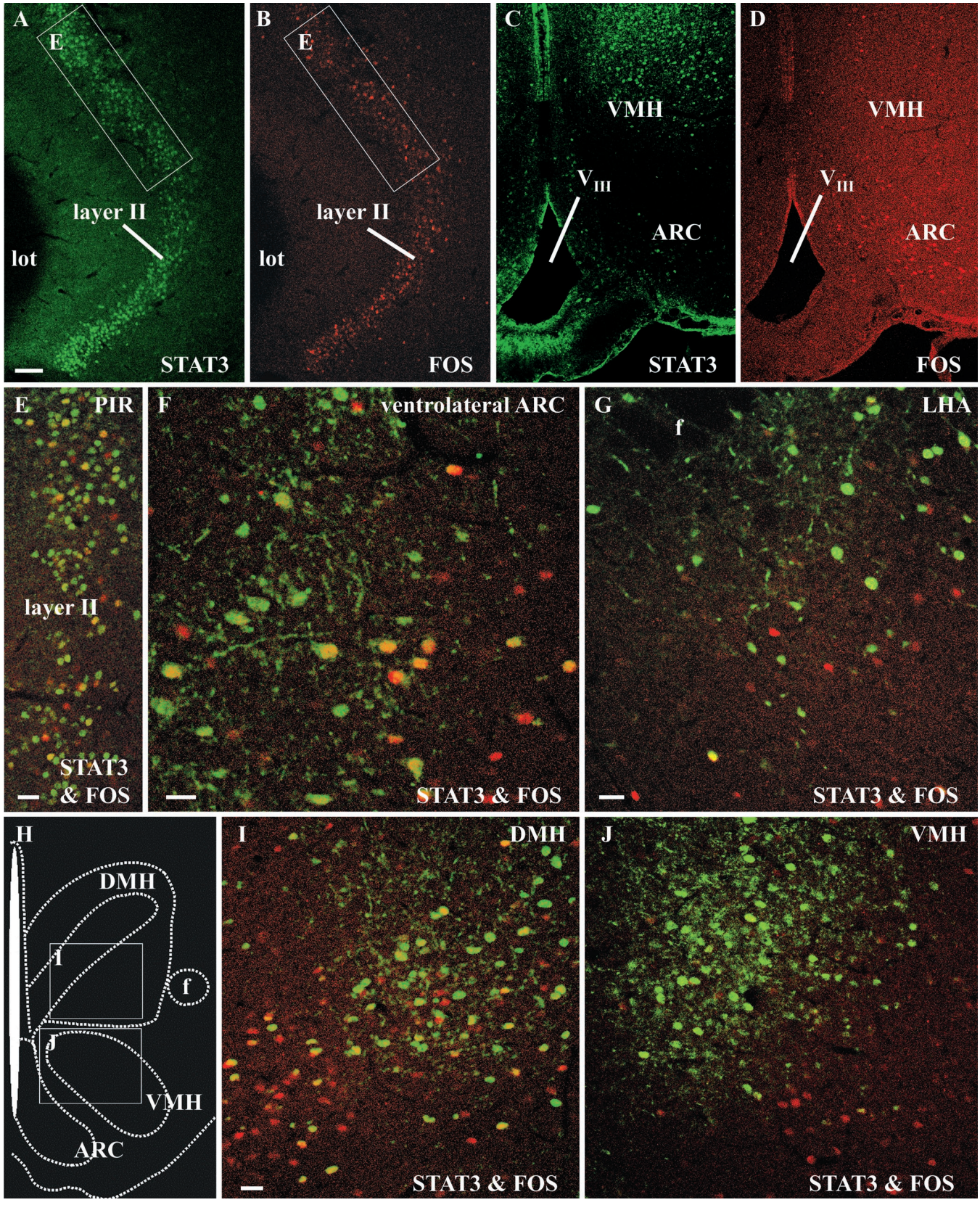

Figure 6. Leptin-translocated nuclear STAT3 and Fos immunoreactivity colocalizes only in a subset of leptin-responsive forebrain neurons. Immunofluorescence photomicrographs of leptin-responsive forebrain structures, such as the PIR (*A*, *B*, *E*), the ARC (*C*, *D*, *F*), ventral aspects of the LHA (*G*), the DMH (*I*), and the VMH (*C*, *D*, *J*), are shown 60 min after intracerebroventricular leptin stimulation. The brain map (*H*) indicates the position of the photomicrographs shown in *I* and *J*. Nuclear STAT3 immunoreactivity (*green*) is compared with the nuclear localization of the protein product of the immediate early gene c-*fos* (*red*). Although within layer II of the PIR many STAT3-labeled (*A*) and Fos-labeled (*B*) nuclei could be detected, the overlay (*E*) at higher magnification (the exact location indicated by the *white rectangles* in *A* and *B*) clearly showed that only a small (*Figure legend continues.*)

tional activation of genes (Ihle, 1996; Darnell, 1997; Takeda and Akira, 2000), among them the immediate early gene c-*fos* (Elmquist et al., 1997, 1998b; Banks et al., 2000) and the SOCS-3 gene (Bjorbaek et al., 1998; Elias et al., 1999). Fos immunohistochemistry has been thoroughly used to investigate leptin actions on the brain. Systemic (Elmquist et al., 1997, 1998b; Wang et al., 1998; Elias et al., 2000; Wilkinson et al., 2000) but also central leptin treatment (van Dijk et al., 1996; Niimi et al., 1999) induced Fos expression in the ventrobasal hypothalamus, with a similar pattern also detected in the present study. However, using Fos analysis, certain hypothalamic Ob-Rb receptor populations seemed to be inaccessible to leptin treatment. One hypothalamic structure in which a discrepancy of high Ob-Rb expression level (Elmquist et al., 1998a; Baskin et al., 1999) with the lack of Fos activation became most evident is the ventromedial ARC (Elmquist et al., 1997, 1998b; Elias et al., 1998). Because inhibitory responses in neurons may not be associated with Fos expression (Chan et al., 1993; Elmquist et al., 1998b), SOCS-3 mRNA expression was consequently used as the first neuroanatomical approach to identify direct leptin-responsive neurons (Bjorbaek et al., 1998; Elias et al., 1999). Within the rat ventrobasal hypothalamus, leptin treatment induced a SOCS-3 expression in areas with high densities of Ob-Rb receptors (Bjorbaek et al., 1998). Both hypothalamic distribution patterns, the leptin-dependent SOCS-3 expression and the constitutive Ob-Rb receptor expression, again resemble the leptin-induced nuclear STAT3 pattern found in the present study. In particular, the SOCS-3 expression and the nuclear STAT3 signals proved to be almost identical in the caudal DMH ventral to its compact formation, as well as in all parts of the ARC, including medial subnuclei, which have been demonstrated to lack a Fos response after leptin treatment. The data collected with both methods, the detection of SOCS-3 mRNA expression and the STAT3 immunohistochemistry, strongly suggest that, unlike Fos immunohistochemistry, these two methods are functional mapping procedures for all leptin targets, whether or not cells are activated or inhibited by leptin.

Recent electrophysiological data have clearly demonstrated an inhibitory leptin action on the neuronal discharge rate of orexin-sensitive ARC neurons, suggesting that neuronal inhibition and not activation is the predominant mode of leptin action in this nucleus. Although in many cases a leptin-induced direct inhibition of neuronal activity in the ARC occurred, some direct activation of neuronal activity also existed (Rauch et al., 2000). In any case, the neuronal discharge rate was rapidly changed in these experiments and therefore, at least initially, these changes occurred independently from genomic effects, e.g., the leptin-induced Fos expression or gene regulation via binding of phosphorylated STAT3 dimers to distinct promoter regions. The putative participation of the STAT3 molecule and its mode of action in such nongenomic, fast neuronal leptin effects remains to be elucidated; however, the intense nerve fiber and axonal STAT3 labeling occurring after leptin application favors the hypothesis of an involvement of axodendritic neuronal processes in fast responses to leptin. In line with electrophysiological data, less Fos-stained than STAT3-labeled cell nuclei may indicate that leptin predominantly induces neuronal inhibition rather than activation in those structures (Spanswick et al., 1997; Rauch et al., 2000). It should be mentioned, however, that these results could also be a reflection of the 60 min time point used in the present study, it being a compromise between the peak of leptin-induced nuclear STAT3 (15–30 min) and nuclear Fos expression (90 min). Those neurons that showed both a nuclear Fos and a STAT3 signal proved to be a minor subpopulation of all STAT3-responsive cells and should be classified as directly activated neurons. Such double-labeled neurons seemed to be prominent in the ventrolateral part of the ARC and in the caudal DMH in a subnucleus ventral to its compact formation. In contrast, within the dorsomedial VMH and in particular within the ventral LHA, only minor colocalization was found, possibly reflecting independent leptin target entities and pathways in the very same nuclei.

REFERENCES

Banks AS, Davis SM, Bates SH, Myers Jr MG (2000) Activation of downstream signals by the long form of the leptin receptor. J Biol Chem 275:14563–14572.

Baskin DG, Schwartz MW, Seeley RJ, Woods SC, Porte Jr D, Breininger JF, Jonak Z, Schaefer J, Krouse M, Burghardt C, Campfield LA, Burn P, Kochan JP (1999) Leptin receptor long-form splice-variant protein expression in neuron cell bodies of the brain and co-localization with neuropeptide Y mRNA in the arcuate nucleus. J Histochem Cytochem 47:353–362.

Bjorbaek C, Uotani S, da Silva B, Flier JS (1997) Divergent signaling capacities of the long and short isoforms of the leptin receptor. J Biol Chem 272:32686–32695.

Bjorbaek C, Elmquist JK, Frantz JD, Shoelson SE, Flier JS (1998) Identification of SOCS-3 as a potential mediator of central leptin resistance. Mol Cell 1:619–625.

Chan RK, Brown ER, Ericsson A, Kovacs KJ, Sawchenko PE (1993) A comparison of two immediate-early genes, c-fos and NGFI-B, as markers for functional activation in stress-related neuroendocrine circuitry. J Neurosci 13:5126–5138.

Chen H, Charlat O, Tartaglia LA, Woolf EA, Weng X, Ellis SJ, Lakey ND, Culpepper J, Moore KJ, Breitbart RE, Duyk GM, Tepper RI, Morgenstern JP (1996) Evidence that the diabetes gene encodes the leptin receptor: identification of a mutation in the leptin receptor gene in db/db mice. Cell 84:491–495.

Cheung CC, Clifton DK, Steiner RA (1997) Proopiomelanocortin neurons are direct targets for leptin in the hypothalamus. Endocrinology 138:4489–4492.

Cusin I, Rohner-Jeanrenaud F, Stricker-Krongrad A, Jeanrenaud B (1996) The weight-reducing effect of an intracerebroventricular bolus injection of leptin in genetically obese fa/fa rats. Reduced sensitivity compared with lean animals. Diabetes 45:1446–1450.

Darnell Jr JE (1997) STATs and gene regulation. Science 277:1630–1635.

Elias CF, Lee C, Kelly J, Aschkenasi C, Ahima RS, Couceyro PR, Kuhar MJ, Saper CB, Elmquist JK (1998) Leptin activates hypothalamic CART neurons projecting to the spinal cord. Neuron 21:1375–1385.

Elias CF, Aschkenasi C, Lee C, Kelly J, Ahima RS, Bjorbaek C, Flier JS, Saper CB, Elmquist JK (1999) Leptin differentially regulates NPY and POMC neurons projecting to the lateral hypothalamic area. Neuron 23:775–786.

Elias CF, Kelly JF, Lee CE, Ahima RS, Drucker DJ, Saper CB, Elmquist JK (2000) Chemical characterization of leptin-activated neurons in the rat brain. J Comp Neurol 423:261–281.

Elmquist JK, Scammell TE, Jacobson CD, Saper CB (1996) Distribution of Fos-like immunoreactivity in the rat brain following intravenous lipopolysaccharide administration. J Comp Neurol 371:85–103.

Elmquist JK, Ahima RS, Maratos-Flier E, Flier JS, Saper CB (1997) Leptin activates neurons in ventrobasal hypothalamus and brainstem. Endocrinology 138:839–842.

Elmquist JK, Bjorbaek C, Ahima RS, Flier JS, Saper CB (1998a) Distributions of leptin receptor mRNA isoforms in the rat brain. J Comp Neurol 395:535–547.

←

subset of layer II neurons coexpressed both transcription factors (*yellow* nuclei), whereas the majority responded with a nuclear translocation of STAT3 only (*green* nuclei). *Red* nuclei belong to those layer II neurons that responded with a nuclear translocation of Fos but not STAT3. Similar results, but with varying degrees of STAT3 and Fos colocalization, were also obtained in the hypothalamic leptin target structures, such as the ventrolateral ARC (*C*, *D*, *F*), the LHA (*G*), the ventral DMH (*I*), and the dorsal VMH (*J*). V_{III}, Third ventricle; *lot*, lateral olfactory tract; *f*, fornix. Scale bars: *A–D*, 100 μm; *E–G*, *I*, *J*, 25 μm.

Elmquist JK, Ahima RS, Elias CF, Flier JS, Saper CB (1998b) Leptin activates distinct projections from the dorsomedial and ventromedial hypothalamic nuclei. Proc Natl Acad Sci USA 95:741–746.

Elmquist JK, Elias CF, Saper CB (1999) From lesions to leptin: hypothalamic control of food intake and body weight. Neuron 22:221–232.

Fei H, Okano HJ, Li C, Lee GH, Zhao C, Darnell R, Friedman JM (1997) Anatomic localization of alternatively spliced leptin receptors (Ob-R) in mouse brain and other tissues. Proc Natl Acad Sci USA 94:7001–7005.

Friedman JM (1998) Leptin, leptin receptors, and the control of body weight. Nutr Rev 56:s38–s46.

Ghilardi N, Skoda RC (1997) The leptin receptor activates janus kinase 2 and signals for proliferation in a factor-dependent cell line. Mol Endocrinol 11:393–399.

Guan XM, Hess JF, Yu H, Hey PJ, van der Ploeg LH (1997) Differential expression of mRNA for leptin receptor isoforms in the rat brain. Mol Cell Endocrinol 133:1–7.

Hakansson M, de Lecea L, Sutcliffe JG, Yanagisawa M, Meister B (1999) Leptin receptor- and STAT3-immunoreactivities in hypocretin/orexin neurones of the lateral hypothalamus. J Neuroendocrinol 11:653–663.

Hakansson ML, Meister B (1998) Transcription factor STAT3 in leptin target neurons of the rat hypothalamus. Neuroendocrinology 68:420–427.

Hakansson ML, Hulting AL, Meister B (1996) Expression of leptin receptor mRNA in the hypothalamic arcuate nucleus: relationship with NPY neurones. NeuroReport 7:3087–3092.

Hakansson ML, Brown H, Ghilardi N, Skoda RC, Meister B (1998) Leptin receptor immunoreactivity in chemically defined target neurons of the hypothalamus. J Neurosci 18:559–572.

Ihle JN (1996) STATs: signal transducers and activators of transcription. Cell 84:331–334.

Lee GH, Proenca R, Montez JM, Carroll KM, Darvishzadeh JG, Lee JI, Friedman JM (1996) Abnormal splicing of the leptin receptor in diabetic mice. Nature 379:632–635.

Leibel RL, Chung WK, Chua Jr SC (1997) The molecular genetics of rodent single gene obesities. J Biol Chem 272:31937–31940.

Lenczowski MJ, Bluthe RM, Roth J, Rees GS, Rushforth DA, van Dam AM, Tilders FJ, Dantzer R, Rothwell NJ, Luheshi GN (1999) Central administration of rat IL-6 induces HPA activation and fever but not sickness behavior in rats. Am J Physiol 276:R652–R658.

Luheshi GN, Gardner JD, Rushforth DA, Loudon AS, Rothwell NJ (1999) Leptin actions on food intake and body temperature are mediated by IL-1. Proc Natl Acad Sci USA 96:7047–7052.

McCowen KC, Chow JC, Smith RJ (1998) Leptin signaling in the hypothalamus of normal rats *in vivo*. Endocrinology 139:4442–4447.

Meister B (2000) Control of food intake via leptin receptors in the hypothalamus. Vitam Horm 59:265–304.

Mercer JG, Hoggard N, Williams LM, Lawrence CB, Hannah LT, Trayhurn P (1996) Localization of leptin receptor mRNA and the long form splice variant (Ob-Rb) in mouse hypothalamus and adjacent brain regions by in situ hybridization. FEBS Lett 387:113–116.

Niimi M, Sato M, Yokote R, Tada S, Takahara J (1999) Effects of central and peripheral injection of leptin on food intake and on brain Fos expression in the Otsuka Long–Evans Tokushima Fatty rat with hyperleptinaemia. J Neuroendocrinol 11:605–611.

Rauch M, Riediger T, Schmid HA, Simon E (2000) Orexin A activates leptin-responsive neurons in the arcuate nucleus. Pflügers Arch 440:699–703.

Rees GS, Ball C, Ward HL, Gee CK, Tarrant G, Mistry Y, Poole S, Bristow AF (1999) Rat interleukin 6: expression in recombinant *Escherichia coli*, purification and development of a novel ELISA. Cytokine 11:95–103.

Saper CB (1998) Neurobiological basis of fever. Ann NY Acad Sci 856:90–94.

Schindler C, Darnell Jr JE (1995) Transcriptional responses to polypeptide ligands: the JAK-STAT pathway. Annu Rev Biochem 64:621–651.

Shindler KS, Roth KA (1996) Double immunofluorescent staining using two unconjugated primary antisera raised in the same species. J Histochem Cytochem 44:1331–1335.

Spanswick D, Smith MA, Groppi VE, Logan SD, Ashford ML (1997) Leptin inhibits hypothalamic neurons by activation of ATP-sensitive potassium channels. Nature 390:521–525.

Strömberg H, Svensson SP, Hermanson O (2000) Distribution of the transcription factor signal transducer and activator of transcription 3 in the rat central nervous system and dorsal root ganglia. Brain Res 853:105–114.

Takeda K, Akira S (2000) STAT family of transcription factors in cytokine-mediated biological responses. Cytokine Growth Factor Rev 11:199–207.

Vaisse C, Halaas JL, Horvath CM, Darnell Jr JE, Stoffel M, Friedman JM (1996) Leptin activation of Stat3 in the hypothalamus of wild-type and ob/ob mice but not db/db mice. Nat Genet 14:95–97.

van Dijk G, Thiele TE, Donahey JC, Campfield LA, Smith FJ, Burn P, Bernstein IL, Woods SC, Seeley RJ (1996) Central infusions of leptin and GLP-1-(7–36) amide differentially stimulate c-FLI in the rat brain. Am J Physiol 271:R1096–R1100.

Wang L, Martinez V, Barrachina MD, Tache Y (1998) Fos expression in the brain induced by peripheral injection of CCK or leptin plus CCK in fasted lean mice. Brain Res 791:157–166.

Wilkinson M, Morash B, Ur E (2000) The brain is a source of leptin. Front Horm Res 26:106–125.

Woods AJ, Stock MJ (1996) Leptin activation in hypothalamus. Nature 381:745.

Woods SC, Seeley RJ, Porte Jr D, Schwartz MW (1998) Signals that regulate food intake and energy homeostasis. Science 280:1378–1383.

Yokosuka M, Xu B, Pu S, Kalra PS, Kalra SP (1998) Neural substrates for leptin and neuropeptide Y (NPY) interaction: hypothalamic sites associated with inhibition of NPY-induced food intake. Physiol Behav 64:331–338.

5.6.

5.6. STEPANYAN, Z., KOCHARYAN, A., PYRSKI, M., HÜBSCHLE, T., WATSON, A.M.D., SCHULZ, S. & MEYERHOF, W. (2003)

Leptin-target neurones of the rat hypothalamus express somatostatin receptors.

J. Neuroendocrinol. **15**: 822-830.

Eigener Anteil an der Publikation:

- Beteiligung an der Versuchsplanung (20 %)
- Durchführung der Versuche (25 %)
- Beteiligung an der Zusammenfassung und Veröffentlichung der Ergebnisse (20 %)

Journal of Neuroendocrinology, 2003, Vol. 15, 822–830

Leptin-Target Neurones of the Rat Hypothalamus Express Somatostatin Receptors

Z. Stepanyan,* A. Kocharyan,* M. Pyrski,* T. Hübschle,* A. M. D. Watson,* S. Schulz† and W. Meyerhof*
*Department of Molecular Genetics, German Institute of Human Nutrition, Potsdam-Rehbrücke, Germany.
†Institute of Pharmacology and Toxicology, Otto-von-Guericke University, Magdeburg, Germany.

Key words: somatostatin, leptin, STAT3, hypothalamus.

Abstract

Hypothalamic leptinoceptive neurones can be visualized by histochemical demonstration of leptin-induced nuclear translocation of the signalling molecule STAT3. We investigated the relationship of the leptinoceptive neurones to the somatostatin signalling system. With double-labelling immunohistochemistry, we studied the colocalization of leptin-activated transcription factor, STAT3, with somatostatin receptor subtypes, sst1, sst2A, sst2B, sst3 and sst4, or the neuropeptide itself, in the rat hypothalamus. Immunoreactivity for all the entities was widely distributed throughout the entire hypothalamus. Despite the wide distribution, only few cases of colocalization of somatostatin with leptin-activated STAT3 were detected in the paraventricular, arcuate and dorsomedial nuclei. A moderate to high degree of colocalization of nuclear STAT3 and all investigated subtypes of somatostatin receptors was found in the lateral and dorsal hypothalamic areas and in the dorsomedial hypothalamic nucleus. Immunoreactivity for sst1, sst2B and sst4 was present in STAT3-containing nuclei of the paraventricular, periventricular, arcuate and ventromedial hypothalamic neurones, as well as in the retrochiasmatic and posterior hypothalamic areas. Despite the wide distribution of sst2A in the rat hypothalamus, few events of colocalization with leptin-activated STAT3 were observed in the dorsomedial nucleus and in the lateral and dorsal hypothalamic areas only. Many leptin-responsive neurones of the dorsal, lateral, periarcuate, perifornical and posterior hypothalamic areas, as well as in the ventromedial and dorsomedial hypothalamic nuclei, displayed sst3 immunoreactivity at their neuronal cilia. These results provide strong anatomical evidence for the direct interaction of leptin and the somatostatin systems in neuroendocrine control loops such as the energy homeostasis, growth or stress response.

Leptin is mainly secreted by adipose tissue and affects feeding behaviour, thermogenesis and neuroendocrine status. Multiple splice variants of leptin receptor mRNA encode at least six leptin receptor isoforms called Ob-Ra–Ob-Rf (1, 2). Of these, only the long receptor isoform, Ob-Rb, is able to efficiently activate the JAK (janus-kinase)-STAT (signal transducers and activators of transcription) signal transduction pathway (3–5). *In vitro*, leptin has been shown to activate STAT1, STAT3, STAT5 and STAT6 (4, 6); however, in the hypothalamus, leptin specifically activates STAT3 (3).

The distribution of the leptin receptor in central nervous system has been described in many studies (7–9). In the hypothalamus, strong leptin receptor immunoreactivity is detected in the arcuate, paraventricular (PVN) and ventromedial hypothalamic nuclei, and also the lateral hypothalamic area (8–10). STAT3-like immunoreactivity is observed in a large number of hypothalamic structures, such as the lateral hypothalamic area, dorsomedial, ventromedial and arcuate hypothalamic nuclei (11). Many leptin receptor-expressing neurones in the rat hypothalamus coexpress STAT3 (12), providing immunohistochemical evidence that leptin acts via STAT3 in hypothalamic neurones.

Consistent with this assumption, leptin leads to the time-dependent stimulation of STAT3 tyrosine phosphorylation (13). Moreover, intravenous (14) or intracerebroventricular (15) leptin administration induces the time-dependent nuclear translocation of STAT3 immunoreactivity in hypothalamic nuclei, with strong nuclear STAT3 signals detectable in the arcuate, ventromedial, dorsomedial hypothalamic nuclei and lateral hypothalamic area. Thus, the detection of nuclear STAT3 immunoreactivity represents a neuroanatomical tool to functionally map central leptin actions.

Many studies demonstrate the connection between leptin target neurones in hypothalamus and other neuropeptide systems. Thus, double-labelling immunohistochemistry showed that leptin receptor is present in neuropeptide Y (NPY) (9, 16) and pro-opiomelanocortin (POMC) (9, 17) neurones of the arcuate hypothalamic

Correspondence to: Professor Wolfgang Meyerhof, Department of Molecular Genetics, German Institute of Human Nutrition, Arthur-Scheunert Allee 114–116, D-14558, Potsdam-Rehbrücke, Germany (e-mail: meyerhof@mail.dife.de).

nucleus, in the corticotropin-releasing hormone (CRH) neurones of the parvocellular division of the PVN and in melanin-concentrating hormone neurones of the lateral hypothalamic area (9). GABA neurones of the ventromedial arcuate nucleus display immunoreactivity for both leptin receptors and STAT3 (18). These observations suggest that different neuropeptides mediate the central actions of leptin and that, on the other hand, leptin modulates other neuropeptides (19–22). Particularly intriguing are reports showing that growth hormone secretion is markedly influenced by body weight, being suppressed in obesity (23) and cachexia (24).

It is well known that somatostatin mediates its biological effects through a family of G-protein coupled receptors containing seven transmembrane domains. Six distinct somatostatin receptor (sst) subtypes, termed sst1, sst2A, sst2B, sst3, sst4 and sst5, have so far been cloned (25, 26), and all are present in the rat central nervous system (27–33).

Little is known about the possible link between leptin and somatostatin. However, pharmacotherapeutic use of the somatostatin analogues lanreotide and sandostatin LAR in patients suffering from acromegaly leads to the decrease of serum leptin levels (34, 35). In the rat hypothalamus, occasional colocalization of somatostatin and leptin receptors was observed in the periventricular hypothalamic nucleus (9). Double-labelling immunohistochemistry performed in sheep hypothalamus showed that all somatostatin immunoreactive neurones in the arcuate, ventromedial and dorsomedial hypothalamic nuclei coexpress Ob-Rb, whereas only a subpopulation of somatostatin neurones in the hypothalamic periventricular area exhibits Ob-Rb immunoreactivity (36). These findings provide a basis for the interaction of leptin and somatostatin; however, the precise mechanisms of this interaction remain to be clarified.

In the present immunohistochemical study, we performed a complete and detailed analysis of the distribution of somatostatin and its receptors in the rat hypothalamus, together with their possible colocalization with leptin-induced STAT3.

Materials and methods

Animals

Adult male Wistar rats (Tierzucht Schönwalde GmbH, Schönwalde, Germany) weighing 180–220 g were individually housed (Max Rubner Laboratory, Bergholz-Rehbrücke, Germany) under light-controlled (12 : 12 h light/dark cycle, lights on at 06.00 h) and temperature-controlled (22 ± 1 °C) conditions. Water and standard chow were available *ad libitum*, and body weight was monitored daily. Animal experimentation was performed in accordance with the German Animal Protection Law (approval number 48-3560-1/2).

Intracerebroventricular cannulation of the lateral ventricle

A modified 23-gauge cannula (Braun, Melsungen, Germany) was stereotaxically placed into the lateral ventricle of rats as described previously (15). The accurate position of the implanted cannula was verified by the intracerebroventricular administration of angiotensin II (50 ng; Bachem Biochemica GmbH, Heidelberg, Germany) in 5 µl of 0.9% pyrogene-free saline (Sigma-Aldrich Chemie GmbH, Steinheim, Germany), 1 week after surgery. Only those animals that drank a minimum of 10 ml water/h were used.

Intracerebroventricular injections

Recombinant murine leptin (3.5 µg; kindly provided by Aventis Pharma, Frankfurt, Germany) diluted in 6 µl of 0.9% pyrogene-free saline (Sigma-Aldrich Chemie) was injected into the lateral ventricle of lightly restrained, conscious rats using a 25-µl Hamilton syringe (Hamilton Bonaduz AG, Bonaduz, Switzerland), connected through a polyethylene tubing to the implanted cannula. The following reasons led us to administer leptin intracerebroventricularly. First, focusing on the action of leptin in the brain (i.e. its hypothalamic satiety centres), we choose the most direct way of central delivery. The mechanism by which leptin enters the brain is still largely unclear. However, it has been shown that there are no differences in STAT3 activation regarding peripheral (14) versus intracerebroventricular (15) injection of leptin. Second, we aimed to compare the results from the present study with those of our previous study (15) in which we applied that same drug-delivery technique.

Thirty minutes after the central administration of leptin, rats were anaesthetized with sodium pentobarbital (60 mg/kg Narcoren; Merial GmbH, Hallbergmoos, Germany) and transcardially perfused with 100 ml of 0.9% saline, followed by 300 ml of ice-cold 4% paraformaldehyde (Sigma-Aldrich Chemie) in 0.1 M phosphate buffer (PB) (pH 7.2). Brains were rapidly dissected and postfixed in the same fixative for 1 h. Tissue was cryoprotected by immersion in 20% sucrose (Merck KGaA, Darmstadt, Germany) in PB for 24 h at 4 °C and then snap-frozen in liquid nitrogen/petroleum ether bath (−60 °C).

Immunohistochemical colocalization studies

Coronal brain sections (30 µm) of the rat hypothalamus (bregma levels from −0.26 to −4.80 mm) were cut in a cryostat (HM505E; Mikrom International GmbH, Walldorf, Germany) for immunohistochemical double-labelling. Immunohistochemistry was performed on free-floating sections preincubated in PB containing 10% normal horse serum (NHS) (Biochrom KG, Berlin, Germany) and 0.3% Triton X-100 (Merck KGaA) for 1 h and then in blocking reagent (NEL700; NEN Life Science Products GmbH, Köln, Germany) for 30 min at room temperature.

For the immunohistochemical double-labelling of somatostatin and STAT3 (n = 11), the mouse monoclonal antihuman somatostatin antibody (1 : 20; V1169; Biomeda Corp., Foster City, CA, USA) and rabbit polyclonal antimouse STAT3 antibody (1 : 10 000; sc-482; Santa Cruz Biotechnology, Inc., Heidelberg, Germany) (11) were applied simultaneously, and incubated for 48–72 h at 4 °C. Both primary antibodies were diluted in PB/2% NHS/0.1% Triton X-100. After rinsing the sections in PB, they were transferred to secondary biotinylated goat anti-rabbit antibody (1 : 200 in PB/2% NHS; Vector BA-1000; Linaris Biologische Produkte, Wertheim-Bettingen, Germany) for 45 min at room temperature. Thereafter, sections were washed with PB and incubated with streptavidin-conjugated horseradish peroxidase (1 : 100 in PB; NEL700; NEN Life Science Products) for 30 min in the dark. After rinsing in PB, sections were transferred to biotinyl tyramide (1 : 100 in amplification diluent provided in the kit; NEL700; NEN Life Science Products) for 10 min in the dark. Then, sections were washed, and immunoreactivity was visualized with fluorescein-conjugated avidin D (1 : 200 in PB; Vector A-200; Linaris Biologische Produkte) for the detection of amplified STAT3 signal and Cy3-conjugated antimouse antibody (1 : 200 in PB; Sigma-Aldrich Chemie) for the detection of somatostatin.

Double-labelling of the STAT3 and different sst subtypes (n = 20) was performed using different primary antibodies raised in the same host species. Thus, sections were first incubated with one of the following antisera: antisst1 (1 : 10 000; 5605) (27), antisst3 (1 : 10 000; 7986) (37), affinity purified antisst2A (2 µg/ml; 6291) (31), antisst2B (2 µg/ml; 5574) (31) or antisst4 (2 µg/ml; 6002) (38) antibodies diluted in PB/2% NHS/0.1% Triton X-100. Staining of different sst subtypes was then detected using the tyramide amplification protocol described above. After incubation with biotinyl tyramide, sections were rinsed in the PB and then incubated for 48–72 h at 4 °C in a second primary antibody for the detection of STAT3 signal (1 : 500 in PB/2% NHS/0.3% Triton X-100; Santa Cruz Biotechnology). Visualization was performed using fluorescein-conjugated avidin D (1 : 200 in PB; Linaris Biologische Produkte) for the detection of staining of sst subtypes and anti-rabbit antibody conjugated with Texas Red (1 : 150 in PB; Vector TI-1000; Linaris Biologische Produkte) for the detection of nonamplified STAT3 signal.

Cross-reactivity between antibodies was discounted by using negative controls where one of the primary antibodies was omitted from the incubation solutions (data not shown).

Analysis of sections

Brain sections were mounted onto chrome alum gelatin-subbed glass slides and coverslipped with Crystal/Mount medium (Biomeda Corp.). Sections were analysed using a fluorescent microscope (Zeiss Axioplan, Jena, Germany). Monochrome 12-bit images were taken using the Spot RT digital camera (Diagnostic Instruments Inc., Visitron Systems GmbH, Puchheim, Germany) and were deblurred by AutoDeblurTM software (Version 7,5; Visitron Systems GmbH). To verify the colocalization scanned images were three-dimensionally reconstructed. Digitized

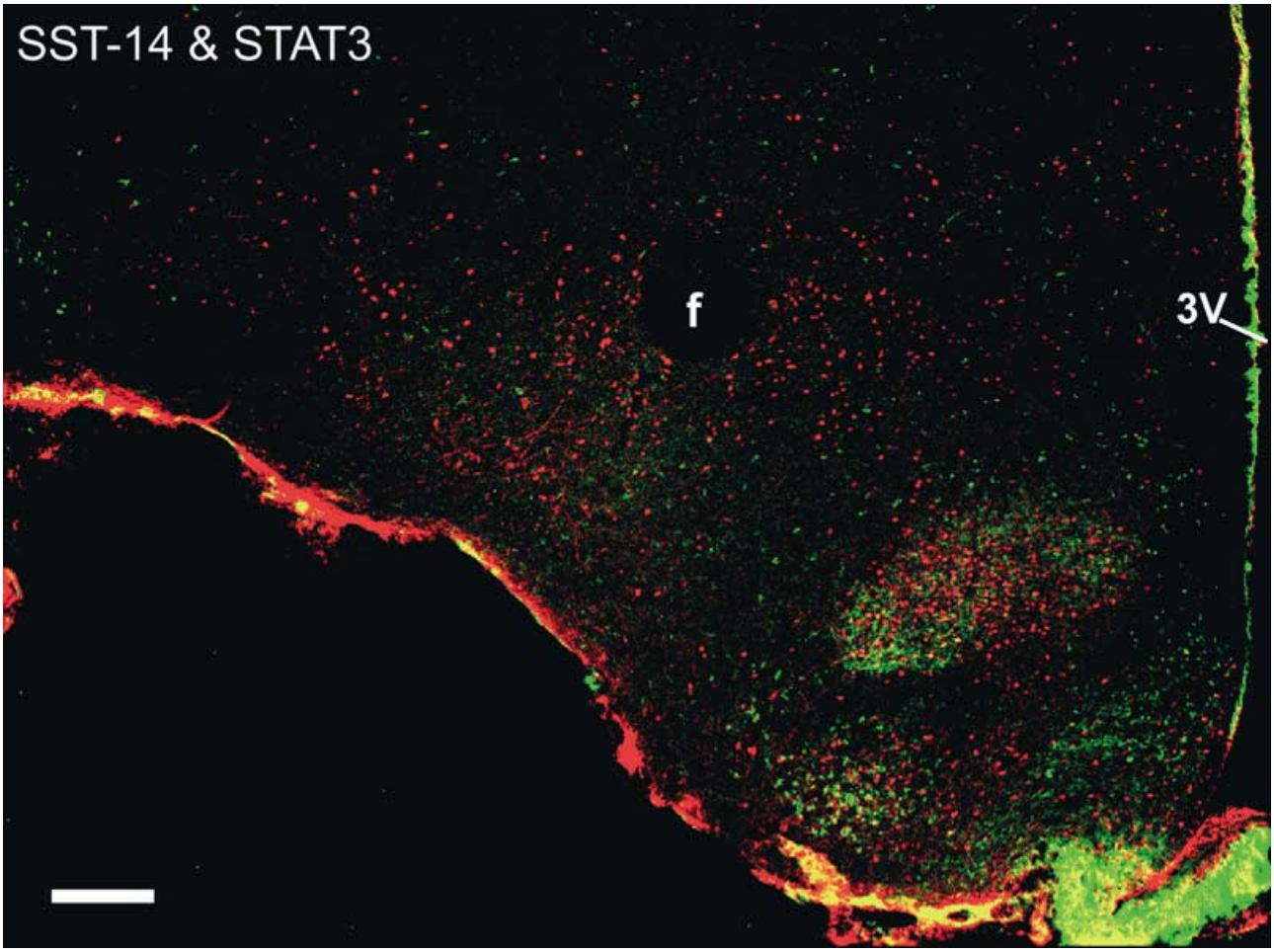

FIG. 1. Immunofluorescence photomicrograph showing the distribution and colocalization of leptin-induced STAT3 (red) with somatostatin (green) in rat hypothalamus (bregma level: −2.56 mm). Monochrome 12-bit images were taken separately for STAT3 and somatostatin immunostaining, and then red colour was chosen for amplified STAT3 signal, and green for nonamplified somatostatin. Scale bar = 200 μm. 3V, third ventricle; f, fornix.

images were minimally edited using MetaMorph 5.0r4 software (Universal Imaging Corp., Visitron Systems GmbH) with regard to contrast and brightness. Quantitative estimates were carried out by counting labelled cells in the field of view at 40 × magnification. At least 20 sections were counted per animal and structure: '–', no cells; '+', 1–4 cells (weak); '++', 5–20 cells (moderate); '+++', 21 and more cells (strong, prominent). The quantification of the colocalization events was performed similarly. Each of the categories '–', no colocalization; '+/–', less than 5% (occasional); '+', from 5% to 20% (intermediate); '++', from 20% to 50% (frequent); and '+++', more than 50% (massive) refer to the number of STAT3 positive cells that coexpressed somatostatin or one of the sst subtypes in a given region. Rat brain regions and nuclei were identified and classified using the rat brain atlas of Paxinos and Watson (39).

Results

Distribution of leptin-activated STAT3

Incubation of the rat brain sections with STAT3 antibody demonstrated the strongest immunoreactivity of leptin-activated STAT3 in the arcuate, ventromedial and dorsomedial hypothalamic nuclei (Figs 1, 2B, 2H and 3B,E,H,K,N,Q). With the exception of the anterior hypothalamic area and the supraoptic nucleus, which were devoid of STAT3 immunoreactive cells, moderate immunostaining for STAT3 was detected in many hypothalamic structures, such as lateral (Fig. 2N), dorsal (Fig. 2K) and posterior hypothalamic areas, retrochiasmatic, periarcuate, perifornical areas and periventricular hypothalamic nucleus (Fig. 2Q). In addition, a weaker labelling for STAT3 was found in the remaining hypothalamic regions (Table 1). The staining patterns of STAT3 described in present study are in full agreement with the data reported previously (15).

Somatostatin and STAT3

The somata and fibre labelling for somatostatin was most dense in the arcuate (Fig. 1) and periventricular hypothalamic nuclei

FIG. 2. Immunofluorescence photomicrographs showing the distribution and colocalization of leptin-induced STAT3 (red) with somatostatin (SST-14), or somatostatin receptors (green) in selected hypothalamic regions. (A–C) sst1 and STAT3 in the dorsomedial hypothalamic nucleus (DM); (D–F) sst2A and STAT3 in the ventral part of premammillary nucleus (PMV); (G–I) sst2B and STAT3 in the arcuate hypothalamic nucleus (Arc); (J–L) sst3 and STAT3 in the dorsal hypothalamic area (DA); (M–O) sst4 and STAT3 in the lateral hypothalamic area (LH); (P–R) SST-14 and STAT3 in the periventricular hypothalamic nucleus (Pe). Arrowheads show selected examples of double-labelled cells, while arrows indicate the absence of colocalization. Scale bar = 25 μm for all panels. 3V, third ventricle.

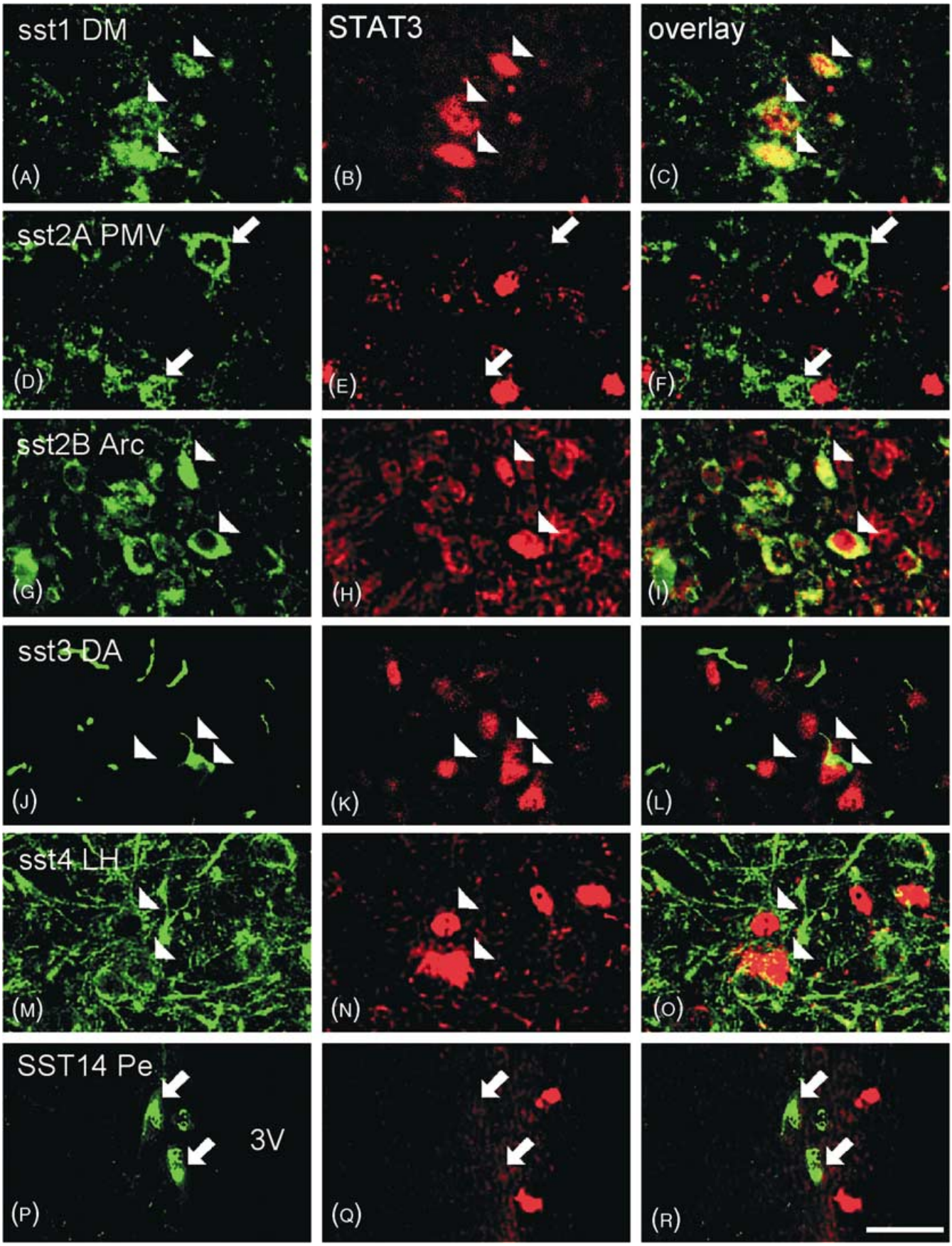
sst1 DM
STAT3
overlay
(A)
(B)
(C)
sst2A PMV
(D)
(E)
(F)
sst2B Arc
(G)
(H)
(I)
sst3 DA
(J)
(K)
(L)
sst4 LH
(M)
(N)
(O)
SST14 Pe
3V
(P)
(Q)
(R)

(Fig. 2P). Prominent staining of fibres was also detected in the ventromedial (Figs 1 and 3P), premammillary and supramammillary hypothalamic nuclei. Somatostatin positive cells were found throughout the entire hypothalamus with the exception of the premammillary, supramammillary, medial and lateral mammillary nuclei, where no labelled cell bodies were evident. Despite the wide distribution of somatostatin in the rat hypothalamus, double-labelling immunohistochemistry revealed occasional cases of colocalization of STAT3 and somatostatin in the PVN, arcuate and dorsomedial hypothalamic nuclei only (Table 1).

Different subtypes of somatostatin receptors and STAT3

Moderate to strong immunostaining for sst1 was found in various hypothalamic structures with the exception of the tuber cinereum and premammillary nucleus, where no immunopositive cell bodies were observed. Cellular staining was the strongest in the arcuate nucleus, whereas the fibre staining was the most prominent in the lateral mammillary nucleus. Double-labelling immunohistochemistry for STAT3 and sst1 revealed colocalization in many of the hypothalamic regions investigated, but not in the suprachiasmatic and medial mammillary nuclei (Table 1). Intermediate colocalization was observed in the lateral hypothalamic area, periventricular, arcuate, ventromedial (Fig. 3C), dorsomedial hypothalamic nuclei (Fig. 2C), posterior, periarcuate and retrochiasmatic hypothalamic areas, as well as in the lateral mammillary and supramammillary nuclei. Frequent cases of colocalization were detected in the PVN, dorsal hypothalamic and perifornical areas.

Cellular and fibre sst2A-immunoreactivity was found in most regions with the strongest cellular staining detected in the arcuate nucleus. However, no fibre labelling was seen in the ventromedial hypothalamic nucleus (Fig. 3D). Despite the wide distribution of sst2A in the rat hypothalamus, only occasional cases of colocalization with STAT3 were confined to the dorsomedial hypothalamic nucleus, lateral and dorsal hypothalamic areas (Table 1).

Sst2B-labelled cell bodies and fibres were numerous and detected throughout the entire hypothalamus. The strongest cellular immunostaining was observed in the arcuate (Fig. 2G) and lateral mammillary nuclei. Double-labelling immunohistochemistry revealed frequent colocalization of sst2B and STAT3 in many hypothalamic areas, including lateral hypothalamic area, PVN, arcuate (Fig. 2I), ventromedial (Fig. 3I), dorsomedial hypothalamic nuclei, dorsal, periarcuate, perifornical and posterior hypothalamic areas. By contrast, no colocalization was detected in the suprachiasmatic, premammillary, lateral mammillary and supramammillary nuclei (Table 1).

In agreement with a previous study (37), sst3-immunoreactivity was selectively restricted to neuronal cilia, primary and nonmotile cilia, considered to be sensory organelles (40). Labelling of these structures was the strongest in the ventromedial hypothalamic nucleus (Fig. 3J). However, weak to moderate densities of labelled cilia were present in other hypothalamic structures including anterior, lateral, dorsal (Fig. 2J) and posterior hypothalamic areas, supraoptic nucleus, PVN, as described earlier (37). In addition, we found sst3-immunostaining in periarcuate, perifornical and retrochiasmatic areas, dorsomedial, premammillary, medial mammillary and supramammillary nuclei. By contrast, sst3 immunoreactivity was absent in the tuber cinereum, arcuate, suprachiasmatic, periventricular and lateral mammillary nuclei. Massive colocalization of sst3 and STAT3 was demonstrated in neurones of the ventromedial hypothalamic nucleus (Fig. 3L) with intermediate colocalization in the lateral, periarcuate, perifornical hypothalamic areas and dorsomedial hypothalamic nucleus (Table 1). Occasional cases of colocalization were found in the dorsal (Fig. 2L) and posterior hypothalamic areas. Because nuclear STAT3 and cilial sst3 signals were difficult to assign to the same cells, we conducted extensive three-dimensional reconstructions. Figure 4 clearly shows that this method allowed the unequivocal colocalization of nuclear and cilial immunostaining.

The sst4 antibody stained numerous hypothalamic structures. Thus, moderate cellular and fibre immunostaining was observed in the tuber cinereum, anterior, lateral (Fig. 2M), dorsal and posterior hypothalamic areas, PVN, arcuate, ventromedial (Fig. 3M), dorsomedial, premammillary, medial and lateral mammillary nuclei. By contrast, no immunopositive cell bodies or fibres were detected in the suprachiasmatic nucleus. Immunohistochemical double-labelling demonstrated intermediate colocalization of STAT3 and sst4 in many hypothalamic regions, including tuber cinereum, periventricular, premammillary, arcuate, ventromedial (Fig. 3O), dorsomedial hypothalamic nuclei, lateral (Fig. 2O), dorsal, periarcuate, retrochiasmatic and posterior hypothalamic areas with frequent colocalization in the PVN and perifornical area. However, no colocalization was found in the medial and lateral mammillary and supramammillary nuclei (Table 1).

Discussion

In the present study, we analysed the expression of somatostatin and different subtypes of its receptors in the rat hypothalamic neurones containing leptin-activated STAT3. The presence of nuclear STAT3 in many neurones of the rat hypothalamus (15) represents the anatomical correlate of the action of leptin. As we show, leptin target neurones of the rat hypothalamus coexpress different sst subtypes, as well as somatostatin itself, which suggests a direct cooperation of the leptin and somatostatin systems. Previous reports have presented anatomical evidence for the interaction of leptin and somatostatin. Thus, all somatostatin immunoreactive neurones in the arcuate, ventromedial and dorsomedial hypothalamic nuclei, and some in the periventricular hypothalamic area of sheep hypothalamus, express Ob-Rb (36), predicting STAT3 nuclear translocation in response to leptin. These data differ from the results of the present study in demonstrating only occasional colocalization of somatostatin and leptin-activated STAT3 in the PVN, arcuate and dorsomedial hypothalamic nuclei, and no colocalization in the ventromedial and periventricular hypothalamic nuclei. This likely reflects differences between ruminant and rodent neuroendocrinology. Despite

FIG. 3. Immunofluorescence photomicrographs showing the distribution and colocalization of leptin-induced STAT3 (red), somatostatin (SST-14) and different subtypes of its receptors (green) in the ventromedial hypothalamic nucleus (VMH). (A–C) sst1 and STAT3; (D–F) sst2A and STAT3; (G–I) sst2B and STAT3; (J–L) sst3 and STAT3; (M–O) sst4 and STAT3; (P–R) SST-14 and STAT3. Arrowheads show examples of double-labelled cells, while arrows indicate the absence of double-labelling. Open arrows or arrowheads indicate cells depicted in the insets at higher magnification. Scale bar = 50 μm for all panels; scale bar = 10 μm for all insets.

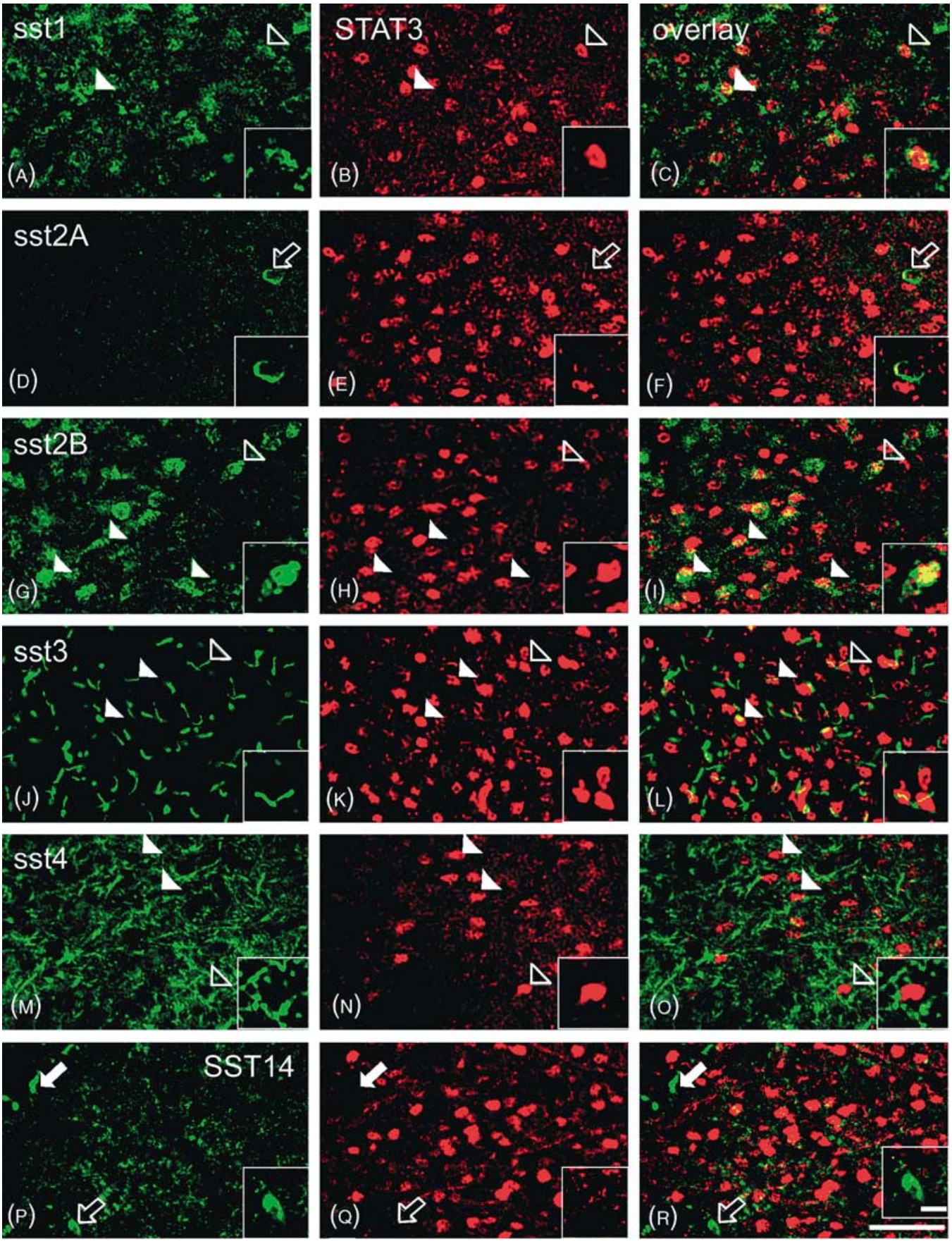
sst1
STAT3
overlay
(A)
(B)
(C)
sst2A
(D)
(E)
(F)
sst2B
(G)
(H)
(I)
sst3
(J)
(K)
(L)
sst4
(M)
(N)
(O)
SST14
(P)
(Q)
(R)

TABLE 1. Regional Distribution and Colocalization of Leptin-Activated STAT3, Somatostatin (SST-14) and Somatostatin Receptors (sst) in the Rat Hypothalamus.

		SST-14			sst1			sst2A			sst2B			sst3		sst4		
Region	STAT3	S	F	Co	S	F	Co	S	F	Co	S	F	Co	R	Co	S	F	Co
Suprachiasmatic nucleus	+	++	++	−	+	++	−	+	+	−	+	++	−	−	−	−	−	−
Tuber cinereum	+	++	++	−	−	+	−	++	++	−	+	++	+	−	−	++	++	+
Anterior hypothalamic area	−	++	++	−	+	+	−	++	++	−	+	++	−	+	−	++	++	−
Lateral hypothalamic area	++	++	++	−	++	+	+	++	++	+−	++	++	++	++	+	++	++	+
Supraoptic nucleus	−	+	+	−	++	++	−	++	+	−	++	+	−	+	−	+	+	−
Paraventricular hypothalamic nucleus	+	++	++	+−	+	++	++	++	++	−	++	+	++	+	−	++	++	++
Periventricular hypothalamic nucleus	++	+++	+++	−	+	+	+	++	++	−	++	++	+	−	−	+	+	+
Arcuate hypothalamic nucleus	+++	+++	+++	+−	+++	+	+	+++	++	−	+++	++	++	−	−	++	++	+
Periarcuate area	++	++	++	−	+	+	+	+	++	−	+	+	++	+	+	+	+	+
Perifornical area	++	++	+	−	+	+	++	+	++	−	+	++	++	+	+	+	++	++
Retrochiasmatic area	++	+	++	−	+	+	+	++	++	−	++	+	+	+	−	+	+	+
Ventromedial hypothalamic nucleus	+++	+	+++	−	++	++	+	+	−	−	++	+	++	+++	+++	++	++	+
Dorsomedial hypothalamic nucleus	+++	++	++	+−	+	+	+	++	+	+−	++	+	++	+	+	++	++	+
Dorsal hypothalamic area	++	++	++	−	+	+	++	++	++	+−	+	++	++	++	+−	++	++	+
Posterior hypothalamic area	++	++	+	−	+	++	+	++	++	−	+	++	++	++	+−	++	++	+
Premammillary nucleus	+	−	+++	−	−	++	−	++	+	−	+	+	−	+	−	++	++	+
Medial mammillary nucleus	+	−	−	−	+	++	−	++	+	−	++	+	+	+	−	++	++	−
Lateral mammillary nucleus	+	−	++	−	+	+++	+	++	+	−	+++	++	−	−	−	++	++	−
Supramammillary nucleus	+	−	+++	−	+	++	+	++	+	−	++	+	−	+	−	+	+	−

Localization: –, no cells; +, 1–4 cells in the field of view (× 40); ++, 5–20 cells in the field of view (× 40); +++, 21 and more cells in the field of view (× 40). Co-localization: –, no colocalization; +/−, occasional, less than 5% of colocalized STAT3 cells; +, intermediate, from 5 to 20% of colocalized STAT3 cells; ++, frequent, from 20 to 50% of colocalized STAT3 cells; +++, massive, more than 50% of colocalized STAT3 cells. S, somata; F, fibres; R, rods; co, colocalization.

the absence of somatostatin and STAT3 colocalization in the rat periventricular hypothalamic nucleus, colocalization of somatostatin and leptin receptor in this structure was described previously using a nonselective Ob-R antibody (9). The periventricular neurones may express the nonsignaling short Ob-R isoforms that do not activate STAT3, but not the long Ob-Rb.

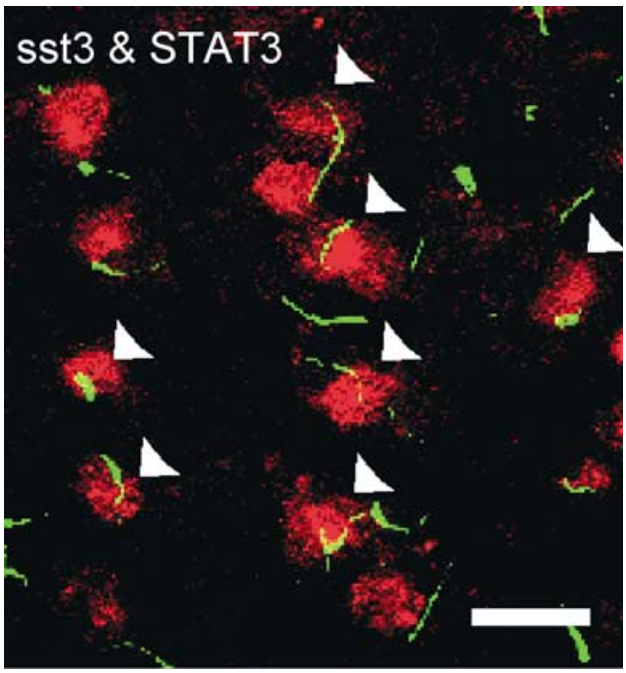

FIG. 4. Three-dimensional reconstruction of a stack of optical images (number of planes = 15, distance between planes = 0.71 μm) showing the colocalization of nuclear STAT3 (red) and cilial sst3 (green) immunostaining. Arrowheads show selected examples of double-labelled cells. Scale bar = 15 μm.

Because various hypothalamic regions have definite physiological functions, colocalization of leptin-activated STAT3 with either somatostatin or its receptors has some functional implications. For example, the PVN, which regulates the neuroendocrine stress response, is heavily labelled with antibodies to somatostatin and all sst subtypes. We found a moderate to high degree of colocalization of nuclear STAT3 with either sst1, sst2B, sst4 or somatostatin in this hypothalamic structure. Interestingly, parvocellular neurones of the rat PVN containing CRH and CART also express leptin receptors (9, 41) and, according to recent data, leptin may be involved in the stress response at the level of hypothalamus (42, 43). In rat, acute and chronic stress increases hypothalamic somatostatin secretion (44) and release (45). Given that somatostatin and/or leptin are involved in the neuroendocrine stress response (46), the colocalization of leptin-activated STAT3 and somatostatin and its receptors in the PVN encourages future investigation of the interaction of leptin and somatostatin system in the regulation of stress.

Leptin and somatostatin also interact to regulate the secretion of growth hormone (19, 20). Leptin administration to fetal rat neuronal culture leads to a time-dependent decrease in somatostatin secretion and somatostatin mRNA expression (47). These findings are in agreement with *in vivo* studies showing that central injection of leptin increases mRNA expression of pituitary growth hormone and hypothalamic growth hormone-releasing hormone (GHRH), whereas somatostatin mRNA expression is reduced (48). Moreover, sst1 and sst2 regulate GHRH in neurones of the arcuate hypothalamic nucleus (49, 50). Our data show that sst1, sst2B and sst4 are present on leptin-responsive neurones of the arcuate nucleus. Together, these results demonstrate that leptin is a metabolic signal that regulates growth hormone secretion in the rat hypothalamus through growth hormone regulatory hormones.

According to our results, leptin-activated STAT3, somatostatin and its receptors, with the exception of sst3, were widely distributed throughout the arcuate hypothalamic nucleus. The arcuate nucleus is considered to be the first target for circulating leptin. Both the NPY/agouti-related protein and POMC/CART neurones in the arcuate nucleus, known to mediate orexigenic and anorexigenic effects, respectively, express the long isoform of the leptin receptor (7, 16, 51–53). In addition, NPY and POMC neurones of the arcuate nucleus have been shown to express STAT3 (12). Leptin can directly effect the gene expression of several neuropeptides (53–56). Moreover, recently conducted investigations demonstrated that GABA neurones of the ventromedial arcuate nucleus coexpress leptin receptors and STAT3 (18). Based on these observations, together with our present findings demonstrating STAT3 and somatostatin colocalization in the arcuate nucleus, we suggest that somatostatin participates in the leptin-mediated regulation of food intake. Several studies support this assumption. It has been reported that somatostatin modulates hourly food intake (57). In addition, somatostatin can alter taste preferences in the rat (58), and may be involved in the regulation of central feeding mechanism in human *anorexia nervosa* (59, 60).

Acknowledgements

This work was supported through a grant, QLG3-CT-1999-00908, from the European Commission.

Accepted 2 June 2003

References

1 Ahima RS, Flier JS. Leptin. *Annu Rev Physiol* 2000; **62:** 413–437.
2 Lee GH, Proenca R, Montez JM, Carroll KM, Darvishzadeh JG, Lee JI, Friedman JM. Abnormal splicing of the leptin receptor in diabetic mice. *Nature* 1996; **379:** 632–635.
3 Vaisse C, Halaas JL, Horvath CM, Darnell JE Jr, Stoffel M, Friedman JM. Leptin activation of Stat3 in the hypothalamus of wild-type and ob/ob mice but not db/db mice. *Nature Genet* 1996; **14:** 95–97.
4 Ghilardi N, Ziegler S, Wiestner A, Stoffel R, Heim MH, Skoda RC. Defective STAT signaling by the leptin receptor in diabetic mice. *Proc Natl Acad Sci USA* 1996; **93:** 6231–6235.
5 Bjorbaek C, Uotani S, da Silva B, Flier JS. Divergent signaling capacities of the long and short isoforms of the leptin receptor. *J Biol Chem* 1997; **272:** 32686–32695.
6 Rosenblum CI, Tota M, Cully D, Smith T, Collum R, Qureshi S, Hess JF, Phillips MS, Hey PJ, Vongs A, Fong TM, Xu L, Chen HY, Smith RG, Schindler C, Van der Ploeg LH. Functional STAT 1 and 3 signaling by the leptin receptor (OB-R); reduced expression of the rat fatty leptin receptor in transfected cells. *Endocrinology* 1996; **137:** 5178–5181.
7 Fei H, Okano HJ, Li C, Lee GH, Zhao C, Darnell R, Friedman JM. Anatomic localization of alternatively spliced leptin receptors (Ob-R) in mouse brain and other tissues. *Proc Natl Acad Sci USA* 1997; **94:** 7001–7005.
8 Shioda S, Funahashi H, Nakajo S, Yada T, Maruta O, Nakai Y. Immunohistochemical localization of leptin receptor in the rat brain. *Neurosci Lett* 1998; **243:** 41–44.
9 Hakansson ML, Brown H, Ghilardi N, Skoda RC, Meister B. Leptin receptor immunoreactivity in chemically defined target neurons of the hypothalamus. *J Neurosci* 1998; **18:** 559–572.
10 Baskin DG, Schwartz MW, Seeley RJ, Woods SC, Porte D Jr, Breininger JF, Jonak Z, Schaefer J, Krouse M, Burghardt C, Campfield LA, Burn P, Kochan JP. Leptin receptor long-form splice-variant protein expression in neuron cell bodies of the brain and co-localization with neuropeptide Y mRNA in the arcuate nucleus. *J Histochem Cytochem* 1999; **47:** 353–362.
11 Stromberg H, Svensson SP, Hermanson O. Distribution of the transcription factor signal transducer and activator of transcription 3 in the rat central nervous system and dorsal root ganglia. *Brain Res* 2000; **853:** 105–114.
12 Hakansson ML, Meister B. Transcription factor STAT3 in leptin target neurons of the rat hypothalamus. *Neuroendocrinology* 1998; **68:** 420–427.
13 McCowen KC, Chow JC, Smith RJ. Leptin signaling in the hypothalamus of normal rats in vivo. *Endocrinology* 1998; **139:** 4442–4447.
14 Hosoi T, Kawagishi T, Okuma Y, Tanaka J, Nomura Y. Brain stem is a direct target for leptin's action in the central nervous system. *Endocrinology* 2002; **143:** 3498–3504.
15 Hubschle T, Thom E, Watson A, Roth J, Klaus S, Meyerhof W. Leptin-induced nuclear translocation of STAT3 immunoreactivity in hypothalamic nuclei involved in body weight regulation. *J Neurosci* 2001; **21:** 2413–2424.
16 Mercer JG, Hoggard N, Williams LM, Lawrence CB, Hannah LT, Trayhurn P. Localization of leptin receptor mRNA and the long form splice variant (Ob-Rb) in mouse hypothalamus and adjacent brain regions by in situ hybridization. *FEBS Lett* 1996; **387:** 113–116.
17 Cheung CC, Clifton DK, Steiner RA. Proopiomelanocortin neurons are direct targets for leptin in the hypothalamus. *Endocrinology* 1997; **138:** 4489–4492.
18 Ovesjo ML, Gamstedt M, Collin M, Meister B. GABAergic nature of hypothalamic leptin target neurones in the ventromedial arcuate nucleus. *J Neuroendocrinol* 2001; **13:** 505–516.
19 Dieguez C, Carro E, Seoane LM, Garcia M, Camina JP, Senaris R, Popovic V, Casanueva FF. Regulation of somatotroph cell function by the adipose tissue. *Int J Obes Relat Metab Disord* 2000; **24:** S100–S103.
20 Watanobe H, Habu S. Leptin regulates growth hormone-releasing factor, somatostatin, and alpha-melanocyte-stimulating hormone but not neuropeptide Y release in rat hypothalamus in vivo: relation with growth hormone secretion. *J Neurosci* 2002; **22:** 6265–6271.
21 Nillni EA, Vaslet C, Harris M, Hollenberg A, Bjorbak C, Flier JS. Leptin regulates prothyrotropin-releasing hormone biosynthesis. Evidence for direct and indirect pathways. *J Biol Chem* 2000; **275:** 36124–36133.
22 Seoane LM, Carro E, Tovar S, Casanueva FF, Dieguez C. Regulation of in vivo TSH secretion by leptin. *Regul Pept* 2000; **92:** 25–29.
23 Ahmad I, Finkelstein JA, Downs TR, Frohman LA. Obesity-associated decrease in growth hormone-releasing hormone gene expression: a mechanism for reduced growth hormone mRNA levels in genetically obese Zucker rats. *Neuroendocrinology* 1993; **58:** 332–337.
24 Takanashi R, Sugawara O, Mernyei M. [Decreased growth hormone secreting cells of the hypophysis in senile cachexia]. *Rinsho Byori* 2001; **49:** 61–65.
25 Bell GI, Reisine T. Molecular biology of somatostatin receptors. *Trends Neurosci* 1993; **16:** 34–38.
26 Hoyer D, Bell GI, Berelowitz M, Epelbaum J, Feniuk W, Humphrey PP, O'Carroll AM, Patel YC, Schonbrunn A, Taylor JE, Reisine T. Classification and nomenclature of somatostatin receptors. *Trends Pharmacol Sci* 1995; **16:** 86–88.
27 Schulz S, Handel M, Schreff M, Schmidt H, Hollt V. Localization of five somatostatin receptors in the rat central nervous system using subtype-specific antibodies. *J Physiol Paris* 2000; **94:** 259–264.
28 Hervieu G, Emson PC. The localization of somatostatin receptor 1 (sst1) immunoreactivity in the rat brain using an N-terminal specific antibody. *Neuroscience* 1998; **85:** 1263–1284.
29 Helboe L, Stidsen CE, Moller M. Immunohistochemical and cytochemical localization of the somatostatin receptor subtype sst1 in the somatostatinergic parvocellular neuronal system of the rat hypothalamus. *J Neurosci* 1998; **18:** 4938–4945.
30 Schindler M, Humphrey PP, Lohrke S, Friauf E. Immunohistochemical localization of the somatostatin sst2(b) receptor splice variant in the rat central nervous system. *Neuroscience* 1999; **90:** 859–874.
31 Schulz S, Schmidt H, Handel M, Schreff M, Hollt V. Differential distribution of alternatively spliced somatostatin receptor 2 isoforms (sst2A and sst2B) in rat spinal cord. *Neurosci Lett* 1998; **257:** 37–40.
32 Stroh T, Kreienkamp HJ, Beaudet A. Immunohistochemical distribution of the somatostatin receptor subtype 5 in the adult rat brain: predominant expression in the basal forebrain. *J Comp Neurol* 1999; **412:** 69–82.
33 Raulf F, Perez J, Hoyer D, Bruns C. Differential expression of five somatostatin receptor subtypes, SSTR1–5, in the CNS and peripheral tissue. *Digestion* 1994; **55:** 46–53.
34 Bolanowski M, Milewicz A, Bidzinska B, Jedrzejuk D, Daroszewski J, Mikulski E. Serum leptin levels in acromegaly – a significant role for adipose tissue and fasting insulin/glucose ratio. *Med Sci Monit* 2002; **8:** CR685–CR689.

35 Tan KC, Tso AW, Lam KS. Effect of Sandostatin LAR on serum leptin levels in patients with acromegaly. *Clin Endocrinol (Oxford)* 2001; **54:** 31–35.
36 Iqbal J, Pompolo S, Murakami T, Clarke IJ. Localization of long-form leptin receptor in the somatostatin-containing neurons in the sheep hypothalamus. *Brain Res* 2000; **887:** 1–6.
37 Handel M, Schulz S, Stanarius A, Schreff M, Erdtmann-Vourliotis M, Schmidt H, Wolf G, Hollt V. Selective targeting of somatostatin receptor 3 to neuronal cilia. *Neuroscience* 1999; **89:** 909–926.
38 Schreff M, Schulz S, Handel M, Keilhoff G, Braun H, Pereira G, Klutzny M, Schmidt H, Wolf G, Hollt V. Distribution, targeting, and internalization of the sst4 somatostatin receptor in rat brain. *J Neurosci* 2000; **20:** 3785–3797.
39 Paxinos G, Watson C. *The Rat Brain in Stereotaxic Coordinates.* San Diego, CA: Academic Press, 1986.
40 Pazour GJ, Witman GB. The vertebrate primary cilium is a sensory organelle. *Curr Opin Cell Biol* 2003; **15:** 105–110.
41 Vrang N, Larsen PJ, Clausen JT, Kristensen P. Neurochemical characterization of hypothalamic cocaine- amphetamine- regulated transcript neurons. *J Neurosci* 1999; **19:** RC5.
42 Stryjewski G, Dalton HJ. Circulating leptin: mediator or marker of the neuroendocrinological stress response? *Crit Care Med* 2001; **29:** 2397–2398.
43 Heiman ML, Ahima RS, Craft LS, Schoner B, Stephens TW, Flier JS. Leptin inhibition of the hypothalamic-pituitary-adrenal axis in response to stress. *Endocrinology* 1997; **138:** 3859–3863.
44 Gillies G. Somatostatin: the neuroendocrine story. *Trends Pharmacol Sci* 1997; **18:** 87–95.
45 Arancibia S, Rage F, Grauges P, Gomez F, Tapia-Arancibia L, Armario A. Rapid modifications of somatostatin neuron activity in the periventricular nucleus after acute stress. *Exp Brain Res* 2000; **134:** 261–267.
46 Pacak K, Palkovits M. Stressor specificity of central neuroendocrine responses: implications for stress-related disorders. *Endocr Rev* 2001; **22:** 502–548.
47 Quintela M, Senaris R, Heiman ML, Casanueva FF, Dieguez C. Leptin inhibits in vitro hypothalamic somatostatin secretion and somatostatin mRNA levels. *Endocrinology* 1997; **138:** 5641–5644.
48 Cocchi D, De Gennaro Colonna V, Bagnasco M, Bonacci D, Muller EE. Leptin regulates GH secretion in the rat by acting on GHRH and somatostatinergic functions. *J Endocrinol* 1999; **162:** 95–99.
49 Tannenbaum GS, Zhang WH, Lapointe M, Zeitler P, Beaudet A. Growth hormone-releasing hormone neurons in the arcuate nucleus express both Sst1 and Sst2 somatostatin receptor genes. *Endocrinology* 1998; **139:** 1450–1453.
50 Lanneau C, Bluet-Pajot MT, Zizzari P, Csaba Z, Dournaud P, Helboe L, Hoyer D, Pellegrini E, Tannenbaum GS, Epelbaum J, Gardette R. Involvement of the Sst1 somatostatin receptor subtype in the intrahypothalamic neuronal network regulating growth hormone secretion: an in vitro and in vivo antisense study. *Endocrinology* 2000; **141:** 967–979.
51 Elmquist JK, Bjorbaek C, Ahima RS, Flier JS, Saper CB. Distributions of leptin receptor mRNA isoforms in the rat brain. *J Comp Neurol* 1998; **395:** 535–547.
52 Schwartz MW, Seeley RJ, Campfield LA, Burn P, Baskin DG. Identification of targets of leptin action in rat hypothalamus. *J Clin Invest* 1996; **98:** 1101–1106.
53 Baskin DG, Breininger JF, Schwartz MW. Leptin receptor mRNA identifies a subpopulation of neuropeptide Y neurons activated by fasting in rat hypothalamus. *Diabetes* 1999; **48:** 828–833.
54 Sahu A. Evidence suggesting that galanin (GAL), melanin-concentrating hormone (MCH), neurotensin (NT), proopiomelanocortin (POMC) and neuropeptide Y (NPY) are targets of leptin signaling in the hypothalamus. *Endocrinology* 1998; **139:** 795–798.
55 Kristensen P, Judge ME, Thim L, Ribel U, Christjansen KN, Wulff BS, Clausen JT, Jensen PB, Madsen OD, Vrang N, Larsen PJ, Hastrup S. Hypothalamic CART is a new anorectic peptide regulated by leptin. *Nature* 1998; **393:** 72–76.
56 Ahima RS, Hileman SM. Postnatal regulation of hypothalamic neuropeptide expression by leptin: implications for energy balance and body weight regulation. *Regul Pept* 2000; **92:** 1–7.
57 Feifel D, Vaccarino FJ. Central somatostatin. a re-examination of its effects on feeding. *Brain Res* 1990; **535:** 189–194.
58 Scalera G, Tarozzi G. Somatostatin administration modifies food intake, body weight, and gut motility in rat. *Peptides* 1998; **19:** 991–997.
59 Stoving RK, Andersen M, Flyvbjerg A, Frystyk J, Hangaard J, Vinten J, Koldkjaer OG, Hagen C. Indirect evidence for decreased hypothalamic somatostatinergic tone in anorexia nervosa. *Clin Endocrinol (Oxford)* 2002; **56:** 391–396.
60 Pincelli AI, Rigamonti AE, Scacchi M, Cella SG, Cappa M, Cavagnini F, Muller EE. Somatostatin infusion withdrawal. studies in the acute and recovery phase of anorexia nervosa, and in obesity. *Eur J Endocrinol* 2003; **148:** 237–243.

5.7.

5.7. HÜBSCHLE, T., HARRÉ, E.-M., MEYERHOF, W., PEHL, U., ROTH, J. & GERSTBERGER, R. (2001c)

The central pyrogenic action of interleukin-6 is related to nuclear translocation of STAT3 in the anteroventral preoptic area of the rat brain.

J. Therm. Biol. **26** (4-5): 299-305.

Eigener Anteil an der Publikation:

- Beteiligung an der Versuchsplanung (90 %)
- Durchführung der Versuche (90 %)
- Beteiligung an der Zusammenfassung und Veröffentlichung der Ergebnisse (90 %)

PERGAMON

Journal of Thermal Biology 26 (2001) 299–305

Journal of
THERMAL BIOLOGY

www.elsevier.com/locate/jtherbio

The central pyrogenic action of interleukin-6 is related to nuclear translocation of STAT3 in the anteroventral preoptic area of the rat brain

Thomas Hübschle*, Eva-Maria Harré, Wolfgang Meyerhof, Ulrich Pehl, Joachim Roth, Rüdiger Gerstberger

Institute of Veterinary Physiology, Justus-Liebig-University, Frankfurter Strasse 100, D-35392 Giessen, Germany

Abstract

(1) In animals treated with i.c.v. pyrogen free saline constitutive STAT3-expression was low and predominantly detected within the cytoplasm of large cells in the medio-caudal hypothalamus. (2) Wistar rats treated with i.c.v. IL-6 (100–200 ng) developed a clear febrile response 90–120 min post treatment and showed a strong STAT3-upregulation and -translocation into cell nuclei at various fore- and hindbrain sites that was already observed 15–30 min after the treatment. (3) The most intense IL-6-induced STAT3-activation pattern was found within the vascular organ of the lamina terminalis and the adjacent ventromedial preoptic area. (4) STAT3-immunohistochemistry therefore represents a novel tool to functionally map IL-6 actions on the brain. The results further support the importance of the anteroventral preoptic area as main central IL-6 target involved in the mediation of fever responses.

Keywords: Fever; Ventromedial preoptic area (VMPO); Vascular organ of the lamina terminalis (OVLT); Cytokines; Signal transducer and activator of transcription (STAT3); Immunohistochemistry

1. Introduction

Central administration of the cytokine and endogenous pyrogen interleukin-6 (IL-6) elicits a variety of (patho-)physiological functions, such as reduction of food intake and locomotor activity, activation of the hypothalamo-pituitary-adrenocortical axis and the mediation of fever response (LeMay et al., 1990; Chai et al., 1996; Plata-Salaman, 1996; Lenczowski et al., 1999). The effects of IL-6 and related cytokines are mediated via the GP130 receptor family. Stimulation of these receptors activate a cytokine-specific signal transduction pathway, the so-called Janus kinase–signal transducer and activator of transcription (Jak-STAT) signalling cascade. IL-6 is known to act through the STAT3-isoform which gets phosphorylated, dimerizes and then translocates into the nucleus, where it regulates gene expression by binding to specific gene promoters, amongst others the promoter of the immediate early gene c-fos (Akira, 1997; Vallieres et al., 1997; Vallieres and Rivest, 1997; Takeda and Akira, 2000). This conversion of an IL-6 stimulus into a long-term genetic action and its exact neuroanatomical location was studied previously in rats, combining systemic and central IL-6 treatment with FOS-immunohistochemistry (Callahan and Piekut, 1997; Niimi et al., 1997) or FOS in situ hybridisation technique (Vallieres et al., 1997). Assessing functionally active central IL-6 target structures, a specific FOS-activation pattern was found within the forebrain. The list of activated brain structures included the hypothalamic paraventricular (PVN) and supraoptic nucleus (SON), the vascular organ of the lamina terminalis

*Corresponding author. Tel.: +49-641-9938155; fax: +49-641-9938159.

E-mail address: thomas.huebschle@vetmed.uni-giessen.de (T. Hübschle).

0306-4565/01/$ - see front matter
PII: S0306-4565(01)00034-1

(OVLT), the subfornical organ, the median eminence and the medial preoptic area (MPO). Non-neuronal cells such as ependymocytes of the lateral and the third ventricles and meningeal cells also showed an intense FOS-activation. Interestingly, systemic treatment with the endotoxin lipopolysaccharide (LPS)—a commonly used experimental fever model—induced a similar pattern of hypothalamic FOS-activation, however, with a more pronounced FOS-response in the ventromedial preoptic area (VMPO) (Sagar et al., 1995; Elmquist et al., 1996).

While FOS-immunohistochemistry has been proven to be a powerful neuroanatomical tool to investigate fever mechanisms regulated via the brain, it has to be noted that inhibitory actions on neurons, such as those induced by endogenous or exogenous pyrogens, might not be associated with FOS-expression (Kovacs and Sawchenko, 1993; Elmquist et al., 1997). Moreover, FOS-analysis in such fever experiments is likely to additionally label indirectly or integratively activated cells. We therefore hypothesised that the combination of central IL-6 treatment with the subsequent immunohistochemical detection of STAT3 should be a helpful method to assess direct IL-6 actions on the brain, irrespective of IL-6-induced neuronal excitation or inhibition. This functional neuroanatomical mapping procedure has been previously used in order to characterise centrally mediated effects of the cytokine leptin (Hübschle et al., 2001). This study describes a novel neuroanatomical tool to map central pyrogenic IL-6 actions on the brain.

2. Materials and methods

2.1. Intracerebroventricular (i.c.v.) cannulation of the lateral ventricle

Male Wistar rats (*Rattus spec.*) with body weights (BW) of 170–230 g were housed individually. Experiments were performed in accordance with the local Ethics Committee (ethics approval number 48-3560-1/2). Lights were on from 06.00 am to 06.00 pm and room temperature (RT) was adjusted to $22 \pm 1^{\circ}C$. Animals had constant access to water and were fed with standard lab chow available *ad libitum*. Animals were anaesthetised with intraperitoneal injections of a ketamine/xylazine solution (100 mg/kg BW Ketamin Gräub, Albrecht, Aulendorf, Germany; 10 mg/kg BW xylazine, Rompun® (2%), Bayer Vital, Leverkusen, Germany). A modified 23 G cannula (Braun, Melsungen, Germany) was stereotaxically inserted (David Kopf, Tujunga, CA, USA) into the left lateral ventricle of the brain. With a general +0.5 mm tooth bar adjustment the coordinates used from Bregma point were 0.4 mm posterior, 1.5 mm lateral and 4 mm ventral (brain surface). After surgery the remaining opening of the cannula was sealed with a plastic blocker and during the recovery periods the probe was checked daily to ensure that it remained sealed. This check was combined with the daily BW measurements. Accuracy of the cannula placement was tested by evaluation of cumulative (60 min) water intake due to i.c.v. bolus application of angiotensin II (50 ng, Bachem Biochemica GmbH, Heidelberg, Germany) dissolved in 5 µl of 0.9% pyrogen free saline (Sigma, Deisenhofen, Germany). Only those animals which showed an adequate drinking response (8–14 ml) were used for further studies. These drink tests were conducted 7–8 days after surgery and 3–4 days prior to central IL-6 stimulation.

2.2. I.c.v. interleukin-6 stimulation

In vivo IL-6 stimulation was performed in conscious animals with a 25 µl Hamilton syringe attached to the i.c.v. cannula via PP30 tubing. The central treatments consisted of an i.c.v. bolus injection of 100–200 ng species homologous rat IL-6 (Dr. Stephen Poole, National Institute for Biological Standard and Control, NIBSC, Potters Bar, U.K.) diluted in 5 µl of pyrogen free saline. Control experiments for both body temperature measurement and histology were carried out with i.c.v. injections of 5 µl of pyrogen free saline (= vehicle).

2.3. Measurement of i.c.v. IL-6-induced fever responses

In order to demonstrate the central pyrogenic action of IL-6, abdominal temperature was measured in three experimental groups, with two groups receiving IL-6 treatment with 100 ($n = 6$) or 200 ng ($n = 7$) and one group serving as control animals ($n = 7$). Body temperature was monitored by use of battery operated biotelemetry transmitters (VM-FH-discs, Mini-Mitter Co., Sunriver, Oregan USA) implanted into the peritoneum directly after the i.c.v. cannulation surgery. A Dataquest IV data acquisition system (Data Sciences Inc., St. Paul, MN, USA) was used for automatic data collection and analysis. Results are expressed as means ± SEM at 15 min time intervals.

2.4. Immunohistochemical STAT3-detection and co-localization with the nuclear DAPI stain

In a further group of animals, histological experiments were performed. Rats (pyrogen free saline-treated $n = 14$, IL-6-treated $n = 17$) were deeply anaesthetised with sodium pentobarbital (60 mg/kg BW, Narcoren, Merial GmbH, Hallbergmoos, Germany) and transcardially perfused with 4% paraformaldehyde in 0.1 M

phosphate buffer (pH 7.2) 15–90 min after central application. The brains were removed and post fixed in the same fixative for 1 h at RT and then the tissue was cryoprotected in 20% sucrose in phosphate buffer overnight at 4°C. Tissue was cut the following day.

Previous studies investigating STAT3-distribution in the rat central nervous system have shown that amplification procedures are a helpful tool to investigate STAT3-immunoreactivity (Strömberg et al., 2000; Hübschle et al., 2001). Therefore, to detect STAT3-signals in brain sections a commercial tyramide amplification kit (NEL700, NEN Life Science Products GmbH, Köln, Germany), based on the catalyzed reporter deposition method, was used. The specificity of the STAT3-antibody (rabbit anti-STAT3-antibody, sc-482, Santa Cruz Biotechnology, Heidelberg, Germany) has clearly been proven (Strömberg et al., 2000). Immunohistochemical pre-absorption control experiments were performed with the control STAT3-peptide (sc-482 P, Santa Cruz Biotechnology, Heidelberg, Germany).

Coronal 20–40 μm brain sections were cut on a freezing microtome (model 1205, Jung, Heidelberg, Germany) or on a cryostat (model HM 500, Microm, Walldorf, Germany). Tyramide amplification staining was performed according to the kit description in a phosphate buffer system (pH 7.2). In detail, sections were placed into 10% fetal calf serum containing 0.3% Triton X-100 for 1 h at RT. Primary STAT3-antibody (1 : 6000–1 : 12000) incubation was performed for 24–48 h at 4°C. The STAT3-antibody was detected with a secondary biotinylated anti-rabbit antibody (1 : 200, Vector BA-1000, Linaris Biologische Produkte, Wertheim-Bettingen, Germany) for 1 h at RT. After amplification the immunohistochemical processing was finished with an avidin biotin horseradish peroxidase complex (Vector Elite Kit, Linaris Biologische Produkte, Wertheim-Bettingen, Germany) which was visualised by either diaminobenzidine hydrochloride (Sigma, Deisenhofen, Germany) reaction in the presence of hydrogen peroxide, or with fluorescein-(FITC-) conjugated avidin D (Vector, Linaris Biologische Produkte, Wertheim-Bettingen, Germany). Finally, sections for the light microscopical analysis were counterstained with cresyl violet and sections stained with fluorescent STAT3-detection were further processed in co-localisation experiments with the nuclear 4′,6-diamidino-2-phenylindole dilactate (DAPI, Molecular Probes Europe BV, Leiden, Netherlands) stain. DAPI staining was achieved by a 1 : 400 DAPI incubation in phosphate buffer for 5 min at RT.

2.5. Microscopical analysis

Sections were cover slipped and analysed using a conventional Zeiss Axioplan light microscope and a Zeiss confocal microscope. Digital images (light microscopy) were taken with a Sony 3-CCD camera using the Zeiss KS 100 software package, digital confocal images (fluorescent microscopy) were taken with an invert Zeiss Laser Scanning Microscope (LSM 410, Zeiss, Jena, Germany). Image editing software (Adobe Photoshop) was used to change the graphic mode from RGB to CYMK, to adjust brightness and contrast and to combine the individual images into figure plates.

3. Results

3.1. IL-6-treatment induces a rise in body temperature

In order to confirm the central pyrogenic action of IL-6 in Wistar rats, i.c.v. IL-6-treatment was performed using similar doses that have previously been reported to induce fever in Sprague-Dawley rats via central mechanisms (Lenczowski et al., 1999). While i.c.v. injection of pyrogen free saline alone resulted in a stress-induced rise of abdominal temperature which lasted for about 1 h, IL-6-treated rats initially showed a similar stress peak that was promptly followed by a further febrile increase in core temperature (Fig. 1). Within 6 h after central stimulation, IL-6 elicited a febrile response characterised by an increase of body temperature from about 37°C to 38.4°C (100 ng/rat dose) and to 39.2°C (200 ng/rat dose), respectively.

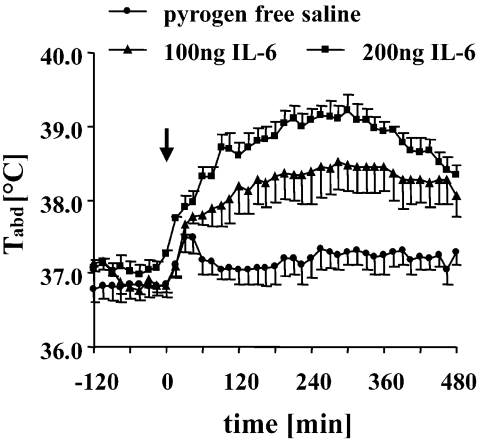

Fig. 1. Effect of intracerebroventricular (i.c.v.) administration of IL-6 on body temperature of Wistar rats. Abdominal body temperature (T_{abd}) was continuously measured before and after i.c.v. treatment with rat-homologous IL-6 (100 ng/rat, $n = 6$ and 200 ng/rat, $n = 7$) or pyrogen free saline ($n = 7$) which was used as vehicle. The time point of i.c.v. bolus injection is indicated by the black arrow. Data are presented as means ± SEM.

3.2. IL-6-treatment induces a time-dependent nuclear translocation of STAT3-immunoreactivity within the brain

In order to investigate the constitutive as well as the IL-6-induced hypothalamic STAT3-expression at the cellular level, STAT3-immunohistochemistry was combined with central IL-6-stimulation. Basal STAT3-expression, as evaluated in the pyrogen free saline treated controls, was at all time points very low and found to be highest in the cytoplasm of large cells of the medio-caudal hypothalamus. Within the rostral hypothalamus and the MPO constitutive STAT3-expression was not even distinguishable from background labelling and therefore only the staining pattern of the cresyl violet counterstaining became visible (Figs. 2A and D). In contrast, i.c.v. bolus application of 200 ng IL-6 induced an intense increase of STAT3-immunoreactivity in various brain areas 30 min after the treatment (Table 1) with strong signals detected in lateral parts of the OVLT, the adjacent VMPO and the SON (Figs. 2B, C and E). In addition, ependymal cells lining the third and lateral ventricles as well as cells of the ventral hypothalamic meninges showed the most intense IL-6-induced increase in STAT3-immunoreactivity (Figs. 2B and E and Table 1). STAT3-antibody specificity was checked via pre-absorption experiments with the control STAT3-peptide. Using sections of an IL-6-treated animal, the over night pre-incubation of the STAT3-antibody with the control peptide led to a markedly reduced STAT3-immunoreactivity as shown in Fig. 2F for the SON, which resembled the STAT3-staining detected within the control situation (Fig. 2D).

The size of the STAT3-stained, round-shaped structures in these hypothalamic areas of IL-6-treated animals indicated a predominant labelling of neuronal cell nuclei (Figs. 2B, C and E). This finding was further analysed by confocal microscopy using the nuclear DAPI stain as a subcellular distribution marker of cell nuclei. Again, 30 min after i.c.v. bolus application of IL-6, similar STAT3-signals were found with fluorescent detection (green signal) in the lateral OVLT and the VMPO (Fig. 3A). Staining of the same section with DAPI revealed all cell nuclei in this brain area, as seen by the blue signal (Fig. 3B). The overlay of IL-6-induced STAT3-immunoreactivity and the DAPI stain is given in Fig. 3C. Indeed, intensively labelled, round-shaped STAT3-signals could be co-localised as DAPI-stained cell nuclei (light blue signal in Fig. 3C and inset).

By varying the post-treatment time from 15 to 90 min, a time dependency of this IL-6-induced nuclear translocation was found. While in the controls at all time points a weak and predominantly non-nuclear signal was observed, a shift of the STAT3-immunoreactivity into cell nuclei was already visible 15 min after the i.c.v. IL-6 application. This nuclear translocation became even

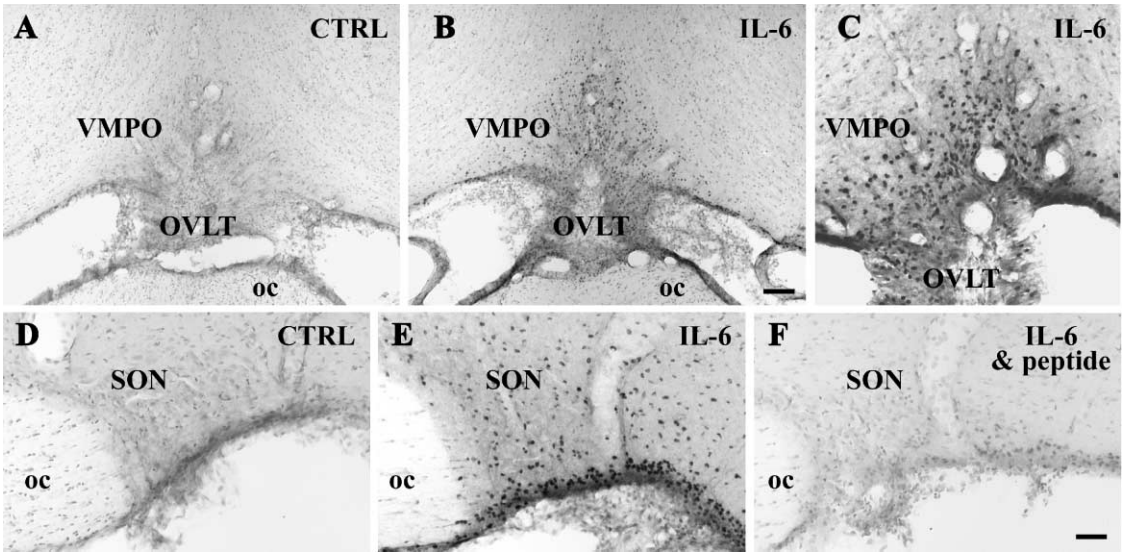

Fig. 2. Hypothalamic IL-6 targets as revealed by the detection of STAT3-immunoreactivity. Immunohistochemical photomicrographs of the vascular organ of the lamina terminalis (OVLT) and the adjacent ventromedial preoptic area (VMPO, A–C) as well as the supraoptic nucleus (SON, D–F) are shown under control conditions (CTRL, A,D, 30 min after pyrogen free saline i.c.v. application) and IL-6-stimulated conditions (IL-6, B,C,E,F, 30 min after 200 ng IL-6 application). Note the strong increase of STAT3-immunoreactivity in the IL-6-treated animals (B,C,E) in the OVLT, VMPO, SON and the nearby meninges as compared to the control situation (A,D). A pre-absorption experiment with the control STAT3-peptide is shown for an IL-6-treated animal (F, 30 min after 200 ng IL-6 i.c.v. application) within the SON. oc = optic chiasm. Bar in A and B represents 100 μm. Bar in C–F represents 50 μm.

Table 1
Relative values of IL-6-induced (30 min, i.c.v. 200 ng/rat) nuclear STAT3-densities in various brain structures as compared to basal nuclear STAT3-expression in the controls (CTRL)

Brain structures	CTRL	IL-6
Hypothalamus		
Anterior hypothalamic area	–	+ +
Arcuate nucleus	+	+
Dorsal hypothalamic area	+	+ +
Dorsomedial nucleus	–	+
Lateral hypothalamic area	–	+ +
Lateral preoptic area, ventral parts	–	+ +
Medial preoptic area	–	+ +
Ventromedial preoptic nucleus	–	+ + +
Median preoptic nucleus	–	+
Paraventricular nucleus	–	+
Periarcuate area	–	+ + +
Periventricular nucleus	–	+
Posterior hypothalamic area	–	+ +
Retrochiasmatic area	–	+ +
Subfornical organ	–	+
Suprachiasmatic nucleus	–	+
Supraoptic nucleus	–	+ + +
Vascular organ of the lamina terminalis	–	+ +
Ventromedial nucleus	–	+
Others		
Area postrema	–	–
Ependymal lining of all ventricles	+	+ + +
Inferior olive, medial parts	–	+ +
Lateral septum	–	+ +
Locus coeruleus	–	+ +
Meninges, in particular at ventral sites	–	+ + +
Nucleus of the solitary tract	–	+ + +
Periaqueductual gray, all parts	–	+
Periventricular		
lateral ventricles	–	+ + +
third ventricle	–	+ + +
aqueduct	–	+
fourth ventricle	–	+ +
Piriform cortex, layer I + II	–	+
Probe site	+ + +	+ + +
Raphe pallidus nucleus	–	+ + +
Thalamic nuclei	–	
medial and lateral habenular nucleus		+ +
mediodorsal thalamic nuclei		+ + +
Ventral tegmental area	–	+ + +
Ventromedial medulla	–	+ + +
Ventrolateral medulla	–	+ +

more pronounced at 30 min and this time point was therefore used for the histological documentation shown in Figs. 2 and 3. When using post-application periods longer than 30 min in IL-6-treated animals, the high intensity of the nuclear STAT3-signal present at 30 min slowly decreased, however, was still detectable after 90 min.

4. Discussion

The cytokine and endogenous pyrogen IL-6 is known to be involved in the coordination of the neural component of the acute phase reaction by inducing sickness behaviour, anorexia, activation of the hypothalamo-pituitary-adrenocortical axis and fever (LeMay et al., 1990; Plata-Salaman, 1996; Lenczowski et al., 1999). The importance of centrally acting IL-6 as a necessary component of the fever response downstream to both endogenous (interleukin-1 beta) and exogenous (LPS) pyrogens, has been demonstrated in an elegant study using IL-6-deficient knock-out mice (Chai et al., 1996). The IL-6 doses used in our study were based on previous i.c.v. application experiments made in Sprague-Dawley rats (Vallieres et al., 1997; Lenczowski et al., 1999). In the present study performed with Wistar rats, i.c.v. IL-6 caused a maximum febrile response at a dose of 200 ng/rat, thereby verifying the IL-6 doses used in the former studies.

Concerning critical brain locations mediating fever responses, lesion studies have revealed the MPO of the rostral hypothalamus including the circumventricular organ OVLT as a primary hypothalamic target. These findings later contributed to the hypothesis that central fever induction pathways involve the blood-brain-barrier lacking circumventricular organs as potential sites where circulating pyrogens interact with the brain via prostaglandin-dependent mechanisms (Blatteis, 1992; Scammell et al., 1996). The close proximity of rostral parts of the VMPO to the OVLT makes this area an attractive brain structure to initiate and mediate febrile responses. Indeed, recent neuroanatomical FOS-studies have pointed to the VMPO as the critical pyrogenic zone in the hypothalamus where fever responses are likely to be initiated (Sagar et al., 1995; Elmquist et al., 1996; Scammell et al., 1996; Niimi et al., 1997; Vallieres et al., 1997). In order to extend the aforementioned neuroanatomical FOS-studies we have employed STAT3-immunohistochemistry after central pyrogenic IL-6-treatment as a marker of IL-6-receptor activation that first of all reveals only direct IL-6 actions and secondly, in contrast to FOS-analysis, is capable to map both activated as well as inhibited neurons. According to the results of in situ hybridisation studies investigating the basal expression of IL-6-receptor mRNA in the rat brain, strong signals have been detected in neurons of the MPO, in particular its ventromedial part in close proximity to the third ventricle (Schöbitz et al., 1993). When assessing functionally active central IL-6-target structures via STAT3-immunohistochemistry, an IL-6-induced nuclear STAT3-translocation was observed 15–30 min after i.c.v. application in various brain regions, with particularly intense STAT3-signals detected in neurons of the anteroventral preoptic area. The overall nuclear STAT3-staining pattern in the MPO

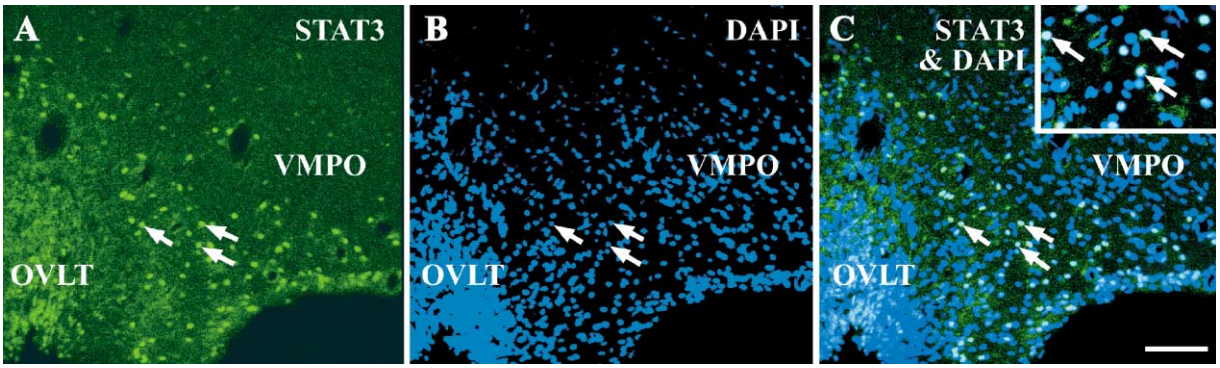

Fig. 3. IL-6 induces a nuclear translocation of STAT3-immunoreactivity in the ventromedial preoptic area (VMPO) and the lateral parts of the vascular organ of the lamina terminalis (OVLT). Immunofluorescence confocal photomicrographs of the OVLT and the adjacent VMPO are shown for an IL-6-stimulated animal (30 min after 200 ng IL-6 i.c.v. application). IL-6-induced STAT3-immunoreactivity in green (A) is compared with the blue nuclear DAPI stain (B). The overlay of these individual confocal images is shown in C. IL-6-treatment induces an intense nuclear STAT3-labelling within the VMPO, OVLT and nearby meninges as proven by the co-localisation with the nuclear DAPI stain (see arrows showing the light blue double labelled cell nuclei in C and its inset). Bar in A–C represents 100 μm.

was similar to that seen with FOS-analysis after systemic LPS treatment (Elmquist et al., 1996), however, the time necessary to induce nuclear translocation of the two transcription factors proved to be different. While nuclear STAT3-signals were already detected 15–30 min after central IL-6-treatment, the first peak of nuclear FOS-protein is known to occur at about 90 min after the stimulation. This suggests that STAT3 might act upstream of immediate early gene c-fos activation in VMPO neurons and—due to the similarity in the FOS- and STAT3-staining patterns—neuronal activation and not inhibition is likely to represent the predominant mode of action involved in the central mediation of fever responses through the VMPO. However, this hypothesis needs to be tested in direct co-localisation studies.

Concerning other thermoregulatory key structures in the hypothalamus, the PVN is one of the major integrative relay nuclei in efferent control of thermoregulatory functions with its autonomic dorsal parvocellular subnucleus receiving direct projections from the anteroventral preoptic area (Elmquist and Saper, 1996; Zhang et al., 2000). Interestingly treatment with endogenous (interleukin-1 beta) and exogenous (LPS) pyrogens induced a massive FOS-response within autonomic and endocrine components of the PVN (Sagar et al., 1995; Elmquist et al., 1996; Callahan and Piekut, 1997; Zhang et al., 2000). In contrast, neither systemic nor central IL-6-treatment led to significant FOS-activation in the PVN (Callahan and Piekut, 1997; Vallieres et al., 1997), strengthened by the present results with almost unchanged nuclear STAT3-signals in the rat PVN after i.c.v. IL-6-application. In line with these findings, basal expression of IL-6-receptor mRNA was not found in the PVN (Schöbitz et al., 1993). So, while the anteroventral preoptic area seems to be the major IL-6 target the PVN is not. However, the PVN should still be regarded as a major integrative and regulatory hypothalamic structure in which thermoregulatory signals—including those initiating and/or mediating IL-6-induced fever—are conveyed towards the autonomic nervous system (Zhang et al., 2000).

In summary, our experiments further support the importance of the anteroventral preoptic area as the pyrogenic zone within the hypothalamus with the cytokine IL-6 being one major mediator of febrile responses in this brain structure. The observed IL-6-induced nuclear STAT3-translocation supports a direct IL-6-action on functionally active IL-6-receptors in this area. The exact IL-6-induced genomic mode of action and its consequences for the febrile response are presently not understood.

Acknowledgements

W. Meyerhof is head of the Molecular Genetics Department, German Institute of Human Nutrition, Arthur-Scheunert-Allee 114-116, D-14558 Potsdam-Rehbrücke, Germany in which part of the work has been performed. The authors thank Dr. Stephen Poole for providing rat recombinant IL-6.

References

Akira, S., 1997. IL-6-regulated transcription factors. Int. J. Biochem. Cell Biol. 29, 1401–1418.

Blatteis, C.M., 1992. Role of the OVLT in the febrile response to circulating pyrogens. Prog. Brain Res. 91, 409–412.

Callahan, T.A., Piekut, D.T., 1997. Differential Fos expression induced by IL-1beta and IL-6 in rat hypothalamus and pituitary gland. J. Neuroimmunol. 73, 207–211.

Chai, Z., Gatti, S., Toniatti, C., Poli, V., Bartfai, T., 1996. Interleukin (IL)-6 gene expression in the central nervous system is necessary for fever response to lipopolysaccharide or IL-1 beta: a study on IL-6-deficient mice. J. Exp. Med. 183, 311–316.

Elmquist, J.K., Saper, C.B., 1996. Activation of neurons projecting to the paraventricular hypothalamic nucleus by intravenous lipopolysaccharide. J. Comp. Neurol. 374, 315–331.

Elmquist, J.K., Scammell, T.E., Jacobson, C.D., Saper, C.B., 1996. Distribution of Fos-like immunoreactivity in the rat brain following intravenous lipopolysaccharide administration. J. Comp. Neurol. 371, 85–103.

Elmquist, J.K., Scammell, T.E., Saper, C.B., 1997. Mechanisms of CNS response to systemic immune challenge: the febrile response. Trends Neurosci. 20, 565–570.

Hübschle, T., Thom, E., Watson, A., Roth, J., Klaus, S., Meyerhof, W., 2001. Leptin-induced translocation of STAT3-immunoreactivity in hypothalamic nuclei involved in body weight regulation. J. Neurosci. 21, 2413–2424.

Kovacs, K.J., Sawchenko, P.E., 1993. Mediation of osmoregulatory influences on neuroendocrine corticotropin-releasing factor expression by the ventral lamina terminalis. Proc. Natl. Acad. Sci. USA 90, 7681–7685.

LeMay, L.G., Vander, A.J., Kluger, M.J., 1990. Role of interleukin 6 in fever in rats. Am. J. Physiol. 258, R798–R803.

Lenczowski, M.J., Bluthe, R.M., Roth, J., Rees, G.S., Rushforth, D.A., van Dam, A.M., Tilders, F.J., Dantzer, R., Rothwell, N.J., Luheshi, G.N., 1999. Central administration of rat IL-6 induces HPA activation and fever but not sickness behaviour in rats. Am. J. Physiol. 276, R652–R658.

Niimi, M., Wada, Y., Sato, M., Takahara, J., Kawanishi, K., 1997. Effect of continuous intravenous injection of interleukin-6 and pretreatment with cyclooxygenase inhibitor on brain c-fos expression in the rat. Neuroendocrinol. 66, 47–53.

Plata-Salaman, C.R., 1996. Anorexia induced by activators of the signal transducer gp 130. Neuroreport 7, 841–844.

Sagar, S.M., Price, K.J., Kasting, N.W., Sharp, F.R., 1995. Anatomic patterns of Fos immunostaining in rat brain following systemic endotoxin administration. Brain Res. Bull. 36, 381–392.

Scammell, T.E., Elmquist, J.K., Griffin, J.D., Saper, C.B., 1996. Ventromedial preoptic prostaglandin E2 activates fever-producing autonomic pathways. J. Neurosci. 16, 6246–6254.

Schöbitz, B., de Kloet, E.R., Sutanto, W., Holsboer, F., 1993. Cellular localization of interleukin 6 recepter mRNA and interleukin 6 receptor mRNA in rat brain. Eur. J. Neurosci. 5, 1426–1435.

Strömberg, H., Svensson, S.P., Hermanson, O., 2000. Distribution of the transcription factor signal transducer and activator of transcription 3 in the rat central nervous system and dorsal root ganglia. Brain Res. 853, 105–114.

Takeda, K., Akira, S., 2000. STAT family of transcription factors in cytokine-mediated biological responses. Cytokine Growth Factor Rev. 11, 199–207.

Vallieres, L., Rivest, S., 1997. Regulation of the genes encoding interleukin-6, its receptor, and gp130 in the rat brain in response to the immune activator lipopolysaccharide and the proinflammatory cytokine interleukin-1 beta. J. Neurochem. 69, 1668–1683.

Vallieres, L., Lacroix, S., Rivest, S., 1997. Influence of interleukin-6 on neural activity and transcription of the gene encoding corticotrophin-releasing factor in the rat brain: an effect depending upon the route of administration. Eur. J. Neurosci. 9, 1461–1472.

Zhang, Y.H., Lu, J., Elmquist, J.K., Saper, C.B., 2000. Lipopolysaccharide activates specific populations of hypothalamic and brainstem neurons that project to the spinal cord. J. Neurosci. 20, 6578–6586.

5.8.

5.8. HARRÉ, E.-M., ROTH, J., PEHL, U., KUETH, M., GERSTBERGER, R. & HÜBSCHLE, T. (2002)

Selected Contribution: Role of IL-6 in LPS-induced nuclear STAT3 translocation in sensory circumventricular organs during fever in rats.

J. Appl. Physiol. **92**: 2657-2666.

Eigener Anteil an der Publikation:

- Beteiligung an der Versuchsplanung (75 %)
- Durchführung der Versuche (25 %)
- Beteiligung an der Zusammenfassung und Veröffentlichung der Ergebnisse (75 %)

J Appl Physiol 92: 2657–2666, 2002.
First published February 8, 2002; 10.1152/japplphysiol.00822.2001.

highlighted topics

Molecular Biology of Thermoregulation
Selected Contribution: Role of IL-6 in LPS-induced nuclear STAT3 translocation in sensory circumventricular organs during fever in rats

EVA-MARIA HARRÉ, JOACHIM ROTH, ULRICH PEHL, MATTHIAS KUETH, RÜDIGER GERSTBERGER, AND THOMAS HÜBSCHLE
Veterinary-Physiology, Justus-Liebig-University Giessen, D-35392 Giessen, Germany

Received 6 August 2001; accepted in final form 6 February 2002

Harré, Eva-Maria, Joachim Roth, Ulrich Pehl, Matthias Kueth, Rüdiger Gerstberger, and Thomas Hübschle. Selected Contribution: Role of IL-6 in LPS-induced nuclear STAT3 translocation in sensory circumventricular organs during fever in rats. *J Appl Physiol* 92: 2657–2666, 2002. First published February 8, 2002; 10.1152/japplphysiol.00822.2001.—Interleukin-6 (IL-6) is regarded as an endogenous mediator of lipopolysaccharide (LPS)-induced fever. IL-6 is thought to act on the brain at sites that lack a blood-brain barrier, the circumventricular organs (CVOs). Cells that are activated by IL-6 respond with nuclear translocation of the signal transducer and activator of transcription 3 molecule (STAT3) and can be detected by immunohistochemistry. We investigated whether the LPS-induced release of IL-6 into the systemic circulation was accompanied by a nuclear STAT3 translocation within the sensory CVOs. Treatment with LPS (100 μg/kg) led to a slight (1 h) and then a strong increase (2–8 h) in plasma IL-6 levels, which started to decline at the end of the febrile response. Administration of both pyrogens LPS and IL-6 (45 μg/kg) induced a febrile response with IL-6, causing a rather moderate fever compared with the LPS-induced fever. Nuclear STAT3 translocation in response to LPS was observed within the vascular organ of the lamina terminalis (OVLT) and the subfornical organ (SFO) 2 h after LPS treatment. To investigate whether this effect was mediated by IL-6, the cytokine itself was systemically applied and indeed an identical pattern of nuclear STAT3 translocation was observed. However, nuclear STAT3 translocation already occurred 1 h after IL-6 application and proved to be less effective compared with LPS treatment when analyzing OVLT and SFO cell numbers that showed nuclear STAT3 immunoreactivity after the respective pyrogen treatment. Our observations represent the first molecular evidence for an IL-6-induced STAT3-mediated genomic activation of OVLT and SFO cells and support the proposed role of these brain areas as sensory structures for humoral signals created by the activated immune system and resulting in the generation of fever.

cytokines; signal transducers and activators of transcription; vascular organ of the lamina terminalis; subfornical organ; area postrema

INFECTIOUS OR INFLAMMATORY stimulation in the periphery of the body results in the generation of a number of centrally mediated characteristic responses. These brain-mediated signs of illness include the generation of fever (17, 37), the activation of the hypothalamic-pituitary-adrenal axis (34), the loss of appetite, and a number of behavioral changes collectively termed sickness behavior (9). Under such infectious conditions, cytokines with a molecular mass of 15–20 kDa are endogenously produced by monocytes, macrophages, and numerous other cell types. Among them, the proinflammatory cytokines interleukin-1β (IL-1β), interleukin-6 (IL-6), and tumor necrosis factor-α (TNF-α) are regarded as key players in the modification of the brain-controlled functions mentioned above. With regard to the febrile response, these cytokines are called endogenous pyrogens (10, 17). Increased release of these cytokines into the general circulation can be experimentally achieved by systemic injections of lipopolysaccharide (LPS) derived from the outer membrane of gram-negative bacteria. Initially, it was thought that the large hydrophilic cytokine proteins could not pass the relatively impermeable blood-brain barrier (BBB) to influence brain structures. However, there are some small brain areas that lack a tight BBB, including the so-called sensory circumventricular or-

Address for reprint requests and other correspondence: T. Hübschle, Veterinary-Physiology, Justus-Liebig-Universität Giessen, Frankfurter Strasse 100, D-35392 Giessen, Germany (E-mail: thomas.huebschle@vetmed.uni-giessen.de).

The costs of publication of this article were defrayed in part by the payment of page charges. The article must therefore be hereby marked "*advertisement*" in accordance with 18 U.S.C. Section 1734 solely to indicate this fact.

gans (CVOs), such as the vascular organ of the lamina terminalis (OVLT), the subfornical organ (SFO), and the area postrema (AP).

First evidence for a role of these sensory CVOs as "windows to the brain" for inflammatory signal molecules is based on classical lesion studies. For example, it has been demonstrated in guinea pigs and sheep that electrolytic lesions of the anteroventral third ventricle area, which includes the OVLT, resulted in a suppression of fever (3, 4). In addition, an interruption of neuronal connections between the OVLT and the anterior hypothalamus, where the febrile resetting of body temperature is regulated, led to an attenuation of fever (12). More recently, it has been reported that electrolytic lesions of the SFO (32) or microinjection of the IL-1 receptor antagonist into the SFO (6) reduced febrile responses. Finally, removal of the AP abolished stimulatory cytokine effects on the hypothalamic-pituitary-adrenal axis activity (19).

Accepting that the sensory CVOs play a crucial role in mediating circulating pyrogenic messages necessary for fever induction in turn leads to two further prerequisites that should be fulfilled. First, a putative endogenous humoral mediator of LPS-induced fever should be measurable in the systemic circulation in close relation to the febrile response. Second, an activation of neurons or other cellular elements within the sensory CVOs needs to be demonstrated. TNF-α, IL-1β, and IL-6 are produced in response to LPS and can be detected in the general circulation with characteristic kinetics. Depending on the route of LPS administration and the injected LPS dose, TNF-α is the first cytokine that appears in the bloodstream (21, 23), followed by very small traces of IL-1β (16), which is frequently not detected at all (17). IL-6, however, is produced during the complete time course of LPS-induced fever, and the circulating levels of IL-6 show an excellent correlation with the febrile changes of body temperature (20, 23). Therefore, IL-6 seems to be an appropriate candidate to act as a humoral signal that may be sensed by the aforementioned CVOs. Measurement of electrical activity of OVLT neurons in brain slices provided first evidence that the firing rates are changed under TNF-α treatment (28). The effect of IL-6 on the electrical activity of neurons within the CVOs has not yet been investigated; however, IL-6 decreased the activity of warm-sensitive neurons in brain slices from the preoptic area (36), an area involved in the central control of temperature regulation.

The effects of IL-6 are mediated via the gp130 cytokine receptor family. Stimulation of these receptors activates a cytokine-specific signal transduction pathway, the so-called Janus kinase-signal transducer and activator of transcription (JAK-STAT) signaling cascade. IL-6 is known to act through the STAT3 isoform, which gets phosphorylated, dimerizes, and then translocates into the nucleus, where it regulates gene expression by binding to specific gene promoters (33). We recently reported (14, 15) that intracerebroventricular microinjections of IL-6 caused a very characteristic pattern of STAT3 translocation into cell nuclei of neurons located in brain areas involved in the generation of fever. Thus STAT3 immunohistochemistry seems to be an excellent tool to demonstrate genomic activation of cells induced by IL-6. If IL-6 is a critical circulating mediator for an inflammatory stimulation of sensory CVOs, it should be possible to demonstrate, during LPS-induced fever, not only the increase of circulating IL-6 but also the parallel IL-6-induced genomic activation of CVOs. Indeed, a recent study reported that treatment with LPS resulted in a nuclear STAT3 translocation in cells of the OVLT (18). In line with this study, our aim was to investigate *1*) the LPS-induced nuclear translocation of STAT3 not only in the OVLT but in all sensory CVOs and *2*) the time dependency of this process. To verify whether LPS-induced nuclear STAT3 translocation might truly reflect a biological activity of IL-6, we injected the cytokine itself and investigated the sensory CVOs with the use of STAT3 immunohistochemistry at distinct time intervals after systemic IL-6 treatment. The results of this study should enable us to state whether there is a role for circulating IL-6 in genomic activation of cells within the sensory CVOs during fever.

MATERIALS AND METHODS

Animals

The study was performed in 99 male Wistar rats (*Rattus spec.*) with body weights of 225 ± 5 g. Experiments were carried out in accordance with the local Ethics Committee (ethics approval numbers GI 20/1-1/96 and GI 18/2-42/00). Animals were housed individually with free access to drinking water and standard laboratory chow. The room temperature (RT) was adjusted to 23 ± 1°C, and lights were on from 7:00 AM to 7:00 PM. The animals were surgically prepared for telemetric body temperature measurement at least 1 wk before the fever experiments.

Substances

Animals were anesthetized with intraperitoneal injections of ketamine-xylazine solution [ketamine-hydrochloride: 100 mg/kg body wt Ketamin Gräub (Albrecht, Aulendorf, Germany); xylazine: 25 mg/kg body wt Rompun (Bayer Vital, Leverkusen, Germany)]. Bacterial LPS derived from *Escherichia coli* (serotype O111:B4, Sigma Chemical, Deisenhofen, Germany) was suspended in sterile pyrogen-free 0.9% saline. A dose of 100 μg/kg body wt was injected intraperitoneally. Controls were treated with the same volume of sterile pyrogen-free 0.9% saline (vehicle). Rat recombinant IL-6 (rrIL-6) was obtained from Dr. S. Poole (National Institute for Biological Standards and Control, Potters Bar, UK), stored at −70°C in stock aliquots of 10 μg in 50 μl of pyrogen-free 0.9% saline, and then injected intraperitoneally in a final volume of 500 μl of sterile 0.9% saline per rat, corresponding to a dose of ~45 μg/kg body wt.

Measurement of Body Temperature

Abdominal temperature was measured by use of biotelemetry transmitters (PDT-4000 E-Mitter, Mini-Mitter) implanted intraperitoneally under general anesthesia. Output (frequency in Hz) was monitored by a receiver placed under each cage (ER-4000 receiver, Mini-Mitter). A data acquisition system (Vital View, Mini-Mitter) was used for automatic

control of data collection and analysis. Body temperature was continuously monitored and recorded at 5-min intervals. For analysis and graphical documentation, temperature data at time intervals of 15 min were used.

Measurement of Bioactive IL-6

Determination of plasma IL-6 was performed by a bioassay based on the dose-dependent growth stimulation of IL-6 on the B9 hybridoma cell line (1). The assay was performed in sterile, 96-well microtiter plates. In each well, 5,000 B9 cells were incubated for 72 h with serial dilutions of biological samples or different concentrations of a human IL-6 standard (code 89/548, National Institute for Biological Standards and Control, South Mimms, UK). The number of living cells after 72 h was measured by use of the dimethylthiazol-diphenyl tetrazolium bromide (MTT) colorimetric assay (13). Plasma samples were prediluted to adjust them to the standard dilution curves. Considering the sample dilution within the assay, the detection limit of the assay was three international units (IU) of IL-6 per milliliter.

Experimental Protocols

LPS-induced circulating IL-6. At selected time points after intraperitoneal injection of 100 μg/kg body wt LPS or vehicle, rats (n = 3–5 per group) were killed for collection of blood via cardiac puncture. Blood samples were immediately centrifuged and stored at −70°C for later measurement of IL-6.

LPS-induced fever. Two groups of rats (n = 7 in each group) were injected intraperitoneally with either 100 μg/kg body wt LPS or an equivalent volume of vehicle. Body temperature was evaluated from 2 h before until 8 h after the time of injection.

IL-6-induced fever. Two groups of rats (n = 5 in each group) were injected intraperitoneally with either 10 μg of rrIL-6 dissolved in 500 μl of sterile 0.9% saline or the solvent alone. Body temperature was evaluated from 2 h before until 8 h after the time of injection.

LPS- or IL-6-induced nuclear STAT3 translocation. To investigate LPS- or IL-6-induced nuclear STAT3 translocation and its putative time dependency, rats were separated into five groups with different postinjection times. Animals of the first group (n = 4 with two IL-6-treated and two vehicle-treated rats) were perfused 30 min, animals of the second group (n = 14, with four LPS-, five IL-6-, and five vehicle-treated animals) were perfused 1 h, animals of the third group (n = 14, with five LPS-, four IL-6-, and five vehicle-treated animals) were perfused 2 h, animals of the fourth group (n = 6, with three LPS-treated and three vehicle-treated animals) were perfused 3 h, and animals of the fifth group (n = 4, with two LPS-treated and two vehicle-treated animals) were perfused 4 h after treatment with the respective substances. Transcardial perfusions with 4% paraformaldehyde in 0.1 M phosphate buffer (pH 7.2) were performed in animals that were deeply anesthetized with ketamine-xylazine. The brains were removed and postfixed in the same fixative for 1 h at RT. The tissue was cryoprotected in 20% sucrose in phosphate buffer overnight at 4°C. Tissue was cut the following day.

STAT3 Immunohistochemistry

To detect STAT3 signals in brain sections, a rabbit anti-STAT3 antibody (sc-482, Santa Cruz Biotechnology, Heidelberg, Germany) was used. The specificity of this STAT3 antibody has clearly been proven (30) and was also demonstrated in our own preabsorption control experiments (14). Previous studies investigating STAT3 distribution in the rat central nervous system have shown that amplification procedures are a helpful tool to investigate STAT3 immunoreactivity (15, 30). Therefore, a commercial tyramide amplification kit (NEL700, NEN Life Science Products, Köln, Germany), based on the catalyzed reporter deposition amplification method, was used.

Coronal 40-μm brain sections were cut on a freezing microtome (model 1205, Jung, Heidelberg, Germany). Tyramide amplification staining was performed according to the kit description in a phosphate buffer system (pH 7.2). In detail, sections were placed into 10% normal horse serum containing 0.3% Triton X-100 for 1 h at RT. Next, sections were transferred into 0.5% blocking powder to block the unspecific tyramine binding sites. Primary STAT3 antibody incubation (1:12,000) was performed for 24–48 h at 4°C. The STAT3 antibody was then detected with a secondary biotinylated anti-rabbit antibody (1:200, Vector BA-1000, Linaris Biologische Produkte, Wertheim-Bettingen, Germany) for 1 h at RT. After amplification, the immunohistochemical processing was finished with an avidin biotin horseradish peroxidase complex (Vector Elite Kit, Linaris Biologische Produkte), which was visualized by diaminobenzidine hydrochloride (Sigma Chemical) reaction in the presence of hydrogen peroxide. Finally, sections were counterstained with cresyl violet and coverslipped with Entellan (Merck, Darmstadt, Germany) for the light microscopic analysis.

Microscopic and Quantitative Histological Analysis

Sections were analyzed with the use of an Olympus BX50 light microscope (Olympus Optical, Hamburg, Germany). Digital images were taken with an Olympus Camedia C-3030 camera, for which we used the Olympus Camedia Master 2.0 software package. Image editing software (Adobe Photoshop) was used to adjust brightness and contrast, to change the graphic mode to CMYK, and to combine the individual images into the figure plates.

The numbers of STAT3-immunoreactive cell nuclei were quantitatively evaluated for the two CVOs (the OVLT and the SFO) 60 and 120 min after systemic treatment with the pyrogens (IL-6 or LPS) and compared with the vehicle control. For each animal, three rostral OVLT sections at similar stereotaxic coordinates and three SFO sections throughout the rostral-to-caudal SFO extension were selected. A microscopic counting grid (200 × 200 μm) was used at 400-fold magnification to determine the number of nuclei stained for STAT3 per three sections within the OVLT or the SFO of each animal investigated. Numbers of stained cell nuclei are represented as means ± SE per OVLT or SFO in four or five animals per group.

Statistics

All statistical calculations were carried out with the Sigmaplot/Sigmastat analysis software (Jandel Scientific, Corte Madera, CA) or Stat View (Abacus Concepts, Berkeley, CA). Mean levels of circulating IL-6 and mean abdominal temperatures of different animal groups are presented as means ± SE. IL-6 in plasma was compared between LPS- and vehicle-treated rats by one-way ANOVA followed by Scheffé's post hoc test. Abdominal temperatures of LPS-treated vs. vehicle-treated rats as well as IL-6-treated vs. vehicle-treated animals were compared by two-way repeated-measures ANOVA followed by an all pairwise Bonferroni's multiple comparison post hoc test. Statistical analysis for the quantitative histological evaluation was performed by one-way ANOVA with subsequent post hoc

analysis. Statistical significance was accepted for all post hoc procedures at $P < 0.05$.

RESULTS

Role of Circulating IL-6 in LPS-Induced Fever

Circulating levels of bioactive IL-6 at distinct time intervals after intraperitoneal injection of LPS or pyrogen-free saline (vehicle) are shown in Fig. 1*A*. Immediately after injection of LPS or vehicle, basal IL-6 levels reached ~20 IU/ml. However, in response to LPS injection, bioactive plasma IL-6 rose to 425 ± 130 IU/ml at 60 min, to 3,010 ± 1,250 IU/ml at 120 min, to 5,360 ± 3,070 IU/ml at 180 min, and to 6,275 ± 2,240 IU/ml at 240 min, respectively. By 480 min postinjection, plasma IL-6 had already decreased to 1,030 ± 565 IU/ml. Injection of saline did not induce changes in basal plasma levels of IL-6, which remained at 21 ± 15 IU/ml. At 120 and 240 min postinjection, IL-6 in plasma of LPS-treated rats was significantly higher than in animals injected with sterile saline ($P < 0.05$).

Changes in body temperature in response to LPS or vehicle are shown in Fig. 1*B*. The injection procedure itself caused a transient stress-induced increase in abdominal temperature of ~0.8°C in both groups. Thereafter, LPS-treated rats developed a robust biphasic fever, with the first peak reaching levels of 38.0°C at 180 min posttreatment and the second peak reaching ~38.8°C at 300–345 min posttreatment. In contrast, body temperature of control animals returned to the preinjection values of ~37.0°C. From 135 to 480 min after the time of injection, body temperature of LPS-treated rats was significantly elevated compared with animals injected with sterile saline ($P < 0.05$).

Figure 1*C* shows the thermal responses of two groups of rats injected with rrIL-6 or vehicle. Again, in both groups, a transient stress-induced rise of abdominal temperature occurred. In saline-treated rats, body temperature returned to the baseline value, whereas treatment with IL-6 caused a rather moderate elevation in body temperature (~37.8°C, lasting 3–4 h), which was less pronounced than that of the febrile response induced by LPS. From 120 to 270 min and again at 300 min after the time of injection, body temperature of IL-6-injected rats was significantly higher than the corresponding value of control rats injected with sterile saline ($P < 0.05$).

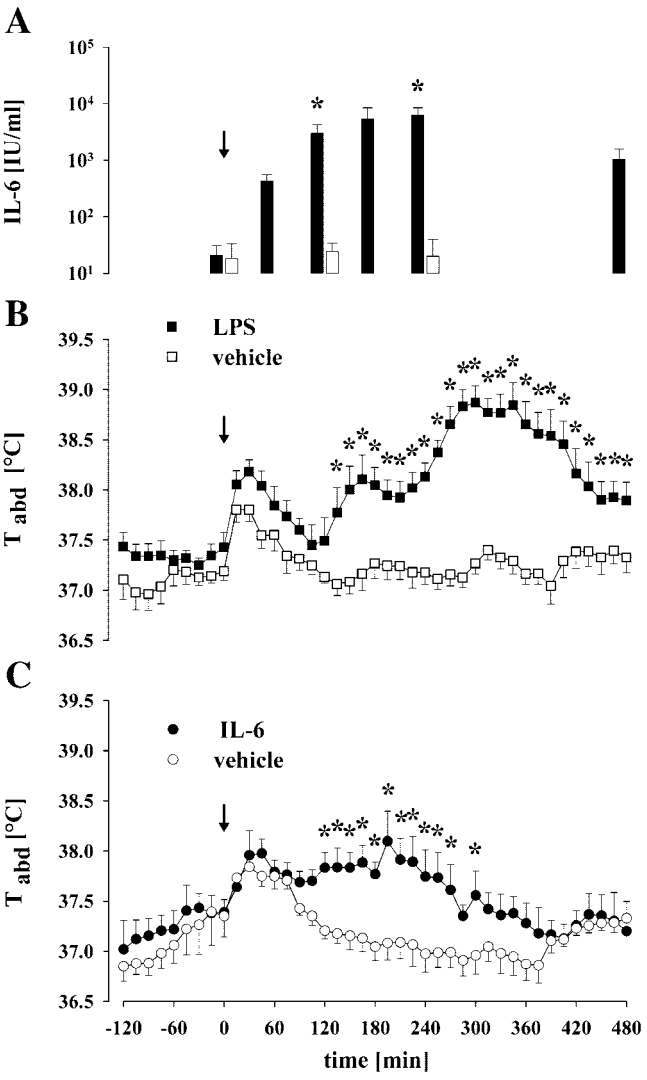

Fig. 1. Lipopolysaccharide (LPS)-induced circulating levels of bioactive interleukin-6 (IL-6) and the febrile responses to intraperitoneal injections of LPS or IL-6 in Wistar rats. *A*: plasma levels of bioactive IL-6 measured at selected time points from injection of LPS (100 μg/kg) or vehicle, with $n = 3$–5 rats per each bar. *B*: abdominal body temperature (T_{abd}) was continuously measured before and after intraperitoneal treatment with LPS (100 μg/kg, $n = 7$ rats) or an equivalent volume of pyrogen-free saline ($n = 7$ rats), which was used as vehicle. *C*: T_{abd} was continuously measured before and after intraperitoneal treatment with rat recombinant IL-6 (45 μg/kg, $n = 5$ rats) or an equivalent volume of pyrogen-free saline ($n = 5$ rats), which was used as vehicle. Time point of intraperitoneal bolus injection of LPS, IL-6, or vehicle is indicated by arrows (*time zero*). All data are presented as means ± SE. *Significant differences between groups ($P < 0.05$). Plasma IL-6 levels of LPS- or vehicle-treated rats were compared by one-way ANOVA followed by Scheffé's post hoc test. Fever curves (LPS vs. vehicle or IL-6 vs. vehicle) were compared by two-way repeated-measure ANOVA followed by an all pairwise Bonferroni's multiple-comparison post hoc test.

Distribution of Cytoplasmic and Nuclear STAT3 Immunoreactivity in the Rat Brain Analyzed Under Control and Pyrogen (IL-6 and LPS)-Stimulated Conditions

In control rats as well as in pyrogen-stimulated animals, basal cytoplasmic STAT3 expression was detected in various brain areas with a similar staining pattern, irrespective of the time point investigated (Table 1). The postinjection time points used for Table 1 (60 and 120 min) are those proven to be necessary to demonstrate pyrogen-induced nuclear STAT3 translocation (see also Figs. 2 and 3).

Brain areas with a moderate to strong cytoplasmic STAT3 expression were predominantly found within the hypothalamus and the medulla. As for the hypothalamus, those areas included the arcuate nucleus, the periarcuate area, the lateral hypothalamic area, the

Table 1. *Distribution of cytoplasmic and nuclear STAT3 immunoreactivity in the rat brain during control and pyrogen-stimulated conditions*

Brain structures	Cytoplasmic STAT3 Expression			Nuclear STAT3 Expression		
	Vehicle (60/120 min)	IL-6 (60 min)	LPS (120 min)	Vehicle (60/120 min)	IL-6 (60 min)	LPS (120 min)
Sensory circumventricular organs						
Area postrema (AP)	++	++	++	+	+	+
Subfornical organ (SFO)	+	+	+	−	++	+++
Vascular organ of the lamina terminalis (OVLT)	+	+	+	−	++	+++
Hypothalamus						
Arcuate nucleus (ARC)	+++	+++	+++	−	−	+
Dorsomedial nucleus (DMH)	−	−	−	−	−	−
Lateral hypothalamic area (LH)	++	++	+	−	−	−
Lateral preoptic area (LPO)	−	−	−	−	−	−
Magnocellular preoptic nucleus (MCPO)	++	++	++	−	−	−
Medial preoptic area (MPA)	−	−	−	−	−	−
Medial preoptic nucleus (MPO)	−	−	−	−	−	−
Median eminence (ME)	++	++	++	−	+	++
Median preoptic nucleus (MnPO)	−	−	−	−	−	−
Paraventricular nucleus (PVN)						
parvocellular subnuclei	+	+	+	−	−	−
magnocellular subnucleus	+	+	+	−	−	−
Periarcuate area (PAA)	++	++	+	−	−	−
Periventricular nucleus (PE)	+	+	++	−	−	−
Retrochiasmatic area (RCH)	++	+	+	−	−	−
Suprachiasmatic nucleus (SCN)	−	−	−	−	−	−
Supraoptic nucleus (SON)	++	++	++	−	−	−
Ventromedial nucleus (VMH)	−	−	−	−	−	−
Ventromedial preoptic nucleus (VMPO)	++	++	+	−	+	−
Septal and basal telencephalic regions						
Lateral septum (LS)	−	−	−	−	−	−
Medial septal nucleus (MS)	++	++	+	−	−	−
Nuclei of the diagonal band of Broca (DB)	++	++	++	−	−	−
Medulla oblongata						
Ambiguus nucleus (Amb)	++	++	++	−	−	−
Cuneate nucleus (Cu)	+++	++	+	−	−	−
Dorsal motor nucleus of the vagus (10)	+++	+++	++	−	−	−
External cuneate nucleus (ECu)	+	+	+	−	−	−
Gracile nucleus (Gr)	++	++	+		−	−
Hypoglossal nucleus (12)	+++	+++	+++	−	−	−
Lateral reticular nucleus (LRt)	+	++	++	−	−	−
Nuclei of solitary tract (Sol)	+	+	+	+	+	+
Spinal trigeminal nucleus (Sp5)	+	−	−	−	−	−
Others						
Cortex, layer 5	+	++	++	−	−	−
Piriform cortex, layer 2	−	−	−	−	−	−
Substantia nigra (SN)	+	+	+	−	−	−
Ependymal lining of all ventricles	++	+	+	−	+	+
Meninges	++	++	++	−	+	+
Choroid plexus	++	++	++	−	+	+

Signal transducer and activator of trancription 3 molecule (STAT3) immunoreactivity relative values are given as qualitative estimates of the densities of cytoplasmic or nuclear STAT3 labeling in representative animals. STAT3 signals were analyzed 60 and 120 min after systemic interleukin-6 (IL-6), lipopolysaccharide (LPS), or vehicle treatment. A four-point scale was used to rate the data: +++ = high density, ++ = moderate density, + = low density, − = no cytoplasmic or nuclear signal. Rat brain nomenclature given here is modified from that used by Swanson (31).

magnocellular and ventromedial preoptic nucleus, the median eminence, the periventricular nucleus, the retrochiasmatic area, and the supraoptic nucleus. Within the medulla oblongata, intense cytoplasmic STAT3 signals were observed in the ambiguus nucleus, the cuneate nucleus, the dorsal motor nucleus of the vagus, the gracile nucleus, the hypoglossal nucleus, and the lateral reticular nucleus. As for those brain structures of particular interest for this study, the CVOs, moderate cytoplasmic STAT3 expression was found within the AP and low cytoplasmic STAT3 signals was found in the SFO and OVLT at all time points investigated and irrespective of the type of treatment.

In contrast, nuclear STAT3 immunoreactivity was only observed in a very limited number of brain structures after both vehicle and pyrogen application. The most intense nuclear signals were detected within the OVLT and the SFO 60 or 120 min after IL-6 or LPS treatment, whereas the respective controls showed no nuclear STAT3 immunoreactivity. This proved to be different for the AP and in some respects also for the solitary tract nuclei, in which at both time points and

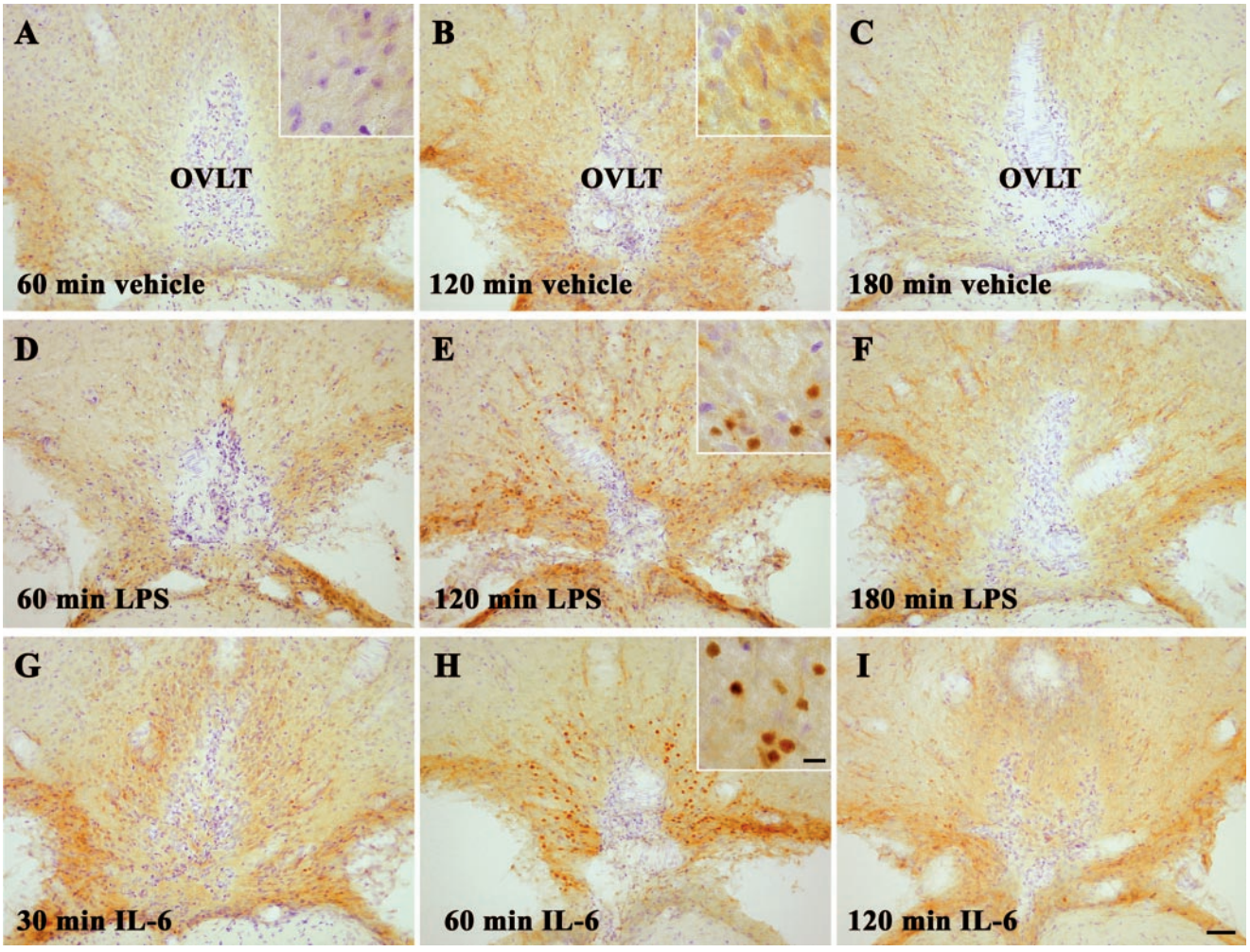

Fig. 2. Systemic treatment with the pyrogens LPS and IL-6 induces a time-dependent nuclear translocation of signal transducer and activator of transcription 3 molecule (STAT3) immunoreactivity in the vascular organ of the lamina terminalis (OVLT). Photomicrographs of the OVLT are shown during LPS-stimulated (*D–F*) and IL-6-stimulated (*G–I*) conditions compared with their respective vehicle treatments (*A–C*). Intraperitoneal vehicle treatment did not result in a nuclear translocation of STAT3 immunoreactivity at all time periods (60–180 min) tested. In contrast, 120 min after an intraperitoneal LPS bolus injection (100 μg/kg), a strong nuclear translocation of STAT3 immunoreactivity was observed in the OVLT (*E*), whereas shorter (*D*, 60 min) or longer (*F*, 180 min) posttreatment LPS periods showed no difference vs. their respective vehicle treatments (60 min: compare *A* vs. *D*; 180 min: compare *C* vs. *F*). Systemic IL-6 treatment (45 μg/kg) also induced a nuclear STAT3 translocation; however, nuclear signals were already observed 60 min after start of treatment (*H*). Shorter (*G*, 30 min) or longer (*I*, 120 min) posttreatment IL-6 periods showed no difference vs. their respective vehicle treatments (30 min: vehicle not shown; 120 min: compare *B* vs. *I*). Note that the specific STAT3 immunoreactivity is depicted from the brown reaction product, due to the immunohistochemical visualization via diaminobenzidine hydrochloride conversion. Specific nuclear STAT3 labeling after systemic LPS and IL-6 application within the OVLT is shown at higher magnifications in the *insets* in *E* and *H* compared with the blue-colored cell nuclei of their respective control situation with the cresyl violet counterstaining, presented in the *insets* in *A* and *B*. Bar for *A–I* = 50 μm. Bar for *insets* = 10 μm.

irrespective of the type of treatment a low nuclear STAT3 expression was observed. As for other brain structures showing nuclear STAT3 signals during pyrogen-stimulated conditions, a low STAT3 expression was found in the arcuate nucleus, the median eminence, the ventromedial preoptic nucleus, the choroid plexus, the ependymal lining of the ventricles, and the meninges. However, the numbers of cells (1–5) that stained positively for STAT3 in these structures were of magnitudes lower than those detected in the two CVOs (the OVLT and SFO) (see Fig. 4).

Systemic IL-6 and LPS Treatment Induces a Time-Dependent Nuclear Translocation of the Transcription Factor STAT3 in the OVLT and SFO

Cytoplasmic STAT3 expression in the OVLT under control conditions (Fig. 2, *A–C*, and Fig. 2, *A* and *B*, *insets*) as well as during pyrogen-stimulated conditions (Fig. 2, *D–I*, and Fig. 2, *E* and *H*, *insets*) was very weak and could hardly be separated from background labeling. In contrast, 120 min after LPS treatment (Fig. 2*E* and *inset* in Fig. 2*E*) or 60 min after IL-6 treatment

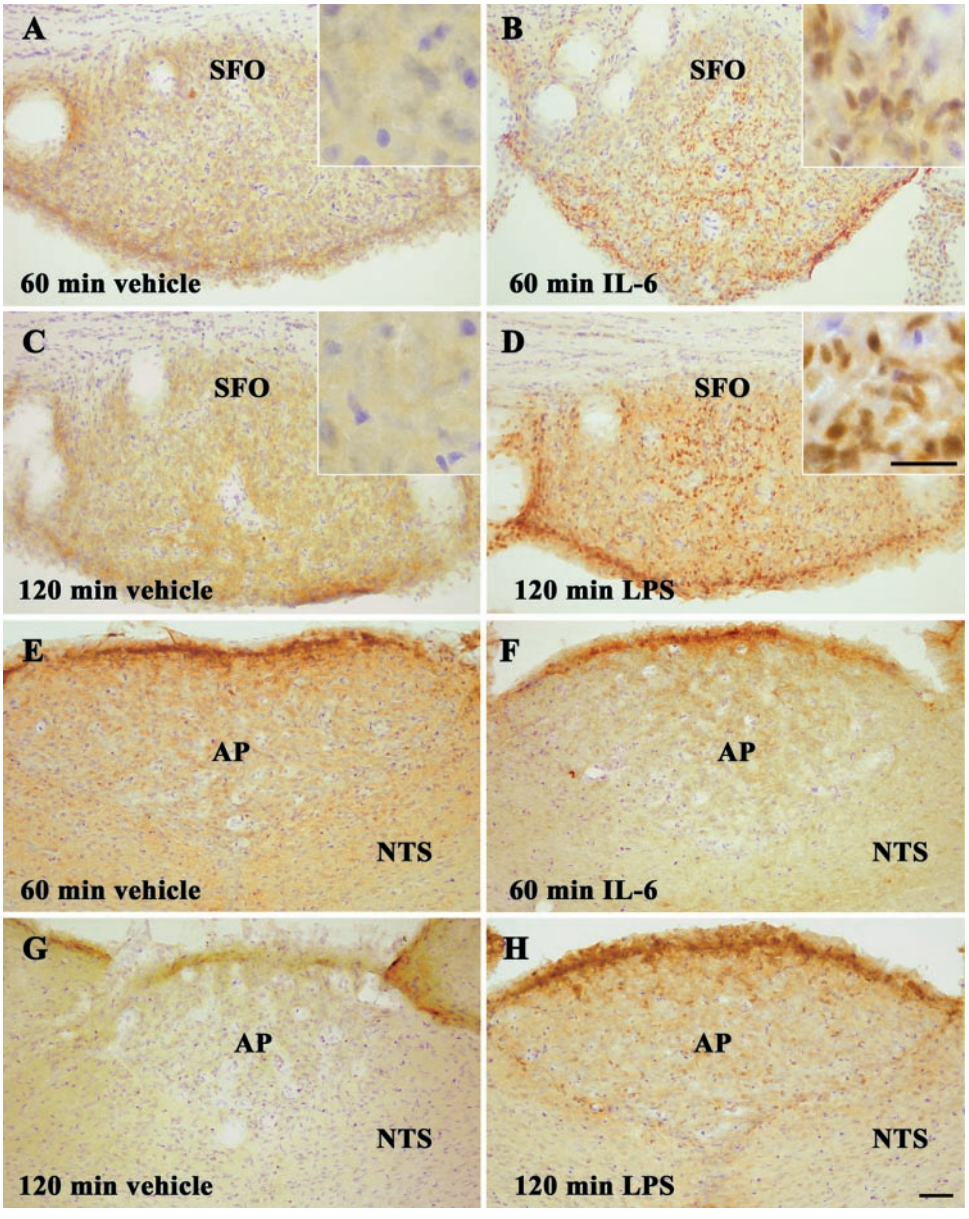

Fig. 3. Systemic treatment with the pyrogens IL-6 and LPS induces a nuclear translocation of STAT3 immunoreactivity in the subfornical organ (SFO) but not in the area postrema (AP). Photomicrographs of the SFO (*A–D* and *insets* in *A–D*) and the AP (*E–H*) are shown during IL-6-stimulated (*B* and *F*) and LPS-stimulated (*D* and *H*) conditions at those time points at which a nuclear STAT3 translocation was observed within the OVLT (see Fig. 2) and compared with their respective vehicle controls (*A*, *C*, *E*, *G*). Sixty and 120 min after intraperitoneal vehicle treatment, no nuclear translocation of STAT3 immunoreactivity was observed in the SFO (*A* and *C* and *insets* in *A* and *C*). In contrast, 60 min after an intraperitoneal bolus injection of rat recombinant IL-6 (45 μg/kg) and 120 min after an intraperitoneal LPS bolus injection (100 μg/kg), a nuclear translocation of STAT3 immunoreactivity was observed in particular in the core of the SFO (*B* and *D* and *insets* in *B* and *D*). In the AP, no obvious change in STAT3 immunoreactivity was observed as a result of IL-6 (*F*) or LPS (*H*) treatment when compared with the respective vehicle controls (*E* and *G*). However, within the AP, cytoplasmic STAT3 expression as well as a few cells with nuclear STAT3 signals could be detected in a band of cells just adjacent to the fourth ventricle (*E–H*). Note that the specific STAT3 immunoreactivity is depicted from the brown reaction product, due to the immunohistochemical visualization via diaminobenzidine hydrochloride conversion. Specific nuclear STAT3 labeling after systemic IL-6 and LPS application within the SFO is shown at higher magnifications in *B* and *D insets* compared with the blue-colored nuclei of their respective control situation with cresyl violet counterstaining and presented in *A* and *C*, *insets*. Bar for *A–H* = 50 μm. Bar for *insets* = 20 μm. NTS, solitary tract nucleus.

(Fig. 2*H* and *inset* in Fig. 2*H*), a nuclear STAT3 translocation and an increase in STAT3 immunoreactivity were observed in cells within rostral aspects of the OVLT. The size and the round shape of the STAT3-labeled cell nuclei (*insets* in Fig. 2, *E* and *H*) compared with the cresyl violet-counterstained neuronal nuclei (*insets* in Fig. 2, *A* and *B*) indicate a predominant nuclear STAT3 translocation in OVLT neurons. All other time intervals investigated showed no difference in STAT3 immunoreactivity between pyrogen- and vehicle-treated animals (for details, see Fig. 2).

Similar to the situation noted for the OVLT, cytoplasmic STAT3 expression within the SFO under control conditions (Fig. 3, *A* and *C*, and *insets* in Fig. 3, *A* and *C*) as well as during pyrogen-stimulated conditions (Fig. 3, *B* and *D*, and *insets* in Fig. 3, *B* and *D*) was low and could hardly be separated from background labeling. In contrast, 60 min after IL-6 treatment (Fig. 3*B* and *inset* in Fig. 3*B*) or 120 min after LPS treatment (Fig. 3*D* and *inset* in Fig. 3*D*), a nuclear STAT3 translocation and an increase in STAT3 immunoreactivity were observed in SFO cells, particularly in cells lying in the core of the SFO (Fig. 3, *B* and *D*). In the case of the SFO, the size and the shape of the STAT3-labeled cell nuclei (*insets* in Fig. 3, *B* and *D*) compared with the cresyl violet-counterstained neuronal nuclei (*insets* in Fig. 3, *A* and *C*) do not suggest a predominant nuclear STAT3 translocation in neurons. All other time intervals investigated showed no difference in STAT3 immunoreactivity between pyrogen- and vehicle-treated animals (data not shown).

Finally, the AP seemed to be the one exception out of the sensory CVOs that did not show a specific pyrogen-induced nuclear STAT3 translocation. Neither 60-min

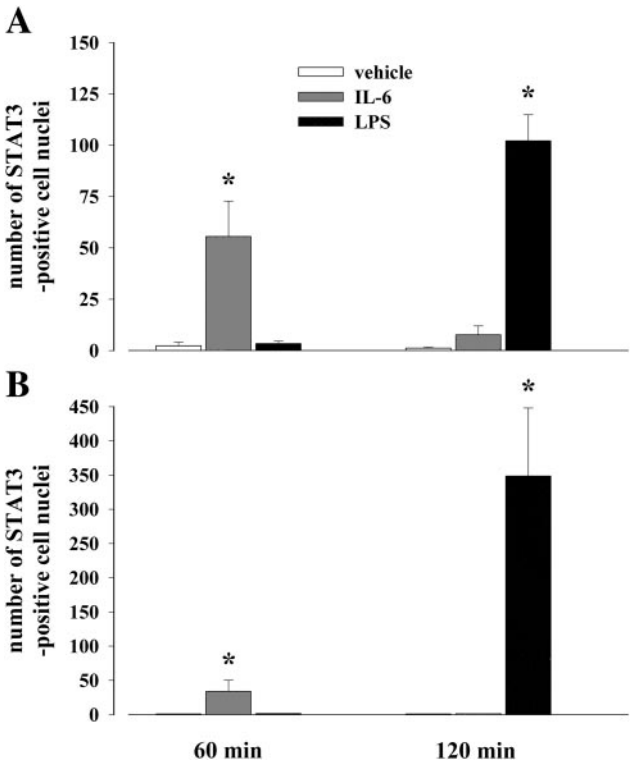

Fig. 4. Quantitative evaluation of the numbers of STAT3-immunoreactive cell nuclei in the OVLT (*A*) and the SFO (*B*) 60 and 120 min after treatment with the pyrogens IL-6 and LPS compared with the vehicle treatment. Data represent means ± SE of cell counts per OVLT section in 4–5 animals per group (60 and 120 min vehicle groups: $n = 5$; 60 min IL-6 group: $n = 5$; 120 min IL-6 group: $n = 4$; 60 min LPS group: $n = 4$; 120 min LPS group: $n = 5$), with 3 OVLT and SFO sections counted for each animal. Statistical analysis was performed by one-way ANOVA with subsequent post hoc analysis, revealing statistical significance at $^*P < 0.05$ compared with the respective vehicle treatment.

IL-6 (Fig. 3*F*) nor 120-min LPS treatment (Fig. 3*H*) induced an obvious difference in nuclear STAT3 signals compared with the respective controls (Fig. 3, *E* and *G*). However, irrespective of the postinjection time interval investigated and the type of treatment, a few AP cells just adjacent to the fourth ventricle displayed nuclear STAT3 labeling. This nuclear STAT3 labeling was often hidden in a line of cells along the fourth ventricle with moderate cytoplasmic STAT3 expression (Fig. 3, *E–H*).

The time dependency of specific nuclear STAT3 translocation was quantitatively verified by counting the STAT3-labeled cell nuclei in the OVLT and SFO (Fig. 4). Although in the vehicle-treated rats at 60 and 120 min none to two cell nuclei were positively labeled within the OVLT and the SFO, treatment with both pyrogens (IL-6 and LPS) significantly increased the number of STAT3-stained nuclei. Sixty minutes after systemic IL-6 application, an increase in STAT3-labeled nuclei up to a number of 56 ± 17 (OVLT) and 34 ± 16 (SFO) was observed, which almost disappeared 120 min after IL-6 treatment, with only 8 ± 4 (OVLT) and 1 ± 1 (SFO) cell nuclei being STAT3 labeled. With 3 ± 1 (OVLT) and 1 ± 1 (SFO) STAT3-labeled nuclei, no significant change was observed 60 min after LPS treatment, but the number of STAT3-positive nuclei rose up to 102 ± 13 (OVLT) and 348 ± 100 (SFO) 120 min after LPS application. This LPS-induced peak in nuclear STAT3 translocation proved to be gone 180 min after LPS application, with only one or two cell nuclei being labeled (not shown, $n = 3$).

DISCUSSION

Role of IL-6 and Sensory CVOs in Fever

IL-6 is regarded as one of the endogenous mediators of LPS-induced fever. In line with this concept, an excellent correlation of bioactive IL-6 in plasma with the febrile changes of body temperature was found during LPS-induced fever in the present investigation and various previous studies (20, 23, 24). This correlation between febrile body temperature and plasma IL-6 alone of course does not prove that fever is really caused by circulating IL-6. However, within the last years, some additional experimental evidence for a critical role of IL-6 in fever has accumulated. Thus it has been shown that the febrile response to LPS or IL-1β is completely abolished in IL-6-deficient ("knockout") mice (8). These mice, on the other hand, develop fever in response to central administration of exogenous IL-6, suggestive of IL-6 gene expression being essential for the manifestation of the febrile response (8). In addition, circulating IL-6 has also been identified as a critical component of fever in an experimental model of localized inflammation in rats (7). However, the results shown in Fig. 1 indicate that IL-6 may participate in, but is clearly not responsible alone for, the febrile response of rats treated with an intraperitoneal injection of LPS, since fever after administration of the relatively high dose of rrIL-6 (45 μg/kg) was rather moderate. In this context, it has been suggested that circulating IL-6 needs a still unidentified "cofactor" to elicit a more pronounced febrile response (7).

If circulating IL-6 is involved in LPS-induced fever, then the question arises of how the pyrogenic message is transported to the thermoregulatory centers in the brain where the febrile response is generated. One current hypothesis is that central fever induction pathways involve the CVOs lacking a BBB as potential sites where circulating pyrogens interact with the brain via prostaglandin-dependent mechanisms (2, 26). Such critical pyrogenic zones in the brain, which were initially revealed in lesion and knife-cut studies, include the medial preoptic area of the rostral hypothalamus and all sensory CVOs (3, 4, 12, 19, 32).

In situ hybridization experiments investigating the constitutive expression of IL-6 receptor mRNA in the rat brain showed strong signals in neurons of the medial preoptic area (27) and low signals within the sensory CVOs (the AP, the OVLT, and the SFO) (35). This is in accordance with our laboratory's recent neuroanatomic results (14, 15) revealing that an IL-6-induced activation of the IL-6 receptor signaling cascade was more pronounced in ventromedial parts of the preoptic area compared with the OVLT or the SFO after central IL-6

application. No nuclear STAT3 translocation was found in the AP after central IL-6 treatment (14). This is once again in line with a recent study (35) showing an upregulation of IL-6-receptor mRNA expression from low to strong (OVLT) and from low to moderate levels (SFO) 3 h after LPS treatment, whereas no changes were induced within the AP. Therefore, in summary, this suggests that, of the sensory CVOs, the OVLT and the SFO seem particularly to represent the target structure for LPS-induced circulating IL-6. In addition, the close proximity of the OVLT to rostral parts of the ventromedial parts of the preoptic area makes both hypothalamic areas an attractive pyrogenic zone that initiates and/or mediates LPS-induced febrile responses with IL-6 as its endogenous pyrogen.

Molecular Aspects of STAT3-Induced Genomic Activation in IL-6- and LPS-Induced Fever

STAT3 is activated in response to ligand binding at the IL-6 cytokine receptor family. Activation of STAT3 involves cytokine-induced dimerization of the gp130 receptor, association of JAKs to the gp130 receptor complex, and JAK-mediated phosphorylation of STAT3. Then phospho-STAT3 dimerizes and translocates into the cell nucleus where it binds to specific response elements of target gene promoters (33). Konsman et al. (18) and also the present study have employed STAT3 immunohistochemistry after systemic LPS treatment as a molecular and neuroanatomic marker of direct IL-6-receptor activation and consequent genomic activation. In the assessment of functionally active central IL-6 target structures, a nuclear STAT3 translocation was predominantly observed within the OVLT and the SFO for both groups: the 60-min rrIL-6-treated and the 120-min LPS-treated group (Table 1 and Figs. 2–4). Although we have no exclusive proof for the involvement of IL-6 as the endogenous mediator of LPS-induced fever that induces nuclear STAT3 translocation in these two CVOs, the similarity of the nuclear STAT3 translocation pattern induced by the pyrogens IL-6 and LPS is striking. The peak in STAT3-labeled cell nuclei occurred 60 min after IL-6 treatment, whereas LPS needed an additional 60 min to exert its peak in nuclear STAT3 translocation. This correlates well with the idea of LPS-induced IL-6 formation (20, 23) and the plasma IL-6 levels being elevated already 1 h after LPS injection (Fig. 1).

On the basis of the initial appearance of nuclear STAT3 translocation, there might seem to exist no obvious correlation between the time point of nuclear STAT3 translocation with the time course of the pyrogen-induced febrile response. However, according to the current concept of how fever is likely to be initiated in the brain, a cytokine-induced genomic activation of prostaglandin synthesis needs to take place (5, 11, 22, 25, 26). This is exactly the point at which STAT3 could exert its role as a transcription factor. Indeed, a gene sequence analysis of the inducible cyclooxygenase 2 (COX2) gene (*Rattus norvegicus*) revealed a STAT3 consensus sequence (29) in the promoter region (66 CTGGRAA 74) of the COX2 gene. Therefore, the time gap in between the pyrogen-induced nuclear STAT3 translocation (60 min for IL-6 and 120 min for LPS) and the maximum febrile response (~200 min for IL-6 and ~300 min for LPS) might be exactly the time necessary for transcription of the COX2 gene and consequent synthesis of prostaglandin E_2.

Perspectives

Our results represent evidence for a genomic activation of important thermoregulatory brain structures by circulating cytokines via the transcription factor STAT3. Although this genomic activation seems to be mediated by blood-borne IL-6, other endogenous mediators of LPS-induced fever, such as TNF-α and IL-1β, also contribute to fever responses induced by bacterial infection. These cytokines use similar intracellular signaling pathways; however, other members of the STAT family and other signaling pathways are thought to be involved. To functionally map cytokine action on the brain, STAT immunohistochemistry offers the opportunity to reveal a cytokine-specific pattern of genomic activation in the brain with distinct STAT molecules as different neuroanatomic markers.

We thank Dr. Stephen Hopkins (University of Manchester, Salford, UK) for providing us with the B9 cell line and for the protocol of the IL-6 assay. We thank Dr. Stephan Barth (Federal Research Centre for Nutrition, Karlsruhe, Germany) for the STAT3 consensus sequence analysis of the COX2 gene. Rat recombinant IL-6 was provided by the BIOMED I program PL-391450 (Dr. Stephen Poole, Herts, UK).

This study was supported by the Deutsche Forschungsgemeinschaft and Research Grant I-572-22.2/1998 to R. Gerstberger by the German-Israeli Foundation.

REFERENCES

1. **Aarden LA, DeGroot ER, Schaap OL, and Landsdorp PM.** Production of hybridoma growth factors by human monocytes. *Eur J Immunol* 17: 1411–1416, 1987.
2. **Blatteis CM.** Role of the OVLT in the febrile response to circulating pyrogens. *Prog Brain Res* 91: 409–412, 1992.
3. **Blatteis CM, Bealer SL, Hunter WS, Llanos QJ, Ahokas RA, and Mashburn TA Jr.** Suppression of fever after lesions of the anteroventral third ventricle in guinea pigs. *Brain Res Bull* 11: 519–526, 1983.
4. **Blatteis CM, Hales JRS, McKinley MJ, and Fawcett AA.** Role of the anteroventral third ventricle region in fever in sheep. *Can J Physiol Pharmacol* 65: 1255–1260, 1987.
5. **Cao CY, Matsumura K, Yamagata K, and Watanabe Y.** Involvement of cyclooxygenase 2 in LPS induced fever and regulation of its mRNA by LPS in the rat brain. *Am J Physiol Regulatory Integrative Comp Physiol* 272: R1712–R1725, 1997.
6. **Cartmell T, Luheshi GN, and Rothwell NJ.** Brain sites of action of endogenous interleukin-1 in the febrile response to localized inflammation in the rat. *J Physiol* 518: 585–594, 1999.
7. **Cartmell T, Poole S, Turnbull AV, Rothwell NJ, and Luheshi GN.** Circulating interleukin-6 mediates the febrile response to localised inflammation in rats. *J Physiol* 526: 653–661, 2000.
8. **Chai Z, Gatti S, Toniatti C, Poli V, and Bartfai T.** Interleukin (IL)-6 gene expression in the central nervous system is necessary for fever in response to lipopolysaccharide or IL-1β: a study on IL-6-deficient mice. *J Exp Med* 183: 311–316, 1996.
9. **Dantzer R, Bluthe RM, Gheusi G, Cremona S, Laye S, Parnet P, and Kelley K.** Molecular basis of sickness behavior. *Ann NY Acad Sci* 865: 132–138, 1998.

10. **Dinarello CA, Cannon JG, and Wolff SM.** New concepts on the pathogenesis of fever. *Rev Infect Dis* 10: 168–189, 1988.
11. **Elmquist JK, Breder CD, Sherin JE, Scammell TE, Hickey WF, Dewitt D, and Saper CB.** Intravenous lipopolysaccharide induces cyclooxygenase-2 like immunoreactivity in rat brain perivascular microglia and meningeal macrophages. *J Comp Neurol* 381: 119–129, 1997.
12. **Hashimoto M, Ueno T, and Iriki M.** What role does the organum vasculosum laminae terminalis play in fever in rabbits? *Pflügers Arch* 429: 50–57, 1994.
13. **Holt I, Cooper RG, and Hopkins SJ.** Relationship between local inflammation, interleukin-6 concentration and the acute phase response in arthritic patients. *Eur J Clin Invest* 21: 479–484, 1991.
14. **Hübschle T, Harré EM, Meyerhof W, Pehl U, Roth J, and Gerstberger R.** The central pyrogenic action of interleukin-6 is related to nuclear translocation of STAT3 in the anteroventral preoptic area of the rat brain. *J Therm Biol* 26: 299–305, 2001.
15. **Hübschle T, Thom E, Watson A, Roth J, Klaus S, and Meyerhof W.** Leptin-induced nuclear translocation of STAT3 immunoreactivity in hypothalamic nuclei involved in body weight regulation. *J Neurosci* 21: 2413–2424, 2001.
16. **Jansky L, Vybiral S, Pospisilowa D, Roth J, Dornand J, Zeisberger E, and Kaminkowa J.** Production of systemic and intrahypothalamic cytokines during the early phase of endotoxin fever. *Neuroendocrinology* 62: 55–61, 1995.
17. **Kluger MJ.** Fever: role of pyrogens and cryogens. *Physiol Rev* 71: 93–127, 1991.
18. **Konsman JP, Luheshi GN, Bluthe RM, and Dantzer R.** The vagus nerve mediates behavioral depression, but not fever, in response to peripheral immune signals: a functional anatomical analysis. *Eur J Neurosci* 12: 4434–4446, 2000.
19. **Lee HY, Whiteside MB, and Herkenham M.** Area postrema removal abolishes stimulatory effects of intravenous interleukin-1β on hypothalamic-pituitary-adrenal axis activity and c-fos mRNA in the hypothalamic paraventricular nucleus. *Brain Res Bull* 46: 495–503, 1998.
20. **LeMay LG, Vander AJ, and Kluger MJ.** Role of interleukin-6 in fever in rats. *Am J Physiol Regulatory Integrative Comp Physiol* 258: R798–R803, 1990.
21. **Long NJ, Kunkel SL, Vander AJ, and Kluger MJ.** Antiserum against tumor necrosis factor enhances lipopolysaccharide fever in rats. *Am J Physiol Regulatory Integrative Comp Physiol* 258: R332–R337, 1990.
22. **Matsumura K, Cao C, Ozaki M, Morii H, Nakadate K, and Watanabe Y.** Brain endothelial cells express cyclooxygenase-2 during lipopolysaccharide-induced fever: light and electron microscopic immunocytochemical studies. *J Neurosci* 18: 6279–6289, 1998.
23. **Roth J, Conn CA, Kluger MJ, and Zeisberger E.** Kinetics of systemic and intrahypothalamic IL-6 and tumor necrosis factor during endotoxin fever in guinea pigs. *Am J Physiol Regulatory Integrative Comp Physiol* 265: R653–R658, 1993.
24. **Roth J, McClellan JL, Kluger MJ, and Zeisberger E.** Attenuation of fever and release of cytokines after repeated injections of lipopolysaccharide in guinea-pigs. *J Physiol* 477.1: 177–185, 1994.
25. **Roth J and de Souza GEP.** Fever induction pathways: evidence from responses to systemic or local cytokine formation. *Braz J Med Biol Res* 34: 301–314, 2001.
26. **Scammel TE, Elmquist JK, Griffin JD, and Saper CB.** Ventromedial preoptic prostaglandin E2 activates fever-producing autonomic pathways. *J Neurosci* 16: 6246–6254, 1996.
27. **Schöbitz B, de Kloet ER, Sutanto W, and Holsboer F.** Cellular localization of interleukin 6 mRNA and interleukin 6 receptor mRNA in rat brain. *Eur J Neurosci* 5: 1462–1435, 1993.
28. **Shibata M and Blatteis CM.** Human recombinant tumor necrosis factor and interferon affect the activity of neurons in the organum vasculosum laminae terminalis. *Brain Res* 562: 323–326, 1991.
29. **Stephanou A, Isenberg DA, Akira S, Kishimoto T, and Latchman DS.** The nuclear factor interleukin-6 (NF-IL6) and signal transducer and activator of transcription-3 (STAT-3) signalling pathways co-operate to mediate the activation of the hsp90beta gene by interleukin-6 but have opposite effects on its inducibility by heat shock. *Biochem J* 330 :189–95, 1998.
30. **Strömberg H, Svensson SP, and Hermanson O.** Distribution of the transcription factor signal transducer and activator of transcription 3 in the rat central nervous system and dorsal root ganglia. *Brain Res* 853: 105–114, 2000.
31. **Swanson LW.** *Brain Maps: Structure of the Brain.* Amsterdam: Elsevier Science, 1992.
32. **Takahashi Y, Smith P, Ferguson A, and Pittman QJ.** Circumventricular organs and fever. *Am J Physiol Regulatory Integrative Comp Physiol* 273: R1690–R1695, 1997.
33. **Takeda K and Akira S.** STAT family of transcription factors in cytokine-mediated biological responses. *Cytokine Growth Factor Rev* 11: 199–207, 2000.
34. **Turnbull AV and Rivier CL.** Regulation of the hypothalamic-pituitary-adrenal axis by cytokines: actions and mechanisms of action. *Physiol Rev* 79: 1–71, 1999.
35. **Vallières L and Rivest S.** Regulation of the genes encoding interleukin-6, its receptor and gp130 in the rat brain in response to the immune activator lipopolysaccharide and the proinflammatory cytokine interleukin-1β. *J Neurochem* 69: 1668–1683, 1997.
36. **Xin L and Blatteis CM.** Hypothalamic neuronal responses to interleukin-6 in tissue slices: effects of indomethacin and naloxone. *Brain Res Bull* 29: 27–35, 1992.
37. **Zeisberger E.** From humoral fever to neuroimmunological control of fever. *J Therm Biol* 24: 287–326, 1999.

5.9.

5.9. HARRÉ, E.-M., ROTH, J., GERSTBERGER, R. & HÜBSCHLE, T. (2003)

Interleukin-6 mediates lipopolysaccharide-induced nuclear STAT3 translocation in astrocytes of rat sensory circumventricular organs.

Brain Res. **980** (1): 151-155.

Eigener Anteil an der Publikation:

- Beteiligung an der Versuchsplanung (75 %)
- Durchführung der Versuche (30 %)
- Beteiligung an der Zusammenfassung und Veröffentlichung der Ergebnisse (75 %)

Available online at www.sciencedirect.com
SCIENCE DIRECT
Brain Research 980 (2003) 151–155
BRAIN RESEARCH
www.elsevier.com/locate/brainres

Short communication

Interleukin-6 mediates lipopolysaccharide-induced nuclear STAT3 translocation in astrocytes of rat sensory circumventricular organs

Eva-Maria Harré, Joachim Roth, Rüdiger Gerstberger, Thomas Hübschle*

Institute of Veterinary-Physiology, Justus-Liebig-University Giessen, Frankfurter Strasse 100, D-35392 Giessen, Germany

Accepted 25 April 2003

Abstract

Pyrogenic treatment with lipopolysaccharide (LPS) or interleukin-6 (IL-6) induces nuclear STAT3 translocation in the vascular organ of the laminae terminalis (OVLT) and the subfornical organ (SFO). STAT3 immunohistochemistry was combined with the detection of marker proteins (glial, neuronal, endothelial) and the nuclear DAPI stain to determine the phenotype of responding cells. At time points with high pyrogen-induced IL-6 plasma levels, nuclear STAT3 signals were co-localized with an astrocytic cell marker. IL-6 might therefore mediate genomic activation of OVLT/SFO astrocytes during LPS-induced fever.

Theme: Endocrine and autonomic regulation

Topic: Neural–immune interactions

Keywords: Signal transducer and activator of transcription; Vascular organ of the laminae terminalis; Subfornical organ; Glia; Fever; Cytokine

The sensory circumventricular organs (CVOs)—the vascular organ of the laminae terminalis (OVLT), the subfornical organ (SFO) and the area postrema (AP)—are characterized by their extensive vasculature and their lack of a normal blood–brain barrier in form of a fenestrated endothelium of the capillaries. The expression of a variety of peptidergic receptors, indicates involvement of the sensory CVOs in communication between the circulation and the central nervous system (CNS) [11]. During infection or inflammation, pro-inflammatory cytokines are released by immune competent cells into the systemic circulation. These cytokines are traditionally regarded as the endogenous mediators of brain-controlled signs of illness which accompany an infectious or inflammatory process such as fever, anorexia or sickness behaviour [2,12]. Since the large hydrophilic cytokine proteins are unable to pass the blood–brain barrier to induce the aforementioned centrally provoked sickness symptoms, the sensory CVOs are regarded as ‘windows to the brain’ for circulating cytokines. Such a role for the CVOs is based on classical studies in which fever could be suppressed or attenuated by lesions of single CVOs [1,14].

Interleukin-6 (IL-6) is the only proinflammatory cytokine that is measurable in significant amounts in the blood during the time course of lipopolysaccharide (LPS)-induced fever [10]. If IL-6 would act as a circulating messenger between the activated immune system and the brain at the level of the sensory CVOs, it should be possible to demonstrate a direct influence of IL-6 on cellular elements located within these brain structures. Stimulation of IL-6-receptors belonging to the gp130 cytokine receptor family activates the Janus kinase-signal transducer and activator of transcription (JAK-STAT) signalling cascade. IL-6 acts through the STAT3 isoform, which after its phosphorylation and subsequent dimerization, translocates from the cytoplasm into the cell nucleus where it regulates gene expression [15]. In rats, systemic administration of LPS as a potent inducer of IL-6 or injection of IL-6 itself caused a characteristic and transient pattern of nuclear STAT3 translocation in cells of the OVLT and SFO [5]. The peak of nuclear STAT3 translocation in these structures occurred 60 min after intraperitoneal (i.p.) injection of IL-6, or 120 min after administra-

*Corresponding author. Tel.: +49-641-9938-155; fax: +49-641-9938-159.

E-mail address: thomas.huebschle@vetmed.uni-giessen.de (T. Hübschle).

0006-8993/03/$ – see front matter
doi:10.1016/S0006-8993(03)02923-8

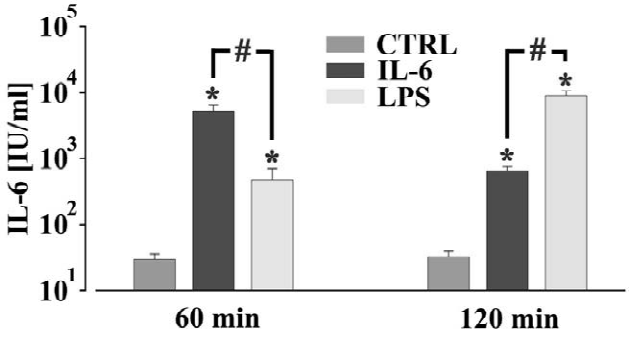

Fig. 1. Plasma IL-6 concentrations 60 and 120 min after systemic treatment with pyrogen-free saline as vehicle (CTRL, 60 min: $n=8$, 120 min: $n=12$), IL-6 (45 μg/kg, 60 min: $n=8$, 120 min: $n=4$) or LPS (100 μg/kg, 60 min: $n=4$, 120 min: $n=11$). All data are presented as means±S.E.M. Log-transformed circulating levels of IL-6 in the different groups were compared by two-way ANOVA followed by the Student–Newman–Keuls post hoc test. Statistical significance was accepted for the post hoc procedure at $P<0.05$. *=Significantly different from the respective vehicle group, #=significant difference between the IL-6- and LPS-groups.

tion of LPS, respectively. Using a 2.5-times higher dose of LPS, Gautron et al. [4] also demonstrated nuclear STAT3 translocation in CVOs (OVLT, SFO and median eminence) but also in some hypothalamic nuclei and in the pituitary. By means of double staining for STAT3 and glial fibrillary protein (GFAP), they further demonstrated LPS-induced nuclear translocation of STAT3 in astrocytes throughout the brain including the OVLT. In contrast, the aim of this study was to investigate the cellular origin of IL-6 induced nuclear STAT3 signals in the sensory CVOs and, for reasons of comparison, the cellular origin of those signals that occur after systemic LPS treatment. Brain sections of the rat OVLT and SFO were analysed in triple labelling experiments with the use of an Olympus BX50 fluorescent microscope, combining STAT3 immunohistochemistry with the immunohistochemical detection of cell specific marker proteins for astrocytes, endothelial, microglial or neuronal cells and with the nuclear DAPI stain.

Male Wistar rats with body weights of 220±5 g were used. Experiments were carried out in accordance with the local ethics committee (ethics approval number GI 18/2-42/00, Regierungspräsidium Giessen). Rat brains were perfused under ketamine–xylazine anaesthesia with 4% paraformaldehyde in 0.1 M phosphate buffer (pH 7.2) and immunohistochemically evaluated 60 min after IL-6 injection and 120 min after LPS treatment. These time points were based on the circulating IL-6 levels measurements shown above and on the temporal pattern of nuclear STAT3 translocation observed in a previous immunohistochemical study [5]. Just before perfusion, blood samples were taken from the left ventricle for determination of plasma IL-6 levels. IL-6 was measured by a specific bioassay based on the dose-dependent growth stimulation of IL-6 on the B9 hybridoma cell line as described previously [5]. Fig. 1 summarizes the circulating levels of bioactive IL-6, measured 60 and 120 min after i.p. injection of the vehicle pyrogen-free saline (CTRL), 45 μg/kg IL-6 or 100 μg/kg LPS. In response to saline administration basal plasma IL-6-levels of 30±6 and 33±6 IU/ml were detected 60 and 120 min post injection, respectively. One hour after IL-6 treatment, significantly increased amounts of this cytokine (5116±1291 IU/ml) were measured. This value declined to 657±94 IU/ml until the end of the second hour after injection of IL-6. Treatment with LPS initially resulted in a moderate but significant rise of plasma IL-6 (471±236 IU/ml) but then in a pronounced significant increase (9088±1679 IU/ml), respectively, 60 and 120 min after pyrogen administration.

To investigate whether pyrogen-induced STAT3 signals in the OVLT and SFO were located in cell nuclei, STAT3 immunohistochemistry was combined with the detection of the nuclear DAPI stain (for details see Ref. [7]). To further determine the cellular origin of nuclear STAT3 signals, 20 and 40 μm brain sections were incubated with rabbit polyclonal anti-STAT3 antibody (anti-STAT3; sc-482, Santa Cruz Biotechnology, Heidelberg, Germany) in combination with a cell-specific marker for astrocytes (mouse monoclonal anti glial fibrillary acidic protein, anti-GFAP; MAB3402, MoBiTec, Göttingen, Germany), oligodendrocytes (mouse monoclonal anti adenomatous polyposis coli, anti-APC; OP80, Calbiochem, VWR Deutschland, Darmstadt, Germany), microglia (mouse monoclonal anti rat cluster of determination 11b (anti-CD11b; MCA-275R, Serotec, Düsseldorf, Germany) or for neurons (mouse monoclonal anti neuron-specific nuclear protein, anti-NeuN; MAB 377, Calbiochem, VWR Deutschland). Based on previous observations that a high percentage of neurons within the rat OVLT and SFO are nitrergic, STAT3 immunohistochemistry was also combined with the NADPH-diaphorase staining [8].)

One hour after systemic IL-6 (45 μg/kg) and 2 h after systemic LPS application (100 μg/kg), STAT3 signals (green colour) could be observed in cells of both CVOs, the OVLT (Fig. 2A–D) and the SFO (Fig. 2E–H). In more detail, the overlay of the STAT3 signals with the DAPI

Fig. 2. Pyrogen-induced nuclear STAT3 translocation in the OVLT (A–D) and SFO (E–H) 1 h after systemic IL-6 (45 μg/kg, A/C/E/G) and 2 h after systemic LPS (100 μg/kg) treatment (B/D/F/H). Almost all intense STAT3 signals (green colour) within the OVLT (C, D) and the SFO (G, H) were localized within the cell nuclei, as shown at high magnification by its co-localization with the nuclear DAPI-stain (blue colour). Strong GFAP immunoreactivity (red colour) was found throughout the OVLT (A–D) and the SFO (E–H). An overlay of the nuclear STAT3 signals (blue–green colour) with GFAP-labelled cells showed a co-localization of some (white arrows in C, D, G, H) but not all (white arrowheads in C, D, G, H) nuclear STAT3 signals with GFAP-labelled astrocytes. Scale bar in A, E, F represents 100 μm, scale bar in B represents 100 μm, scale bar in C, D, H represents 25 μm, scale bar in G represents 50 μm.

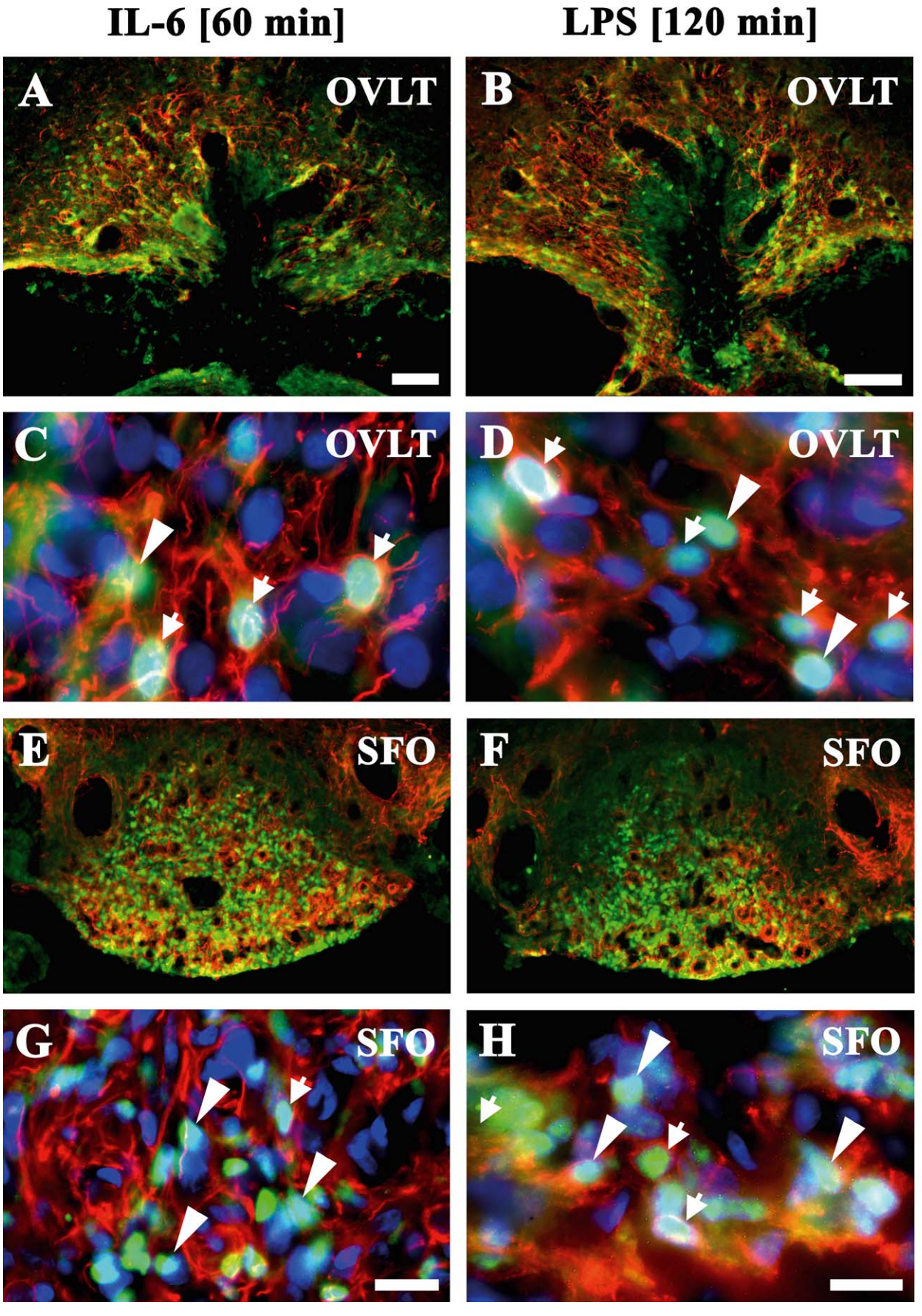
IL-6 [60 min]
LPS [120 min]
A
OVLT
B
OVLT
C
OVLT
D
OVLT
E
SFO
F
SFO
G
SFO
H
SFO

stained cell nuclei (blue colour) revealed, that almost all intense STAT3 signals within the OVLT (Fig. 2C and D) and the SFO (Fig. 2G and H) were localized within the cell nuclei as shown at higher magnification. This proved to be true for both pyrogen treatments with either IL-6 (Fig. 2C and G) or LPS (Fig. 2D and H) application at the respective time points. In saline-treated control rats, nuclear STAT3 signals were not observed within the OVLT and SFO (not shown).

Strong GFAP immunoreactivity (red colour) was found throughout the OVLT (Fig. 2A–D) and the SFO (Fig. 2E–H). An overlay of the nuclear STAT3 signals (blue–green colour) with GFAP-labelled cells showed co-localization of some (white arrows in Fig. 2C, D, G, H) but not all (white arrowheads in Fig. 2C, D, G, H) nuclear STAT3 signals with GFAP-labelled astrocytes. Therefore, only a subpopulation of those cells responding with nuclear STAT3 translocation were astrocytes, suggesting the existence of OVLT and SFO cells distinct from astrocytes which also responded to the IL-6 (Fig. 2C, G) or LPS treatment (Fig. 2D, H) at the respective time points. In contrast, co-localization of pyrogen-induced nuclear STAT3 signals with any of the other cell-specific marker proteins could not be established within both CVOs (not shown). Very few brain endothelial cells contained nuclear STAT3 signals, but these vessels were located outside the CVOs investigated.

One general question arising from the results presented in this study is, whether LPS-induced activation of STAT3 in the OVLT and SFO is mediated by IL-6. We [5] and others [4,9] previously reported, that peripheral administration of bacterial LPS induced a dose- and time-dependent nuclear translocation of STAT3 in various brain areas and predominantly activated cells of the CVOs, which lack a tight blood–brain barrier. Cytokines are putative endogenous mediators of LPS-induced STAT3 activation and stimulate the so-called gp130 receptor family [15]. The group of cytokines signalling through the gp130 receptor subunit includes IL-6, IL-11, CNTF, LIF and others. Leptin is another hormone-like cytokine which is induced by LPS [3]. Its binding to functionally active leptin receptors after central or systemic in vivo application leads to nuclear translocation of phosphorylated STAT3 [6,7].

The following arguments support the view that nuclear STAT3 translocation in OVLT and SFO in response to LPS is mediated by IL-6. (i) IL-6 is induced by LPS 2 h after LPS administration at exactly the same time points at which nuclear STAT3 translocation was most pronounced in the CVOs [5] and high levels of bioactive IL-6 were measurable in the systemic circulation. (ii) Circulating levels of IL-6 measured 1 h after i.p. injection of 45 μg/kg IL-6 or 2 h after i.p. injection of 100 μg/kg LPS were similar (Fig. 1). Under both conditions the peak of circulating IL-6 was associated with the highest number of nuclear STAT3 signals in the OVLT and SFO [5]. (iii) An identical spatial pattern of nuclear STAT3 translocation occurred 1 h after IL-6 and 2 h after of LPS application within the OVLT and the SFO. (iv) IL-6-receptors were present within the OVLT and SFO and their expression in both CVOs is even up regulated by systemic LPS treatment [16].

Accepting that circulating IL-6 is the signal which induces nuclear STAT3 translocation in cells within the OVLT and SFO then leads to two interesting questions. (i) What phenotypes of OVLT and SFO cells are activated by blood borne IL-6? and (ii) what is the functional relevance of the genomic activation observed in both sensory CVOs? To determine the phenotype and cellular origin of pyrogen-induced nuclear STAT3, we and others [4] used a variety of cell specific-marker proteins for co-localization studies. Gautron et al. [4] injected 250 μg/kg LPS, a 2.5-fold higher dose than used in this study and observed nuclear STAT3 translocation not only in sensory CVOs, but in the pituitary and to some degree also in the hypothalamus, the preoptic area, the cortex and the hippocampus. As for the phenotype of cells they revealed that nearly all STAT3 positive cell nuclei in the brain parenchyma are surrounded by GFAP immunoreactivity. This finding was interpreted as a more or less exclusive activation of astrocytes by the applied inflammatory stimulus. In general, we confirmed the findings of Gautron et al. [4] as far as many pyrogen-induced nuclear STAT3 signals were found in the OVLT and SFO and a subpopulation of them could be co-localized with the astrocytic cell marker GFAP. The new aspect of the present study, however, is the documentation of an almost identical co-localization pattern of nuclear STAT3 signals with GFAP under both pyrogen treatments, again suggestive of an IL-6 mediated STAT3 activation during LPS stimulation in both CVOs. In the OVLT as well as in the SFO a significant portion of nuclear STAT3 signals were not co-localized with GFAP-positive cells. This clearly indicated the existence of pyrogen-responding OVLT and SFO cells distinct from astrocytes and we therefore hypothesize that other cell types, for example neurons, microglia, endothelial cells or even blood borne macrophages and neutrophils might as well be activated by circulating IL-6. Indeed, microtubule-associated protein 2 (MAP2)—a neuronal cell marker—has been co-localized with phosphorylated nuclear STAT3 after focal cerebral ischemia in rats [13]. This finding showed that activation of STAT3 by ischemia-induced cytokines of the IL-6-family can occur in brain cells of neuronal origin. We therefore co-analysed pyrogen-induced nuclear STAT3 signals, which appeared in OVLT and SFO cells, with NeuN, a neuronal marker protein or NADPH-diaphorase, a marker for nitrergic neurons. Both attempts failed and nuclear STAT3 signals were not detected in NeuN- or NADPH-positive cells of the OVLT and SFO. Similar negative results were obtained when we tried to co-localize nuclear STAT3 signals with endothelial or microglial cell marker proteins. Thus at present, we are unable to propose the phenotype of those STAT3 responsive cells in the

OVLT and SFO, which were not co-localized with GFAP. At the moment we can only speculate on the functional relevance of IL-6 activated OVLT and SFO astrocytes. This important issue clearly merits further investigations and it would be of particular interest to identify those genes that are modulated by the IL-6 activated transcription factor STAT3 and further establish their role in fever and other brain-controlled signs of illness.

Acknowledgements

This study was supported by the Deutsche Forschungsgemeinschaft (DFG). We thank Dr. Stephen Hopkins (University of Manchester, UK) for providing us with the B9 cells and informing us about important details of the IL-6-assay, and Dr. Stephen Poole (NIBSC, Herts., UK) for providing rat recombinant IL-6 within the BIOMED program PL-391450 of the European Community.

References

[1] C.M. Blatteis, S.L. Bealer, W.S. Hunter, Q.J. Llanos, R.A. Ahokas, T.A. Mashburn Jr., Suppression of fever after lesions of the anteroventral third ventricle in guinea pigs, Brain Res. Bull. 11 (1983) 519–526.

[2] R. Dantzer, Cytokine-induced sickness behavior: where do we stand?, Brain Behav. Immun. 15 (2001) 7–24.

[3] B.N. Finck, K.W. Kelley, R. Dantzer, R.W. Johnson, In vivo and in vitro evidence for the involvement of tumor necrosis factor-α in the induction of leptin by lipopolysaccharide, Endocrinology 139 (1998) 2278–2283.

[4] L. Gautron, P. Lafon, M. Chaigniau, G. Tramu, S. Layé, Spatiotemporal analysis of signal transducer and activator of transcription 3 activation in rat brain astrocytes and pituitary following peripheral immune challenge, Neuroscience 112 (2002) 717–729.

[5] E.-M. Harré, J. Roth, U. Pehl, M. Kueth, R. Gerstberger, T. Hübschle, Molecular biology of thermoregulation selected contribution: role of IL-6 in LPS-induced nuclear STAT3 translocation in sensory circumventricular organs during fever in rats, J. Appl. Physiol. 92 (2002) 2657–2666.

[6] T. Hosoi, T. Kawagishi, Y. Okuma, J. Tanaka, Y. Nomura, Brain stem is a direct target for leptin's action in the central nervous system, Endocrinology 143 (2002) 3498–3504.

[7] T. Hübschle, E. Thom, A. Watson, J. Roth, S. Klaus, W. Meyerhof, Leptin-induced nuclear translocation of STAT3 immunoreactivity in hypothalamic nuclei involved in body weight regulation, J. Neurosci. 21 (2001) 2413–2424.

[8] M. Jurzak, H.A. Schmid, R. Gerstberger, NADPH-diaphorase staining and NO-synthase immunoreactivity in circumventricular organs of the rat, in: K. Pleschka, R. Gerstberger (Eds.), Integrative and Cellular Aspects of Autonomic Functions: Temperature and Osmoregulation, John Libbey Eurotext, Paris, 1994, pp. 451–459.

[9] J.P. Konsman, G.N. Luheshi, R.M. Bluthe, R. Dantzer, The vagus nerve mediates behavioral depression, but not fever, in response to peripheral immune signals: a functional anatomical analysis, Eur. J. Neurosci. 12 (2000) 4434–4446.

[10] L.G. LeMay, A.J. Vander, M.J. Kluger, Role of interleukin-6 in fever in rats, Am. J. Physiol. 258 (1990) R798–R803.

[11] M.J. McKinley, R. Gerstberger, M.L. Mathai, B.J. Oldfield, H.A. Schmid, The lamina terminalis and its role in fluid and electrolyte homeostasis, J. Clin. Neurosci. 6 (1999) 289–301.

[12] J. Roth, G.E.P. De Souza, Fever induction pathways: evidence from responses to systemic or local cytokine formation, Braz. J. Med. Biol. Res. 34 (2001) 301–314.

[13] S. Suzuki, K. Tanaka, S. Nogawa, T. Dembo, A. Kosakai, Y. Fukuuchi, Phosphorylation of signal transducer and activator of transcription-3 (Stat3) after focal cerebral ischemia in rats, Exp. Neurol. 170 (2001) 63–71.

[14] Y. Takahashi, P. Smith, A. Ferguson, Q.J. Pittman, Circumventricular organs and fever, Am. J. Physiol. 273 (1997) R1690–R1695.

[15] K. Takeda, S. Akira, STAT family of transcription factors in cytokine-mediated biological responses, Cytokine Growth Factor Rev. 11 (2000) 199–207.

[16] L. Vallières, S. Rivest, Regulation of the genes encoding interleukin-6, its receptor and gp130 in the rat brain in response to the immune activator lipopolysaccharide and the proinflammatory cytokine interleukin-1β, J. Neurochem. 69 (1997) 1668–1683.

5.10.

5.10. YOSHIDA, K., NAKAMURA, K., MATSUMURA, K., KANOSUE, K., KÖNIG, M., THIEL, H.-J., BOLDOGKÖI, Z., TOTH, I., ROTH, J., GERSTBERGER, R. & HÜBSCHLE, T. (2003)

Neurons of the rat preoptic area and the raphe pallidus nucleus innervating the brown adipose tissue express prostaglandin E receptor subtype EP3.

Eur. J. Neurosci. **18** (7): 1848-1860.

Eigener Anteil an der Publikation:

- Beteiligung an der Versuchsplanung (90 %)
- Durchführung der Versuche (40 %)
- Beteiligung an der Zusammenfassung und Veröffentlichung der Ergebnisse (90 %)

European Journal of Neuroscience, Vol. 18, pp. 1848–1860, 2003

Neurons of the rat preoptic area and the raphe pallidus nucleus innervating the brown adipose tissue express the prostaglandin E receptor subtype EP3

Kyoko Yoshida,[1,4] Kazuhiro Nakamura,[2] Kiyoshi Matsumura,[3] Kazuyuki Kanosue,[4] Matthias König,[5] Heinz-Jürgen Thiel,[5] Zsolt Boldogköi,[6] Ida Toth,[6] Joachim Roth,[1] Rüdiger Gerstberger[1] and Thomas Hübschle[1]
[1]Veterinary-Physiology, and [5]Institute of Virology, Justus-Liebig-University Giessen, Frankfurter Strasse 100 and 107, D-35392 Giessen, Germany
[2]Department of Morphological Brain Science, Graduate School of Medicine, and
[3]Department of Intelligence Science and Technology, Graduate School of Informatics, Kyoto University, Kyoto, Japan
[4]Department of Physiology, School of Allied Health of Sciences, Osaka University, Osaka, Japan
[6]Laboratory of Neuromorphology, Semmelweis University of Medicine, Budapest, Hungary

Keywords: central control of non-shivering thermogenesis, fever, pseudorabies virus, thermoregulation, viral tracing technique

Abstract

The major effector organ for thermogenesis during inflammation or experimental pyrogen-induced fever in rodents is the brown adipose tissue (BAT). Prostaglandin E2 (PGE_2) microinjection into the medial preoptic area (POA) of rats leads to hyperthermia through an increase in BAT thermogenesis and induces pyrogenic signal transmission towards the raphe pallidus nucleus (RPa), a brainstem nucleus known to contain sympathetic premotor neurons for BAT control. The medial POA has a high expression of prostaglandin E receptor subtype EP3 (EP3R) on POA neurons, suggesting that these EP3R are main central targets of PGE_2 to mediate BAT thermogenesis. To reveal central command neurons that contain EP3R and polysynaptically project to the BAT, we combined EP3R immunohistochemistry with the detection of transneuronally labelled neurons that were infected after injection of pseudorabies virus into the BAT. Neurons double-labelled with EP3R and viral surface antigens were particularly numerous in two brain regions, the medial POA and the RPa. Of all medial POA neurons that became virally infected 71 h after BAT inoculation, about 40% expressed the EP3R. This subpopulation of POA neurons is the origin of a complete neuronal chain that connects potential PGE_2-sensitive POA neurons with the BAT. As for the efferent pathway of pyrogenic signal transmission, we hypothesize that neurons of this subpopulation of EP3R expressing POA neurons convey their pyrogenic signals towards the BAT via the RPa. We additionally observed that two-thirds of those RPa neurons that polysynaptically project to the interscapular BAT also expressed the EP3R, suggesting that RPa neurons themselves might possess prostaglandin sensitivity that is able to modulate BAT thermogenesis under febrile conditions.

Introduction

Metabolic heat production of the brown adipose tissue (BAT) as a major thermoregulatory effector organ is induced under various (patho-)physiological conditions such as cold exposure, overeating and fever (Dascombe *et al*., 1989). With respect to fever occurring in rodents, evidence has accumulated regarding BAT as the major organ for thermogenesis during inflammation or experimentally pyrogen-induced fever (Rothwell, 1992). Amongst the pyrogens known to cause BAT activation are the endotoxin lipopolysaccharide (LPS), several cytokines and the E series of prostaglandins (PGE). According to the current concept of how fever is initiated in response to peripheral challenge of the immune system, cytokine-dependent formation of prostaglandin E2 (PGE_2) in the post-capillary walls is followed by activation of neuronal PGE receptors, which in turn trigger the neural circuitry for fever induction (Elmquist *et al*., 1997; Matsumura *et al*., 1998; Yamagata *et al*., 2001).

Correspondence: Dr Thomas Hübschle, as above.
E-mail: Thomas.Huebschle@vetmed.uni-giessen.de

Received 19 March 2003, revised 14 July 2003, accepted 28 July 2003

doi:10.1046/j.1460-9568.2003.02919.x

With regard to the location of prostaglandin action, the preoptic area (POA) seems to play a crucial role (Feldberg & Saxena, 1971; Stitt, 1973; Williams *et al*., 1977; Blatteis & Sehic, 1997). Injection of PGE_2 into the POA of rats induces pronounced hyperthermia through an increase in BAT thermogenesis that seems to be purely regulated by efferent outflow towards the sympathetic nervous system (Amir & Schiavetto, 1990). Studying Fos protein expression as a neuroanatomical tool to detect stimulus-induced neuronal activation, a PGE_2-sensitive pyrogenic zone has been located in the most ventromedial regions of the POA just adjacent to the vascular organ of the lamina terminalis, a hypothalamic structure with an open blood–brain barrier that has been hypothesized as the site at which circulating cytokines might induce PGE_2 production to initiate fever (Scammel *et al*., 1996).

Amongst mice deficient in distinct PGE receptor expression, only those lacking the prostaglandin E receptor subtype EP3 (EP3R) fail to show a febrile response to pyrogenic challenge with PGE_2, interleukin-1β or LPS, thereby stressing the importance of the EP3R in the febrile response and BAT thermogenesis (Ushikubi *et al*., 1998). In accordance with this finding, a high expression of EP3R is observed especially within cell bodies and dendrites of POA neurons (Nakamura

et al., 1999, 2000). This suggests that EP3R on POA neurons are targets of PGE_2 to exert its febrile action. In line with this hypothesis, our functional experiments have recently shown that microinjections of PGE_2 into the medial POA induce pyrogenic signals that were directly transmitted towards the raphe pallidus nucleus (Nakamura *et al*., 2002), a brainstem structure known to contain premotor neurons controlling sympathetic drive of BAT functions (Morrison *et al*., 1999).

However, the complete neuronal chain that connects potential PGE_2-sensitive POA neurons with the BAT has not yet been neuroanatomically demonstrated. The present study therefore combines EP3R immunohistochemistry with the detection of transneuronally labelled neurons that were infected after injection of pseudorabies virus (PRV) into the BAT. Using this analysis we plan to reveal central neurons that express EP3R and polysynaptically project to the sympathetic BAT innervation. We expect that we will be able histologically to confirm our earlier study on the role of PGE_2-sensitive POA neurons in BAT/fever control (Nakamura *et al*., 2002) and further demonstrate additional potential pyrogenic pathways that might transmit PGE_2-induced signals for BAT thermogenesis under fever conditions.

Materials and methods

Propagation of pseudorabies virus

The attenuated Bartha strain of pseudorabies virus (PRV-Ba) was propagated using standard cell culture procedures. Briefly, a porcine kidney fibroblast cell line (PK-15) was used for propagation and titration. Cells were grown in Dulbecco's modified minimum essential medium supplemented with 5% heat-inactivated fetal calf serum and 0.5 mg/mL gentamycin at 37 °C in a CO_2 incubator. Infected cells were frozen and thawed three times, followed by centrifugation to remove cell debris. Then virus aliquots were stored at −70 °C until they were used for the inoculation procedure. The titre of the PRV-Ba stocks was 8.03 TCID50/mL.

Animals

The study was performed in 22 male Wistar rats (*Rattus* spec.) with body weights (BW) of 230 ± 5 g (mean ± SEM). All experiments were carried out in accordance with the local Ethics Committee (ethics approval number GI 18/2 – No. 13/2002). Animals were housed individually with free access to water and standard laboratory chow. The room temperature (RT) was adjusted to 23 ± 1 °C and lights were on from 07:00 to 19:00 h.

Inoculation procedure

Rats were anaesthetized with intraperitoneal (i.p.) injections of ketamine-xylazine solution at 100 mg/kg BW ketamine hydrochloride (Pharmacia Upjohn, Erlangen, Germany) and 25 mg/kg BW Rompun (Bayer Vital, Leverkusen, Germany). The interscapular BAT was exposed and PRV-Ba was injected at three different sites of the right BAT pad with an injection volume of 1 μL each. The injections were made with a 5-μL Hamilton syringe (Hamilton, Bonaduz, Switzerland) and the syringe was kept in place for 30 s. Any efflux from the point of puncture was immediately adsorbed with sterile cotton buds. The wound was closed and the rats were allowed to survive up to 3 days. To demonstrate the time-dependent hierarchical infection of the brain, different post-infection times were chosen until the animals were transcardially perfused.

Immunohistochemistry

Transcardial perfusion was performed in deeply anaesthetized rats (60–100 mg/kg BW, i.p. sodium pentobarbital, Narcoren, Merial GmbH, Hallbergmoos, Germany) with 100–200 mL of 0.9% saline followed by ice-cold 400–500 mL of 4% paraformaldehyde diluted in 0.1 M phosphate buffer (PB, pH 7.2). Brains and spinal cords were removed, post-fixed for 4–8 h in the same fixative and then transferred into a 20% sucrose/PB solution overnight. Brains and spinal cord were cut the next day at 30 μm on a freezing microtome (model 1205, Jung, Heidelberg, Germany). Whereas brain sections were stained immunohistochemically for both EP3R and viral antigens, spinal cord sections were analysed for PRV antigens only.

Immunohistochemical detection of EP3R was performed with the anti-EP3R rabbit polyclonal antibody using the protocol described by Nakamura *et al*. (1999, 2000) with slight modifications. Briefly, free floating coronal brain sections were incubated for 1 h at RT in PB containing 10% normal horse serum (NHS) and 0.3% Triton X-100. Then primary antibody incubation was performed for 24–48 h at 4 °C with the affinity-purified anti-EP3R antibody (2 μg/mL) in PB containing 0.1% Triton-X-100 and 2% NHS. EP3R staining was completed with a biotinylated secondary donkey anti-rabbit IgG (1 : 100, AP182B, Chemicon, Hofheim, Germany) followed by visualization with diaminobenzidine hydrochloride reaction in the presence of hydrogen peroxide. Sections were washed, mounted onto gelatine-coated glass slides and coverslipped with Entellan (Merck, Darmstadt, Germany).

Immunofluorescent double labelling detection of both EP3R and viral surface antigens was performed as follows. Free floating coronal brain sections cut at 30 μm were incubated in PB containing 10% NHS and 0.3% Triton X-100 for 1 h at RT. Then a co-incubation of both primary antibodies was made with the sections for 24–48 h at 4 °C using the anti-EP3R antibody (2 μg/mL) and a specific antiserum against acetone-inactivated PRV raised in goat (1 : 20 000, generous gift from Lynn W. Enquist), diluted each in PB containing 0.1% Triton-X-100 and 2% NHS. Sections were washed and an avidin–biotin blocking was performed according to the kit description (Vector Laboratories, Linaris, Wertheim, Germany). In a next step a co-incubation of both secondary antibodies was made with a biotinylated donkey anti-rabbit IgG (1 : 100, AP182B, Chemicon, Hofheim, Germany) and an Alexa Fluor 488-conjugated donkey anti-goat IgG (1 : 500, Molecular Probes, MoBiTec, Göttingen, Germany), diluted each in PB containing 0.1% Triton-X-100 and 2% NHS for 90 min at RT. Fluorescent EP3R staining was completed with 1 h incubation at RT of Cy3-conjugated streptavidin (Jackson ImmunoResearch, dianova GmbH, Hamburg, Germany) diluted 1 : 1000 in PB. Sections were washed, mounted onto gelatine-coated glass slides and cover slipped with anti-fading PB/glycerol solution.

Spinal cord sections were analysed for viral surface antigens using a similar protocol as described above for fluorescent detection. However, the final visualization was made by diaminobenzidine hydrochloride reaction in the presence of hydrogen peroxide.

Microscopical analysis and brain maps

Brain and spinal cord sections were analysed with a conventional light/fluorescent microscope (Olympus BX50, Olympus Optical, Hamburg, Germany) and an inverted confocal Leica microscope (Leica DM IRBE, Bensheim, Germany) equipped with the appropriate filter sets to detect the fluorescent conjugates Alexa Fluor 488 and Cy3. Bright-field images were taken with an Olympus Camedia C-3030 digital camera (Olympus Optical, Hamburg, Germany). Fluorescence microscopy was performed using a Spot Insight B/W digital camera (Diagnostic Instruments, Visitron Systems, Puchheim, Germany). Confocal fluorescence images were taken at the Leica DM IRBE (Leica). Image editing software (MetaMorph 5.05, Adobe Photoshop) was used to adjust brightness and contrast, to change the graphic mode to four-colour (CMYK) and to combine the individual images into the figure plates.

To demonstrate the degree of viral infection that occurred throughout the brain in an animal already showing infection within the preoptic area, rat BAT 17 with a post-infection time of 71 h was chosen as the representative animal. Digital brain maps of the Paxinos Watson Rat brain atlas (Paxinos & Watson, 1998) were modified using Corel Draw software to match the infection seen within BAT 17. PRV infection was analysed in detail in sections of the forebrain, midbrain and brainstem at eight levels caudal to Bregma point (see Fig. 2A and B). This brain map analysis was accomplished by a semiquantitative table analysis (Table 1) comparing viral infection of BAT 17 with infection that occurred at the same Bregma levels in animals of either the same (BAT 16, 71 h) or the other survival time groups (BAT 13–15, 18, 54–71 h). In addition, the degree of double labelling for viral surface antigens and EP3R was semiquantitatively analysed in the late post-infection time group (BAT 16, 17). Data shown for both analysis procedures represent the numbers of PRV-infected neurons as well as the numbers of double-labelled neurons within a particular brain nucleus of one representative section at the different Bregma levels investigated (for Bregma levels see Fig. 2A and B and Table 1). For the table analysis, an attempt was made to standardize the comparison between the groups, based on the relative degree of infection detected within the paraventricular nucleus of the hypothalamus. This approach has been used effectively by others and ourselves utilizing the viral tracing technique (Jansen *et al*., 1992; Rotto-Percelay *et al*., 1992; Ter Horst *et al*., 1996; Hübschle *et al*., 1998). The terminology used to describe brain structures was modified from the rat brain map atlas of Paxinos & Watson (1998).

Quantitative analysis and statistics

The double labelling immunohistochemistry for EP3R and viral surface antigens was analysed qualitatively (see Fig. 3) and quantitatively (see Figs 4 and 5 and Table 1). Within two brain areas the degree of double labelling was most pronounced, namely (i) in the caudal brainstem raphe nuclei and there in particular within the rostral raphe pallidus nucleus (RPa), and secondly (ii) within the medial POA of the rostral hypothalamus, including ventral aspects of the median preoptic nucleus (MnPO) (for details see Table 1). Therefore, these two brain structures were chosen for the quantitative and statistical analysis. Counts were made on the computer screen from confocal digital images of the respective brain structure using Adobe Photoshop software. In detail, digital images of the brain sections were taken with the 40-fold objective at the confocal Leica microscope. Although one image proved to be enough to cover the outlines of the RPa, seven adjacent images were necessary to cover the medial POA (see Fig. 4, insets a–g). For the statistical analysis shown in Fig. 5 all cell counts of the seven individual medial POA images were combined to represent cell numbers for the whole medial POA of one forebrain section. For each animal three adjacent sections of the rostral RPa (at about −11.30 mm caudal to Bregma point) as well as the medial POA (at about −0.26 mm caudal to Bregma point) were analysed and all cell count data were combined to mean values for the respective animal. The time-dependent infection of the brain was additionally taken into consideration and further analysed using three rats each with a post-infection time of 54 h (BAT 7, 14, 18) or 66 h (BAT 8, 13, 14) and five animals (BAT 9, 11, 12, 16, 17) for the 71-h survival time. The quantitative data on the RPa and the medial POA shown in Fig. 5 therefore finally represent means (three RPa or medial POA sections per individual animal) of the means (animals of a distinct post-infection time group) ± SEM.

Statistics was performed with the SigmaPlot/SigmaStat analysis software (SPSS Science Software GmbH, Erkrath, Germany). Differences between the post-infection time groups were tested for the RPa with one-way ANOVA followed by the *post hoc* Tukey test. A statistical significance was accepted for $P < 0.05$.

Results

In accordance with our previous studies (Nakamura *et al*., 1999, 2000, 2001, 2002), EP3R-like immunoreactivity (EP3R-LI) on cell bodies of neurons was widely observed throughout the brain. Within the POA, EP3R-LI neurons were equally densely spread in its medial subnuclei including the ventral MnPO, the medial preoptic nucleus, the ventromedial preoptic nucleus (VMPO) and medial parts of the ventrolateral preoptic nucleus (VLPO) (Fig. 1A). After injection of PRV-Ba into the interscapular BAT of rats, neurons within the POA became virally infected as previously demonstrated by two different groups (Oldfield *et al*., 2002; Cano *et al*., 2003). Interestingly, these PRV-infected neurons were found with a similar distribution in the very same medial subnuclei of the POA, in which EP3 receptor expressing neurons are concentrated (Fig. 1A and B).

Distribution of PRV-infected neurons 71 h after BAT inoculation

Viral infection throughout the brain of the rat BAT 17 was considered as being representative for the 71-h post-infection time group. The distribution of PRV-infected neurons in this animal is schematically presented in the brain maps of Fig. 2A and B at eight different Bregma levels along the neuroaxis at which most prominent viral infection was observed.

The 71-h post-infection time was the time point chosen to observe a substantial number of infected forebrain neurons. Within the forebrain, infection was most prominent in the hypothalamus (Fig. 2A) with a tendency of a higher number of PRV-infected hypothalamic neurons on the side ipsilateral to BAT injection. At Bregma −0.26 mm, viral infection was observed within several subnuclei of the medial POA, which included the ventral MnPO, the medial preoptic nucleus, the VMPO and the VLPO. In addition, some virally infected neurons were seen more laterally within the parastrial nucleus. Further caudally, at Bregma levels −1.4 to −1.8 mm infection was most pronounced in the parvocellular subnuclei of the hypothalamic paraventricular nucleus (PVN) and in individual dispersed neurons located throughout the retrochiasmatic area (RCh). Some virally infected neurons were additionally observed within the anterior hypothalamic area (AHA), the lateral hypothalamic area (LHA), the zona incerta, the supraoptic nucleus (SON) and the suprachiasmatic nucleus. Within the caudal hypothalamus (Bregma −3.3 mm) many infected neurons were found in the LHA, the dorsal and the posterior hypothalamic area (DA, PH). Moderate infection was seen in lateral parts of the arcuate nucleus (ARC) and the adjacent periarcuate area (PAA). However, very little or no viral infection was observed within the ventromedial hypothalamic nucleus, as previously described after PRV inoculation into the interscapular BAT of rats (Oldfield *et al*., 2002; Cano *et al*., 2003) and Siberian hamsters (Bamshad *et al*., 1999). Within the dorsomedial hypothalamic nucleus (DMH), the compact subnucleus also showed no PRV-infected cells, whereas other DMH subnuclei and in particular the dorso-lateral part showed some PRV-infected neurons.

Extrahypothalamic forebrain sites that showed a substantial number of virally infected neurons proved to be the motor cortex and to some extent the adjacent somatosensory cortex (M/SS). In particular, layer 4 and 5 neurons in rostral aspects of the M/SS (Bregma −0.26 mm) on the side contralateral to BAT injection were labelled.

At the midbrain Bregma level −8.3 mm (Fig. 2B) the most heavily infected area proved to be the ventrolateral periaqueductal grey (VLPAG). Infected VLPAG neurons were observed bilaterally with no dominance for the ipsi- or contralateral side. Infection was also

TABLE 1. Time-dependent infection of brain structures after PRV-Ba injection into the right interscapular BAT and colocalisation of EP3R

	PRV-Ba infection						EP3R and PRV-Ba	
	54 h		66 h		71 h		71 h	
Brain nuclei	BAT 15	BAT 18	BAT 13	BAT 14	BAT 16	BAT 17	BAT 16	BAT 17
Bregma −0.26 mm								
Preoptic area								
Medial POA	−/−	−/−	−/−	−/−	+/+	++/+	+/+	+/+
Median preoptic nucleus*	−	−	−	−	+	+	+	+
Parastrial nucleus	−/−	−/−	−/−	−/−	−/−	5/3	−/−	−/−
Vascular organ of the lamina terminalis*	−	−	−	−	+	++	4	+
Ventrolateral preoptic nucleus	−/−	−/−	−/−	−/−	4/3	5/3	−/−	−/1
Ventromedial preoptic nucleus	−/−	−/−	−/−	−/−	3/2	4/3	−/−	−/1
Cortex								
Motor/Somatosensory cortex§	−/−	−/−	−/−	−/−	−/+	1/++	−/−	−/−
Bregma −1.40 mm								
Hypothalamus								
Anterior hypothalamic area	−/−	−/−	−/−	−/−	−/−	3/−	−/−	1/−
Lateral hypothalamic area	−/−	−/−	−/−	−/−	−/−	1/3	−/−	−/−
Medial POA	−/−	−/−	−/−	−/−	4/2	3/−	2/1	1/−
Paraventricular nucleus	3/2	2/1	+/+	+/3	++/+	++/+	−/1	1/1
Retrochiasmatic area*	−	−	−	−	2	2	1	2
Suprachiasmatic nucleus	−/−	−/−	−/−	1/−	4/2	+/3	−/−	−/−
Bregma −1.80 mm								
Hypothalamus								
Anterior hypothalamic area	−/−	−/−	−/−	−/−	4/3	2/1	−/−	−/−
Lateral hypothalamic area/Zona incerta§	−/−	2/−	1/−	−/1	+/+	2/1	2/1	−/1
Paraventricular nucleus	+/+	+/3	++/++	++/++	++/++	++/++	−/−	1/−
Retrochiasmatic area*	−	−	−	−	+	++	5	+
Supraoptic nucleus	−/−	−/−	−/−	−/−	−/−	−/2	−/−	−/1
Cortex								
Motor/Somatosensory cortex§	−/−	−/−	−/−	−/−	−/2	2/+	−/−	−/−
Bregma −3.30 mm								
Hypothalamus								
Arcuate nucleus/Periarcuate area§	1/−	−/−	3/4	2/1	+/+	+/+	+/5	4/2
Dorsal/Posterior hypothalamic area§	−/−	−/−	4/+	2/+	++/+	++/++	4/3	2/−
Dorsomedial hypothalamic nucleus	−/−	−/−	2/1	1/−	+/+	+/+	−/−	−/−
Lateral hypothalamic area	−/−	−/−	+/+	4/+	++/++	++/++	2/2	−/1
Bregma −8.30 mm								
Midbrain								
Periaqueductal grey	−/−	−/−	+/3	5/3	++/++	++/++	2/3	1/−
Pontine reticular nucleus/ Ventrolateral tegmental area§	−/−	−/−	+/1	3/1	++/++	++/++	3/1	1/1
Bregma −9.80 mm								
Brainstem								
A5-region/Rostroventrolateral medulla§	4/3	3/2	+/+	+/+	++/++	++/++	+/+	+/4
Locus coeruleus/Subcoeruleus nucleus§	2/1	−/−	+/+	+/−	++/++	++/++	4/3	5/3
Pontine reticular nucleus	−/−	−/−	4/1	2/1	++/+	++/++	1/−	−/−
Raphe magnus nucleus/Raphe pallidus nucleus*§	−	−	5	+	++	++	++	++
Below and lateral to pyramidal tract*	−	−	−	−	2	5	1	4
Bregma −11.30 mm								
Brainstem								
A5-region	1/1	−/−	5/1	4/2	5/3	+/+	2/2	5/+
C3-, B4-region/Dorsal paragigantocellular nucleus*§	4	−	+	+	++	++	1/2	−/1
Gigantocellular reticular nucleus/ Lateral paragigantocellular nucleus§	2/−	−/−	++/++	++/++	++/++	++/++	+/+	4/+
Intermediate reticular nucleus	−/−	−/−	2/1	2/1	−/1	5/1	−/−	−/−
Raphe magnus nucleus/Raphe obscurus nucleus*§	4	−	++	++	++	++	+	+
Raphe pallidus nucleus*	3	+	+	+	++	++	++	++
Rostroventrolateral medulla	−/1	+/+	4/2	−/4	+/+	+/+	1/2	2/−
Below and lateral to pyramidal tract*	2/1	3/1	+/4	4/5	+	+	+	+

(Continued on next page)

TABLE 1. continued

Brain nuclei	PRV-Ba infection						EP3R and PRV-Ba	
	54 h		66 h		71 h		71 h	
	BAT 15	BAT 18	BAT 13	BAT 14	BAT 16	BAT 17	BAT 16	BAT 17
Bregma −13.80 mm								
Brainstem								
Area postrema*	−	−	1	1	+	++	−	1
Caudoventromedial medulla	−/−	−/1	+/+	+/+	++/+	++/++	4/3	2/−
Intermediate reticular nucleus	−/−	−/−	3/1	1/1	+/+	+/+	−/−	−/−
Lateral reticular nucleus/Caudo-ventrolateral reticular nucleus§	−/−	−/−	5/4	+/5	++/+	++/++	3/2	4/1
Nucleus of the solitary tract	−/−	−/−	2/1	1/−	+/+	+/+	1/1	−/1
Raphe obscurus nucleus*	1	1	+	4	+	+	+	+
Raphe pallidus nucleus*	+	4	+	+	+	+	+	+

Where the solidus (/) is used, the left and right hand symbols indicate infection on the ipsi- and contralateral side, respectively. *No separation of ipsi- and contralateral data; §combined analysis of brain nuclei. ++, ≥21 PRV-Ba-infected or double-labelled cells; +, 6–20 PRV-Ba-infected or double-labelled cells; −, no PRV-Ba-infected or double-labelled cells; numbers 1–5 indicate actual counts of PRV-Ba-infected or double-labelled cells.

determined in the oral part of the pontine reticular nucleus and the ventrolateral tegmental area. One further caudal pontine brain area showing some virally infected neurons 71 h post-inoculation was the parabrachial nucleus and in particular its lateral and medial subnuclei. The vast majority of infected parabrachial nucleus neurons was detected around the Bregma levels −8.80 to −9.16 mm.

Using the post-infection time of 71 h, many infected brain nuclei were found within the medulla oblongata (Bregma levels −9.8 to −13.8 mm), amongst them several ventrally located nuclei as well as the locus coeruleus (LC), the subcoeruleus nucleus (SubC), the intermediate reticular nucleus, the area postrema and the solitary tract nucleus (Fig. 2B). No dominance of infection for either the ipsi- or the contralateral side could be determined. Ventrally located medullary sites with strong infection proved to be all caudal raphe nuclei, the RPa, raphe magnus nucleus (RMg), raphe obscurus nucleus (ROb) and those nuclei located immediately lateral to them, such as the gigantocellular reticular nucleus (GiA), lateral paragigantocellular nuclei (LPGi), rostroventrolateral (RVL), caudoventromedial (CVM) and caudoventrolateral reticular nuclei (CVL). As for the RPa, infection proved to be strongest in the rostral RPa at about Bregma level −11.3 mm. Further caudally the number of infected RPa neurons was markedly diminished.

Stepwise PRV infection 54–71 h after BAT inoculation

Viral infection observed in BAT 17 (the representative animal of the 71-h post-infection group) was compared with viral infection that occurred in rats of the same or the other survival time groups (54 and 66 h) using a semi-quantitative analysis procedure. The degree of infection is shown in Table 1, revealing a clear time-dependent spread of the virus to hierarchically higher brain sites as well as a increase of viral infection in a particular brain structure during this time course.

Whereas infection in animals with 71-h survival time was already prominent in many hypothalamic and cortical structures, a markedly decreased number of PRV-infected neurons was observed in forebrain structures of the 66-h post-injection group. In more detail, there was a lack of labelling within the POA, cortex, parastrial nucleus, RCh, AHA and SON. However, some potentially hypothalamic third-order neurons showed viral infection, such as neurons of the parvocellular PVN,

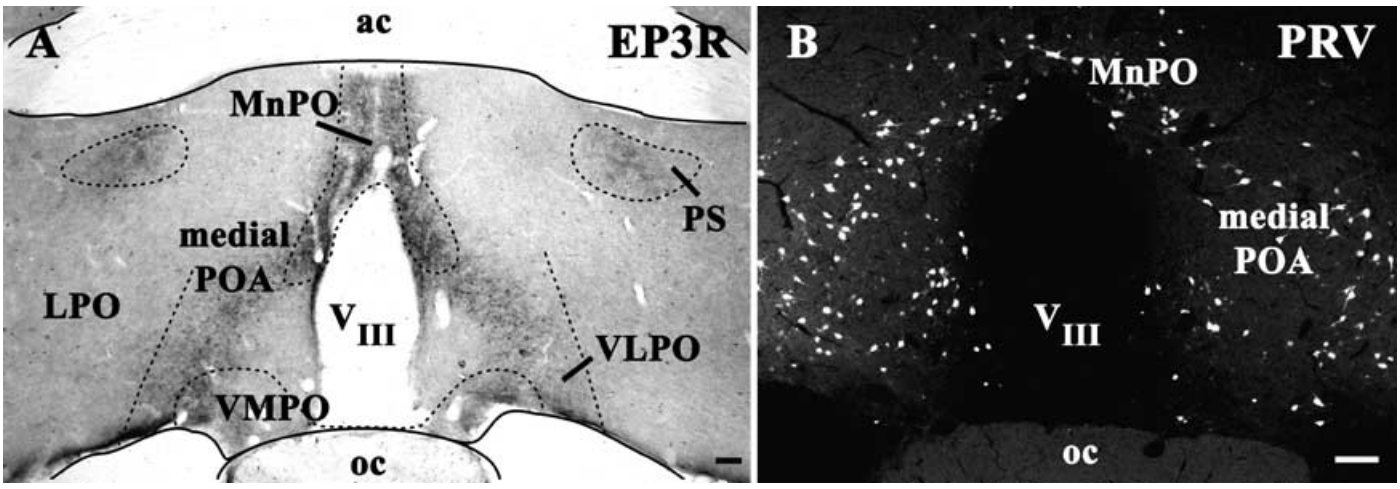

FIG. 1. Photomicrographs from rat brain, illustrating the POA distribution of prostaglandin E receptor subtype EP3 (EP3R) immunoreactive cells (A) as compared with pseudorabies virus (PRV)-labelled neurons 71 h after PRV injection into the right interscapular brown adipose tissue (B). Scale bars represent 100 μm. ac, anterior commissure; LPO, lateral POA; MnPO, median preoptic nucleus; POA, preoptic area; oc, optic chiasm; PS, parastrial nucleus; V_{III}, third ventricle; VLPO, ventrolateral preoptic nucleus; VMPO, ventromedial preoptic nucleus.

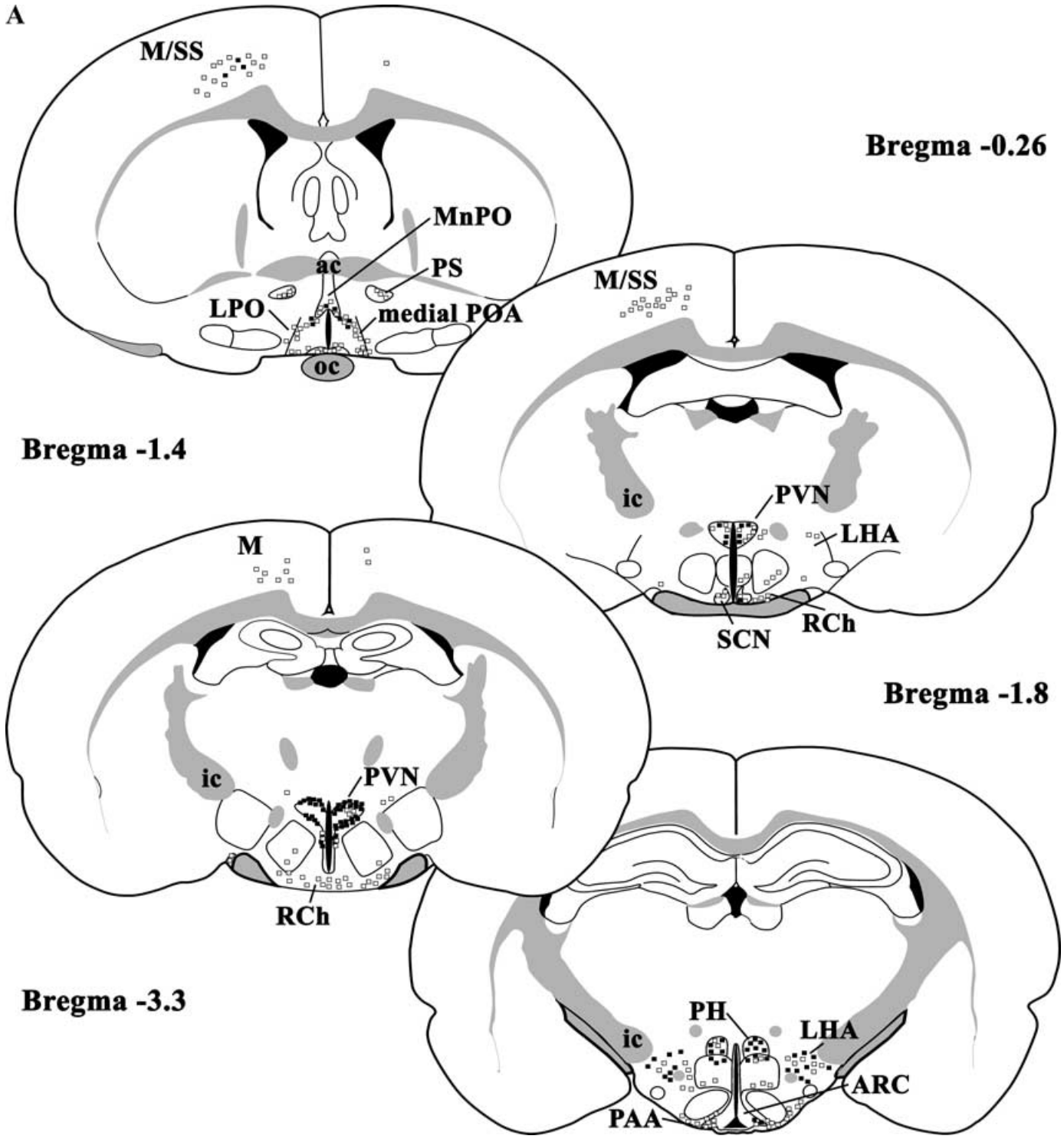

FIG. 2. Brain maps showing the distribution of PRV-infected neurons in coronal sections from rostral (A, Bregma −0.26 to −3.30 mm) to caudal (B, Bregma −3.30 to −13.80 mm) rat brain levels after PRV injection into the right interscapular brown adipose tissue (BAT). The distribution of infected neurons is taken from a representative experiment with a survival time of 71 h (rat BAT 17, see also Table 1). Open squares represent 1 infected neuron and black filled squares represent a cluster of five infected neurons. A5, A5 noradrenaline cells; ac, anterior commissure; AP, area postrema; ARC, arcuate nucleus; CVL, caudoventrolateral reticular nucleus; CVM, caudoventromedial reticular nucleus; GiA, gigantocellular reticular nucleus, alpha part; ic, internal capsule; IRt, intermediate reticular nucleus; LC, locus coeruleus; LHA, lateral hypothalamic area; LPGi, lateral paragigantocellular nucleus; LPO, lateral POA; LRt, lateral reticular nucleus; M/SS, motor/sensory cortex; MnPO, median preoptic nucleus; POA, preoptic area; NTS, solitary tract nucleus; oc, optic chiasm; PAA, periarcuate area; PAG, periaqueductal grey; PH, posterior hypothalamic area; PnO, pontine reticular nucleus, oral part; PS, parastrial nucleus; PVN, paraventricular hypothalamic nucleus; py, pyramidal tract; RCh, retrochiasmatic nucleus; RMg, raphe magnus nucleus; ROb, raphe obscurus nucleus; RPa, raphe pallidus nucleus; RVL, rostroventrolateral reticular nucleus; SCN, suprachiasmatic nucleus; SubC, subcoeruleus nucleus; VLPAG, ventrolateral periaqueductal grey; VLTg, ventrolateral tegmental area.

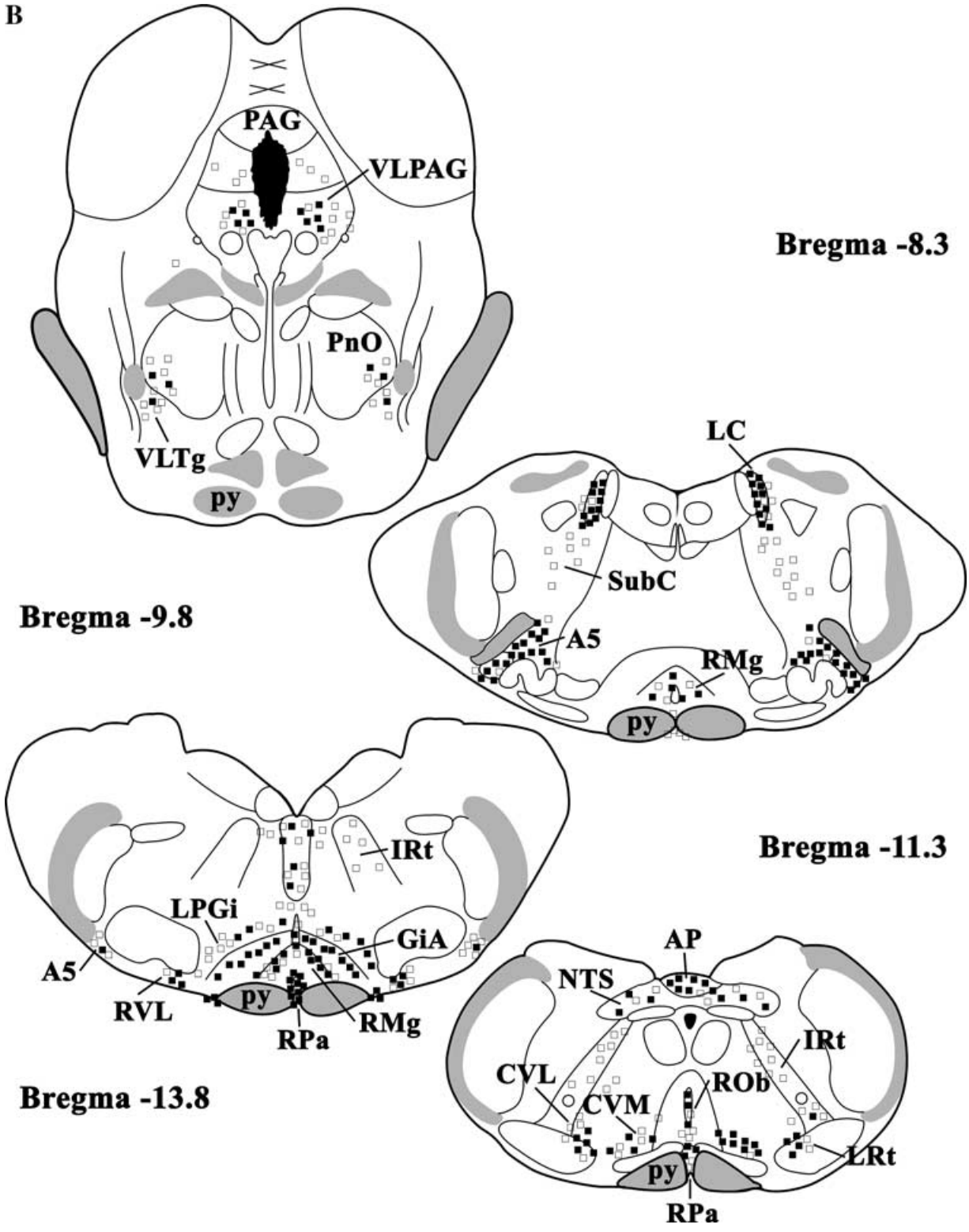

FIG. 2. continued

LHA, DA, PH, lateral ARC and PAA. Amongst those hypothalamic nuclei, the PVN as a major exception already showed a high number of infected neurons. At 54 h post infection, the overall number of infected neurons was again strongly reduced as compared with the 66-h survival time group. Several brain nuclei showed PRV-infected neurons, such as the PVN, LHA, PAA, LC, SubC, A5 noradrenaline cell area, RVL, GiA, the C3-B4 regions and the caudal raphe nuclei. Amongst them the PVN and the RPa already contained a relatively high number of infected cells, as compared with the other brain structures labelled after 54 h post-injection.

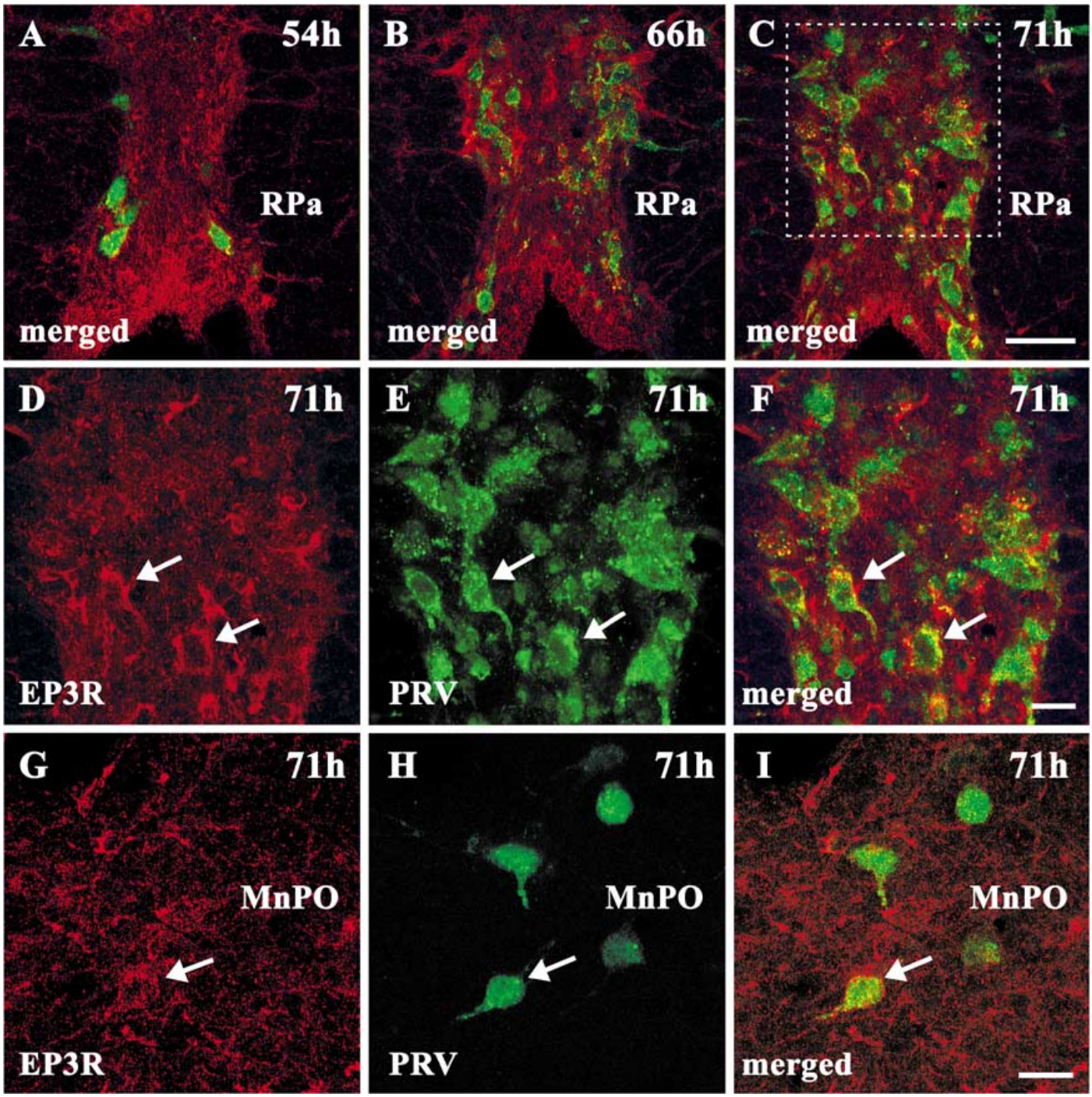

FIG. 3. Prostaglandin E receptor subtype EP3 (EP3R) immunoreactive neurons in the raphe pallidus nucleus (RPa, A–F) and the median preoptic nucleus (MnPO, G–I) project to the interscapular brown adipose tissue (BAT) of the rat. Confocal microscopical images show EP3R immunoreactivity in red and pseudorabies virus (PRV-) infected neurons in green. Note the time-dependent increase of PRV infection in the rostral raphe pallidus nucleus (A–C) as shown for animals with 54–71 h survival time. The dotted square in C is further enlarged in D–F and reveals that neurons of the raphe pallidus nucleus that became virally infected after BAT injections express EP3R immunoreactivity. Co-localization is indicated by the white arrows. Virally infected neurons of the medial POA, as shown here for the MnPO, also express EP3R immunoreactivity (G–I, white arrow). Scale bar in A–C represents 50 μm, scale bars in D–I represent 20 μm.

PRV-infected neurons that express prostaglandin E receptor subtype EP3 within the rostral raphe pallidus and the medial POA

Neurons double-labelled with EP3R and viral surface antigens were particularly numerous in two brain regions, within the caudal brainstem raphe nuclei, in particular there in the rostral RPa, as well as within the medial POA including ventral aspects of the MnPO (Table 1, Figs 3–5). Whereas the number of PRV-infected neurons increased with longer post-infection time for the RPa (Fig. 3A–C, in green), PRV-infected neurons within several subnuclei of the medial POA could only be detected within the 71-h post-infection time group, as shown for the MnPO in Fig. 3H and I. To analyse the number of double-labelled neurons within the RPa and the medial POA (see white arrows in Fig. 3D–I), cell counts were performed.

Such cell counts are shown in Fig. 4 in a brain map analysis of a POA section at about Bregma level −0.26 mm taken from BAT 17, the representative animal of the 71-h survival time group. The cell numbers and their location are shown for EP3R-positive, PRV-positive and double-labelled cells within the medial POA. About 50% of all medial POA neurons that became virally infected after PRV injection into the right interscapular BAT also expressed the EP3R (Fig. 4).

A more detailed quantitative analysis and statistical examination of the virally infected cells that express EP3R was performed for both brain structures, the RPa and the medial POA. For the medial POA, we observed that of all PRV-infected neurons a subpopulation of about 40% also expressed the EP3R. For the RPa, we found no differences in the total number of EP3R-LI cells amongst the different post-infection time groups (Fig. 5). By contrast, a time-dependent significant increase in the number of PRV-infected RPa neurons occurred with longer survival times ($P < 0.05$). The cell number of double-labelled neurons significantly increased from 6.0 ± 0.19 (54 h) to 18.6 ± 1.0 (66 h) and to 25.2 ± 1.2 (71 h), respectively ($P < 0.05$). These actual cell numbers were then recalculated into percentage of double-labelled cells of either all EP3R-positive cells or all PRV-infected cells within the RPa. The percentage of those RPa cells expressing the EP3R and showing viral infection significantly increased with longer survival times from $11.7 \pm 0.5\%$ (54 h) to $36.6 \pm 2.1\%$ (66 h) and to $50.1 \pm 1.7\%$ (71 h), respectively ($P < 0.05$). However, the percentage of double-labelled neurons of all PRV-infected cells within the RPa did not change with longer survival time. This was still of particular interest because approximately two-thirds (65–76%) of those RPa neurons that polysynaptically project to the BAT also expressed the EP3R and this proved to be independent of the investigated post-infection time points.

For the medial POA, the total number of EP3R-LI cells amongst the different post infection time groups was not determined (Fig. 5, nd). No viral infection could be observed within the medial POA, when using the shorter survival times (Fig. 5, 'ni'). Therefore, the quantitative analysis for the medial POA is restricted to the 71-h post-infection time group. The actual cell number of double-labelled neurons within the medial POA (9.7 ± 1.7 cells) seemed to be surprisingly low when compared with the total number of EP3R-positive cells (117.5 ± 6.5). However, when the percentage of double-labelled cells of all PRV-infected cells within the medial POA was calculated, it became obvious that about 40% of those medial POA neurons that polysynaptically project to the BAT also expressed the EP3R.

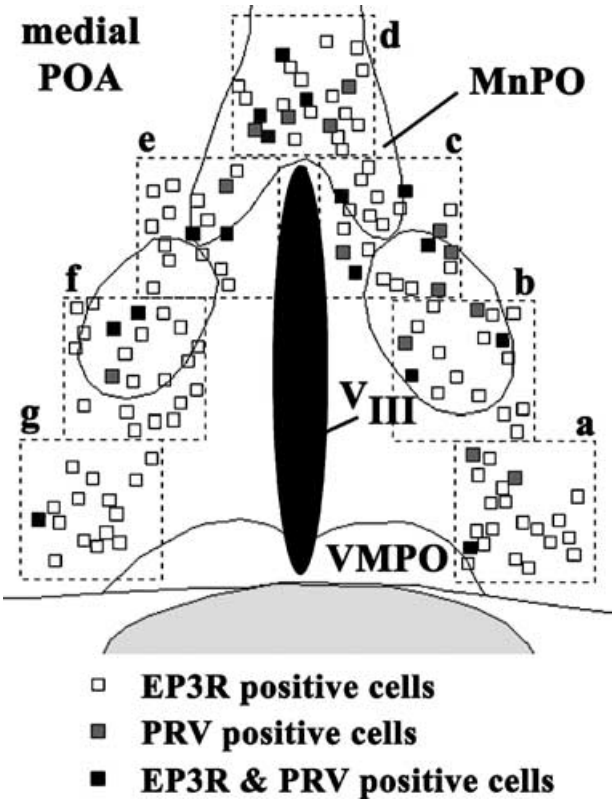

FIG. 4. Brain map of the rat medial preoptic area (POA, at about Bregma −0.3 mm) illustrating the distribution and co-localization of prostaglandin E receptor subtype EP3 (EP3R)-positive cells with neurons that show viral infection after pseudorabies virus (PRV) injection into the right interscapular brown adipose tissue (BAT). The data are taken from a representative experiment with a survival time of 71 h (rat BAT 17, see also Fig. 2A and B and Table 1). EP3R-positive cells are indicated by the open squares, PRV-positive neurons by the filled grey squares and double-labelled cells by the filled black squares. The distribution and co-localization was documented with the help of a detailed analysis of seven adjacent confocal photomicrographs (a–g, dotted squares) covering several subnuclei of the medial POA, including the median preoptic nucleus (MnPO) and the ventromedial preoptic nucleus (VMPO). This analysis was also used to document quantitatively the percentage of EP3R/PRV co-labelling within the medial POA (see Fig. 5).

Other PRV-infected brain structures showing a lower degree of prostaglandin E receptor subtype EP3 co-localization

Other supraspinal brain structures also showed a substantial number of co-labelled neurons within the 71-h post-infection group (Table 1, Fig. 6); however, the degree of EP3R and viral antigen co-localization on cell bodies was visibly lower. This was partly because those areas often showed no clustered accumulation of double-labelled cells as in the RPa and parts of the medial POA, but a more spread and dispersed labelling of co-localized cells. In Fig. 6 the hierarchical order of infected brain nuclei during an early stage of infection (first appearance of infection in a particular brain structure) was schematically combined with the occurrence of a substantial number (more than five) of PRV-infected cells that express the EP3R at 71 h post-infection. Brain nuclei with such substantial to high amounts of double-labelled cells were highlighted with grey ellipses. Besides those two brain areas with highest amounts of PRV and EP3R co-localization (RPa and medial POA, for details see above) other brainstem nuclei showed a moderate number of double-labelled cells. Amongst these were the classical sympathetic premotor areas the A5 region, the rostroventrolateral and ventromedial medulla as well as the GiA, the LPGi and the SubC. In addition, caudal raphe nuclei neurons other than from the RPa, such as neurons from the RMg, the ROb and neurons beneath and lateral to the pyramidal tract, showed some co-labelling.

Within the hypothalamus some spread, individual co-labelled cells were located in its ventral aspects within the RCh and the PAA as well as in the dorsal and posterior hypothalamus. Further rostrally the vascular organ of the lamina terminalis also showed some co-localized cells. The sympathetic outflow to the interscapular BAT, which might be driven by central PGE_2 action under febrile conditions, could also be modulated via these supraspinal structures.

Discussion

Non-shivering thermogenesis occurs under various (patho-)physiological conditions such as cold exposure, overeating and fever. Therefore, it is not surprising that widespread brain areas can be found as the neuroanatomical basis for central BAT control in the rat (Oldfield *et al.*, 2002; Cano *et al.*, 2003; present study). The similarity in the pattern of brain PRV infection within these studies might favour the idea of a common overlapping central sympathetic outflow. Abundant evidence

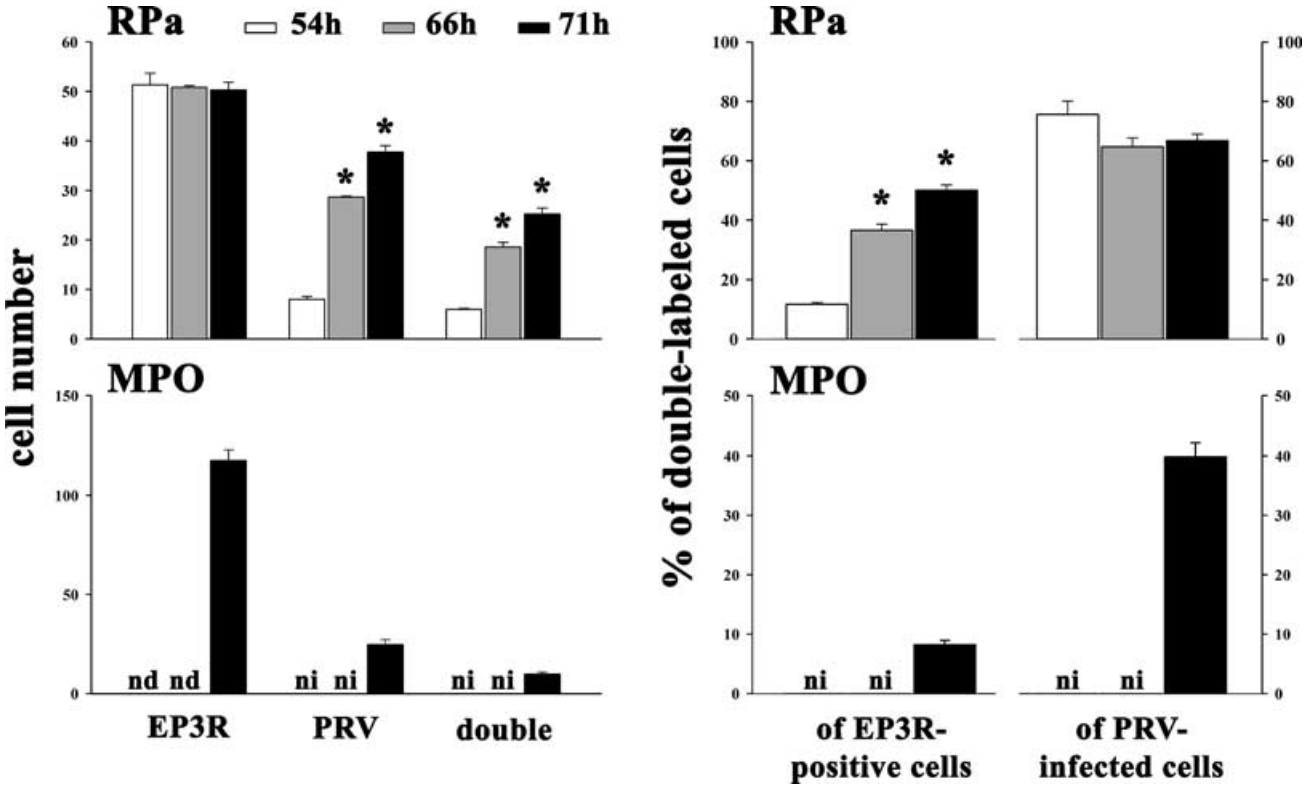

FIG. 5. Quantitative co-localization analysis investigating cells with prostaglandin E receptor subtype EP3 (EP3R) immunoreactivity and neurons that show viral infection after pseudorabies virus (PRV) injection into the right interscapular brown adipose tissue. The cell number and the percentage of double-labelled cells for the raphe pallidus nucleus (RPa) is depicted from the upper bar charts. The data for the medial preoptic area (MPO) are given in the lower bar graphs. For each animal three sections of the rostral RPa (at about Bregma −11.3 mm, $N = 3$–5) and three sections of the MPO (at about Bregma −0.26 mm, $N = 5$) were used for the analysis of the respective post-infection time (white bars = 54 h; grey bars = 66 h, black bars = 71 h). Values are given as mean ± SEM. Statistical analysis was performed by one-way ANOVA with subsequent *post hoc* Tukey test analysis, revealing a statistical significance at $^{*}P < 0.05$. nd, not determined; ni, no infection observed.

has been provided to show that the central control of sympathetic outflow to interscapular BAT of the rat is strongly exerted by the hypothalamus, a major brain area involved in thermoregulation and feeding behaviour. On the basis of these three PRV studies, however, involvement of distinct anatomical circuitries in central BAT control during cold exposure, overeating or fever has now been established, being most obvious at the level of the hypothalamus. Whereas the ventromedial parvocellular PVN was shown to be important in the control of cold-evoked thermogenesis (Cano *et al*., 2003), it seems that brain nuclei of the caudo-basal hypothalamus such as the lateral ARC, RCh, PAA, LHA and the perifornical area might control body heat generation after overeating (Oldfield *et al*., 2002). By contrast, the present study suggests that the medial POA within the rostral hypothalamus seems to control non-shivering thermogenesis under conditions of prostaglandin-dependent fever. In more detail, this neuroanatomical study describes the prevalence of prostaglandin E receptor subtype EP3-expressing neurons in efferent pathways to the interscapular BAT, thereby providing information on those brain structures that could directly influence sympathetic BAT control via prostaglandin-sensitive mechanisms.

In general, our results show that such a central BAT control might be modulated by several supraspinal groups of neurons located throughout the brain. Different stimulus-specific neural pathways might exist to modulate BAT functions under different (patho-)physiological circumstances. Nevertheless, our anatomical data predominantly point to two hot spots that might influence the central control of BAT functions under PGE_2-fever, namely the medial POA and the rostral RPa.

BAT thermogenesis controlled by PGE_2-sensitive neurons of the medial POA

Our functional experiments have recently shown that PGE_2 microinjection into the medial POA elicited pyrogenic signals that are transmitted to the rostral RPa (Nakamura *et al*., 2002), a brainstem nucleus known to contain premotor neurons controlling sympathetic drive of BAT functions (Morrison *et al*., 1999). Indeed, the present tract-tracing study neuroanatomically confirms that neurons within the medial POA equipped with the prostaglandin E receptor subtype EP3 have polysynaptical projections to the interscapular BAT, thereby supporting the functional studies by Scammel *et al*. (1996) and Nakamura *et al*. (2002). The quantitative analysis showed that about 40% of those medial POA neurons that polysynaptically project to the BAT also expressed the EP3R. However, several uncertainties on the role of PGE_2-sensitive medial POA neurons in central BAT control became evident and need to be addressed.

The cellular responses to PGE_2 depend on the expression of specific EP receptor subtypes on brain cells and, during fever, distinct neuronal PGE_2 receptor subtypes may regulate brain functions in a region-specific manner. There is a debate as to which particular prostaglandin E receptor subtypes are crucial for fever production (Oka *et al*., 1994, 2000; Ushikubi *et al*., 1998; Zhang & Rivest, 2000). It has been suggested that the EP1 receptor subtype mediates prostaglandin-induced hyperthermia, whereas EP3R was found to be involved in the regulation of thermal hyperalgesia as well as fever generation in response to both exogenous and endogenous pyrogens (Oka *et al*., 1994; Hosoi *et al*., 1997; Ushikubi *et al*., 1998). Studies in which the

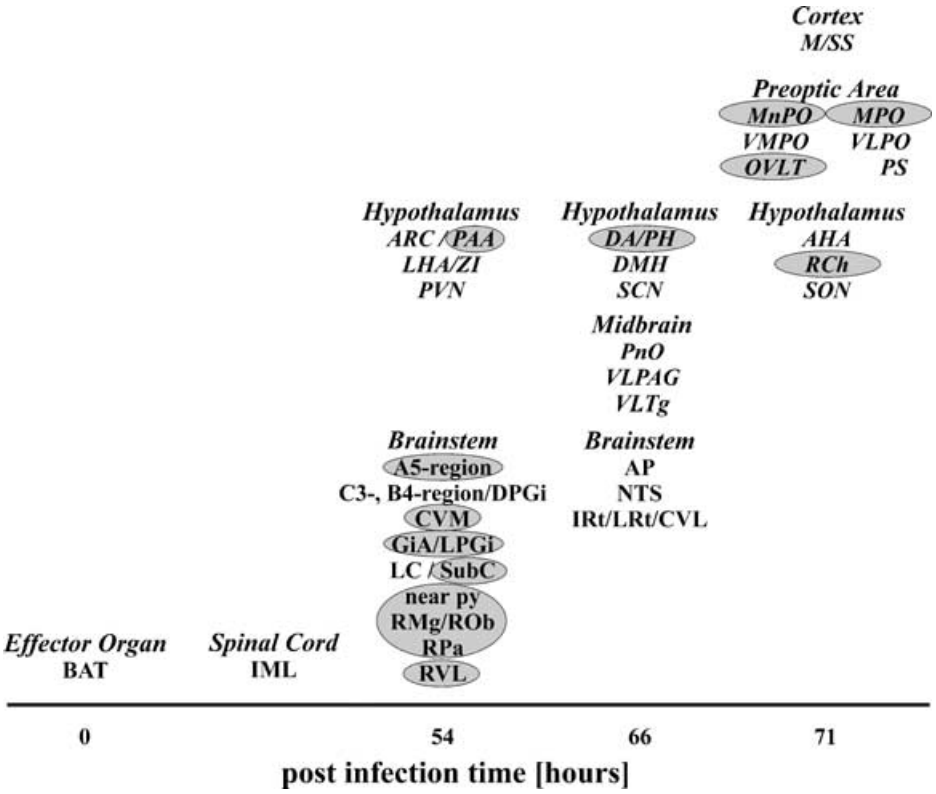

FIG. 6. Time-ordered list of brain structures infected after pseudorabies virus injection into the right interscapular brown adipose tissue (BAT) and evidence of its co-localization with the prostaglandin E receptor subtype EP3 (EP3R). Three post-infection time points (54, 66 and 71 h) were investigated. Note that only the first appearance of the virus in a particular brain structure is listed at the respective post-infection time point. Note also that only those brain structures showing a substantial number of co-localization (more than five) of virally infected neurons with the EP3R from the 71-h post-infection group were considered within this diagram. Such brain structures are highlighted with grey ellipses. The analysis was performed in the same representative animals (BAT 13 – BAT 18) and at the same Bregma levels (−0.26 to −13.8 mm) as shown in Table 1. The brain nuclei nomenclature and their abbreviations are given within the list of abbreviations.

EP3R gene in mice was deleted provides strong evidence that EP3R is required at least for the initial fever phase (< 1 h) after pyrogenic challenges (Ushikubi *et al*., 1998). Intense expression of EP3R is known for the ventral MnPO, the medial preoptic nucleus and the adjacent medial POA (see Fig. 1A and Nakamura *et al*., 1999, 2000; Ek *et al*., 2000). These are exactly those subnuclei of the medial POA in which in the present study the vast majority of virally infected neurons were found expressing the EP3R. Viral infection within the VMPO was observed to a much lesser extent and consequently fewer double-labelled neurons were determined for this POA structure. The VMPO has been described as the most PGE_2-sensitive pyrogenic zone within the medial POA (Scammel *et al*., 1996), but the expression of at least the prostaglandin E receptor subtype EP3 was found to be low to moderate (Nakamura *et al*., 1999, 2000; Oka *et al*., 2000). By contrast, a very strong expression of prostaglandin E receptor subtype EP4 was determined with *in situ* hybridization for the VMPO (Oka *et al*., 2000). As for the functional relevance of the VMPO prostaglandin E receptor subtype EP4R in the febrile response, it seems that this PGE_2 receptor subtype mediates the effects of circulating cytokines via activation of neurons producing corticotrophin-releasing hormone (CRF) and the hypothalamic–pituitary–adrenal axis (Zhang & Rivest, 2000). One possible means of EP4R action within the medial POA would thus involve efferent VMPO projections towards the hypothalamic PVN CRF-producing neurons (Scammel *et al*., 1998).

In conclusion, it seems that distinct PGE receptor subtype-specific fever pathways emerge from the POA and give rise to parallel efferent pathways connected to autonomic regulatory brain regions involved in febrile responses. For example, EP4R-expressing POA neurons seem to act via the VMPO–PVN axis (Oka *et al*., 2000; Zhang & Rivest, 2000), whereas a subpopulation of EP3R-expressing POA neurons efferently convey pyrogenic signals directly towards the RPa (Nakamura *et al*., 2002), known to contain sympathetic premotor neurons for BAT control (Loewy, 1981; Morrison *et al*., 1999). A further alternative fever pathway could involve PGE_2-sensitive projections from the POA to the dorsomedial hypothalamus. A recent study suggests that the PGE_2-induced thermogenic action elicited by POA microinjections is adjusted through the neuronal activity within the DMH (Zaretskaia *et al*., 2003). Indeed our data show PRV-infected neurons within the DMH at exactly the same DMH site (dorso-lateral DMH at about Bregma −3.30 mm) that proved to be most effective in the Zaretskaia *et al*. (2003) study. However, in no single case could a PRV-infected DMH neuron be co-localized with the EP3R, thereby excluding a putative DMH-intrinsic PGE_2 sensitivity that might be important for central BAT control. The distinct region-specific expression of different PGE receptor subtypes within POA neurons and their distinct efferent projections might therefore help to control different neuronal effector functions or reciprocally modulate each other's activities, as previously suggested by Ek *et al*. (2000).

BAT control by neurons of the rostral raphe pallidus nucleus and its putative modulation by local PGE_2 action

Throughout the entire brain, the largest number of neurons that expressed the EP3R and became virally infected after BAT inoculation

was found within the rostral RPa. There is no doubt that a subpopulation of RPa neurons represent sympathetic premotor neurons for BAT control (Morrison *et al*., 1999) and possess direct projections to the intermediolateral cell column (Loewy, 1981). As revealed by conventional tracing studies, medullary raphe nuclei neurons in turn receive projections from various brain areas, amongst them also projections from the POA (Simerly & Swanson, 1988; Hermann *et al*., 1997; Murphy *et al*., 1999). We previously observed that pyrogenic transmission from the EP3R-expressing POA neurons via direct projections to RPa neurons is likely to be GABAergic and that under febrile conditions the EP3R-mediated release of the tonic inhibition of GABAergic inputs from the POA to these RPa neurons triggers the activation of BAT thermogenesis (Nakamura *et al*., 2002).

As previously shown, there is an abundant expression of the EP3R on RPa neurons (Ek *et al*., 2000; Nakamura *et al*., 2000, 2001), and this is in agreement with results obtained here. The present tract-tracing experiments clearly demonstrate that both EP3R-positive as well as EP3R-negative neurons in the RPa polysynaptically project to the interscapular BAT, constituting about 70% and 30% of PRV-positive cells, respectively. There are thus two alternative mechanisms that could explain the role of RPa neurons in premotor BAT control.

1. EP3R-negative RPa premotor neurons. Based on the knowledge that EP3R-expressing neurons within the RPa are predominantly serotonergic, but that non-serotonergic RPa neurons respond with Fos-expression to intracerebroventricular PGE_2 administration (Nakamura *et al*., 2001, 2002), one hypothesis would be that those 30% of PRV-infected RPa neurons that do not express the EP3R are likely to play the dominant role in PGE_2-induced BAT thermogenesis. Microinjections of the $GABA_A$ receptor agonist muscimol into the RPa blocked PGE_2-induced BAT thermogenesis, most likely via the suppression of the PGE_2-triggered activation of non-serotonergic RPa neurons (Nakamura *et al*., 2002). This is in line with the suggestion that sympathetic premotor neurons in the RPa send excitatory projections to the preganglionic sympathetic neurons controlling BAT functions, as demonstrated by electrical RPa stimulation and by disinhibition of RPa with a GABA antagonist (Morrison *et al*., 1999).
2. EP3R-positive RPa premotor neurons. Alternatively, it would be also feasible that EP3R-positive serotonergic neurons of the RPa could be locally inhibited by PGE_2 and that the resulting suppressed serotonergic transmission towards the intermediolateral cell column neurons may in turn enhance BAT thermogenesis under febrile conditions. This hypothesis is compatible with the view that PGE_2 exerts suppressive effects on cells expressing EP3 receptors, most likely via a decrease in cyclic AMP levels as a consequence of inhibition of the adenylate cyclase activity (Negishi *et al*., 1995). Indeed, 5-hydoxytryptamine has been reported to play an important role in regulating excitability of IML sympathetic preganglionic neurons; however, it induces powerful excitation rather than inhibition of IML neurons (Pickering *et al*., 1994). Whether the preganglionic sympathetic neurons controlling interscapular BAT functions respond in the same way is not yet known. If they do, the hypothesis of a PGE_2-induced suppression of serotonergic transmission from the RPa towards IML neurons would not explain the activation of BAT thermogenesis that usually occurs under PGE_2 fever. This important issue clearly merits further investigation. Nevertheless, the data presented here support the idea that EP3R-expressing neurons of the RPa might themselves possess prostaglandin sensitivity that is able to modulate BAT thermogenesis under febrile conditions either independently or in concert with other descending hypothalamic pathways.

Acknowledgements

We thank L. W. Enquist (Princeton University, Princeton, USA) and R. R. Miselis (School of Veterinary Medicine, University of Pennsylvania, Philadelphia, USA) for providing the goat anti-PRV antiserum. K.Y. was supported by a fellowship Grant-in-Aids for Scientific Research no. 12307001 from the Ministry of Education, Science and Culture of Japan. K.N. is a research fellow of the Japan Society for the Promotion of Science. This work was supported by the Deutsche Forschungsgemeinschaft grant SFB 535 to H.-J.T. and a Research Grant no. I-572–22.2/1998 to R.G. by the German–Israeli Foundation (G.I.F).

Abbreviations

A5, A5 noradrenaline cells; ac, anterior commissure; AHA, anterior hypothalamic area; AP, area postrema; ARC, arcuate nucleus; B4, B4 serotonin cells; BAT, brown adipose tissue; BW, body weight; C3, C3 adrenaline cells; CVL, caudoventrolateral reticular nucleus; CVM, caudoventromedial reticular nucleus; DA, dorsal hypothalamic area; DMH, dorsomedial hypothalamic nucleus; DPGi, dorsal paragigantocellular nucleus; EP3R, prostaglandin E receptor subtype EP3; EP4R, postaglandin E receptor subtype EP4; EP3R-LI, EP3R-like immunoreactivity; GiA, gigantocellular reticular nucleus; ic, internal capsule; IML, intermediolateral cell column; IRt, intermediate reticular nucleus; LC, locus coeruleus; LHA, lateral hypothalamic area; LPGi, lateral paragigantocellular nucleus; LPO, lateral POA; LPS, lipopolysaccharide; LRt, lateral reticular nucleus; M/SS, motor and somatosensory cortex; MnPO, median preoptic nucleus; MPO, medial preoptic area; NHS, normal horse serum; NTS, solitary tract nucleus; oc, optic chiasm; OVLT, vascular organ of the lamina terminalis; PAA, periarcuate area; PAG, periaqueductal grey; PGE, E series of prostaglandin; PGE_2, prostaglandin E2; PH, posterior hypothalamic area; PnO, pontine reticular nucleus; POA, preoptic area; PRV, pseudorabies virus; PRV-Ba, Bartha strain of pseudorabies virus; PS, parastrial nucleus; PVN, hypothalamic paraventricular nucleus; py, pyramidal tract; RCh, retrochiasmatic area; RMg, raphe magnus nucleus; ROb, raphe obscurus nucleus; RPa, raphe pallidus nucleus; RVL, rostroventrolateral reticular nucleus; SCN, suprachiasmatic nucleus; SON, supraoptic nucleus; SubC, subcoeruleus nucleus; V_{III}, third cerebral ventricle; VLPAG, ventrolateral periaqueductal grey; VLPO, ventrolateral preoptic nucleus; VLTg, ventrolateral tegmental area; VMPO, ventromedial preoptic nucleus.; ZI, zona incerta.

References

Amir, S. & Schiavetto, A. (1990) Injection of prostaglandin E2 into the anterior hypothalamic preoptic area activates brown adipose tissue thermogenesis in the rat. *Brain Res.*, **528**, 138–142.

Bamshad, M., Song, C.K. & Bartness, T.J. (1999) CNS origins of the sympathetic nervous system outflow to brown adipose tissue. *Am. J. Physiol.*, **276**, R1569–R1578.

Blatteis, C.M. & Sehic, E. (1997) Prostaglandin E2: a putative fever mediator. In Mackowiak, P.A. (Ed.), *Fever Basic Mechanisms and Management*. Lippincott-Raven, Philadelphia, pp. 117–145.

Cano, G., Passerin, A.M., Schiltz, J.C., Card, J.P., Morrison, S.F. & Sved, A.F. (2003) Anatomical substrates for the central control of sympathetic outflow to interscapular adipose tissue during cold exposure. *J. Comp. Neurol.*, **460**, 303–326.

Dascombe, M.J., Rothwell, N.J., Sagay, B.O. & Stock, M.J. (1989) Pyrogenic and thermogenic effects of interleukin 1 beta in the rat. *Am. J. Physiol.*, **256**, E7–E11.

Ek, M., Arias, C., Sawchenko, P. & Ericsson-Dahlstrand, A. (2000) Distribution of the EP3 prostaglandin E (2) receptor subtype in the rat brain: relationship to sites of interleukin-1-induced cellular responsiveness. *J. Comp. Neurol.*, **428**, 5–20.

Elmquist, J.K., Scammell, T.E. & Saper, C.B. (1997) Mechanisms of CNS response to systemic immune challenge: the febrile response. *Trends Neurosci.*, **20**, 565–570.

Feldberg, W. & Saxena, P.N. (1971) Further studies on prostaglandin E1 fever in cats. *J. Physiol. (Lond.)*, **219**, 739–745.

Hermann, D.M., Luppi, P.-H., Peyron, C., Hinckel, P. & Jouvet, M. (1997) Afferent projections to the rat nuclei raphe magnus, raphe pallidus and reticularis gigantocellularis pars α demonstrated by iontophoretic application of choleratoxin (subunit b). *J. Chem. Neuroanat.*, **13**, 1–21.

Hosoi, M., Oka, T. & Hori, T. (1997) Prostaglandin E receptor EP3 subtype is involved in thermal hyperalgesia through its action in the preoptic hypothalamus and the diagonal band of Broca in rats. *Pain*, **71**, 303–311.

Hübschle, T., McKinley, M.J. & Oldfield, B.J. (1998) Efferent connections of the lamina terminalis, the preoptic area and the insular cortex to submandibular and sublingual gland of the rat traced with pseudorabies virus. *Brain Res.*, **806**, 219–231.

Jansen, A.S.P., Ter Horst, G.J., Mettenleiter, T.C. & Loewy, A.D. (1992) CNS cell groups projecting to the submandibular parasympathetic preganglionic neurones in the rat: a retrograde transneuronal viral cell body labelling study. *Brain Res.*, **572**, 253–260.

Loewy, A.D. (1981) Raphe pallidus und raphe obscurus projections to the intermediolateral cell column in the rat. *Brain Res.*, **222**, 129–133.

Matsumura, K., Cao, C., Ozaki, M., Morii, H., Nakadate, K. & Watanabe, Y. (1998) Brain endothelial cells express cyclooxygenase-2 during lipopolysaccharide-induced fever: light and electron microscopic immunocytochemical studies. *J. Neurosci.*, **18**, 6279–6289.

Morrison, S.F., Sved, A.F. & Passerin, A.M. (1999) GABA-mediated inhibition of raphe pallidus neurones regulates sympathetic outflow to brown adipose tissue. *Am. J. Physiol.*, **276**, R290–R297.

Murphy, A.Z., Rizvi, T.A., Ennis, M. & Shipley, M.T. (1999) The organization of preoptic-medullary circuits in the male rat: evidence for interconnectivity of neural structures involved in reproductive behavior, antinociception and cardiovascular regulation. *Neuroscience*, **91**, 1103–1116.

Nakamura, K., Kaneko, T., Yamashita, Y., Hasegawa, H., Katoh, H., Ichikawa, A. & Negishi, M. (1999) Immunocytochemical localization of prostaglandin EP3 receptor in the rat hypothalamus. *Neurosci. Lett.*, **260**, 117–120.

Nakamura, K., Kaneko, T., Yamashita, Y., Hasegawa, H., Katoh, H. & Negishi, M. (2000) Immunohistochemical localization of prostaglandin EP3 receptor in the rat nervous system. *J. Comp. Neurol.*, **421**, 543–569.

Nakamura, K., Li, Y.Q., Kaneko, T., Katoh, H. & Negishi, M. (2001) Prostaglandin EP3 receptor protein in serotonin and catecholamine cell groups: a double immunofluorescence study in the rat brain. *Neuroscience*, **103**, 763–775.

Nakamura, K., Matsumura, K., Kaneko, T., Kobayashi, S., Katoh, H. & Negishi, M. (2002) The rostral raphe pallidus nucleus mediates pyrogenic transmission from the preoptic area. *J. Neurosci.*, **22**, 4600–4610.

Negishi, M., Sugimoto, Y. & Ichikawa, A. (1995) Molecular mechanisms of diverse actions of prostanoid receptors. *Biochim. Biophys. Acta*, **1259**, 109–119.

Oka, T., Aou, S. & Hori, T. (1994) Intracerebroventricular injections of prostaglandin E2 induces thermal hyperalgesia in rats: the possible involvement of EP3 receptors. *Brain Res.*, **663**, 287–292.

Oka, T., Oka, K., Scammell, T.E., Lee, C., Kelly, J.F., Nantel, F., Elmquist, J.K. & Saper, C.B. (2000) Relationship of EP (1–4) prostaglandin receptors with rat hypothalamic cell groups involved in lipopolysaccharide fever responses. *J. Comp. Neurol.*, **428**, 20–32.

Oldfield, B.J., Giles, M.E., Watson, A., Anderson, C., Colvill, L.M. & McKinley, M.J. (2002) The neurochemical characterisation of hypothalamic pathways projecting polysynaptically to brown adipose tissue in the rat. *Neuroscience*, **110**, 515–526.

Paxinos, G. & Watson, C. (1998) *The Rat Brain in Stereotaxic Coordinates*, 4th edn. Academic Press, San Diego.

Pickering, A.E., Spanswick, D. & Logan, S.D. (1994) 5-Hydoxytryptamine evokes depolarizations and membrane potential oscillations in rat sympathetic preganglionic neurones. *J. Physiol. (London)*, **480**, 109–121.

Rothwell, N.J. (1992) Eicosanoids, thermogenesis and thermoregulation. *Prostagl. Leukotr. Essent. Fatty Acids*, **46**, 1–7.

Rotto-Percelay, D.M., Wheeler, J.G., Osorio, F.A., Platt, K.B. & Loewy, A.D. (1992) Transneuronal labelling of spinal interneurones and sympathetic preganglionic neurones after pseudorabies virus injections in the rat medial gastrocnemius muscle. *Brain Res.*, **574**, 291–306.

Scammell, T.E., Elmquist, J.K., Griffin, J.D. & Saper, C.B. (1996) Ventromedial preoptic prostaglandin E2 activates fever-producing autonomic pathways. *J. Neurosci.*, **16**, 6246–6254.

Scammel, T.E., Griffin, J.D., Elmquist, J.K. & Saper, C.B. (1998) Microinjection of a cyclooxygenase inhibitor into the anteroventral preoptic region attenuates LPS fever. *Am. J. Physiol.*, **274**, R783–R789.

Simerly, R.B. & Swanson, L.W. (1988) Projections of the medial preoptic nucleus: a *Phaseolus vulgaris* leucoagglutinin anterograde tract-tracing study in the rat. *J. Comp. Neurol.*, **270**, 209–242.

Stitt, J.T. (1973) Prostaglandin E1 fever induced in rabbits. *J. Physiol. (Lond.)*, **232**, 163–179.

Ter Horst, G.J., Hautvast, R.W., De Jongste, M.J. & Korf, J. (1996) Neuroanatomy of cardiac activity-regulating circuitry: a transneuronal retrograde viral labelling study in the rat. *Eur. J. Neurosci.*, **8**, 2029–2041.

Ushikubi, F., Segi, E., Sugimoto, Y., Murata, T., Matsuoka, T., Kobayashi, T., Hizaki, H., Tuboi, K., Katsuyama, M., Ichikawa, A., Tanaka, T., Yoshida, N. & Narumiya, S. (1998) Impaired febrile response in mice lacking the prostaglandin E receptor subtype EP3. *Nature*, **395**, 281–284.

Williams, J.W., Rudy, T.A., Yaksh, T.L. & Viswanathan, C.T. (1977) An extensive exploration of the rat brain for sites mediating prostaglandin-induced hyperthermia. *Brain Res.*, **120**, 251–262.

Yamagata, K., Matsumura, K., Inoue, W., Shiraki, T., Suzuki, K., Yasuda, S., Sugiura, H., Cao, C., Watanabe, Y. & Kobayashi, S. (2001) Coexpression of microsomal-type prostaglandin E synthase with cyclooxygenase-2 in brain endothelial cells of rats during endotoxin-induced fever. *J. Neurosci.*, **21**, 2669–2677.

Zaretskaia, M.V., Zaretsky, D.V. & DiMicco, J.A. (2003) Role of the dorsomedial hypothalamus in thermogenesis and tachycardia caused by microinjection of prostaglandin E2 into the preoptic area in anaesthetized rats. *Neurosci. Lett.*, **340**, 1–4.

Zhang, J. & Rivest, S. (2000) A functional analysis of EP4 receptor-expressing neurones in mediating the action of prostaglandin E2 within specific nuclei of the brain in response to circulating interleukin-1beta. *J. Neurochem.*, **74**, 2134–2145.

6. Literaturverzeichnis (eigene Publikationen sind hervorgehoben)

Armitage G, Harris RBS, Hervey GR and Tobin G (1984) The relationship between energy expenditure and environmental temperature in congenitally obese and non-obese Zucker rats. Journal of Physiology (London) 350: 197-207.

Aston-Jones G and Card JP (2000) Use of pseudorabies virus to delineate multisynaptic circuits in brain: opportunities and limitations. Journal of Neuroscience Methods 103: 51-61.

Barney CC, Williams JS and Kuiper DN (1991) Thermal dehydration-induced thirst in rats: role of angiotensin II. American Journal of Physiology 61: R1171-R1175.

Bernard C (1878-1879) Lecons sur les phénomènes de la vie communs aux animaux et aux végétaux, 2 Bände, Baillière, Paris, Frankreich.

Bishai I and Coceani F (1996) Differential effects of endotoxin and cytokines on prostaglandin E2 formation in cerebral microvessels and brain parenchyma: implications for the pathogenesis of fever. Cytokine 8: 371-376.

Blatteis CM, Bealer SL, Hunter WS, Llanos-Q J, Ahokas RA and Mashburn TA Jr. (1983) Suppression of fever after lesions of the anteroventral third ventricle in guinea pigs. Brain Research Bulletin 11: 519-526.

Blatteis CM, Hales JRS, McKinley MJ and Fawcett AA (1987) Role of the anteroventral third ventricle region in fever in sheep. Canadian Journal of Physiology and Pharmacology 65: 1255-1260.

Blatteis CM and Sehic E (1997) Prostaglandin E2: a putative fever mediator. In: Mackowiak PA (Ed), Fever basic mechanisms and management. Lippincott-Raven, Philadelphia pp. 117-145.

Boulant JA (2000) Role of the preoptic-anterior hypothalamus in thermoregulation and fever. Clinical Infection and Disease 31 (5): 157-161.

Callahan TA and Piekut DT (1997) Differential Fos expression induced by IL-1beta and IL-6 in rat hypothalamus and pituitary gland. Journal of Neuroimmunology 73: 207-211.

Cannon WB (1932) The wisdom of the body. Norton Press, New York.

Card JP, Rinaman L, Schwaber JS, Miselis RR, Whealy ME, Robbins AK and Enquist LW (1990) Neurotropic properties of Pseudorabies virus: uptake and transneuronal passage in the rat central nervous system. The Journal of Neuroscience 10: 1974-1994.

Chai Z, Gatti S, Toniatti C, Poli V and Bartfai T (1996) Interleukin (IL)-6 gene expression in the central nervous system is necessary for fever response to lipopolysaccharide or IL-1 beta: a study on IL-6-deficient mice. Journal of Experimental Medicine 183: 311-316.

Dinarello CA, Cannon JG, Mancilla J, Bishai I, Lees J and Coceani F (1991) Interleukin-6 as an endogenous pyrogen: induction of prostaglandin E2 in brain but not in peripheral blood mononuclear cells. Brain Research 562 (2): 199-206.

Elmquist JK, Elias CF and Saper CB (1999) From lesions to leptin: hypothalamic control of food intake and body weight. Neuron 22: 221-232.

Eriksson S, Hjelmqvist H, Keil R and Gerstberger R (1997) Central application of a nitric oxide donor activates heat defense in the rabbit. Brain Research 774 (1-2): 269-273.

Feldberg W and Saxena PN (1971) Further studies on prostaglandin E1 fever in cats. Journal of Physiology (London) 219: 739-745.

Fregly MJ and Rowland NE (1996) Centrally mediated vasodilation of the rat`s tail by angiotensin II. Physiology and Behavior 60: 861-865.

Friedman JM (1998) Leptin, leptin receptors, and the control of body weight. Nutritional Reviews 56: s38-s46.

Gerstberger R (1999) Nitric oxide and body temperature control. News in Physiological Science 14: 30-36.

Gerstberger R, Barth SW, Horowitz M, Hudl K, Patronas P and Hübschle T (2001) Differential activation of nitrergic hypothalamic neurons by heat exposure and dehydration. In: Thermotherapy for Neoplasia, Inflammation and Pain, Kosaka M, Sugahara T, Schmidt KL and Simon E (Eds). Springer-Verlag, Tokyo. pp. 43-62.

Guan XM, Hess JF, Yu H, Hey PJ and van der Ploeg LH (1997) Differential expression of mRNA for leptin receptor isoforms in the rat brain. Molecular and Cellular Endocrinology 133: 1-7.

Hainsworth FR and Epstein AN (1966) Severe impairment of heat-induced saliva-spreading in rats recovered from lateral hypothalamic lesions. Science 153: 1255-1257.

Hainsworth FR and Stricker EM (1971) Evaporative cooling in the rat: differences between salivary glands as thermoregulatory effectors. Canadian Journal of Physiology and Pharmacology 49: 573-580.

Hainsworth FR, Stricker EM and Epstein AN (1968) Water metabolism of rats in the heat: dehydration and drinking. American Journal of Physiology 214: 983-989.

Hammel HT (1965) Neurons and temperature regulation. In: Physiological Controls and Regulations, Yamamoto WS and Brobeck JR (Eds). Saunders Press, Philadelphia. Pp. 71-97.

Hammel HT (1968) Regulation of internal body temperature. Annual Reviews of Physiology 30: 641-710.

Harré E-M, Roth J, Pehl U, Küth M, Gerstberger R and Hübschle T (2002) Selected Contribution: Role of interleukin-6 in lipopolysaccharide-induced nuclear STAT3 translocation in sensory circumventricular organs during fever in rats. Journal of Applied Physiology 92: 2657-2666.

Harré E-M, Roth J, Gerstberger R and Hübschle T (2003) Interleukin-6 mediates lipopolysaccharide-induced nuclear STAT3 translocation in astrocytes of rat sensory circumventricular organs. Brain Research 980 (1): 151-155.

Horowitz M, Argov D and Mizrahi R (1983) Interrelationships between heat acclimation and salivary cooling mechanism in conscious rats. Comparative Biochemistry and Physiology A 74 (4): 945-949.

Horowitz M, Kaspler P, Simon E and Gerstberger R (1999) Heat acclimation and hypohydration: involvement of central angiotensin II receptors in thermoregulation. American Journal of Physiology 277: R47-R55.

Hübschle T, McKinley MJ and Oldfield BJ (1998) Efferent connections of the lamina terminalis, the preoptic area and the insular cortex to submandibular and sublingual gland of the rat traced with pseudorabies virus. Brain Research 806: 219-231.

Hübschle T, Mathai ML, McKinley MJ and Oldfield BJ (2001a) Multisynaptic neuronal pathways to the submandibular and sublingual gland from the lamina terminalis in the rat - A model for the role of the lamina terminalis in the control of osmo- and thermoregulatory behaviour. Clinical and Experimental Pharmacology and Physiology 28 (7): 558-569.

Hübschle T, Thom E, Watson A, Roth J, Klaus S and Meyerhof W (2001b) Leptin-induced nuclear translocation of STAT3-immunoreactivity in hypothalamic nuclei involved in body weight regulation. The Journal of Neuroscience 21 (7): 2413-2424.

Hübschle T, Harré E-M, Meyerhof W, Pehl U, Roth J and Gerstberger R (2001c) The central pyrogenic action of interleukin-6 is related to nuclear translocation of STAT3 in the anteroventral preoptic area of the rat. Journal of Thermal Biology 26 (4-5): 299-305.

Hunter WS, Sehic E and Blatteis CM (1994) Fever and the organum vasculosum laminae terminalis: another look. In: Temperature Regulation: Recent Physiological and Pharmacological Advances, Milton AS (Ed), Birkhäuser Verlag, Basel.

Iqbal J, Pompolo S, Murakami T and Clarke IJ (2000) Localization of long-form leptin receptor in the somatostatin-containing neurons in sheep hypothalamus. Brain Research 887: 1-6.

Ivanov AI and Romanovsky AA (2002) Fever responses of Zucker rats with and without fatty mutation of the leptin receptor. American Journal of Physiology 282 (1): R311-R316.

Jansen AS, Ter Horst GJ, Mettenleiter TC and Loewy AD (1992) CNS cell groups projecting to the submandibular parasympathetic preganglionic neurons in the rat: a retrograde transneuronal viral cell body labeling study. Brain Research 572: 253-260.

Jurzak M, Schmid HA and Gerstberger R (1994) NADPH-Diaphorase staining and NO-synthase immunoreactivity in circumventricular organs of the rat brain. In: Integrative and Cellular Aspects of Autonomic Functions: Temperature and Osmoregulation, Pleschka K and Gerstberger R (Eds), John Libbey Eurotext, Paris, pp. 451-460.

Kanosue K, Matsuo R, Tanaka H and Nakayama T (1986) Effect of body temperature on salivary reflexes in rats. Journal of the Autonomic Nervous System 6 (3): 233-237.

Kanosue K, Nakayama T, Tanaka H, Yanase M and Yasuda H (1990) Modes of action of local hypothalamic and skin thermal stimulation on salivary secretion in rats. Journal of Physiology (London) 424: 459-471.

LeMay LG, Vander AJ, and Kluger MJ (1990) Role of interleukin 6 in fever in rats. American Journal of Physiology 258: R798-R803.

Lenczowski MJ, Bluthe RM, Roth J, Rees GS, Rushforth DA, van Dam AM, Tilders FJ, Dantzer R, Rothwell NJ and Luheshi GN (1999) Central administration of rat IL-6 induces HPA activation and fever but not sickness behaviour in rats. American Journal of Physiology 276: R652-R658.

Lomniczi B (1988) Aujeszky´s Disease (Pseudorabies) in Laboratory and Captive Animals. In: Virus Diseases in Laboratory and Captive Animals, Darai, G (Ed), Martinus Nijhoff Publishers, Boston USA.

Maskrey M, Wiggins PR and Frappell PB (2001) Behavioral thermoregulation in obese and lean Zucker rats in a thermal gradient. American Journal of Physiology 281 (5): R1675-R1680.

Mathai ML, Hübschle T. and McKinley MJ (2000) Central angiotensin receptor blockade impairs thermolytic and dipsogenic responses to heat exposure in rats. American Journal of Physiology 279 (5): R1821-R1826.

Matsuda T, Hori T and Nakashima T (1992) Thermal and PGE2 sensitivity of the organum vasculosum laminae terminalis region and preoptic area in rat brain slices. Journal of Physiology (London) 454: 197-212.

McKinley MJ, Bicknell RJ, Hards DK, McAllen RM, Vivas L, Weisinger RS and Oldfield BJ (1992) Efferent neural pathways of the lamina terminalis subserving osmoregulation. Progress in Brain Research 91: 395-402

McKinley MJ, Pennington GL and Oldfield BJ (1996) Anteroventral wall of the third ventricle and dorsal lamina terminalis: headquarters for control of body fluid homeostasis? Clinical and Experimental Pharmacology and Physiology 23: 271-281.

Meister B (2000) Control of food intake via leptin receptors in the hypothalamus. Vitamins and Hormons 59: 265-304.

Mercer JG, Hoggard N, Williams LM, Lawrence CB, Hannah LT and Trayhurn P (1996) Localization of leptin receptor mRNA and the long form splice variant (Ob-Rb) in mouse hypothalamus and adjacent brain regions by in situ hybridization. FEBS Letters 387: 113-116.

Mettenleiter TC (1994) Pseudorabies (Aujeszky`s disease) virus: state of the art. Acta Veterinaria Hungarica 42 (2-3): 153-177.

Morrison SF, Sved AF and Passerin AM (1999) GABA-mediated inhibition of raphe pallidus neurones regulates sympathetic outflow to brown adipose tissue. American Journal of Physiology 276: R290-R297.

Nagashima K, Nakai S, Tanaka M and Kanosue K (2000) Neuronal circuitries involved in thermoregulation. Autonomic Neuroscience 85 (1-3): 18-25.

Nakamura K, Kaneko T, Yamashita Y, Hasegawa H, Katoh H, Ichikawa A and Negishi M (1999) Immunocytochemical localization of prostaglandin EP3 receptor in the rat hypothalamus. Neuroscience Letters 260: 117-120.

Nakamura K, Kaneko T, Yamashita Y, Hasegawa H, Katoh H and Negishi M (2000) Immunohistochemical localization of prostaglandin EP3 receptor in the rat nervous system. Journal of Comparative Neurology 421: 543-569.

Nakamura K, Matsumura K, Kaneko T, Kobayashi S, Katoh H and Negishi M (2002) The rostral raphe pallidus nucleus mediates pyrogenic transmission from the preoptic area. The Journal of Neuroscience 22: 4600-4610.

Nakayama T (1985) Thermosensitive neurons in the brain. Japanese Journal of Physiology 35 (3): 375-389.

Niimi M, Wada Y, Sato M, Takahara J and Kawanishi K (1997) Effect of continuous intravenous injection of interleukin-6 and pretreatment with cyclooxygenase inhibitor on brain c-fos expression in rat. Neuroendocrinology 66: 47-53.

Patronas P, Horowitz M, Simon E and Gerstberger R (1998) Differential stimulation of c-Fos expression in hypothalamic nuclei of the rat brain during short-term acclimation and mild dehydration. Brain Research 798: 127-139.

Penfield W (1929) Diencephalic autonomic epilepsy. Archives of Neurology and Psychiatry 22: 358-374.

Plata-Salaman CR (1996) Anorexia induced by activators of the signal transducer gp 130. Neuroreport 7: 841-844.

Ranels HJ and Griffin JD (2003) The effects of prostaglandin E2 on the firing rate activity of thermosensitive and temperature insensitive neurons in the ventromedial preoptic area of the rat hypothalamus. Brain Research 964: 42-50.

Renzi A, Lopes RA, Sala MA, Camargo LA, Menani JV, Saad WA and Campos GM (1990) Morphological, morphometric and stereological study of submandibular glands in rats with lesion of the anteroventral region of the third ventricle (AV3V). Experimental Pathology 38 (3): 177-187.

Ritter RC and Epstein AN (1974) Saliva lost by grooming. A major item in the rat`s water economy. Behavioral Biology 11: 581-585.

Romanovsky AA, Sugimoto N, Simons CT and Hunter WS (2003) The organum vasculosum laminae terminalis in immune-to-brain febrigenic signaling: a reappraisal of lesion experiments. American Journal of Physiology 285 (2): R420-R428.

Ross G, Hübschle T, Pehl U, Braun HA, Voigt K, Gerstberger R and Roth J (2003) Fever induction by localized subcutaneous inflammation in guinea pigs: the roles of cytokines and prostaglandins in this experimental fever model. Journal of Applied Physiology 94: 1395-1402.

Roth J, McClellan JL, Kluger MJ und Zeisberger E (1994) Attenuation of fever and release of cytokines after repeated injections of lipopolysaccharide in guinea pigs. Journal of Physiology (London) 447 (1): 177-185.

Roth J, Hübschle T, Pehl U, Ross G and Gerstberger R (2002) Influence of systemic treatment with cyclooxygenase inhibitors on lipopolysaccharide-induced fever and

circulating levels of cytokines and cortisol in guinea-pigs. European Journal of Physiology - Plügers Archiv 443 (3):411-417.

Roth J, Harré E-M, Rummel C, Gerstberger R and Hübschle T (2004) Signaling the brain in systemic inflammation: Role of sensory circumventricular organs. Frontiers in Bioscience 9: 290-300.

Rothwell NJ (1992) Eicosanoids, thermogenesis and thermoregulation. Prostaglandines Leukotriene and Essential Fatty Acids 46: 1-7.

Saad WA, Guarda IFMS, Camargo LAA, Santos TAFB, Guarda RS, Saad WA, Simoes S and Rodrigues JA (2003) Role of nitric oxide of the median preoptic nucleus (MnPO) in the alterations of salivary flow, arterial pressure and heart rate induced by injection of pilocarpine into the MnPO and intraperitoneally. Brazilian Journal of Medical and Biological Research 36: 897-905.

Sagar SM, Sharp FR and Curran T (1988) Expression of c-Fos protein in brain: Metabolic mapping at the cellular level. Science 240: 1328-1331.

Saper CB (1998) Neurobiological basis of fever. Annuals of the New York Academy of Science 856: 90-94.

Scammell TE, Elmquist JK, Griffin JD and Saper CB (1996) Ventromedial preoptic prostaglandin E2 activates fever-producing autonomic pathways. The Journal of Neuroscience 16: 6246-6254.

Schöbitz B, de Kloet ER, Sutanto W and Holsboer F (1993) Cellular localization of interleukin 6 mRNA and interleukin 6 receptor mRNA in rat brain. European Journal of Neuroscience 5: 1462-1435.

Simon E (1999) Thermoregulation as a switchboard of autonomic nervous and endocrine control. Japanese Journal of Physiology 49: 297-232.

Stepanyan Z, Kocharyan A, Pyrski, M, Hübschle T, Watson A, Schulz S and Meyerhof W (2003) Leptin target neurons of rat hypothalamus express somatostatin receptors. Journal of Neuroendocrinology 15: 822-830.

Stitt JT (1973) Prostaglandin E1 fever induced in rabbits. Journal of Physiology (London) 232: 163-179.

Takahashi Y, Smith P, Ferguson A and Pittman QJ (1997) Circumventricular organs and fever. American Journal of Physiology 273: R1690-1695.

Travis KA and Johnson AK (1993) In vitro sensitivity of median preoptic neurons to angiotensin II, osmotic pressure, and temperature. American Journal of Physiology 264: 1200-1205.

Ushikubi F, Segi E, Sugimoto Y, Murata T, Matsuoka T, Kobayashi T, Hizaki H, Tuboi K, Katsuyama M, Ichikawa A, Tanaka T, Yoshida N and Narumiya S (1998) Impaired febrile response in mice lacking the prostaglandin E receptor subtype EP3. Nature 395: 281-284.

Vallières L and Rivest S (1997) Regulation of the genes encoding interleukin-6, its receptor and gp130 in the rat brain in response to the immune activator lipopolysaccharide and the proinflammatory cytokine interleukin-1ß. Journal of Neurochemistry 69: 1668-1683.

Vallières L, Lacroix S and Rivest S (1997) Influence of interleukin-6 on neural activity and transcription of the gene encoding corticotrophin-releasing factor in the rat brain: an effect depending upon the route of aministration. European Journal of Neuroscience 9: 1461-1472.

Whyte DG and Johnson AK (2002) Lesions of periventricular tissue surrounding the anteroventral third ventricle (AV3V) attenuate salivation and thermal tolerance in response to a heat stress. Brain Research 951(1): 146-149.

Williams JW, Rudy TA, Yaksh TL and Viswanathan CT (1977) An extensive exploration of the rat brain for sites mediating prostaglandin-induced hyperthermia. Brain Research 120: 251-262.

Yoshida K, Nakamura K, Matsumura K, Kanosue K, König, M, Thiel H-J, Boldogköi Z, Toth I, Roth J, Gerstberger R and Hübschle T (2003) Neurons of the rat preoptic area and the raphe pallidus nucleus innervating the brown adipose tissue express prostaglandin E receptor subtype EP3. European Journal of Neuroscience 18 (7): 1848-1860.

Zhang YH, Lu J, Elmquist JK and Saper CB (2000) Lipopolysaccharide activates specific populations of hypothalamic and brainstem neurons that project to the spinal cord. The Journal of Neuroscience 20: 6578-6586.

Zhang YH, Lu J, Elmquist JK and Saper CB (2003) Specific roles of cyclooxygenase-1 and cyclooxygenase-2 in lipopolysaccharide-induced fever and Fos expression in rat brain. Journal of Comparative Neurology 463 (1): 3-12.

7. Danksagung

Mein besonderer Dank gilt meinem langjährigen Betreuer und Doktorvater Prof. Dr. R. Gerstberger, der durch seine stets freundschaftliche und konstruktive Unterstützung und Förderung wesentlichen Anteil an meiner wissenschaftlichen Laufbahn hat und damit die Entstehung dieser Arbeit erst ermöglichte. Unter seiner wissenschaftlichen Anleitung und menschlichen Führung habe ich mich sehr wohl gefühlt. Er gab mir die Chance, meinen eigenen wissenschaftlichen Weg zu suchen und zu finden. Die Beteiligung am Aufbau der Arbeitsgruppe Gerstberger an der Veterinär-Physiologie der JLU Giessen war für mich eine wichtige und lehrreiche Erfahrung, die ich nicht missen möchte. Ein herzliches Dankeschön für die gemeinsame Zeit.

Ganz besonders danken möchte ich auch meinem Kollegen und Zimmernachbarn PD Dr. Joachim Roth (genannt J.R.). Die vielen wissenschaftlichen und privaten Hilfeleistungen, die freundschaftliche Atmosphäre, die außerordentlich produktive Zusammenarbeit haben uns zusammen mit unseren technischen Assistentinnen (Bärbel, Doreen, Jola) zu einem Team im Team werden lassen. Es war für mich außerordentlich hilfreich einen derart erfahrenen „Uni-Mann“ an meiner Seite zu haben. Ich habe durch ihn etliches in Forschung und Lehre dazugelernt.

Es gab Freunde, Mitarbeiter und Kollegen, ohne die dieses Werk so nicht entstanden wäre. Ein herzliches Dankeschön an Prof. Dr. E. Simon, Dr. U. Pehl, Prof. Dr. M.J. McKinley, Dr. B.J. Oldfield, Dr. M.L. Mathai, Dr. R. McAllen, Ayse, Liana, David, Nana, Puspha, Yossi, Anna, Prof. W. Meyerhof, Prof. S. Klaus, Dr. E.-M. Harré, Netzwerkadministrator M. Küth, Dr. I. Toth, Dr. Z. Boldogköi, Dr. M. König, Prof. Dr. H.-J. Thiel, Prof. Dr. K. Kanosue, Prof. Dr. K. Matsumura, Dr. K. Nakamura und Dr. K. Yoshida.

Allen anderen hier namentlich nicht genannten Mitarbeiterinnen und Mitarbeitern des Instituts für Veterinär-Physiologie der JLU Giessen, des Deutschen Instituts für Ernährungsforschung (DIfE) in Potsdam-Rehbrücke, des Max-Planck-Instituts für physiologische und klinische Forschung, W.G. Kerckhoff-Institut in Bad Nauheim und des Howard-Florey-Instituts in Melbourne, Australien möchte ich für die gute und kollegiale Arbeitsatmosphäre danken.

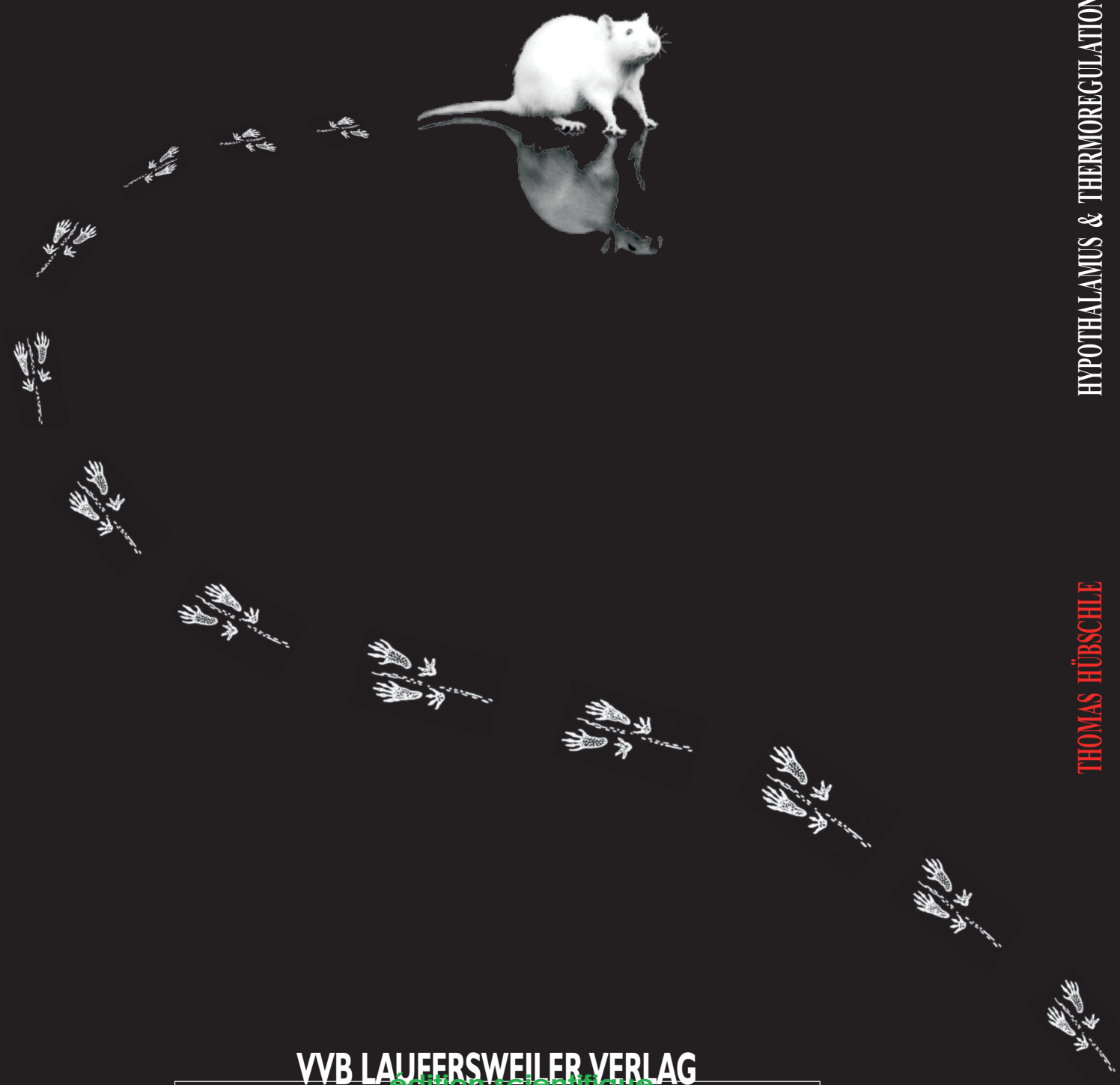

HYPOTHALAMUS & THERMOREGULATION

THOMAS HÜBSCHLE

VVB LAUFERSWEILER VERLAG
édition scientifique

VVB LAUFERSWEILER VERLAG
GLEIBERGER WEG 4
D-35435 WETTENBERG

Tel: +49-(0)6406-4413 Fax: -72757
Email: vvb-ips@t-online.de
www.doktorverlag.de

ISBN 3-89687-681-3

9 783896 876812

VVB